A ROLE FOR TCTP IN NEURAL CIRCUITRY FORMATION

Cláudio André Gouveia Martins Roque

UNIVERSIDADE DE COIMBRA

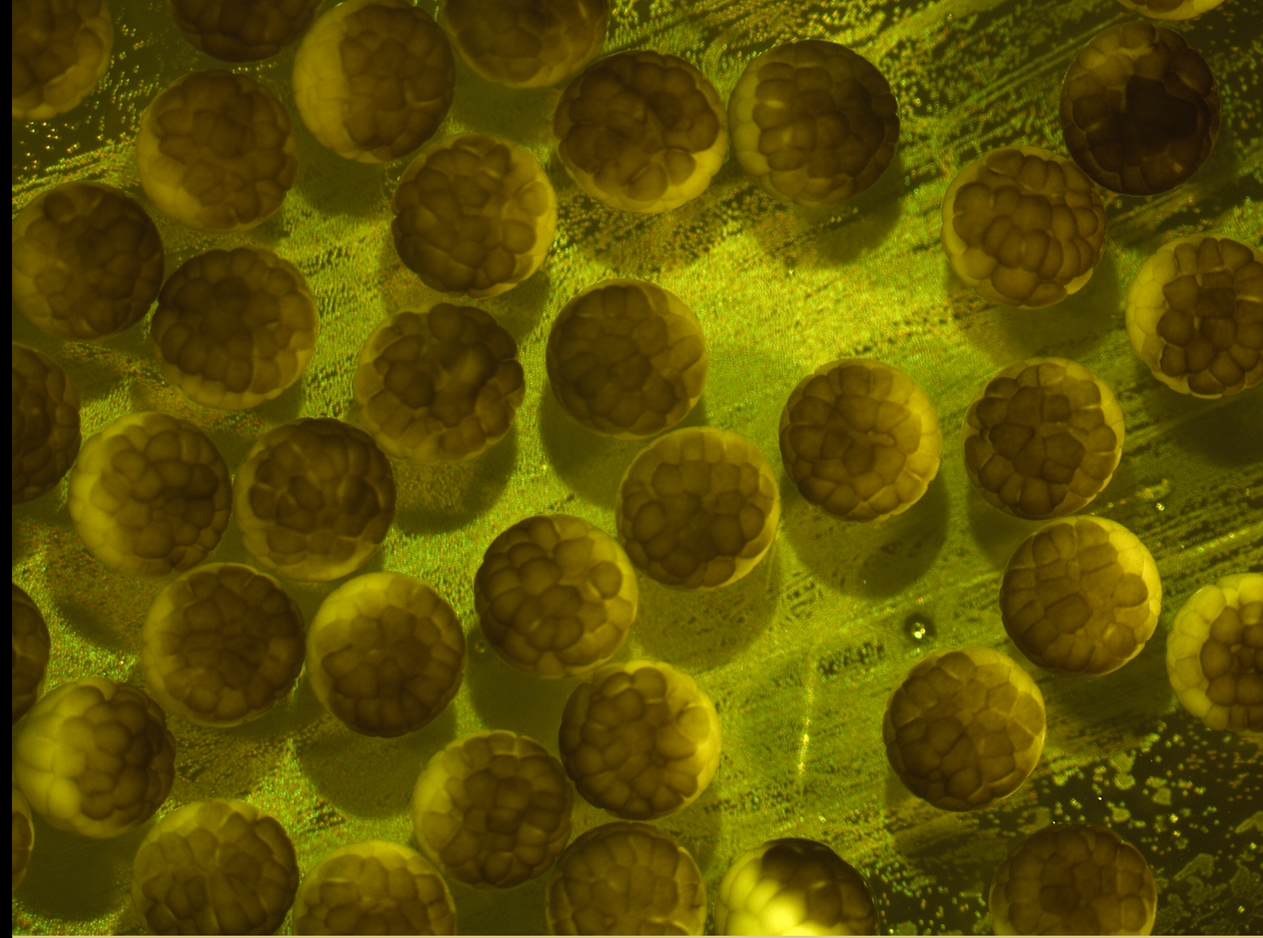

Cláudio André Gouveia Martins Roque

A ROLE FOR TCTP IN NEURAL CIRCUITRY FORMATION

Tese de doutoramento em Biociências, ramo de especialização em Biologia Celular e Molecular,
orientada pela Doutora Christine Elizabeth Holt e com co-orientação do Doutor Carlos Jorge Alves Miranda Bandeira Duarte,
e apresentada ao Departamento de Ciências da Vida da Faculdade de Ciências e Tecnologia da Universidade de Coimbra.

Fevereiro de 2015

· U C ·

UNIVERSIDADE DE COIMBRA

A Role for Tctp in Neural Circuitry Formation

Cláudio André Gouveia Martins Roque

Universidade de Coimbra

2015

Este trabalho foi realizado no Departamento de Fisiologia, Desenvolvimento e Neurociências da Universidade de Cambridge, ao abrigo do Programa Doutoral em Biologia Experimental e Biomedicina organizado pelo Centro de Neurociências e Biologia Celular da Universidade de Coimbra. A sua realização foi suportada pela bolsa de doutoramento SFRH / BD / 33891 / 2009.

About the cover: Animal view of stage 6 ½ *Xenopus laevis* blastulas, 3 and a half hours post-fertilization.

Aos meus pais

Prefácio

O trabalho apresentado nesta dissertação resulta unicamente da minha atividade de investigação e não inclui contribuições de outrem, excepto quando explicitamente referenciado no texto.

O corpo destes resultados será submetido para publicação numa revista científica internacional:

Roque CM, Wong HW, and Holt CE. *Cancer-associated Tctp Regulates Axon Pathfinding by Promoting Mitochondrial Homeostasis.*

Certifico ainda que toda e qualquer secção aqui incluída, e que venha a constar dessa publicação, foi redigida somente por mim.

Agradecimentos

Ao Centro de Neurociências e Biologia Celular cabe o primeiro agradecimento. Tenho a oportunidade concedida pelo Programa Doutoral em Biologia Experimental e Biomedicina como única – *life-changing* – e todos os dias me senti grato por ela.

I would like to thank my supervisor, Professor Christine Holt, for making this research possible through her continuous support, guidance, and the allowed freedom to grow as a scientist. These years with you have left a profound mark in me.

Coube-me a honra de poder contar o Professor Carlos Duarte como segundo orientador. Mesmo que maioritariamente à distância, retive das nossas conversas inspiração prolongada, e tomo para mim como modelo o seu trabalho, dedicação, e forma de estar. Sei hoje que gostava que tivesse sido o meu orientador "de todos os dias".

I owe you big time, Hovy. Thank you for your crucial help, and, most of all, the kindness and uplifting attitude you have continously shown me.

Xana Almeida, Harsh Bhatt, Nikki Coutts, Stefanie Dudczig, Tomasz Dyl, Jie He, Aih Cheun Lee, Julie Qiaojin Lin, Ryan MacDonald, Julia Oswald, Siân Richards, Vasja Urbančič: can I put you all in a box and take you home with me?

Porque sem fim, deixo contigo o último obrigado, Inês. Não teria chegado tão longe sem ti.

Table of Contents

Sumário

Com os seus cerca de 86 mil milhões de neurónios [1], o cérebro humano é constituído por uma rede intrincada de processos axonais e dendríticos complexamente interligados, e que, como um todo coerente, nos permite reconhecer sinais com origem no meio externo e responder de forma consciente sobre este. A formação de ligações precisas entre as diversas áreas do sistema nervoso assume, portanto, um papel fundamental no garante das suas funções.

Numa primeira fase, os programas de conectividade neuronal desenvolvem-se no decurso da embriogénese. Em concreto, após a formação e subsequente migração do neurónio, este estende um axónio que se expande de modo estereotipado até à vizinhança do seu alvo pós-sináptico. Os mecanismos de navegação axonal dependem de uma sequência de marcos moleculares distribuídos pelo sistema nervoso embrionário, os quais são integrados ao nível do cone de crescimento, uma estrutura ameboide com capacidades sensoriais e motoras, existente no extremo distal do axónio. Ao longo das últimas três décadas, um vasto leque de estudos foi permitindo perceber que o cone de crescimento é dotado de um certo grau de autonomia funcional [2], facto claramente ilustrado pela capacidade inalterada revelada por axónios embrionários seccionados – isto é, separados dos seus corpos celulares – para se orientarem corretamente *in vivo* [3]. Sabe-se hoje que esta flexibilidade de atuação advém, em parte, da regulação local do proteoma axonal promovida pelos sinais moleculares presentes no meio extracelular embrionário. A tradução local de novas proteínas despoletada por estes factores permite, por exemplo, alterações rápidas ao nível do citoesqueleto [4-6] e da expressão de receptores na membrana celular do cone de crescimento [7], assim como potenciar mecanismos de manutenção axonal e mitocondrial [8-10]. É, no entanto, o carácter transversal do transcriptoma axonal – o número de espécies de ARNm localizados no compartimento axonal situa-se na ordem dos milhares [11-15] – que porventura nos dá verdadeiramente conta da importância funcional deste processo celular.

Nos estudos laboratoriais conducentes a esta tese, foi estudada a participação da Tctp (do acrónimo inglês, translationally controlled tumor protein) nos processos de conectividade neuronal, usando como modelo a projeção retinotectal da rã-de-unhas-

-africana (*Xenopus laevis*). A Tctp é uma proteína conservada filogeneticamente [16], relevante ao nível de processos de sobrevivência [17] e de crescimento celular [18, 19], e bem caracterizada em particular no âmbito da oncogénese [20]. A motivação inicial para estudar a Tctp neste contexto surgiu da identificação do ARNm que codifica a Tctp entre os mais abundantemente expressos no compartimento axonal de diversas populações neuronais [11-14], incluindo em células ganglionares da retina, indicando que esta proteína detém um papel local relevante, mas por explorar, no campo da neurobiologia.

A minha contribuição original mais significativa para o conhecimento prende-se com a identificação do envolvimento da Tctp na regulação do desenvolvimento axonal através da sua função de suporte à homeostasia mitocondrial. Especificamente, a depleção da Tctp durante a embriogénese resulta em projeções retinotectais que não granjeiam alcançar a zona-alvo no mesencéfalo aquando do estádio de desenvolvimento normal. Os axónios deficitários em Tctp apresentam uma disfunção e menor densidade mitocondrial, bem como dinâmicas de transporte mitocondrial alteradas; contudo, tais manifestações não se traduzem em decréscimos globais da biogénese ou da massa destes organelos, pelo que se infere um fenótipo com repercussões predominantemente axonais. Documento ainda a interação intra-axonal da Tctp com duas oncoproteínas anti-apoptóticas da família Bcl-2 – a Mcl1 (do acrónimo inglês, myeloid cell leukemia 1) e a Bcl-X_L (Bcl-2-like protein 1) – e aumentos nos níveis de expressão da P53 e da forma ativada da Caspase-3 no cone de crescimento de axónios desprovidos da Tctp.

Estes resultados indicam que a Tctp regula o desenvolvimento axonal pela sua ação nos mecanismos de homeostasia celular. O meu estudo sugere, portanto, que à Tctp cabe uma função de fundamental relevância nos mecanismos de formação dos circuitos neuronais em vertebrados.

Summary

With 86 billion neurons in the human brain [1], the ordered array of neuronal pathways is an exceptionally complex web of accurately connected axonal and dendritic processes, ultimately allowing us to perceive the world and respond consciously to it. Precise wiring of the nervous system is therefore the cornerstone of its intricate functions.

Neuronal connectivity begins to take shape during embryonic development, when post-migratory newborn neurons send out a single threadlike axon that extends in a highly directed manner to the vicinity of its appropriate target region. Axon pathfinding relies on molecular 'guideposts' presented in the embryonic landscape and integrated by the growth cone, an amoeboid, sensory structure at the tip of developing axons first identified by the legendary Ramón y Cajal [21]. Studies in the past three decades have revealed that a certain degree of functional autonomy is endowed upon this cellular outpost [2], perhaps best exemplified by the demonstration that axons separated from their cell bodies can still navigate correctly *in vivo* [3]. It is now evident that this flexibility partly arises from the local regulation of the axonal proteome in response to extracellular cues. The local translation of new proteins elicited by these factors allows for rapid alterations in cytoskeleton dynamics [4-6], guidance receptor expression [7], substrate adhesion [22], as well as promoting axonal and mitochondrial maintenance [8-10]. The recent appreciation of the complexity of the axonal transcriptome, with thousands of mRNAs identified [11-15], clearly illustrates the functional significance of this homeostatic mechanism.

Here, I pioneered the study of translationally controlled tumor protein (Tctp) in the context of neural connectivity using the *Xenopus laevis* (African clawed frog) retinotectal projection as an *in vivo* model system. Tctp is an evolutionary conserved pro-survival protein implicated in cell growth [16-19] and particularly well-studied in cancer pathogenesis [20], where its expression is often found upregulated and correlates with indicative markers of aggressive disease [23-25]. Significantly, across diverse neuronal populations, including retinal ganglion cells, the *tpt1* transcript, which encodes for Tctp, is ranked among the most enriched in the axonal compartment [11-14], suggestive of an unexplored relevant role in neurobiology.

My most significant original contribution to knowledge is the identification of Tctp as a cell-autonomous checkpoint for axon development through its support of mi-

tochondrial homeostasis. Specifically, Tctp deficiency during embryogenesis results in shorter retinotectal projections that fail to reach their target at the appropriate developmental window. Tctp-depleted axons exhibit mitochondrial dysfunction, decreased mitochondrial density and defects in mitochondrial dynamics, but Tctp knockdown embryos have intact mitochondrial biogenesis and mass, arguing for a phenotype with predominantly axonal repercussions. Furthermore, I document that axonal Tctp interacts with Bcl-2 pro-survival oncoproteins myeloid cell leukemia 1 (Mcl1) and Bcl-2-like protein 1 (Bcl-X_L), and that Caspase-3 activation and increased P53 levels are found in growth cones depleted of Tctp.

Overall, the data I have collected over the course of my research indicate that Tctp regulates axon development by impacting on the homeostatic mechanisms of the neuron. My findings thus suggest a novel and fundamental role for Tctp in vertebrate neural circuitry formation.

Note on Gene Nomenclature

For overall clarity and consistency, *Xenopus* gene nomenclature guidelines were used throughout this dissertation [26].

Note that the *tumor protein, translationally-controlled 1* (*tpt1*) gene, is transcribed into *tpt1* mRNA, which encodes for Tctp protein.

1. Introduction

A – Axon Development

The arrangement of retinal neurons in the brain reflects that of the light-sensitive cells in the retina and, ultimately, the visual world. The computing power such organization commands is staggering: in each eye we have approximately 126 million photoreceptors, connecting to 540 million visual cortex cells [27]. In between, processing of information in the visual system begins at the very first synapse, to the extent that when leaving the eye, each electric signal relays not a point of light but a *pattern* of light. In lower vertebrates, independent of the birthplace in the retina, retinal ganglion cell (RGC) axons extend towards the optic nerve head, where they collect to exit the eye and form the optic nerve. Once past the midline optic chiasm[a] in the ventral diencephalon, retinal ganglion cell axons turn dorsally and grow to the optic tectum, their most prominent synaptic target in the midbrain, where they terminate and arborize in a topographic array that, in essence, copies the spatial map on the retina into the brain **(Figure 1.1)**. Likewise, several other stereotyped trajectories of axonal growth are concurrently established in the embryonic brain; so, how do axons succeed in finding their way?

[a] Binocular vision requires that information from both eyes converge on the same areas of the brain. At the optic chiasm, axons from specific regions of the retina, project either contralaterally or ipsilaterally, enabling those neurons that share visual space to converge on the same brain hemisphere. By contrast, fish and birds do not extend ipsilateral projections for they do not have binocular vision.

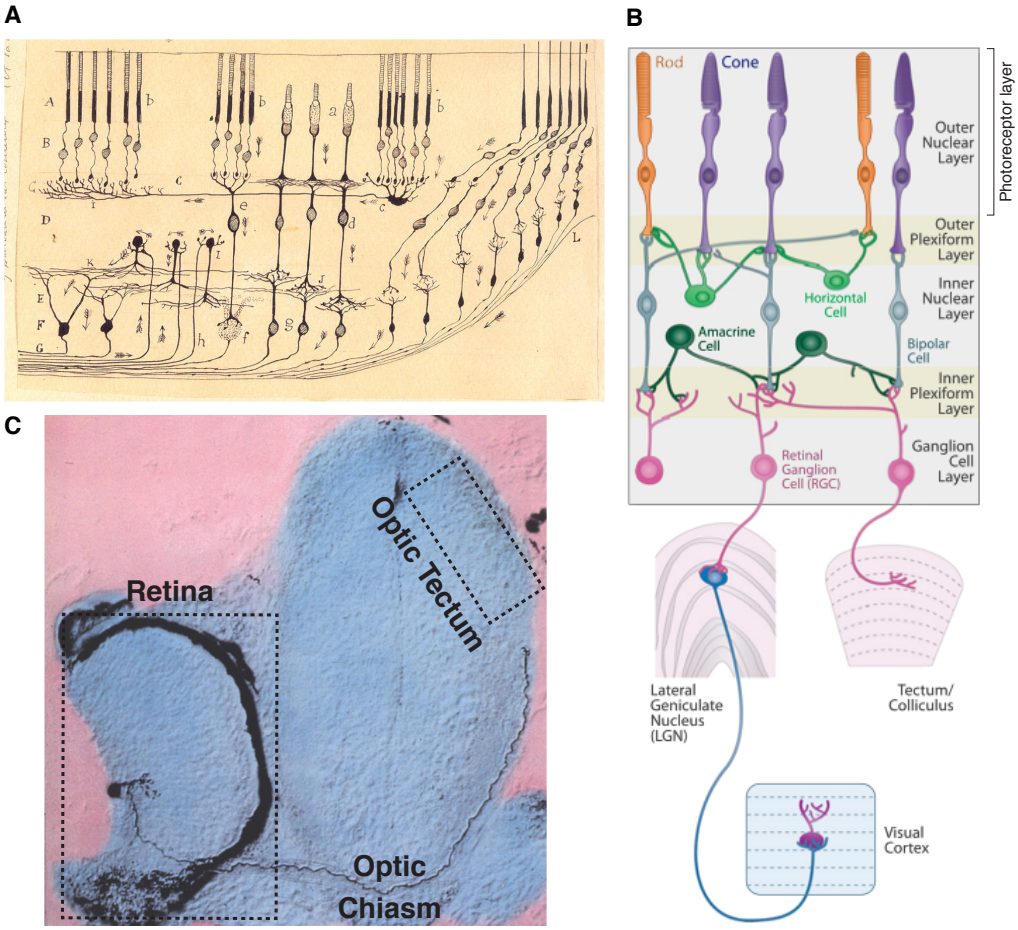

Figure 1.1 – Overview of the visual system. (A) Hand-drawn representation of the mammalian retinal structure by Santiago Ramón y Cajal. (B) Global organization of the visual system. Note that the optic tectum in lower vertebrates is the anatomic equivalent of the superior colliculus in mammals. In higher mammals (e.g. in cats and humans) the dorsal lateral geniculate (LGN) in the thalamus is instead the main target in the diencephalon. *From Sanes and Zipursky* (2010) [28]. (C) *Xenopus laevis* transverse section showing a single retinal ganglion cell with its axon growing through the optic pathway en route to the optic tectum. *Adapted, courtesy of Christine Holt.*

A.1 Principles of Axon Guidance

Historically, the neuroscience field debated two explanatory hypotheses regarding the wiring of the nervous system. The 'resonance theory' explained the developmental patterning of the central nerve tracts on a purely mechanical basis, by schemes of initially non-selective growth that, based on the validity of the connection formed, were later maintained or eliminated [29, 30]. A second framework proposed that selective chemical or electrical forces guided neuronal connections and found initial support in the experiments of John Langley in the late ninetieth century [31]. The extensive studies of Roger Sperry on how regenerating frog retinal ganglion cell axons[a] are arranged when re-innervating their target categorically proved the latter hypothesis [32-34]. In

[a] Unlike their mammalian counterparts, central axons regenerate well in lower vertebrates, thus their utilization in such experiments.

his most dramatic experiment, Sperry rotated the eye 180º on its dorsoventral axis after severing the optic nerve and noted that it lead to the animal having inverted vision; that is, the axons were originating from reversed positions in the eye yet managing to find their appropriate synaptic connections in the brain. He concluded that "the cells and fibers of the brain and cord must carry some kind of individual identification tags, presumably cytochemical in nature, by which they are distinguished one from another almost, in many regions, to the level of the single neuron" [34], a molecular view of the structuring of the nervous system which remains largely unchallenged to date [35].

Indeed, observations *in vivo* of developing axonal projections have revealed that their growth is highly directed, with axons navigating along a prescribed trajectory en route to their respective synaptic targets and making very few errors of navigation in the process [36-39]. Growing axons encounter successive spatial signals – guidance cues – with each section of the trajectory governed by distinct attractive or repulsive guidance mechanisms [40]; *id est*, axon trajectories are seemingly divided into shorter segments [41-43], thus reducing the effort of navigating towards a distant target – in the order of centimetres in some instances, or a thousand-fold the diameter of the cell body – to the simpler task of reaching consecutive intermediate points.

What are the mechanisms that govern the stereotyped axon growth in each segment of their trajectory? Classically, four evolutionary conserved families of signaling molecules that function as instructive guidance cues are described for their widespread roles in axon guidance: netrins, semaphorins, slits and ephrins **(Figure 1.2)** [44]. Two additional classes of molecules with roles in axon guidance and originally characterized in other settings have been more recently recognized: morphogens (members of the Wnt, Hedgehog, and Bone Morphogenic Protein families), and various molecules classified primarily as growth factors [44]. Importantly, the actions of these cues are not mutually exclusive, but rather coordinately act to ensure an unerring navigation. For example, commissural axons, a particularly well-studied and illustrative guidance paradigm, are attracted to the ventral midline by members of the Netrin family [43], the morphogen Sonic Hedgehog (Shh) [45] and the prototypic angiogenic factor Vegf [46], all exerting complementary effects; synchronously, roof plate cells in the dorsal midline secrete bone morphogenic proteins (BMPs) which act as chemorepellents and provide a decisive *forward* push on their ventral journey [47]. Thus, the involvement of various instructive signals even along a short trajectory considerably diminishes the likelihood of guidance errors and promotes the necessary fidelity in the establishment of neuronal connections **(Figure 1.3)**.

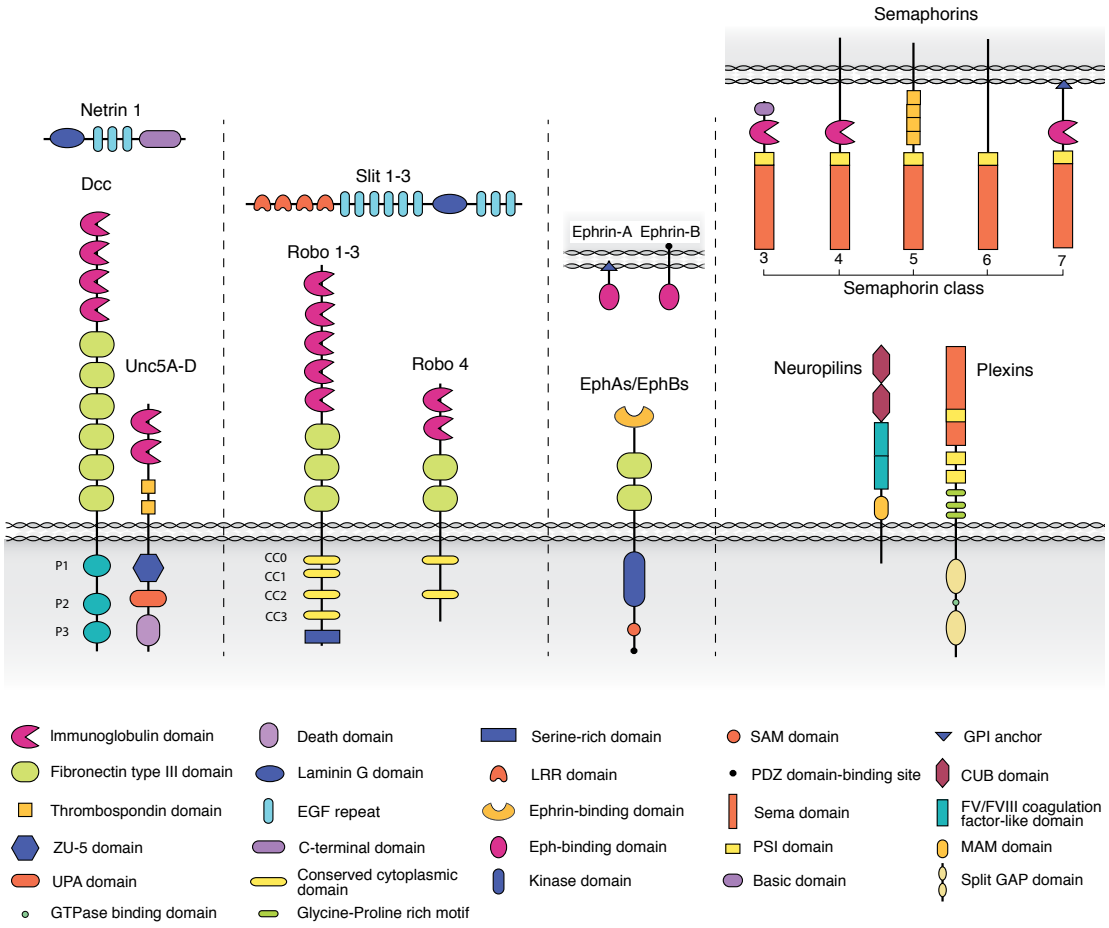

Figure 1.2 – Families of axon guidance molecules. Schematic representation of the four 'canonical' ligand/receptor families of signaling proteins involved in axon guidance. Netrins comprise a family of extracellular proteins related to laminin and are the vertebrate homologues of the Unc-6 protein identified in *Caenorhabditis elegans*. In vertebrates, the Netrin family is formed by three secreted (Netrin-1, Netrin-3 and Netrin-4) and two glycosylphosphatidylinositol (GPI)-linked membrane proteins (Netrin-G1 and Netrin-G2). From worms to vertebrates, secreted Netrins can function as attractive cues to some axons and repulsive to others, depending on the complement of receptors present and cellular context. Netrin-1 attraction is mediated by receptors of the deleted in colorectal cancer (Dcc) family, which are members of the immunoglobulin superfamily of cell adhesion molecules. By contrast, Netrin-mediated repulsion is dependent on the combinatorial actions of Dcc and Unc-5 receptors, which belong to the immunoglobulin gene superfamily. More recently, the highly conserved Down syndrome cell adhesion molecule (Dscam) has been characterized as a Netrin-1 receptor, mediating attractive guidance to commissural axons in collaboration with Dcc [48, 49]. Semaphorins constitute a family of secreted, transmembrane and GPI-anchored proteins that were originally identified as repulsive axon guidance cues. Semaphorin input is signalled predominantly through members of the Plexin family, though many secreted semaphorins, including the first vertebrate semaphorin to be identified (Semaphorin 3A), do not bind these receptors directly but instead neuropilins, which act as semaphorin co-receptors. Downstream of receptor activation, signaling pathways activated by semaphorins promote the local disassembly of the cytoskeleton and substrate adhesion contacts, counteracting axon outgrowth and/or inducing repulsive guidance responses [49, 50]. Slits are large secreted glycoproteins identified in the late 90s as axonal repellents and mediators of axon branching. The actions of Slit proteins are primarily intermediated by receptors of the Roundabout (Robo) family, which, like Dcc, are part of the immunoglobulin superfamily. Ephrin ligands are cell surface signaling molecules that function exclusively as short-range guidance ▶

cues, binding Eph receptors and producing bidirectional output signals at points of contact between cells. Class A ephrins are anchored to the cell surface via GPI-linkages, whereas class B ephrins are transmembrane proteins and, as a general rule, interact with EphA and EphB receptors, respectively. Eph receptors constitute the largest family of receptor tyrosine kinases [49, 51]. All the receptors described herein have single-pass transmembrane domains.

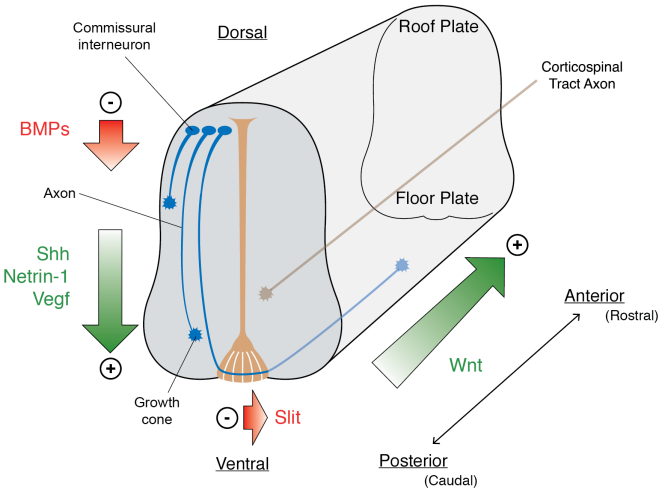

Figure 1.3 – The concerted action of multiple guidance cues upholds fidelity in axon guidance mechanisms. The development of commissural axons in the spinal cord is accurately directed by a combination of repellent (denoted by the red colour and minus sign) and attractive (green and plus sign) factors in the spinal cord to achieve. BMPs - bone morphogenic proteins; Shh - sonic hedgehog; Vegf - vascular endothelial growth factor. See text for details. *Adapted from Fundamental Neuroscience, 3th Edition* [348].

Upon crossing the midline, commissural axons are faced with a rostral-to-caudal decreasing gradient of Wnt molecules in the spinal cord instructing an anterior turn in the direction of the brain. Similarly, caudally projecting corticospinal tract axons are guided by Wnts along the longitudinal axis **(Figure 1.3)**, illustrating another fundamental aspect of guidance mechanisms: different axons may have contrary responses to the same cue[a][52, 53]. In turn, if the intermediate target is understood as attractive, how can axons move onwards to the following segment of the pathway? Ingeniously, axonal growth cones are capable of altering their responsiveness to guidance factors to such an extent that a territory initially sensed as permissive is subsequently perceived as repulsive. In the case of commissural axons, in addition to secreting Netrin-1, the floor plate cells also produce repellents of the Slit family [54, 55] **(Figure 1.3)**. These axons can cross the midline unaffected by the repulsive cue because they are initially insensitive to it. However, upon passing the midline, they become responsive to the Slit gradient due to an increase in the expression and function of its receptors [56] and,

a Although incompletely defined, the divergent responses to Wnt gradients partially reflect the expression of distinct surface receptors.

concomitantly, to a loss of responsiveness to Netrin-1 [57]. Thus, just as important as the mechanisms that accurately guide axons through the pathway, are the coordinate switches from attraction to repulsion that ensure their progression past the intermediate targets.

In addition to *chemical* signals, growth cones are instructed by cell-cell and cell-matrix *physical* adhesions that provide not only an effective roadmap for navigation but also an essential platform for growth cone motility [58]. In the context of growth cone steering, adhesive molecules can be encountered upon contact with neighbouring cells (cell-cell adhesion) or, indirectly, through the binding to components of the surrounding extracellular matrix (cell-matrix adhesion). These contacts can be mediated by members of the integrin, cadherin and, most prominently, immunoglobin (IgG) superfamilies **(Figure 1.4)** [58, 59]. Though much of the initial work on neural connectivity was dedicated to identifying factors that mediate adhesion to substrates, many cell adhesion molecules with neuronal expression were shown to promote surprisingly subtle axon guidance defects upon biochemical or genetic loss-of-function. Nonetheless, experiments with fly *fasII* mutants[a] provided a breakthrough understanding of how the selective expression of adhesion receptors can shape neural connectivity; specifically, despite still projecting in roughly correct trajectories, ultrastructural analysis of *fasII* mutants embryos showed defasciculation phenotypes along the longitudinal tracts where Fasciclin II is selectively expressed [60]. Furthermore, selective cell adhesion events underlie another major feature in the wiring of the nervous system: the stepwise nature of the process [61]. Notably, whereas the very first axons advance when the embryonic brain is still relatively small and 'uncomplicated', most later-born neurons face an expanding and increasingly complex environment. Fittingly, as the brain matures, pioneer tracts can serve as scaffolds for many of the later developing axons for at least some parts of their trajectory [62-64]. Such scheme, in which successive waves of axons extend to their targets along preexisting tracts, much simplifies the elaboration of the complex three-dimensional neuritic web of the brain.

A.2 The Dynamic Growth Cone

A colourful analogy pictures the growth cone on its journey as both 'vehicle' and 'navigator' [58]. And indeed, guidance cues are instructive signaling molecules that modulate whether the growth cone turns, extends or retracts in pursue of a new direction; *id*

[a] *fasII*, encodes for the neural cell adhesion molecule Fasciclin II, which is the fly orthologue of prototypic *NCAM* in vertebrates.

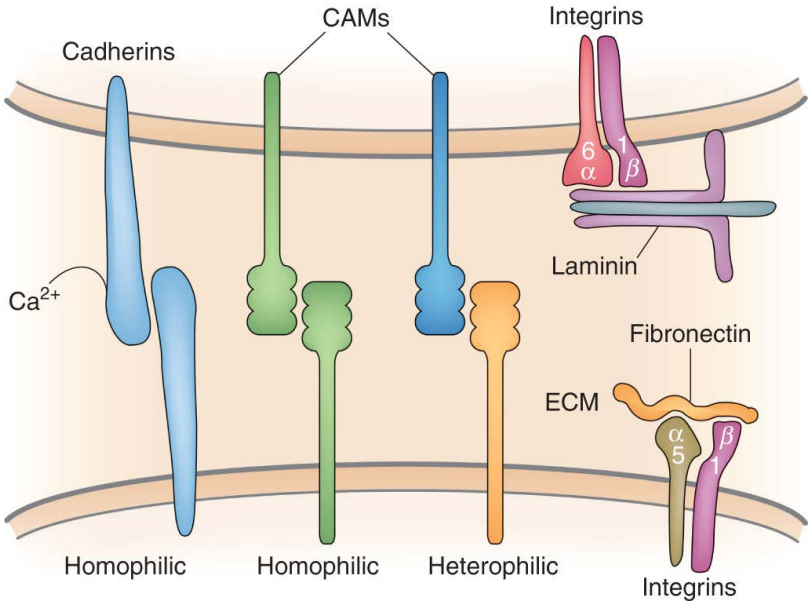

Figure 1.4 – Overview of major cell-cell and cell-matrix adhesive interactions regulating axon guidance. In the process of axon pathfinding, adhesive contacts are primarily mediated by cell adhesion molecules (CAMs), namely cadherins, integrins, and members of the immunoglobulin (Ig) superfamily of cell adhesion molecules (IgCAMs). Cadherins are calcium-binding adhesive molecules that mostly function in homophilic cross-bridges. Differently, integrins participate in cell-matrix, as well as cell-cell interactions (not depicted here). Integrin heterodimers are composed of various combinations of α and β subunits, which generate multiple affinity profiles. The immunoglobulin superfamily is comprised of either transmembrane or GPI-anchored proteins, with extracellular Ig-like domains and fibronectin type III repeats. Some IgCAMs can associate in homophilic contacts, while others interact through heterophilic cross-bridges. Of note, the cytosolic domains of some CAMs can engage with adapter proteins that act as direct or indirect (through downstream signaling cascades) linkers to the cytoskeleton. [65, 66]. *Image sourced from Development of the Nervous System, 3th Edition* [349].

est, guidance signals, one way or another, must impinge on the dynamics of the growth cone motility machinery. Thus, as important as understanding the molecular environment the growth cone navigates, is to know how these spatial cues are integrated and how they shape its responses.

To this end, learning the structure of the growth cone is critical to decipher the nature of its plastic and protrusive behaviours. Although functionally indissociable, the distribution of the actin and microtubule cytoskeletons in the growth cone define two distinct compartments: the *central domain*, enclosing tightly bundled microtubules in addition to various organelles (e.g., mitochondria), and the *peripheral domain*, composed of a dense meshwork of branched actin networks supporting lamellipodia-like veils and long, polarized actin fibrils highlighting several transient filopodia that incessantly scout the environment [58]. At the interface between these two domains lies the *transition zone*, an actomyosin contractile arc that regulates both actin and microtubule cytoskeletons **(Figure 1.5)** [67, 68].

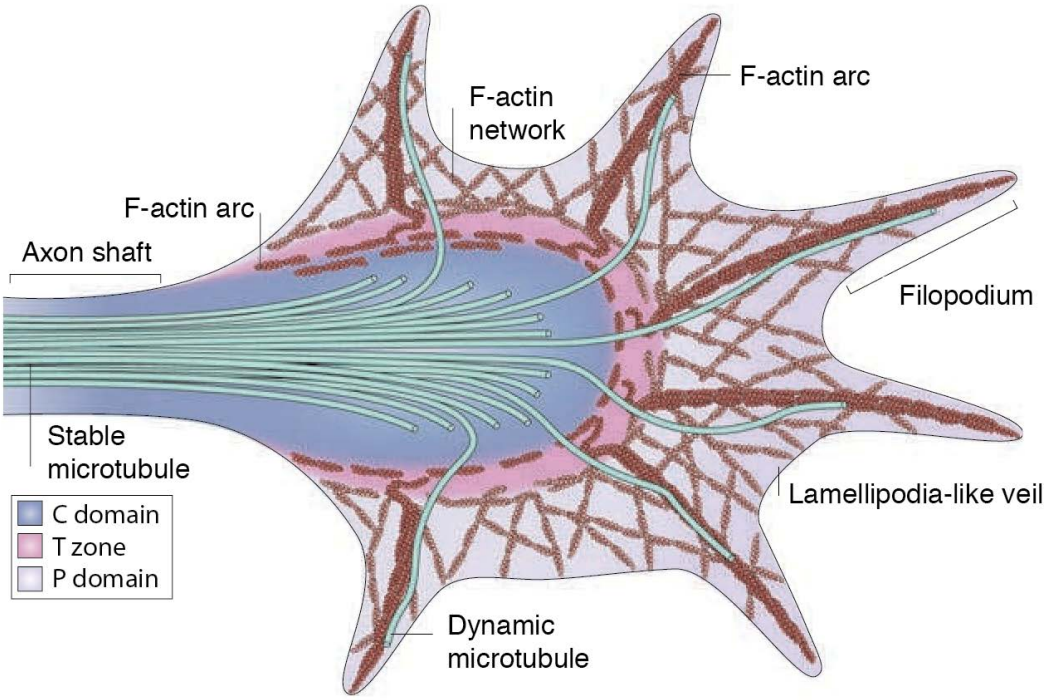

Figure 1.5 – The growth cone 'vehicle'. As Ramón y Cajal famously described it, the growth cone is "(...) endowed with exquisite chemical sensitivity, rapid amoeboid movements, and a certain motive force (...)" [3]. The growth cone is a dynamic structure acted upon by spatial cues in the environment which bias the behaviour of its cytoskeleton machinery. C domain - central domain; T zone - transition zone; P domain - peripheral domain. See text for details. *From Lowery and Van Vactor* (2009) [58].

As with migratory cells, the forward-crawling motion of a growth cone is dependent on its cytoskeleton, and particularly the dynamic properties of actin. The 'actin motor' is propelled by a continuous myosin-based rearward flux of filamentous (F)-actin from the leading edge of the growth towards its central domain (termed 'actin retrograde flow') in combination with F-actin treadmilling, which involves the constant recycling of depolymerized actin monomers from the transition zone to the leading edge, where they re-polymerize. Without productive adhesive contacts, the actin retrograde flow rapidly equalizes polymerization-depolymerization rates and no net contribution to forward movement is made. However, when filopodia encounter an adhesive substrate, a molecular complex that functions as a clutch is formed between the receptors and the actin cytoskeleton that, in essence, tethers the F-actin fibrils and attenuates retrograde flow [58, 69]. Simultaneously, F-actin polymerization at the leading edge continues[a], pushing the peripheral domain forward and, as a result, protrusion of the growth cone occurs.

[a] Or is even stimulated, as the signaling cascades initiated by some guidance cues can lead to the activation of Rho GTPases and downstream effectors that promote actin polymerization.

In parallel, adhesion events selectively shape the dynamics of the microtubule cytoskeleton, particularly, at their onset[a], the population of individual microtubule polymers that actively explore the peripheral domain [70, 71]. Specifically, it has been demonstrated that these highly dynamic microtubules explore filopodia along F-actin bundles and are necessary as scaffolding platforms for the localized accumulation of key signaling components of the navigation machinery at strongly attached filopodia [72, 73]. Hence, a productive attachment of a filopodium onto a permissive substrate or cell induces a localized increase in actin polymerization that is 'encouraged' further by invading microtubules. In this way, filopodia act both as distal guidance sensors and 'points of attachment' to the substrate, continuously searching the molecular environment and generating the required tension for growth cone progression [74].

Spatial bias can also be introduced into the system by guidance cues. Indeed, many chemotropic factors ultimately converge on signaling cascades (e.g. Rho family GTPases) that modulate actin dynamics, and their differential activation across the growth cone compartment can lead to localized changes in the rate of actin polymerization or depolymerization [75, 76]. Graded distributions of 'positive', attractive cues can invoke an asymmetric increase in actin polymerization rates that promotes protrusion preferentially in the direction of the attractive gradient; conversely, repulsive signals decrease polymerization or increase catastrophe events on the nearside, favoring protrusion away from the 'source' [58]. Some guidance cues have also been shown to regulate microtubule dynamics, particularly by modulating the activity of proteins associated with the plus-end of microtubules [59, 77, 78].

A.3 Asymmetric Endocytosis and Exocytosis in the Growth Cone

Though distal membrane stores were identified four decades ago [79, 80], only recently has regulated plasma membrane trafficking at the tip of developing axons emerged as a major contributing aspect to chemotropic growth cone decisions alongside the cooperative interaction between cytoskeleton and adhesion machineries [81-84]. Nonetheless, it is now increasingly evident that asymmetric membrane trafficking across the growth cone plasma membrane – in the form of endocytosis and exocytosis – arises at the onset of guidance cue responses.

Kamiguchi and colleagues provided the first demonstration that polarized vesicle dynamics mediates chemotactic responses in growth cones, by showing that a

---

a In a later phase of the steering mechanism, bundled microtubules in the central domain extend into the area of new growth and effectively commit the growth cone as a whole in a new direction.

gradient of chemoattractants stimulates the centrifugal transport of vesicle-associated membrane protein 2 (Vamp2)-positive exocytic vesicles along microtubules towards the gradient side of the growth cone. It was also shown that this type of exocytosis operates exclusively in attractive turning responses and does not mediate axon outgrowth [81]. Conversely, the same group later reported that a repulsive chemotactic gradient promotes the asymmetric removal of growth cone plasma membrane on the side facing the stimulus via clathrin-mediated endocytosis, and that this event is required and sufficient for repulsive turning [82]. Taken together, these findings support the notion that a polarized disturbance of membrane trafficking across the growth cone is sufficient to promote a directional turning response towards the side undergoing more exocytosis or, alternatively, less endocytosis [85].

Given that differential membrane trafficking temporally precedes any detectable cytoskeletal rearrangements, it appears likely that membrane remodeling imparts a decisive contribution to initiate turning responses [59, 85], although, to the best of my knowledge, only two studies have addressed this issue directly in the context of asymmetric stimulation [83, 84], [a][86, 87]. Most notably, Hines et al. demonstrated that a repulsive myelin-associated glycoprotein (Mag) gradient provokes a polarized clathrin-mediated endocytic response and, concurrently, a localized remodeling of cell adhesion components, including the loss of β_1-integrin receptors on the side of the growth cone experiencing the negative stimulus [83]. Thus, asymmetric membrane trafficking can allow the growth cone to rapidly adjust its adhesiveness across its axis – an essential step to commence a chemotactic turning response, as I have described above.

A.4 The Optic Pathway

The optic pathway **(Figure 1.6)**, comprised of the axons of retinal ganglion cells – the sole output neurons of the retina – joins the retina to the optic tectum/superior colliculus, and has served as a particular suitable model to study the mechanisms of axon guidance, for it entails diverse molecular environments through which retinal growth cones must precisely navigate [b][3, 34, 88-91].

---

a Outside the 'asymmetric' paradigm, it is well established the involvement of the endocytic and exocytic pathways in the modulation of signaling nodes in the growth cone. For example, endocytosis of Dcc and Neuropilin 1 receptors upon collapse-inducing Netrin 1 and Semaphorin 3A stimulation, selectively adjusts their surface availability and desensitizes the growth cone transiently to its environment.

b In particular, the *Xenopus laevis* retinotectal tract offers a number of attractive reasons for its continued utilization in studies addressing the mechanisms of axon guidance. First, *X. laevis* embryos develop externally and can be obtained throughout the year by *in vitro* fertilization. They require minimal daily care to maintain and grow rapidly, allowing the researcher to run successive experiments in a matter of days. Protocols for culturing *X. laevis* eye explants are well established and retinal neurons develop *in vitro* at ▶

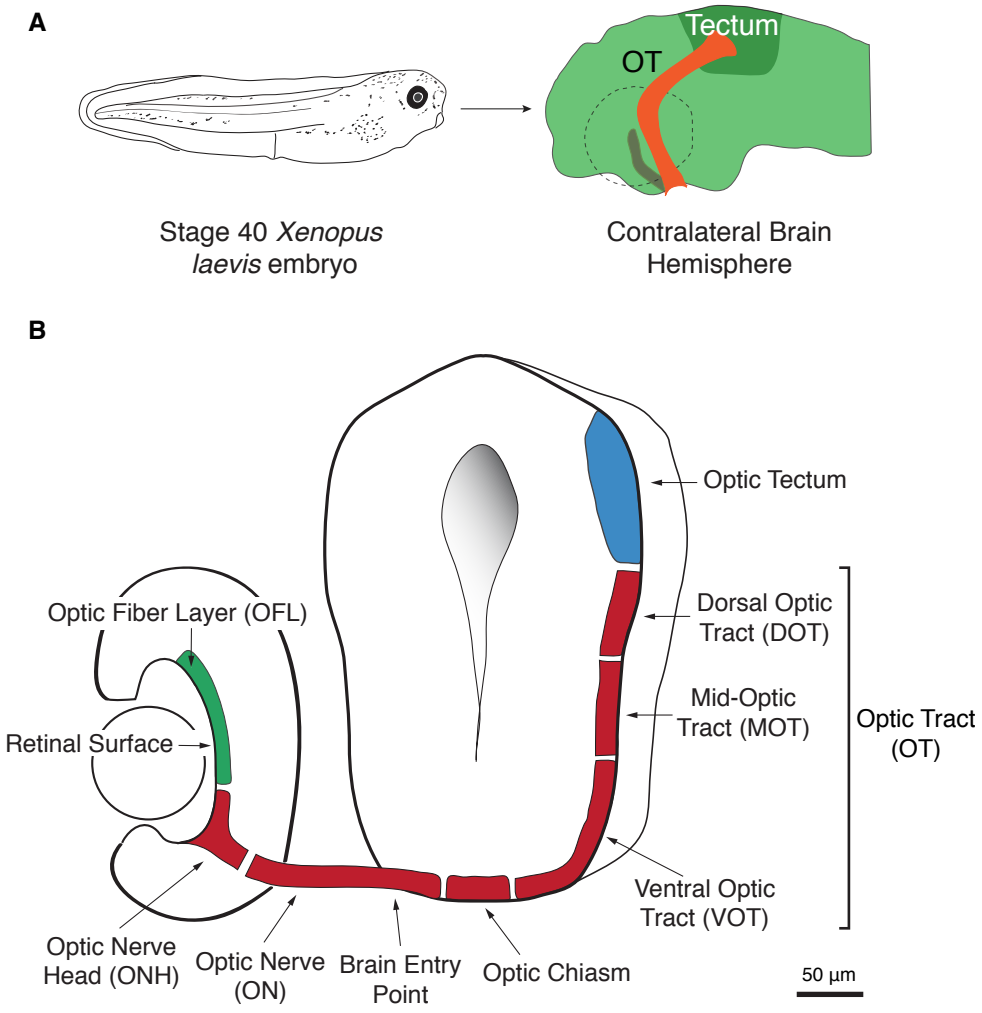

Figure 1.6 – Diagram of the embryonic *Xenopus laevis* retinotectal pathway. Lateral (A) and transverse (B) views of the optic pathway. Inside the neural retina, retinal ganglion cell axons extend radially along the retinal surface towards the optic nerve head/optic disk, where they collect to exit the eye and form the optic nerve. Once past the midline optic chiasm in the ventral diencephalon, retinal ganglion cell axons turn dorsally. Subsequently, in the mid-optic tract, retinal ganglion cell axons turn caudally to reach the optic tectum (pioneer axons complete their stereotypic journey as early as stage 37/38). For anatomical clarity, the retinotectal projection in (B) is divided into nine discrete regions. The doted circumference in (A) denotes the opposite retina (in respect to the viewpoint of the illustration), from where the depicted axon projection originates. OT- optic tract; scale bar: 50 µm. *The illustration in (B) was redrawn from Holt* (1989) [92].

room temperature without requiring growth factors, thus permitting the functional exploration of individual guidance cues without extra factors in the culture media. Plus, a myriad of techniques are available to the experimenter to effectively manipulate gene expression in a targeted fashion and follow live growing axons *in vivo*, making the *X. laevis* visual system a stellar, all-round model to study axon guidance.

The journey of retinal ganglion cell axons starts in the retina, extending radially along the optic fiber layer (OFL) before converging at the optic disc and extending through the optic nerve head (ONH) to exit the eye. Upon completing differentiation, extracellular matrix (ECM) components of the basal lamina provide the necessary stimuli to polarize the emergence of retinal ganglion cell axons on the basal pole of their cell bodies [93]. Subsequently, as retinal ganglion cell axons extend towards the optic disc, their growth is confined to the optic fiber layer in the inner surface of the retina. This is achieved by the actions of negative signals inhibiting awry navigation into the outer layers of the retina and the embryonic lens, acting in concert with attractive cues promoting growth centrally [94-96]; in particular, a high central–low peripheral wave of the morphogen Sonic Hedgehog is involved in regulating the directed growth of retinal ganglion cell axons towards the optic disc [97], whereas repulsive gradients of Slit2 and the proteoglycan chondroitin sulfate (Cspg) are present at higher levels peripherally [98, 99]. Next, the growth cones of retinal axons are guided into the optic nerve head by Netrin-1 [100], which here functions 'locally', unlike its *modus operandi* in the spinal cord, where it acts as a long-range diffusible cue to guide commissural axons towards the ventral midline [101].

After exiting the eye, the optic nerve steers through the embryonic optic stalk and enter the brain at the optic chiasm in the ventral diencephalon, where retinal ganglion cell axons either cross the midline and extend to the contralateral hemisphere or, alternatively, remain ipsilateral. In *Xenopus* tadpoles, all retinal ganglion cell axons grow contralaterally at the optic chiasm before metamorphosis [102][a]. As retinal growth cones approach the chiasm, Slits and Sonic Hedgehog, which are expressed in the ventral-most diencephalic region, function as inhibitory cues to retinal ganglion cell axons, effectively establishing the coordinates of the optic chiasm in the midline neuroaxis [95]. At the chiasm, Sonic Hedgehog works as an inhibitor of retinal ganglion cell axon extension, in opposition to its attractive role inside the retina. In fact, it has been shown *in vitro* that Sonic Hedgehog elicits contrary responses in retinal ganglion cell growth cones depending on the concentration used in the assay [97]. Hence, different levels of Sonic Hedgehog expression in the retina and chiasm may partly explain the

[a] *Xenopus laevis* tadpoles – *id est*, pre-metamorphic animals – were used throughout the laboratory research I conducted.

differential behaviors exhibited by retinal ganglion cell axons in respect to the same cue [95], as has been demonstrated in other instances [103, 104]. Once at the chiasm, distinct subpopulations of retinal ganglion cell axons respond oppositely to Ephrin-Bs expressed by radial glia, as initial studies in *Xenopus* indicated [102]. The mechanism was later elucidated in mouse: Ephrin-B2-mediated repulsion is determined by the expression of EphB1 protein in the growth cone of ipsilaterally projecting retinal ganglion cells emerging from the temporoventral crescent. Conversely, contralaterally projecting axons emanating from the dorsal and ventral regions of the retina do not express EphB1, and are therefore insusceptible to the repulsive influence of Ephrin-B2 [105].

Once in the optic tract, retinal axons are restrained to a path adjacent to the telencephalon as they extend dorsally through the diencephalon. Initial axon progression from the optic chiasm is dependent on Growth associated protein (Gap)-43 function to overcome the inhibitory regional environment [106, 107]. Similarly to other discrete segments of the optic pathway, retinal ganglion cell growth cones are guided within the optic tract by inhibitory Cspg and Slit cues, which prevent aberrant intrusions into the telencephalon and inappropriate domains of the diencephalon [108-112]. As for a molecular mechanism, initial biochemical studies in *Xenopus* found evidence implicating N-cadherin in the ordered formation of the optic tract [113], which was followed a few years later by the demonstration that N-cadherin-mediated cell adhesion is inactivated downstream of repulsive Slit signals [114]. Furthermore, Slit 2 has been shown to promote the rapid, protein-synthesis dependent upregulation of the actin-depolymerizing protein Cofilin in retinal growth cones, suggesting also a role for local translation in the path-restraining effects operated by Slits [115]. Subsequently, repellent Semaphorin 3A and Slit signals at the mid-optic tract impose a caudal turn in the direction of the optic tectum, and effectively demarcate the last section of optic tract [22, 116]. In specific, the Holt laboratory has shown recently that NF-protocadherin local synthesis evoked by Semaphorin 3A in retinal growth cones facilitates the accurate navigation at the mid-optic tract caudal turn, which suggests that an effective cross-talk exists between the two signaling systems and help to shape the formation of the optic pathway [22].

As they near the target area, retinal ganglion cell axons begin to defasciculate from the compact bundle of the optic tract. Finally, in addition to the signals discussed in the next section, entry into the target region is partly defined by the transition from an environment highly rich in fibroblast growth factor, the optic tract, which promotes axonal growth, to a territory where very little of it is present, the optic tectum [117].

A.5 Axon Guidance at the Optic Tectum

From the optic tract, retinal ganglion cell axons enter the optic tectum/superior colliculus anteriorly; here, retinal axons significantly slow down as they extend along the anterior-posterior axis of the optic tectum/superior colliculus, and their growth cones become more complex and eventually begin to branch [3, 118]. However, important interspecies differences arise at this stage: the initial development of retinotectal topography in frog and fish is a much more precise process than in chicks or rodents, the other two major vertebrate models that have been utilized to study such mechanisms. Indeed, in the former duo, retinal ganglion cell axons extend to, or just about to, a defined territory within the tectum and afterwards arborize from the back of the growth cone; differently, in mouse and chick, axons initially grow well past their specific targets, instead establishing contacts through interstitial branches formed along the axon shaft at the anterior-posterior location of their correct termination zone [119].

As I have briefly introduced before, the retinotectal projection, like other sensory systems of the body, is organized topographically; that is, retinal ganglion cells with neighboring points of origin within the retina maintain neighboring relationships in the target field. Ultimately, it is this correct neuroanatomical representation that allows us to perceive the visual space as a contiguous, coherent whole. In lower vertebrates, the temporo-nasal axis of the retina is represented along the anterior-posterior axis of the optic tectum, whereas the ventro-dorsal retinal axis maps along the dorso-ventral axis [102]. A similar arrangement is observed in mammals: the temporo-nasal retina projects along the anterior-posterior axis of the superior colliculus, and ventro-dorsal regions along its lateral-medial axis. Consequently, the two-dimensional map of the visual world on the optic tectum/superior colliculus is effectively maintained, albeit inverted, in respect to that on the retina. As Sperry deduced from his experiments, each point in the optic tectum/superior colliculus seems to have a unique molecular ‘post code’ defined by gradients of topographic guidance molecules orthogonally distributed; in turn, these ‘molecular coordinates’ are matched by unique profiles of guidance receptors on the surface of each retinal ganglion cell axon. Hence, both innervating neurons

and their targets are chemically specified in a complementary fashion to promote appropriate synaptic contacts [119].

Though the exact complement of ligands and receptors may differ between species, the extent of anterior-posterior mapping is largely determined by repulsive interactions between Ephrin-A ligands expressed on the optic tectum/superior colliculus and EphA-expressing retinal axons. In particular, quantitative differences, rather than qualitative, account for the astonishing fidelity of the system: EphAs have a graded high-temporal to low-nasal expression pattern in the retina, matched by a overall low-to-high complementary gradient of Ephrin-As distributed along the anterior-posterior axis of the optic tectum/superior colliculus[a]. Simply put, temporal axons are repulsed by relative lower concentrations of Ephrin-As because they express higher EphAs levels. Consequently, their progression is halted along the anterior-posterior axis at 'more anterior' positions, and how much so is determined by the actual amount of EphAs each individual growth cone expresses. On the other hand, nasal retinal ganglion cell axons, which express lower levels of EphAs, solely become repulsed by relative higher – therefore more posterior – concentrations of Ephrin-As [119, 120].

Mechanisms contributing to topographic mapping along the optic tectum/superior colliculus dorso-ventral/lateral-medial axis are more incompletely defined. Effectively, dorso-ventral/lateral-medial order begins to be established within the optic tract itself as retinal ganglion cell axons defasciculate, a process known as *pre-target sorting* [121, 122]. Then, similarly to anterior-posterior topographic mechanisms, graded distributions of EphB/Ephrin-B help to further refine dorso-ventral/lateral-medial mapping in the optic tectum/superior colliculus. Specificically, both EphBs and Ephrin-Bs are expressed in the retina, albeit in opposite gradients: Ephrin-Bs have a high dorsal to low ventral expression pattern, while EphBs have an overall low-to-high distribution along the dorso-ventral retinal axis. Although *in vivo* loss- and gain-of-function studies clearly support the notion that EphB/Ephrin-B signaling is important for dorso-ventral/lateral-medial mapping [123, 124], neither EphBs nor Ephrin-Bs are expressed as a discernible dorso-ventral/lateral-medial gradient in the tectum/superior colliculus, impairing definite conclusions about their mode of action [119, 120]. Nonetheless, as with the nasotemporal representation, other molecules have been shown to participate in dorso-ventral/lateral-medial topographic decisions, including Wnts, which have a graded expression pattern in the chick optic tectum and mouse superior colliculus [119,

a Note that Eph/Ephrin dyads are bidirectional cell surface signaling molecules and, by their very nature, do not function as long-range diffusible guidance molecules, but as contact-dependent signals.

120]. Therefore, like elsewhere in the nervous system, multiple cues acting in concert are necessary to establish a truly accurate neuroanatomical representation of the visual world.

A.6 Mitochondria, Axon Maintenance and Survival

Since, as a general rule, neuronal cells cannot be replaced throughout the individual's lifetime [125], the upkeep of functional neural circuits must necessarily rely on effective axonal protective mechanisms. Classical conjectures supported the view that the process of axonal degeneration ensued from deficient sustenance from the cell body (e.g. as a result of cell body death) [126]. However, it is now well established that the axonal degenerative cascade can be actively promoted by *in situ* death pathways, and, similarly, is counteracted by locally acting and, to some extent, axon-specific pro-survival mechanisms [126]. Moreover, adequate metabolic provision – and hence mitochondria, where much of the interplay between pro-degenerative and protective factors occurs [126, 127] – is pivotal to axon integrity and function, as the demand for energy, metabolites and calcium buffering is particularly elevated at axons terminals (e.g. to support synaptic transmission) [128]. Indeed, many mitochondrial dysfunctions trigger neurodegenerative disorders with prominent axonal phenotypes[a][129-131], suggesting that axons are particularly vulnerable to mitochondrial compromise. A growing axon is all the more dependent on adequate mitochondrial operation, as it requires the continuous provision of energy for its expansion in the developing brain. It follows that neurons, with their elongated and complex morphologies, must tightly operate, as well as preserve, a damage-prone mitochondrial network to maintain functionality and integrity.

During the development of the nervous system, the refinement of neural circuits results from the selective preservation and elimination of axons: target areas are initially innervated by an exuberant number of processes, which is followed by the pruning of inapt connections and maintenance of the valid ones [126]. The original postulate of the "neurotrophic hypothesis" explained this phenomenon on the basis of target field-derived signals and their limited availability [132]. It is now known that, in addition to neurotrophic growth factors, neuronal activity also potentiates the maintenance of functional connections partly through its promotion of mitochondria-acting

a The integral role of mitochondria in axonal physiology is truly appreciated when one considers the substantial list of neurodegenerative diseases associated with mitochondrial defects including Alzheimer's, Parkinson's and Huntington's disease, but also retinal ganglion cell-specific pathologies, such as dominant optic atrophy and Leber's hereditary optic neuropathy.

axon survival pathways [126]. Of particular note, the axon survival-promoting effects triggered by neurotrophin stimulation is abolished when axonal protein synthesis is inhibited, suggesting that, at least to some extent, this neuroprotective signaling mode relies on locally synthesized factors to bring about its neuroprotective effects [133]. *Id est*, the preservation of neural circuits depends on a finely tuned network of axon-localized protective factors [11, 126, 133].

B – Axonal mRNA Localization and Local Protein Synthesis

The synapse underlies one the neuron's most striking features: the axon-dendrite duality, with the inherent cellular and molecular polarization of the nerve cell it encompasses [134]. Necessarily asymmetric in function, these two compartments receive an independent assortment of organelles, membrane components and molecules from the cell body [135]. Subcellular RNA localization has emerged as a particularly prevalent and cost-efficient mechanism of outsourcing genomic information in these highly polarized cells, where the site of transcription can be far removed from the final destination of the protein [2, 136]. Specific transcripts can be precisely localized to subcellular compartments using the 'address' information harboured in their untranslated regions (UTRs), which function as *cis*-acting platforms for regulatory RNA-binding proteins (RBPs) and small non-coding RNAs [136, 137]. Subsequently, local, 'on-site' synthesis confers both spatial and temporal precision, as the new protein is present only where and when a biological demand for it exists [138]. It is this mRNA-based mechanism that, for example, allows the growth cone to enjoy a certain degree of functional autonomy in its guidance process [2]. Still, it was not until the recent appreciation of the complexity of the axonal transcriptome – several independent genome-wide screens have identified thousands of mRNAs localizing in the axonal compartment of embryonic and adult neuronal cells [11-15] – that the functional significance of this cellular mechanism was really fully grasped. It is thus not surprising that deregulated RNA localization and translation are at the core of many neurodevelopment and neurodegenerative diseases [139-142].

B.1 Regulation of Axonal mRNA Translation

Protein synthesis inhibition in severed axons can hinder the ability of the growth cone to respond *in vitro* to a plethora of extrinsic – attractive or repulsive – guidance factors [2]. These guidance signals promote rapid alterations of the local proteome by modulating the activation of the mechanistic target of rapamycin (mTOR) pathway, which, as a master regulator of mRNA translation, acts as a global rheostat to the process of protein

synthesis [2], [a][143], [b][144, 145].

However, whereas attractive cues like Netrin-1 or brain-derived neurotrophic factor (Bdnf) induce β-actin synthesis to build up the growth cone cytoskeleton [4, 5], repellent factors such as Slit 2b and Semaphorin 3A elicit *de novo* synthesis of proteins that promote cytoskeletal disassembly (e.g. RhoA and Cofilin) [6, 115], implying that different protein synthesis-inducing signals regulate the translation of distinct groups of transcripts. But since the mTOR pathway controls the translational output at a global level, how does one account for such fine regulation of the growth cone proteome?

The main strategy utilized to achieve translational specificity is centred on *trans*-acting factors – such as RNA-binding proteins and microRNAs (miRNAs) – which associate with specific mRNAs to regulate their axonal transport, stability and translation [137]. For example, the zipcode-binding protein 1 (Zbp1), a well-characterized RNA-binding protein, has affinity for a conserved 54-nucleotide long motif – termed the *zipcode* – located in the 3'UTR of the *actb* (β-actin) mRNA; on encountering Bdnf, a signaling cascade is triggered within the growth cone compartment resulting in Src-dependent phosphorylation of Zbp and translational derepression of *actb* mRNA [146, 147]. Drawing on these and other reports [2], current models speculate that different *trans*-acting factors, each associating with a unique cohort of mRNAs, are independently regulated by distinct guidance cues, thus allowing for the translation of specific sets of transcripts [148] **(Figure 1.7)**.

B.2 Scope of the Axonal Transcriptome

The prevailing view at the turn of the century was that axons did not synthesize proteins [2, 149]. This notion has since been overwhelmingly dismissed, as evidence linking local mRNA translation to many aspects of axonal biology accumulated. It is now known that axonal mRNA translation regulates not only growth cone guidance decisions [5-7, 22, 144], where its involvement was originally studied, but also axon elongation [150, 151],

---

[a] mTORC1 exerts its actions through the phosphorylation of ribosomal protein S6 kinase 1 (p70S6K1/2) and eukaryotic translation initiation factor 4E binding protein 1 (eIF4E-BP1), which associate with mRNAs and control translation initiation and the overall progression of the translation mechanism.

[b] The ubiquitin proteasome system (UPS) also plays a central role in regulating the axonal proteome in response to some guidance signals. For example, the chemotropic response elicited by Netrin-1 results from the coordinate regulation of the local proteome by protein synthesis and degradation mechanisms.

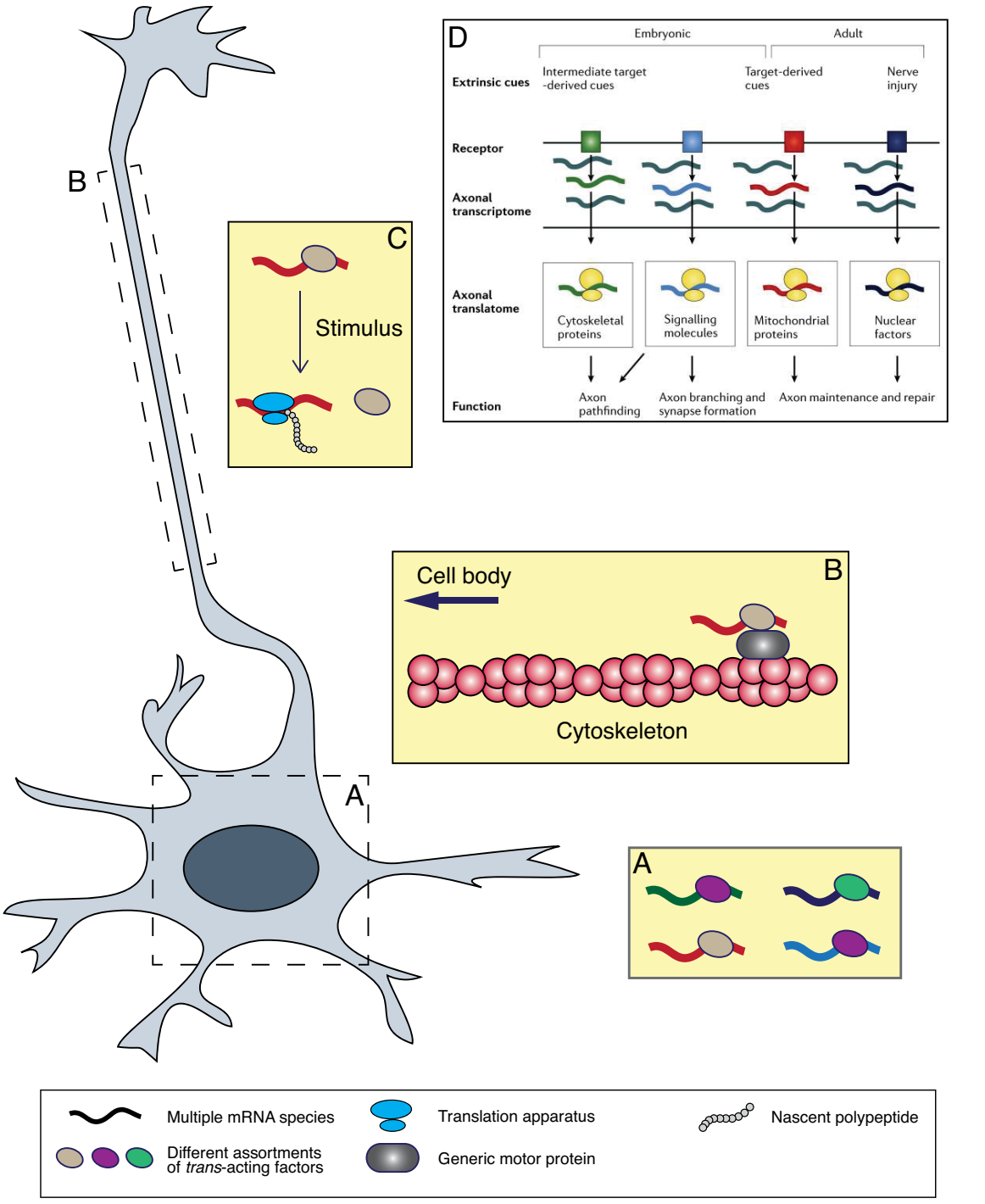

Figure 1.7 – Axonal mRNA localization and local protein synthesis: an overview. (A) Subcellular targeting of specific mRNAs depends on the recognition of 'localization-coding' *cis*-acting elements by nuclear and cytoplasmic *trans*-acting factors (TAFs), which collectively associate as part of higher-order messenger ribonucleoprotein (mRNP) complexes [130]. Most of the *cis*-acting axon-targeting elements that have been identified are situated in the 3'UTR of the mRNA, and are ▶

◀ 'decoded' by various TAFs operating synchronously [129, 130]. Commonly, distally targeted messages have longer 3'UTRs than their soma-localizing counterparts, and unique 'address' information is present in these additional segments [11]. 3'UTR diversity mainly arises from differential 3'-end processing mechanisms such as alternative polyadenylation [262]. Some mRNAs are known to share similar *cis*-acting motifs and to be regulated by a common set of TAFs, a property that allows functionally related cohorts of transcripts to be conjointly translated with temporal and spatial precision [2, 130]. (B) Upon recruiting additional adapter proteins (not depicted), mRNPs are 'shipped' along cytoskeletal tracts by motor-based active transport mechanisms towards their subcellular destination in the axonal compartment. Notably, mRNAs are maintained in a translationally dormant state during the assembly and transport phases [2, 130]. (C and D) By modulating the activation of mTOR signaling and, in parallel, eliciting changes in the binding affinity of specific TAFs, various local stimuli, including guidance cues, can bring about concerted alterations in gene expression programs [2, 130]. *Panel 'D' taken from Jung, Yoon, and Holt* (2012) [2].

synapse formation [2], axon maintenance [9, 11, 152], and nerve injury and axon regeneration responses [153-156], among other processes [2].

Significantly, the diversity of neurobiological functions associated with local protein synthesis underlines another crucial aspect of axonal RNA localization: the dynamic nature of the local transcriptome. Indeed, even within the same population, comparative profiling of two different developmental stages has revealed that axons contain 'age'-specific mRNA pools. For example, mRNAs encoding for branching-promoting cytoskeletal proteins and synaptic vesicle proteins, which intuition suggests to be irrelevant during the pathfinding stages, are only found enriched in the transcriptome of target-arrived axons [2, 12].

Nevertheless, it is noteworthy that all the axonal populations analysed to date appear to have a common core of transcripts, such as those encoding for mitochondrial proteins, ribosomal proteins and other factors involved in the protein synthesis process, components of the cytoskeleton, as well as proteins related to signal transduction [2], suggesting their encoded proteins are implicated in the maintenance of constitutive axonal functions. Moreover, several of these independent genome-wide screens have also found cancer-linked transcripts to be well represented in axonal mRNA populations [11-13], denoting potential shared mechanisms in developmental processes and cancer pathogenesis. Accordingly, the *tpt1*[a] transcript, which encodes for translationally controlled tumor protein (Tctp), is ranked among the most enriched in the axonal compartment across diverse embryonic and adult neuronal populations[b][11, 13, 14], including

a Gene name: *tumor protein, translationally-controlled 1*.

b In the study performed by Gumy et al., which used rat embryonic sensory neurons, *tpt1* mRNA ranks as the 31th most enriched in the axonal compartment [13]; in Taylor et al. analysis, using rat naïve cortical axons aged to maturity in culture, *tpt1* mRNA appears in the 11th position [14]; in the sequential analysis of gene expression (SAGE) screen conducted by Antonella Riccio's group in rat perinatal sympathetic neurons, the *tpt1* transcript placed as the 5th most abundant message [11].

Xenopus laevis retinal ganglion cells [12], raising the possibility of an important, and still entirely unexplored, subcellular function.

C – The Translationally Controlled Tumor Protein

Tctp is a small, multifunctional, evolutionarily conserved protein implicated in cell growth [18, 19] and tumorigenesis [23-25, 157]. Initially discovered in 1982 as an abundant mRNA in untranslated, partially suppressed messenger ribonucleoprotein (mRNP) complexes in mouse sarcoma ascites cells [158], it was further characterized as a protein whose rate of synthesis is greatly enhanced in growing versus non-growing Ehrlich ascites tumour cells [159, 160]. Tctp has been identified in a multitude of tissues [24, 161] and is involved in cellular functions as diverse as DNA damage and allergy responses (incidentally, it is also known as Histamine-releasing factor[a]) [162, 163]. As its high degree of sequence conservation suggests, Tctp plays an essential, but still not fully realized, role in development, as loss of *tpt1* expression in mice results in embryonic lethality [17, 164].

C.1 Gene and mRNA Structure

The human *tpt1* gene is arranged in six exons intercalated by five introns, in addition to a relatively well-characterized upstream promoter region. Exon 1 spans the entire 5'UTR and the first 9 codons of the coding sequence, and exon 6 encompasses in its entirety the 3'UTR of the mRNAs. To the best of my knowledge, an identical exon/intron organization is present in higher vertebrates and mammals. Likewise, in *Xenopus laevis*, the *tpt1* gene structure follows the same arrangement [165].

The human *tpt1* promoter contains two highly conserved cAMP response element (CRE) sites, suggesting that *tpt1* is under transcriptional control by cAMP signaling [166]. Moreover, Amson et al. and Chen et al. have both identified a P53-responsive element in the promoter region of *tpt1*, albeit with ambiguous downstream outcomes. Indeed, Amson et al. reported that P53 represses *tpt1* expression [24], whereas Chen et al. described it as an inducer of *tpt1* transcription [167]. Significantly, mammalian genomes retain a large number (up to 15 in humans) of processed *tpt1* pseudogenes [161, 168]. I stress these findings because of emerging evidence implicating pseudogenes and other non-coding RNAs as competing endogenous RNAs (ceRNAs) during develop-

a Other aliases include 'Fortilin', 'P23' in *Homo sapiens* and 'P21' in *Mus musculus*.

ment and disease [169]. In this regard, transcribed *tpt1* pseudogenes could potentially modulate the availability of miRNAs that regulate *tpt1* mRNA translation and thus greatly shape its biological functions.

In humans and rabbits, the *tpt1* gene is transcribed into two virtually identical mRNAs, except for the length of their 3'UTRs. In *Homo sapiens*, the *tpt1* mRNA isoforms are 843 and 1163 nucleotide long, and arise from the differential usage of two alternative polyadenylation signals [168]. In the same study, Thiele et al. went on to characterize qualitatively and quantitatively the distribution of both transcripts in a number of human tissues, including various regions of the brain. Although ubiquitously distributed, it was found that the expression of *tpt1* mRNA variants differs considerably in quantity and proportion between tissues (and also in the different brain regions analysed), leading the authors to conclude that the *tpt1* gene is under extensive transcriptional regulation [168]. However, the biological significance behind the existence of the two *tpt1* mRNA isoforms has remained unaddressed.

Of particular note, the 5'UTR of *tpt1* transcripts starts with a canonical 5'-terminal oligopyrimidine (TOP) motif, a typical feature of transcripts selectively regulated at the translational level by mTORC1 [161, 170],[a][171, 172]. Lastly, due to its complex secondary structure, the translation of *tpt1* mRNA is suggested to be negatively regulated by the double-stranded RNA-dependent (dsRNA) protein kinase R (Pkr) under serum starvation conditions [173].

C.2 Protein Structure

Not only has Tctp remained highly conserved throughout evolutionary history, but its primary sequence also lacks significant homology with any other known protein [16]. Brioudes et al. provide possibly the best evidence in support of its conservation: *Drosophila melanogaster* Tctp can fully rescue *Arabidopsis thaliana* Tctp knockouts, and vice versa [174]. It is a relatively small, hydrophilic protein, composed of 172 amino acid residues[b] and with a predicted molecular weight of approximately 19.5 kDa. Fur-

---

a This *cis*-regulatory motif is found in a subset of mRNAs regulated by mTORC1 that shifts to the translationally active polysome fraction when resting cells are induced to grow or proliferate. Invariably, it consists of a cytosine residue at the cap site, followed by an uninterrupted run of 4-15 pyrimidines. Except for the initial cytosine, the sequence of the TOP motif varies significantly between different mRNAs of this class, even within the same species. The TOP motif has been traditionally described in mRNAs encoding for ribosomal proteins and other proteins associated with the translational apparatus.

b Tctp is a 172-amino acid protein in *Homo sapiens*, *Pan troglodytes, Rattus norvegicus*, *Mus musculus*, *Oryctolagus cuniculus* (rabbit), *Gallus gallus*, *Drosophila melanogaster*, and *Xenopus laevis*; ▶

thermore, no known organelle localization signal exists in its sequence [a][175].

Tctp tertiary structure comprises three α-helices (H1, H2 and H3; the two long α-helices, H2 and H3, form a α-helical hairpin) and nine β-strands organized in two distorted β-sheets. The packing of structural elements gives rise to two hydrophobic cores within Tctp. Also of note, the portion of the protein encompassing residues 39-66 is presumed disordered [b][16, 17] **(Figure 1.8)**.

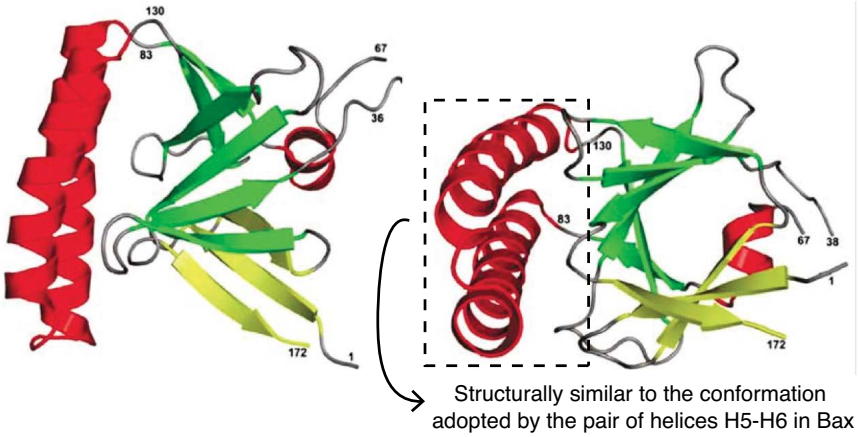

Figure 1.8 – The three-dimensional structure of Tctp. The crystal structure of *Homo sapiens* Tctp, shown here in two different orientations, contains three α-helices (H1, H2 and H3; coloured in red) and two distorted β-sheets (green and yellow). The desorded portion of the protein (residues 39-66) is not shown because of it not being visible in the electron density map. Although no relevant amino acid homology exists, the α-helical hairpin formed by helices H2 and H3 (boxed structural unit) has been observed to possess similitudes with the H5-H6 helices of Bax [17]. *Adapted from Susini et al.* (2008) [17].

Initial structural analysis revealed similarities between the core Tctp fold and the mammalian suppressor of yeast Sec4 (Mss4) [16], which is suggested to function as a chaperone [176, 177], and methionine sulfoxide reductase gene B (MsrB) [178], a repair enzyme for proteins inactivated by methionine residue oxidation [179]. However, the biological significance of these findings is still elusive. More recently, the α--helical hairpin formed by helices H2 and H3 of human Tctp as been noted to share structural resemblances with the H5-H6 helices of Bax, a pro-apoptotic member of the Bcl-2 family of proteins **(Figure 1.8)**. As detailed in a subsequent section, this study

◀ in *Danio rerio*, 171 amino acids; in *Arabidopsis thaliana* and *Schizosaccharomyces pombe*, 168 amino acids.

a Curiously, although it also lacks any known secretion signal in its primary sequence, Tctp can be secreted by cells.

b The three-dimensional structure of *Schizosaccharomyces pombe* Tctp was solved first by heteronuclear NMR spectroscopy; later, the crystal structure of human Tctp was solved at 2.0 Å resolution. Attesting the conservation of this protein throughout phylogeny, both groups reported the same 'signature' motifs, which I briefly describe here.

went on to demonstrate that Tctp antagonizes Bax pro-apoptotic function by inhibiting its dimerization in the mitochondrial outer membrane (MOM) [17].

C.3 Biological Functions

Despite enjoying increasing attention from many areas in the field of Biology, which has translated in its association with a variety of physiological and pathological processes, a clear and unified understanding regarding Tctp is yet to emerge. Still, the near-ubiquitous expression profile of Tctp, in combination with the fact that this protein has remained highly conserved throughout phylogenetic evolution, suggests that Tctp holds an important cellular role. A comprehensive systematization attempt would perhaps include Tctp in three main functional categories: cell growth, cell survival, and immunity.

C.3.1 Cell Growth

Tctp expression has been intimately linked to growth across phylogeny and in multiple contexts [18, 19, 174, 180, 181]. The first *in vivo* clue linking Tctp to growth came from a large-scale screen in *Caenorhabditis elegans* that used RNA interference to target approximately 86% of the worm's predicted genes, establishing that Tctp depletion elicited a slow-growth phenotype [18]. Later, in *Drosophila melanogaster*, Tctp knockdowns were shown to have reduced cell size, cell number and organ size. The authors of this study went on to demonstrate that Tctp displays guanine nucleotide exchange activity towards the Ras homolog enriched in brain (Rheb) GTPase, thus identifying Tctp as a positive modulator of mTOR [19], a master kinase behind cell growth [143], [a][182]. Similarly, *tpt1*$^{-/-}$ mouse embryos – which die *in utero* between E6.5 and E9.5 – show overall growth defects and a reduction in the number of cells populating the epibast [17, 164]. Curiously, overexpression of Tctp also elicits a slow-growth phenotype in mammalian cells [183], indicating that a tight regulation of Tctp expression levels is necessary in order for cells to maintain growth homeostasis. Unlike in animals, Tctp does not regulate postmitotic growth in *Arabidopsis thaliana*; rather, plant Tctp appears to exclusively govern mitotic growth by impacting on the duration of the cell cycle [174]. During mitosis, Tctp specifically localizes to the mitotic spindle [184], and is phosphorylat-

[a] A role for Tctp has a guanine nucleotide dissociation inhibitor (GDI) has also been proposed by Cans et al.; in their study, the authors reported that Tctp stabilizes eEF1A in its GDP-bound form by impairing the GDP exchange reaction triggered by eEF1Bβ. Thus, not only has Tctp been proposed to modulate global mTOR signaling, but also to regulate the elongation step of protein translation.

ed by Polo-like kinase 1 [185][a]; in particular, overexpression of a phosphorylation-incompetent form of Tctp increases the frequency of phenotypes associated with mitotic catastrophe (e.g. multinucleation) [185]. Additionally, the laboratory of John Gurdon, recipient of the Nobel Prize in Medicine or Physiology in 2012, has demonstrated that Tctp activates the transcription of *oct4* and *nanog*, early pluripotency genes, during nuclear reprogramming [186], a finding that might help explaining the abnormal number of epiblastic cells observed in *tpt1*$^{-/-}$ mouse embryos.

C.3.2 Cell Survival

Loss of *tpt1* expression in mice results in increased apoptosis during embryogenesis and early lethality [17, 164], supporting the notion that Tctp is a guardian of the integrity of the cell. Indeed, Tctp shows protective effects against apoptosis in serum-deprived cells [187], and enhances chemoresistance in etoposide-, taxol-, or 5-fluorouracil treated cells [188, 189]. Although it lacks the characteristic Bcl-2 homology domains shared by the members of the Bcl-2 family[b] [126, 127], Tctp has been shown to interact with the anti-apoptotic proteins myeloid cell leukemia 1 (Mcl1), Bcl-2-like protein 1 (Bcl-X_L), and Bcl-2-related protein A1 (A1, as known as Bfl1 in humans) [189-191]. In particular, the N-terminal region of Tctp was shown to be required for its association with Bcl-X_L, and was recognized as fundamental for its anti-apoptotic activity [189]. Moreover, the data collected by Liu et al. suggests that Tctp modulates Mcl1 biological activity by promoting its stability[c] [190]. While it does not interact directly with Bcl-2 associated X protein (Bax), Susini et al. reported that Tctp inhibits Bax dimerization in the mitochondrial outer membrane (MOM) [17]. According to the model put forward by the authors, Tctp is able to inhibit Bax-induced mitochondrial outer membrane permeabilization by associating with Mcl1 and Bcl-X_L, thereby antagonizing this key step

---

a Polo-like kinases regulate various mitotic (M)-phase-specific events, including centrosome maturation and mitotic spindle formation.

b The Bcl-2 protein family – which includes Mcl1 and Bcl-X_L, known Tctp interactors with anti-apoptotic functions, but also executioner pro-apoptotic effectors (e.g. Bcl-2 associated X protein, Bax; Bcl-2 homologous antagonist/killer, Bak) and BH3 (Bcl-2 homology 3)-only initiators (e.g. Bcl-2-associated death promoter, Bad; P53 upregulated modulator of apoptosis, Puma) – plays a key role mediating mitochondrial integrity by regulating the permeabilization of the mitochondrial outer membrane (MOM). Mechanistically, the pro-survival members of the Bcl-2 family (e.g Mcl1 and Bcl-X_L) operate by sequestering initiator and executioner pro-apoptotic proteins (e.g. Bax), thus preventing the release of Cytochrome c from the mitochondrial intermembrane space and subsequent activation of caspases; as such, the interactions between the members of this family are dictated by local equilibria that are dependent on their relative protein concentrations and binding affinities.

c Mcl1 half-life ranges between 30 to 40 minutes.

of the apoptotic cascade [17]. More recently, Tctp has also been shown to interact with apoptotic peptidase-activating factor 1 (Apaf1) [192], a key component of the apoptosome [193].

On a different note, a proteomic screen aimed at detecting differently expressed proteins upon exposure to a low-dosage of gamma rays – ionizing radiation is commonly used in investigations on the mechanisms involved in DNA damage responses – identified Tctp, among a plethora of other regulated proteins, as the most sensitive to this treatment, suggesting a potential relevant role for Tctp in DNA damage sensing and repair [163]. Notably, increased Tctp levels were detected in human cells as early as 30 minutes after irradiation. Moreover, the authors of this study went on to demonstrate that Tctp upregulation upon exposure to ionizing radiation – which was particularly prominent in the nuclei of irradiated cells – was dependent on ataxia-telangiectasia mutated (Atm) kinase, and elicited protective effects against radiation-induced DNA damage, altogether suggesting that Tctp may promote genomic integrity in cells subjected to DNA-damaging agents [163]. More recently Hong et al. demonstrated that, in *Drosophila melanogaster*, Tctp mutants display increased radiation sensitivity during development, as well as marked deficiencies in terms of chromosome stability [194].

C.3.3 Allergic Response of the Host

In addition to its numerous roles within the cell, extracellular Tctp displays histamine-releasing activity and other cytokine-like functions [175]. Historically, the presence of histamine-releasing activity in the supernatants of cultured peripheral blood mononuclear cells prompted research efforts in the pursuit of the factors behind this activity, which culminated in 1995 with the identification of Tctp [162]. In particular, Tctp – or, as termed then by MacDonald et al., Histamine-releasing factor (Hrf) – was demonstrated to enhance or prime the release of histamine from human basophils in an Immunoglobulin E (IgE)-dependent mechanism [162]. Apart from promoting the release of histamine, Tctp has later been associated with other cytokine-like actions, including the induction of Th2-type cytokines and chemoattractants [175], and the stimulation of B cell activation and function [180]. In addition, since the original report by MacDonald et al. [162], many studies have supported the notion that secreted Tctp/Hrf only develops cytokine-like functions following some kind of structural rearrangement triggered by the inflammatory extracellular environment that arises during an allergic response

[175]. It is now known that Tctp/Hrf is secreted as a monomer but is required to dimerize via an intermolecular disulphide bond to gain its cytokine-like activity [195].

C.4 Signals Regulating Tctp Expression Levels

Several lines of study have established that Tctp cellular levels are regulated in response to extra- and intracellular signals, including growth signals and certain cytokines [159, 163, 196, 197]. In fact, the naming of Tctp as a 'translationally controlled' protein reflects the original observations regarding the regulation of Tctp expression [198]: while the rate of Tctp protein synthesis was greatly enhanced in growing versus non-growing Ehrlich ascites tumour cells, such upregulation was neither associated with a concomitant increase in *tpt1* mRNA levels nor was it blocked by transcription inhibitors [159][a]. In 1994, Bommer et al. demonstrated that Tctp protein synthesis is well correlated with the phosphorylation and consequent activation of the eukaryotic translation initiation factor 4E (eIF4E) under mitogenic stimulation [199], a result that found support in recent genome-wide studies profiling mTOR-regulated mRNAs [171, 200].

In spite of these findings, it was later recognized that Tctp is also regulated at the transcriptional level [201-203]. Indeed, the expression of *tpt1* gene is now known to be governed by a number of conditions and stresses, including during a vitamin D-induced cell death program in glioma cells [203], macrophage activation [204], in earthworms exposed to heavy metals in their habitat [202], ammonium starvation in yeast [205], or in response to increased intracellular calcium concentrations [206]. More recently, the *tpt1* gene has been shown to be upregulated by androgens in the context of prostate cancer [25].

C.5 Tctp Expression in the Nervous System

Although the expression of *tpt1* mRNA in many areas of the adult human brain[b] was reported in a study published in 2000 [168], little is known about its functions in neuronal biology. The early notion that Tctp is mainly expressed in mitotically active tissues, associated with its relative low expression level in the brain [161, 168], has perhaps potentiated this almost complete disregard for the study of Tctp in the context of neurodevelopment and neurophysiology. However, recent evidence has challenged this

---

a Its classification as a 'tumour protein' denotes the origin of the material from which the cDNA of the human *tpt1* homolog was obtained: a mammary tumour.

b Including the amygdala, caudate nucleus, cerebellum, cerebral cortex, frontal lobe, occipital lobe, temporal lobe, hippocampus, medulla oblongata, thalamus, and spinal cord.

view, for many independent genome-wide profiling studies have identified *tpt1* mRNA among the most enriched in the axonal compartment across diverse embryonic and adult neuronal populations, including embryonic retinal ganglion cells [12], neonatal sympathetic neurons [11], embryonic and adult sensory neurons [13], and cortical and hippocampal neurons derived from embryonic E18 rats and matured in culture [14], denoting of an important role in axons. Of note, Tctp protein levels were found downregulated in the temporal cortex of Alzheimer's disease patients, and in the temporal cortex, caudate nucleus and thalamus of individuals with Down syndrome [207]. Collectively, these reports suggest that Tctp expression in the nervous system remains important after development and that it may contribute to cellular homeostasis.

C.6 Tctp in Malignancy

The association between Tctp and tumorigenesis dates back to its discovery in the early 1980s [158, 208]. Tctp has since been found overexpressed in a multitude of cancer cell lines [20, 209, 210], though true recognition as a fundamental player in cancer pathogenesis came much later [23]. Pioneering investigations by Telerman and colleagues on the mechanisms behind tumour reversion identified *tpt1* as the most differently expressed transcript between the malignant and reverted states, showing a steep down-regulation in reverted cells (248 reads in tumour cells versus 2 in revertants) [23], [a][211]. Of note, in the same study, knockdown experiments targeting *tpt1* mRNA increased by approximately 30% the reversion of malignant phenotypes [23]. More recently, the same group reported that Tctp represses P53 expression, a key regulator of apoptosis and tumour suppression, by promoting its degradation [24]. In this latter study, Tctp was found to exert its modulation on P53 by preventing the auto-ubiquitination of Mdm2[b]. In parallel, P53 was shown to directly repress *tpt1* transcription, leading the authors to conclude that a reciprocal negative feedback loop exists between Tctp and P53 [24], [c][167]. Moreover, in a cohort of 508 breast cancer patients, a high-Tctp

---

a Although extremely rare, tumour reversion is the process by which some malignant cells overcome their cancerous programs and return to their initial 'normal' state.

b The data reported by the authors suggest that Tctp competes with Numb, an inhibitor of P53 ubiquitination, for binding to Mdm2-P53 complexes. Mdm2 is an E3 ubiquitin protein ligase and a major antagonist of P53, as it mediates the ubiquitination and proteosomal degradation of this protein. Thus, by preventing Mdm2 self-ubiquitination, Tctp effectively promotes its biological activity.

c As I have alluded to in a previous section, this finding has been questioned recently. Indeed, Chen et al. later reported that P53 *upregulates* Tctp transcription and identified a P53-responsive element in the promoter region of the *Mus musculus tpt1* gene [167].

expression profile, which was observed in a fraction of these cancers, correlated with indicative markers of aggressive disease (e.g. poor differentiation). The same study has also recognized Tctp expression as an independent prognostic factor in breast cancer patients [24]. In line with these findings, Tctp expression levels in glioma tumours were later found significantly elevated when compared to normal brain tissues [157]. In addition, a high-Tctp expression status was shown to correlate with clinicopathological markers of advanced disease, and Tctp expression established as an independent prognosis factor in patients with these tumours. Overall, individuals with glioma and higher Tctp expression profiles were noted to have shorter survival times [157].

D – Environmental Regulation of Cancer Cell Invasion

Motility and invasiveness are traits central to malignancy and growth cone migration alike. Indeed, for carcinoma cells to break away from the primary tumour, increased actin polymerization at the leading edge must necessarily accompany the acquisition of a neoplastic phenotype; and just like a navigating growth cone, cancer metastasization is highly modulated by the tumour environment. Notably, the four families traditionally described for their role as environmental guidance cues in axon pathfinding (ephrins, semaphorins, netrins and slits, and respective receptors) have emerged as important regulators of cancer progression, in particular during the phases of primary tumour growth and dissemination [43, 48, 51, 212], suggesting that similar signaling may operate in both contexts. Hence, it is perhaps not surprising that frequent mutations were discovered in canonical axon guidance genes in tumours derived from pancreatic ductal adenocarcinoma patients [213], or that several independent genome-wide screens have found cancer-linked transcripts to be well-represented in axonal mRNA populations [11-13]. In effect, the merits of solidifying these links are fully embodied by recent, on-going and soon to start cancer clinical trials targeting 'axon guidance' molecules, including Semaphorin 4D [244], Neuropilin-1 [245], EphA2 [246], and EphB4 [247-249].

In this section, I consider the acquisition of an invasive phenotype in the framework of cancer dissemination and attempt to find common ground between this process and the mechanisms of neural circuitry formation.

D.1 Epithelial-to-Mesenchymal Transition in Metastatic Invasion and Neuronal Development

During metastatic dissemination, individual or small groups of cells escape from the primary tumour, locally invading the surrounding extracellular matrix and stromal cell layers. The subsequent cell-biological events – intravasation into the microvasculature of the blood systems, extravasation from the bloodstream at distant sites, adaptation to a new microenvironment and, finally, launch of proliferative programs anew – although also heavily dependent on microenvironmental cues, bear smaller mechanistic resemblance to growth cone migration and, thus, are conceptually less important for the present discussion.

The discovery within tumours of cancer stem cells (CSTs)[a] with significantly enhanced tumour-initiating potential demonstrated that cancers are formed by a heterogeneous population of hierarchically organized cells [214]. This is a relevant idea to bring forth because many of the biological phenotypes associated with tumour malignancy – motility, invasiveness, self-renewal and a heightened resistance to cell death – are now known to be derived from this subpopulation of cells. In fact, it is hypothesized that cancer stem cells are the driving force behind tumour dissemination. However, an important distinction – that between *intrinsic* and *induced* cancer stem cells – is deemed necessary for the purpose of this discussion: intrinsic cancer stem cells are assumed to be a constitutive part of primary tumours since the earliest stages of tumour development; differently, the tumour microenvironment may induce non-cancer stem cells into a cancer stem cell-like state through an epithelial-to-mesenchymal transition program [215], which encompasses changes in adhesion, an overall loss of apico-basolateral polarity, as well as the acquisition of migratory and invasive attributes [216, 217].

Throughout organogenesis, a reciprocal and dynamic relationship develops between cells and their surroundings, which is necessary for the association of cells into functional multicellular tissues. Particularly, the extracellular matrix, in addition to working as a physical support frame of tissue architecture, also provides cells with direct survival and differentiation factors. Hence, it is reasonable to expect that deregulated signals from the microenvironment to have the potential to destabilize tissue homeostasis and induce derivative phenotypes, even in the absence of a genetic susceptible background [218]. This notion is actually overtly accepted in the field of oncology: it is well established, for example, that higher stromal densities potentiate the likelihood of developing breast cancer [219, 220]. Indeed, accumulating evidence shows that, during the early phases of tumour progression, the initially homeostasis-protecting stromal confines of the tumour may be converted to growth and metastasis-promoting as a consequence of the mobilization of a variety of bone marrow-derived cells, including fibroblasts, myofibroblasts, macrophages, neutrophils, mesenchymal stem cells, and lymphocytes [215, 221]. The recruitment of these cells, and the ensuing release of signaling factors by them (e.g. Wnt, transforming growth factor-β and fibroblast growth factor), forms a reactive microenvironment that can trigger tumour cells to undergo an epithelial-to-mesenchymal transition (EMT) program and acquire a motile and invasive phenotype [215].

---

a Otherwise known as tumour-initiating cells or cancer-initiating cells.

A comparable process has been shown to occur during the development of the neocortex. Here, once neural precursor cells become committed to a neuronal fate, they delaminate from the pseudostratified epithelium in the ventricular zone where they originate and migrate in the direction of the pia. Recently, an epithelial-to-mesenchymal transition-related mechanism has been proposed to bring about the transformation of these neural precursor cells into migrating neurons [222]. In specific, Scratch 1 and Scratch 2, important transcription factors of the Snail superfamily that govern the program of the epithelial-to-mesenchymal transition, were shown to be up-regulated downstream of proneural transcription factors (namely Neurogenin 1, Neurogenin 2, or Ascl1) and to effectively promote the departure of committed cells from the ventricular zone [222]. Thus, the aforementioned study provides a relevant link between the earliest steps of neuronal migration and the acquisition of invasive properties by cancer cells. First, the epithelial sheet from where carcinoma cells[a] evade can be equated to the neuroepithelium where neural progenitor cells originate in the ventricular zone (e.g. the two share cell-cell junctions and the same apicobasal polarity). Second, in both cases a mesenchymal phenotype is acquired, enabling the subsequent migratory phase. And third, because the Wnt pathway, mentioned above for its implications in the acquisition of cancer stem cell-like traits, is reported to induce the expression of Neurogenin 1 in neural precursor cells [223], one of the upstream proneural transcription factors known to regulate EMT-promoting Scratch proteins **(Figure 1.9)** [222].

Moreover, although not studied directly in the context of axon-dendrite polarization, the signaling mechanisms behind the program of epithelial-to-mesenchymal transition have, likewise, been suggested to orchestrate the process of axon specification [224]. In particular, this work provides *in vivo* evidence for a role in axon specification of the signaling cascade triggered by transforming growth factor-β, one of the most potent known inducers of epithelial-to-mesenchymal transition [217].

In conclusion, while more studies are required, the events in early neuronal morphogenesis, like those shaping an induced cancer stem cell-like phenotype during tumorigenesis, may indeed share significant mechanistic similarities. Namely, in both contexts cells lose epithelial traits, including cell-cell junctions and overall polarity, and develop a motile and invasive phenotype. Also, Wnt and transforming growth factor-β-mediated signaling function upstream of all of these processes[b][225], further sug-

---

a Tumours with an epithelial origin, denominated carcinomas, constitute approximately 80% of life-threating cancers.

b Wnt signaling is also a well-established driver of neuronal polarization.

gesting that an co-opted program may exist.

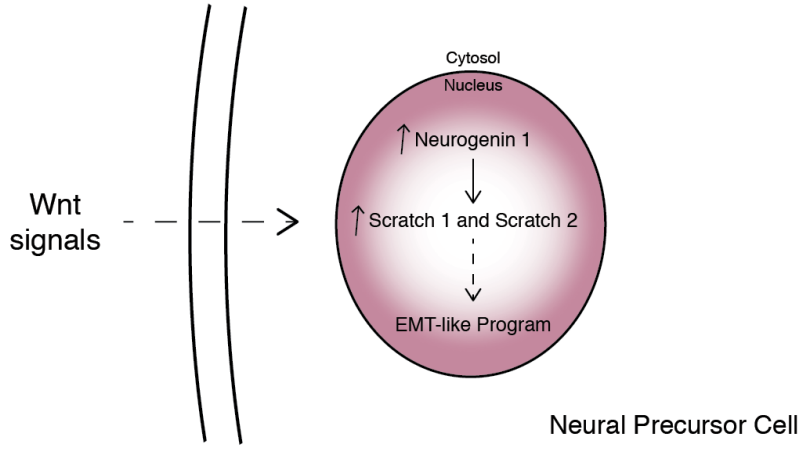

Figure 1.9 – Hypothetical regulation of epithelial-to-mesenchymal transition-like programs at the onset of neuronal migration. The Wnt pathway is known to support the acquisition of a neuronal fate by neural precursor cells in part by promoting the expression of Neurogenin 1, a proneural transcription factor [223]. In turn, Neurogenin 1-regulated Scratch 1 and Scratch 2 have been show to regulate neuronal migration mechanisms via an EMT-like program [222].

D.2 Axon Guidance Molecules in Cancer Progression

A short incursion into the history of the 'canonical' axon guidance molecules reveals that their association to cancer dates back to their initial discovery. The *epha1* gene, for example, was cloned from a carcinoma cell line in 1987 in a screen for novel tyrosine kinase receptors with oncogenic potential, and the first Ephrin ligand was as well described by a group working in the context of cancer [51]. Likewise, the gene encoding for the prototypical Netrin-1 receptor Dcc was originally identified as a tumour suppressor in advanced stages of colorectal carcinoma progression (hence its designation deleted in colorectal cancer) [48]. Only in the mid-1990s did their association to axon pathfinding begin to emerge [43, 101].

D.2.1 Netrin Signaling in Cancer

Key properties of tumour dissemination include not only the acquisition of a migratory phenotype, but also a heightened propensity to survive [215]. In this Netrin-1 signals play an instrumental role, because the Dcc/Unc5 family functions as 'dependence receptors', a specific class of receptors that may mediate cell-death programs depending on the absence of ligands [226]. Indeed, when netrins are present, Dcc/Unc5 receptors form dimeric or multimeric complexes and induce mitogen-activated protein kinase (Mapk)-, focal adhesion kinase (Fak)- and Akt (also known as protein kinase b)-dependent signals; however, if disengaged, an apoptotic signal is triggered instead.

The presence of Netrin-1 in the surrounding tissue can thus act as a regulatory death signal to tumour cells expressing these receptors, particularly when the number of cancer cells outweighs the availability of the ligand, or when metastatic cells disseminate into tissues where Netrin-1 expression is absent or only weakly present.

It follows from the existence of dependence receptors that cancer cells must somehow override the 'safeguard' inhibitory influence on growth such constraints impose [48]. To this end, three main strategies have been documented in human tumours: 1) receptor downregulation or loss-of-function, as originally shown in colorectal cancers [227]; 2) upregulation of Netrin-1 expression, which has been found in a large number of breast cancers that develop secondary tumours [228]; 3) downregulation or loss of pro-apoptotic partners that participate in the dependence receptor-evoked death pathway [229].

Analogously, in addition to being necessary for commissural axon attraction towards the ventral midline [101], Netrin-1 has been shown to inhibit the pro-apoptotic activity mediated by Dcc in developing axons, where it also functions as a dependence receptor [230].

D.2.2 Semaphorin Signaling in Cancer

Semaphorin research in the context of tumorigenesis has focused primarily on elucidating the contribution of this family to the formation of tumour vasculature, where its various members can elicit anti- or pro-angiogenic effects. Given that the proliferation of cancer cells depend on adequate supplies of oxygen and nutrients [231], it comes as no surprise that the expression of semaphorins or their receptors has frequently been encountered deregulated in tumours. As a general rule, the levels of pro-angiogenic semaphorins are upregulated in tumour cells, whereas semaphorins that convey inhibitory signals to the vasculature are downregulated [212]. This notable versatility in semaphorin-mediated effects is partly due to the diversity of signaling receptors – including the receptor tyrosine kinases vascular endothelial growth factor receptor type 2 (Vegfr2), erythroblastic leukemia viral oncogene homologue 2 (Erbb2), and hepatocyte growth factor receptor (Hgfr) – that can associate with plexins and neuropilins upon semaphorin binding [212]. That is, semaphorin signaling in many instances is cell context-dependent.

In turn, these considerations very much echo semaphorin-mediated mechanisms during brain development. For example, Semaphorin 3E/Plexin D1-mediated attractive or repulsive chemotropic responses are known to be dependent on the expression pro-

file of Neuropilin-1 [232]. Even more remarkable is the finding linking the association of Vegfr2 with PlexinD1/Neuropilin-1 receptor complexes to the axon growth promoting effects elicited by Semaphorin 3E in subicular neurons [233].

D.2.3 Eph/Ephrin Bidirectional Signaling in Cancer

The transmembrane Eph-Ephrin cell communication system relays two-way – bidirectional – signals: upon ligand binding, the 'forward' signaling arm impinges in the Eph-expressing cell and is mainly mediated by the receptor's kinase domain, whereas the 'reverse' arm acts on the Ephrin-expressing counterpart through associated Src family kinases [51]. As the history of their discovery suggests, Eph receptors and ephrins are abundantly expressed in cancer cells as well as in the tumour microenvironment, and, in many cellular contexts, including cancer, Eph-Ephrin signals promote morphological and behavioural changes reminiscent of an epithelial phenotype by effectively enhancing cell-cell contacts and suppressing cell invasiveness [51, 234]. It stands to reason, then, why perturbations to this signaling system are prone to initiate malignant phenotypes.

Indeed, during cancer pathogenesis, Eph-Ephrin signaling has been implicated in many steps of the tumorigenic cascade, including tumour proliferation, angiogenesis and dissemination, and their expression, particularly that of Eph receptors, is often found deregulated at advanced cancer stages and is well correlated with tumour progression and patient survival. However, their actions are complex, even paradoxical at times, rendering attempts to provide generalizations of their effects rather inconsequent. That being said, it is often the case that the expression levels of Eph receptors and Ephrin ligands are regulated discordantly in the context of cancer and, in consequence, oncogenic cell-cell crosstalk develops between cancer cells and their environment [51]. Hence, as highlighted by their roles in neural circuit formation, a finely tuned regulation of the Eph system is crucial for the maintenance of tissue homeostasis.

D.2.4 Slit Signaling in Cancer

The strongest evidence implicating Slit-Robo signaling in cancer progression comes from comparative genomic studies using clinically homogenous tumour samples [213, 235]. In both instances, in addition to modifications in well-established cancer-related genes, prevalent mutations and copy-number variations (CNVs) were reported for Slit and Robo genes in tumours derived from patients diagnosed with liver fluke-associated cholangiocarcinoma [235] and pancreatic ductal adenocarcinoma [213]. Particular-

ly, low *Robo2* and high *Robo3* mRNA expression were independently correlated with poor patient prognosis in the latter study [213][a,b]. These data, together with previous evidence from invasive cancers of the lung, breast, kidney and cervix, strongly suggest that deregulated Slit-Robo signaling may be a common tumorigenic feature of many human cancers [48, 236].

Slit2, a particularly well-studied ligand, has been shown to inhibit tumour cell migration in medulloblastoma and glioma models *in vitro* and *in vivo* [237, 238]. Although the exact intricacies of its mode of action are yet to be fully elucidated, Slit-Robo signaling in physiological contexts is known to sustain the activation of glycogen synthase kinase 3β (Gsk3β) by inhibiting Akt; in turn, Gsk3β in its active form phosphorylates β-catenin, which results in its export from the nucleus and a consequent loss of its transcriptional activity. Concurrently, Gsk3β also promotes the degradation of Snail1 through the ubiquitin-proteasome pathway[c]. These events have a double effect on E-cadherin, a key molecule involved in stabilizing cell-cell junctions: first, there is an accumulation of β-catenin at the plasma membrane, where it interacts and stabilizes E-cadherin; second, because Snail1 is a strong transcriptional repressor of E-cadherin expression, its degradation effectively augments E-cadherin cellular levels **(Figure 1.10)**. Hence, normal Slit-Robo signaling can prevent cell migration in part by potentiating cell-cell adhesive contacts[d]. By contrast, attenuated Slit-Robo signaling leads to the inactivation Gsk3β, which relieves the modulation it previously exerted on the nuclear pool of β-catenin. This impacts on the expression of E-cadherin and, simultaneously, limits the association between β-catenin and E-cadherin at the membrane, thus weakening adhesive contacts between cells. In addition, the nuclear localization of β-catenin also promotes the canonical Wnt signaling arm, which, as discussed above, is a strong inducer of the epithelial-to-mesenchymal transition program [48, 213, 236, 239-241].

---

a Robo3 has been shown to negatively regulate Robo2 signaling in commissural axons; the upregulation of its transcripts in pancreatic cancers suggests that a similar mechanism may operate in this context, as hypothesized by the authors of the study.

b Incidentally, some genes encoding for semaphorins ligands and receptors were also found to harbor alterations in these tumours.

c The Snail transcription factors, as discussed above, are important regulators of the epithelial-to-mesenchymal transition program.

d Other significant mechanisms, such as the inhibition of the key actin cytoskeleton regulator Cdc42 by Slit-Robo-specific GTPase-activating protein (srGAP), additionally contribute to the global effects observed downstream of homeostatic Slit-Robo signals, in this case by hindering cell motility.

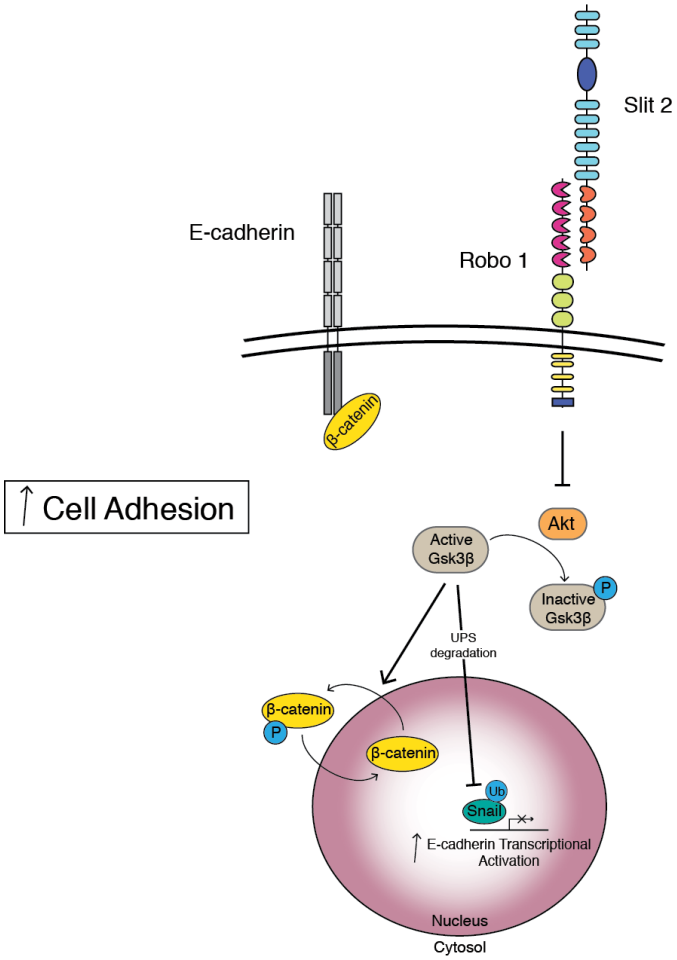

Figure 1.10 – Modes of Slit/Robo signaling with impact on cell adhesion. P- phosphorylation event; Ub- denotes a UPS-mediated mechanism. See text for details.

D.3 The 'Seed and Soil' Affinity Hypothesis

Finally, it seems fruitful to mention the seminal work of Stephen Paget, an English surgeon who published in 1889 what has come to be known as the *'seed and soil' hypothesis*, for it embodies an idea quite akin to that implied in Sperry's chemoaffinity postulate. Paget noted, in the process of analysis of more than 900 autopsy records, that tumour metastasis contains an organ-specific, non-random character: "The evidence seems to me irresistible that in cancer of the breast the bones suffer in a special way (…) Some bones suffer more than others; the disease has its *seats of election*" [242]. From these observations, he equated that metastases depend on certain cancer cells – the 'seeds' – having a specific affinity for the environment of certain organs – the 'soil' – correctly concluding, with sound resemblance to modern day theories of neural circuit formation, that only when both 'seed' and 'soil' were compatible would metastasis form [216, 243].

E – Focus of this Thesis

From the influence of the environment, to the modulation of cellular adhesive contacts, or the build up of protrusive actin dynamics necessary for motility, the initial challenges experienced by a metastatic cancer cell resemble in many ways the obstacles continuously overcome by a navigating growth cone as it progresses through the complex embryonic environment. Moreover, the significant subcellular prevalence of transcripts encoding for cancer-associated proteins in diverse axonal populations, together with accumulating evidence implicating the deregulated expression of axon guidance molecules in tumour pathogenesis, underline the striking cellular and molecular commonalities that exist between both processes. Thus, it is reasonable to assume that by learning more about the properties of growth and migration during development, a better understanding of disease-associated cell invasion strategies can be attained; vice versa, it is likely that the knowledge gathered in the context of tumorigenesis can be partly transduced to the field of axon guidance.

Herein, motivated by the parallels between growth cone and metastatic migration, I studied a tumorigenic protein during the early development of neuronal circuitry. Using the *Xenopus laevi*s retinotectal projection as an *in vivo* model system, and from a RNA-centric perspective, I examined the involvement of Tctp in axon pathfinding and dissected the cellular and molecular consequences of its deficiency in neurodevelopment. Given that the identification of *tpt1* as a potential candidate of study stemmed from genome-wide profiling screens [11-14], I initially sought to confirm the presence of this mRNA species in the axonal compartment of retinal ganglion cells. The experimental validation of this premise permitted me to form the basis for the objectives of my research: the characterization of how the expression of axonal Tctp is locally regulated and, in parallel, the evaluation of its potential involvement in the process of axon guidance. The range of phenotypes detected in embryos depleted of Tctp eventually led me to pursue a third research aim, which focused on understanding the contribution of Tctp to axonal biology. In particular, I studied how mitochondrial function is affected in Tctp-depleted axons, and linked Tctp, through its interplay with the Bcl-2 protein family, to the survival machinery of the axon.

2. Experimental Procedures

***Xenopus laevis* Embryos**

Xenopus laevis embryos were obtained by *in vitro* fertilization, raised in 0.1X Modified Barth's Saline (0.88 mM NaCl, 0.01 mM KCl, 0.024 mM $NaHCO_3$, 0.1 mM HEPES, 8.2 μM $MgSO_4$, 3.3 μM $Ca(NO_3)_2$, 4.1 μM $CaCl_2$) at 14-22 ºC and staged according to Nieuwkoop and Faber [250]. All animal experiments were approved by the University of Cambridge Ethical Review Committee.

Retinal Cultures

Unless otherwise noted, eye primordia were dissected from anesthetized stage 32 embryos, rinsed and then plated on culture dishes pre-coated with poly-L-lysine (10 μg/mL, Sigma) and laminin (10 μg/mL, Sigma). Cultures were incubated at 20 ºC in 60% L15 minimal medium (Life Technologies) for 24 hours before experimentation and/or fixation.

In Situ Hybridization (ISH) and Fluorescent In Situ Hybridization (FISH)

ISH on transverse cryosections of fixed embryos was performed as described previously [251]. Digoxigenin-labelled RNA probes were generated from linearized IMAGE clones (*tpt1* IMAGE ID: 5542512); sequence-specific probes were derived from PCR amplicons with primers containing SP6 or T7 promoter sequences at 5' end. Photomicrographs were taken with a Zeiss microscope equipped with a Micropublisher 5.0 RTV

camera (Qimaging). For whole-mount ISH, stage 40 *Xenopus laevis* embryos were processed as described elsewhere [252, 253] using the same probes as described above for the ISH on transverse cryosections methodology; processed embryos were imaged on an agarose bed using a Leica MZ FLIII inverted microscope equipped with a Micropublisher 5.0 RTV camera. FISH probe design followed documented guidelines [254] and probes were 3'-labeled with DIG oligonucleotide tailing kit (Roche); FISH procedure on retinal growth cones was then carried out as described with minor variations [12].

FISH antisense probe sequence in 5'-3' orientation

TAGATATCCGAGAACATTTCGTCTTCAGTGATGCAGTCCTTGTAGATGA

ATCATCAATTGCACCTTCTTCTCTTTGGATTACCTTGCCTTCAACTTC

CCTTGATGTAATTCTTGTAAGAGTCCTTGGTGAAGCCTGTTTCCTGAA

GGGGTTCATTCTTTCTCCGGTGTAAAACTGATAGTTTTTGAAATTTCGAAG

Immunostaining of Retinal Sections

Anesthetized embryos were fixed in 4% paraformaldehyde (vol/vol) in phosphate buffered saline (PBS) overnight at 4ºC, washed and incubated in 30% sucrose (wt/vol) in PBS for 2 hours at 4ºC before sectioning. Transverse 12 µm cryosections were processed using standard immunohistochemistry protocols (blocking solution: 10% heat-inactivated goat serum, 1% bovine serum albumin, 0.5% Triton X-100 in 1X PBS). Antibodies: rabbit anti-Tctp (1:500, kind gift from J. Kubiak); mouse anti-Calbindin D-28k (1:1000, Swant); rabbit anti-Calretinin (1:1000, Millipore); rabbit anti-GAD65/67 (1:200, Abcam) mouse anti-Rhodopsin (1:200, Novus Biologicals), mouse anti-Opsin (1:1000, Sigma). Alexa Fluor 488 phalloidin (Life Technologies) was used at 1:40. Nuclei were labelled with 0.1 µg/mL DAPI (Life Technologies) at the last wash step before mounting. Alexa Fluor secondary antibodies (Life Technologies) were used throughout at 1:1000. Antigen retrieval with steaming 0.01 M sodium citrate (0.05% Tween 20, pH 6.0) was carried out prior to staining for Tctp. Processed sections were visualized with a Nikon Eclipse 80i and photographed with a Hamamatsu ORCA-ER camera.

Laser-capture Microdissection and RNA Extraction

Per experiment, ~140 stage 33/34 eye explants were plated on PET (polyethylene terephthalate) membrane slides (Leica Microsystems), pre-coated with poly-L-lysine (10 µg/mL; Sigma) and laminin (10 µg/mL, Sigma), and cultured for 32-36 hours. As described previously [12], retinal cultures were fixed (4% paraformaldehyde, 4% sucrose

in 1X PBS) for 10 minutes, subsequently dehydrated through an ethanol series and air-dried before capture. To aid visualization, the membrane stain FM 1-43FX (Life Technologies) was added 20 minutes before fixation. Samples were processed using the Leica LMD6000 system. RNA was extracted immediately after with RNAqueous-Micro kit (Life Technologies) according to manufacturer's instructions. Unlike Zivraj et al. [12], a linear amplification was not used prior to RACE, RT-PCR or RT-qPCR procedures. Control RT-PCR reactions were performed using OneStep RT-PCR kit (QIAGEN); the presence of microtubule-associated protein-2 (*map2*), histoneH4 (*hist1h4a*), and β-actin (*actb*) transcripts was evaluated before running the each RACE PCR or RT-qPCR experiment

5' and 3' Rapid Amplification of cDNA Ends (RACE PCR)

Eye and pure axonal extracts were processed with SMARTer RACE cDNA Amplification Kit (Clontech) according to manufacturer's instructions. RACE PCR was performed using Advantage HF 2 PCR kit (Clontech). Following gel extraction, PCR products were TA-cloned and sequenced in both orientations.

Quantification of *tpt1* mRNA Isoforms by RT-qPCR

Eye and axonal RNA extracts were prepared as detailed above. QIAGEN QuantiTect SYBR Green RT-PCR kit was used in combination with Roche LightCycler 480 Real-Time PCR system. Manufacturer's guidelines were followed thoroughly except for primer concentration – 0.4 μM instead of 0.5 μM was found optimal. Primer design intently kept amplicon size below 150 base pairs to ensure optimal amplification efficiency. Due to the inexistence of introns in the 3'UTR of the *tpt1* gene, it is impossible to design primers specific to the unique region of *tpt1*-L and spanning an exon-intron boundary, as an optimal primer set for RT-PCR would. Hence, when designing primers specific to the coding region of *tpt1*, exon-intron boundaries were, as well, intently avoided. To overcome potential pipetting errors during the initial reaction assembly, each reaction was run in quadruplicate. Reaction volume was 10 μL per well. Following reaction assembly, plates were centrifuged at 1,500 x *g* for 2 minutes at 4ºC. Standard curves for the calculation of amplification efficiency were run independently from the actual experiments [255]. Relative quantification data was obtained following the ΔΔCt method using Roche's LightCycler 480 data analysis module. *actb* (beta-actin) mRNA was used as reference for data normalization. As an additional quality control for the axonal RNA preparations, and similarly to the controls performed in the axonal RACE PCR experiments, the presence of microtubule-associated protein-2 (*map2*)

and histone H4 (*hist1h4a*) transcripts was evaluated by RT-PCR before running each RT-qPCR experiment (data not shown).

The real-time cycling reaction conditions, as per manufacturer's guidelines, were as follows:

Reverse transcription	30 minutes, 50ºC
PCR Initial Activation Step	15 minutes, 95ºC
Polymerase Chain Reaction (45 cycles)	
Denaturation	15 seconds, 94ºC
Annealing	30 seconds, 57ºC
Extension	30 seconds, 72ºC
Data acquisition	15 seconds, 72ºC

Melting Curve

1 minute at 95ºC
1 minute at 40ºC
0.11ºC/second increments from 40ºC to 95ºC and continuous fluorescence readings

MS2 *In Vivo* Biotin Tagged RNA Affinity Purification (MS2-BioTRAP): Cell Culture and Metabolic Stable Isotope Labelling for SILAC[a] Mass Spectrometry

Human Embryonic Kidney (HEK) two hundred and ninety-three stable cell lines expressing MS2-HB ($293^{MS2\text{-}HB}$) were a gift from Marian Waterman (University of California, Irvine) [256]. The methodology followed here and in subsequent steps drew profusely on the procedure described in Tsai et al. original technical report [256]. Briefly, to ensure complete isotope incorporation in the proteome, $293^{MS2\text{-}HB}$ cells were grown for seven doublings in SILAC DMEM Media containing unlabelled arginine (^{12}C and ^{14}N) and lysine (^{12}C and ^{14}N) amino acids (Dundee Cell Products) or in SILAC DMEM Media containing ^{13}C and ^{15}N labelled arginine and ^{13}C and ^{15}N labelled lysine (Dundee Cell Products) supplemented with 10 % (vol/vol) dialyzed foetal bovine serum (FBS, Pierce Biotechnology), 50 units/mL of penicillin + 50 µg/mL of streptomycin (Pen Strep, Life Technologies), and 3 µg/mL of puromycin (for cell selection, Life Technolo-

a SILAC: Stable Isotope Labeling by Amino Acids in Cell Culture.

gies). For the purpose of assessing isotope incorporation, a one-dimension SDS-PAGE gel was run, Coomassie stained (Colloidal Blue Staining Kit, Life Technologies), and analysed at the Cambridge Centre for Proteomics (data not included).

MS2-BioTRAP: Cloning of pRL-*Rluc*-*MS2*-*tpt1*-3'UTR

Due to the necessary inclusion of non-related sequence elements in the final DNA product if traditional cloning methods were to be applied (e.g. restriction sites), the synthesis of the *MS2* stem loop repeats upstream of the *Homo sapiens tpt1* 3'UTR was commissioned to a manufacturer of custom DNA products (GENEWIZ).

Ordered sequence:

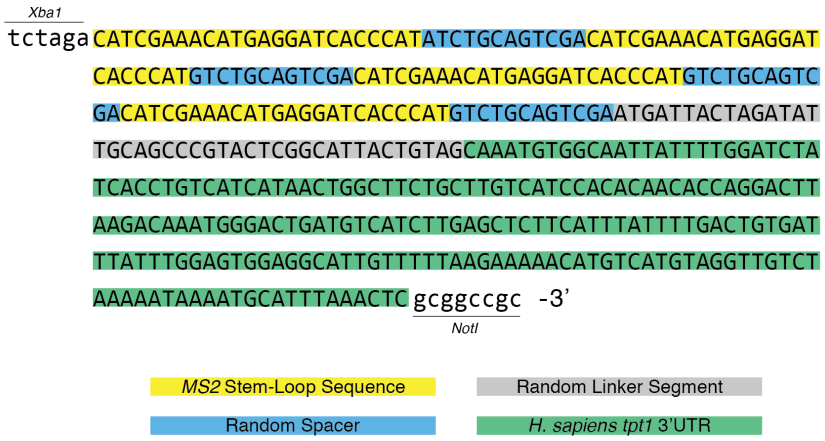

This custom-made MS2-*tpt1*-3'UTR insert (shipped ligated to a pUC57 plasmid) and the pRL-SV40 Renilla luciferase reporter plasmid (Promega) were digested with XbaI and NotI for 3 hours. Afterwards, New England Biolabs' Antarctic Phosphatase catalysis of 5' phosphate groups was used to prevent vector self-ligation. The digested vector was then run on an agarose gel and the band corresponding to the insert extracted with PureLink Quick Gel Extraction Kit (Life Technologies). Insert and vector were ligated overnight at 16ºC at a 6:1 ratio before transformation, and successful insertions were confirmed by DNA sequencing. The pRL-*Rluc*-MS2-Control construct was generated in a similar fashion; namely, the custom-made MS2-*tpt1*-3'UTR insert was used as the starting DNA material for a PCR reaction with the following primer pair: 5'-GCTAACTCTAGACATCGAAACATGAGGATCACCC-ATA-3' and 5'-ATTCTAGCGGCCGCCTACAGTAATGCCGAGTACGGG-3'. Primer design included unique restriction sites (XbaI and NotI recognition sites in the forward and reserve primers, respectively) and six extra nucleotides upstream of the restriction site. Subsequent steps were executed in parallel to the pRL-*Rluc*-MS2-*tpt1*-3'UTR cloning procedure.

MS2-BioTRAP: Renilla Luciferase/Firefly Luciferase RT-qPCR and Dual Luciferase Reporter Assay

On the day before transfection, $293^{MS2\text{-}HB}$ cells [256] were trypsinized and plated in a 24-well plate. Volumes were adjusted so that cells were ~80-90% confluent on the day of transfection. For normalization proposes, cells were co-transfected with pRL-*Rluc*-MS2-*tpt1*-3'UTR or pRL-*Rluc*-MS2-Control (experimental vectors) and Promega's pGL3-Control Vector (which expresses Firefly luciferase) using Lipofectamine 2000 (Life Technologies). Since both pRL and pGL3 plasmids contain the SV40 early enhancer/promoter, and to minimize possible *trans* effects between promoters on the co-transfected plasmids which could potentially affect reporter gene expression, a ratio of 10:1 between experimental and control plasmids, respectively, was used (1 µg:100 ng).

Twenty-four hours post-transfection, RNA extracts were prepared using RNeasy Micro Kit (QIAGEN) following the instructions provided by the manufacturer. Of particular note, the cell lysate was passed five times through a blunt 20-gauge needle fitted to a syringe to ensure homogeneity before transferring the lysate to the spin column. Moreover, 2-mercaptoethanol at 1% (vol/vol) was added to Buffer RLT, and an on-column DNase digestion step was included in the protocol). For robustness, four biological replicates per transfection condition were prepared. QIAGEN QuantiTect SYBR Green RT-PCR kit was used in combination with a Roche LightCycler 480 Real-Time PCR system. Manufacturer's guidelines were followed thoroughly.

Alternatively, twenty-four hours post-transfection, the activities of both firefly and *Renilla* luciferases were measured sequentially using the Dual-Luciferase Reporter Assay (Promega) system according to manufacturer's instructions on a TD-20/20 single-tube luminometer (Turner Biosystems).

MS2-BioTRAP: Cell Transfection, Affinity Purification and Sample Preparation for Mass Spectrometry

Briefly, 'light' and 'heavy' $293^{MS2\text{-}HB}$ cells cultured in five 150-mm plates to approximately 80-90% confluence were transfected with pRL-*Rluc*-MS2-*tpt1*-3'UTR or pRL-*Rluc*-MS2-Control using Lipofectamine 2000 (Life Technologies). Forty-eight hours post-transfection, and before harvesting by scrapping, cells were washed with ice-cold PBS[a] and RNA-protein complexes cross-linked by ultra-violet illumination (energy

[a] All steps, except otherwise expressly mentioned, were performed on ice or with ice-cold reagents.

delivered: 400 mJ/cm^2) on an ice tray using a Stratalinker 1800 (Stratagene). 'Light' and 'heavy' cell pellets were lysed using a denaturing lysis buffer (8M Urea, 300 mM NaCl, 50 mM NaH_2PO_4, 0.5% (vol/vol) Nonidet P-40, 1 mM phenylmethylsulfonyl fluoride (PMSF)[a], and a protease inhibitor cocktail (Halt Protease Inhibitor Cocktail from Pierce Biotechnology, used at 1:100), sonicated at medium intensity settings three times for 15-second intervals, centrifuged at 14,000 x *g* for 15 minutes at 4ºC, and clarified through 1.6 um GD/X Glass Microfiber filters (Whatman). Equal amounts of 'light' and 'heavy' lysates, determined by protein concentration, were then mixed, which was followed by the addition of previously-washed Dynal streptavidin M-280 magnetic beads (Life Technologies; approximately 1 µL of bead slurry per 20 µg of protein).

After completing the affinity purification procedure, beads were equilibrated in ice-cold 25 mM NH_4HCO_3 aqueous solution (approximately thirty bed volume), resuspended in 250 µL of a trypsin solution (Promega's Tryping Gold, Mass Spectrometry Grade; 10 ng/µL of acetic acid-reconstituted trypsin in 25 mM NH_4HCO_3 aqueous solution), and digested overnight at 37ºC with gentle agitation. Digested samples were taken on the following morning to the Cambridge Proteomics Centre for spectrometric analysis. Differently from Tsai et al. methodology [256], the liquid chromatography-tandem mass spectrometry (LC-MS/MS) run was prolonged for three hours instead of performing a strong-cation fractionation (SCX) step. In total, three independent mixed samples and submissions were completed.

Finally, the enrichment of RNA-binding proteins in the "*tpt1* 3'UTR" condition was judged based on SILAC ratios (the fraction of the heavy to light peptides); reproducible identifications were then studied for correlation on the STRING (Search Tool for the Retrieval of Interacting Genes/Proteins) database.

Translation-blocking Morpholino Antisense Oligonucleotides

Antisense *tpt1*-MO and control-MO were designed and supplied by GeneTools: 5'-ATCATGTTGGCGGCCTAAGTGTTGT-3' and 5'-CCTCTTACCTCAGTTACAATTTATA-3', respectively. Fluorescein-tagged (3'end) morpholinos were used throughout, except when mitochondrion targeted GFP (mt-GFP) was to be subsequently electroporated.

Blastomere Microinjection

Embryos were injected as previously described [89]. Injections were preformed at the 4-cell stage in one or both dorsal blastomeres as detailed in the main text. mRNA was

a All reagents purchased from Sigma-Aldrich, unless otherwise stated.

delivered at 90 pg/blastomere. *tpt1*-MO and control-MO were injected at 12 ng/blastomere.

Retina-targeted Electroporation

Plasmid DNA electroporation was carried out on stage 28-30 embryos as described previously [90] using eight consecutive 18 V pulses of 50-millisecond duration, delivered at 1-second intervals. Membrane RFP (gap-RFP) and/or mitochondria targeted-GFP (mtGFP, gift from M. Coleman) were delivered at 1 mg/μL.

Netrin-1 Stimulation

After 24 hours incubation, explants were bathed in 600 ng/mL recombinant mouse Netrin-1 (reconstituted in PBS containing 0.1% [wt/vol] bovine serum albumin) for 5 minutes and fixed in 2% (vol/vol) paraformaldehyde, 7.5% (wt/vol) sucrose; BSA (0.1%) was used as control. Cycloheximide (25 μM, Sigma) and rapamycin (10 nM, Sigma) were bath-applied to cultures 2 minutes prior to the addition of Netrin-1.

Ephrin-A1 Stimulation

As described elsewhere [257], to pre-aggregate proteins, recombinant mouse Ephrin-A1-Fc (a recombinant chimera between mouse Ephrin-A1 and human IgG_1 Fc region[a]; R&D Systems) or human IgG_1 Fc peptide (supplied by Jackson Immunoresearch Labs) was incubated with a goat antibody against the human Fc region (Jackson Immunoresearch Labs). Specifically, anti-human IgG, Fc fragment specific antibody (100 μL, diluted at 0.9 mg/mL) was incubated with Ephrin-A1-Fc (100 μL of 100 μg/mL stock) or 100 μL of IgG_1 Fc peptide (100 μL, diluted at 100 μg/mL). After gentle agitation for 45 minutes at room temperature, protein aggregates were bath-applied to retinal cultures for 10 minutes (unless otherwise specified) at a 1:10 dilution (final concentration: 5 μg/mL) before fixation. Cultures were subsequently processed for quantitative immunofluorescence analysis.

Quantitative Immunofluorescence

Quantitative immunofluorescence was carried out largely as described [22]. Cells were fixed in 2% (vol/vol) paraformaldehyde, 7.5% (wt/vol) sucrose for 20 minutes, washed in PBS and permeabilized for 3 minutes with saponin (1 mg/mL in PBS). Standard immunocytochemistry protocols were followed henceforth (blocking solution: 5%

a Fragment crystallizable (Fc) region.

heat-inactivated goat serum in 1X PBS). Fluorescence intensity (mean pixel intensity per unit area) was measured in non-collapsed growth cones using Openlab or Volocity software (PerkinElmer). Measurements were taken using masks obtained by manually tracing growth cones in corresponding bright-field images. Background fluorescence was then subtracted from total growth cone fluorescence and data were normalized to the mean immunofluorescence intensity of the control group and expressed as percentage. A Nikon Eclipse TE2000-U inverted microscope was used for all image acquisitions. Antibodies: rabbit anti-Tctp (1:500, gift from J. Kubiak); rabbit anti-$p_{S235/236}$rpS6 (1:500, Upstate); mouse anti-'mono- and polyubiquitinylated conjugates' (FK2 clone; 1:500, Millipore); mouse anti-P53 (1:300, Abcam); rabbit anti-Active Caspase-3 (1:200, Abcam). Alexa Fluor secondary antibodies (Life Technologies) were used throughout at 1:1000.

Cloning and *In Vitro* Transcription of Kaede-S and Kaede-L

Generation of chimeric *tpt1*-Kaede constructs made use of TA-cloned RACE fragments and an empty pKaede-S1 cloning vector (accession number: AB085641). The *tpt1* 5'UTR was amplified with the following primer pair: 5'-TCAGCAGAATTCCCTTTTCTCTCCCCACCCTCCG-3' and 5'-TCGCGTGGATCCGTTGGCGGCCTAAGTGTTGTAATG-3' (forward and reverse primer, respectively). Primer design included unique restriction sites in the 5' end (EcoRI and BamHI sites in the forward and reserve primers, respectively). As the amplified fragment was shorter that 100bp, QIAGEN's MinElute Reaction Cleanup Kit was used to purify the resulting DNA product. The pKaede-S1 cloning vector and the *tpt1* 5'UTR insert were subsequently digested with EcoRI and BamHI for 3 hours. New England Biolabs' Antarctic Phosphatase catalysis of 5' phosphate groups was used to prevent vector self-ligation. The digested vector was then run on an agarose gel and gel extracted with PureLink Quick Gel Extraction Kit (Life Technologies). Insert and vector were ligated overnight at 16ºC at a 6:1 ratio before transformation. Successful cloning was confirmed by DNA sequencing.

The resulting *tpt1* 5'UTR–Kaede fusion construct was used in succeeding cloning steps. Overall, the *tpt1* 3'UTRs cloning involved an equivalent strategy. The *tpt1*-S 3'UTR was amplified with the following primer pair: 5'-CGCACTGCAGCATTCCGTTTGGTTCTTCCATCTT-3' (forward primer) and 5'-GGGCCCATATGACAGTGGAGAATCATGGGCTTTAT-3' (reverse primer). The *tpt1*-L 3'UTR was amplified with the following primer pair: 5'-CGCACTGCAGCATTCCGTTTGGTTCTTCCATCTT-3' (forward primer) and 5'-CGCGGCCATATGTTGTTTAATTCTGTCTTTATTCAGGATC-3' (reverse primer). Here, the

forward primer design included a PstI restriction site (note that this primer was used in the amplification of both short and long 3'UTRs) and both reverse primers contained a NdeI site.

In the last step of the devised cloning strategy, a T3 phage polymerase promoter was added immediately upstream of the 5'UTR using the following primer combinations: 5'-AATTAACCCTCACTAAAGGCCTTTTCTCTCCCCACCCTCCG-3' and 5'-GGGCCCATATGACAGTGGAGAATCATGGGCTTTAT-3' (forward and reverse primers, respectively, for Kaede-S); 5'-AATTAACCCTCACTAAAGGCCTTTTCTCTCCCCACCCTCCG-3' and 5'-CGCGGCCATATGTTGTTTAATTCTGTCTTTATTCAGGATC-3' (forward and reverse primers, respectively, for the Kaede-L construct). Resulting products were run on an agarose gel and gel purified. Isolated products were then TA-cloned and positive insertions identified by sequencing.

Capped Kaede mRNAs were synthesized from linearized plasmids using mMESSAGE mMACHINE T3 Transcription kit (Life Technologies); a poly(A) tail was subsequently added to DNase-treated reactions using Poly(A) Tailing Kit (Life Technologies). Before delivery, the resultant RNA was column-purified in accordance to manufacturer's instructions (RNeasy Mini Kit, Qiagen).

Kaede Translation Reporters in Cultured Axons

Experiments with Kaede reporters were performed as described previously with minor alterations [5, 89]. Eye primordia were dissected from anesthetized stage 24 Kaede-positive embryos and cultured for 14-18 hours before imaging. Culture dishes were pre-coated with poly-L-lysine (10 μg/mL, Sigma) and fibronectin (10 μg/mL, Sigma). RGC axons were manually severed from cell bodies using a mounted pin holder. Before netrin-1 (600 ng/ml) or control stimulation (0.1% BSA), Kaede green was partially photoconverted with two 5-second pulse of 405-nm laser illumination. Images were acquired at 5-minute intervals using an UltraView VoX spinning disk confocal imaging system (PerkinElmer) on an Olympus IX81 microscope. For data analysis, growth cone outlines were traced in Volocity; fluorescence recovery was calculated from background-corrected intensity measurements by normalizing green fluorescence change ($F - F_0$) as percentage change of fluorescence intensity $(F - F_0)/F_0$, where F_0 is the fluorescence intensity at 0 minutes and F that of the subsequent time points.

DiI Labeling of Retinal Axons

As described [22], embryos were fixed overnight at 4 ºC in 4% paraformaldehyde in

PBS; after a quick wash in PBS, retinal ganglion cell axons were labelled by intraocular injection of the fluorescent carbocyanine DiI ($DiIC_{18}(3)$, Life Technologies). Dye crystals were dissolved in 100% ethanol at ~25 mg/μL and heated to 65 ºC for five minutes before use. Fourteen to twenty hours at 19-22 ºC were allowed for proper diffusion before proceeding. Then, the contralateral (in respect to the dye-injected eye) brain hemisphere was dissected, mounted in 1X PBS and immediately visualized on a Nikon Eclipse TE2000-U inverted fluorescent microscope and photographed with a Hamamatsu ORCA-ER camera. Optic projection length was normalized to the distance between the optic chiasm and the posterior boundary of the tectum, two easily recognizable morphological landmarks on bright-field/red-channel superimposed images; data were subsequently normalized to the mean projection length of the control group.

In Vivo Imaging of Axon Pathfinding

Live imaging of pathfinding retinal axons was performed as documented elsewhere [22]. *tpt1*-MO- or con-MO-injected embryos were electroporated with gap-RFP and/or mt-GFP. Anesthetized embryos, selected on the basis of healthy appearance, were restrained before skin and dura were carefully removed above the contralateral optic tract. They were then transected below the heart and mounted in an imaging chamber consisting of two superimposed Gene Frame adhesive frames (Thermo) on oxygenated Permanox slides (Nunc). Images were acquired every 15 minutes for up to 2 hours using an UltraView VoX spinning disk confocal imaging system on an Olympus IX81 microscope or, alternatively, a Nikon Eclipse 80i setup. Axon outgrowth was analysed with Volocity (PerkinElmer); axons were scored as 'stalled' if their outgrowth was ≤ 10 μm over a 2-hour period.

In Vivo Imaging of Transected Axons

Gap-RFP was delivered by eye-targeted electroporation to wild-type stage 28 embryos, when the first retinal ganglion cell axons have just exited the eye, and axon extension kinetics were analysed 21-24 hours later (stage 37/38), when most axons are growing up the optic tract towards the optic tectum. Just before imaging, the optic nerve was manually transected, and con-MO or *tpt1*-MO was delivered subcellularly by targeted brain electroporation. Of note, transected retinal ganglion cell axons can continue to grow and navigate accurately *in vivo* for up to 3 hours, well within the 1-hour perior of this experiment. Differently from the protocol described above, images were acquired every 15 minutes for up to 1 hour using an a Nikon Eclipse 80i setup.

Analysis of Photoreceptor Degeneration

Transverse retinal sections probed for opsin or rhodopsin and counterstained with DAPI were used, respectively, in cone and rod photoreceptor phenotypic analyses. Photoreceptor inner segment length was taken as the average of the distance between the DAPI signal in the outer nuclear layer (*id est*, photoreceptor cell bodies), and that of the outer segment markers, across a number of points (at least five) in the retinal hemi-circumference. Differently, the number of cells without an identifiable outer segment was normalized to the length of the outer nuclear layer to calculate the percentage of photoreceptor neurons with degenerative phenotypes. Cone and rod analysis were conducted independently, and measurements were made using Volocity (PerkinElmer).

ATP Bioluminescence Assay

As documented [258], paired retinae from stage 37/38 embryos were dissected in 1x Modified Barth's Saline with MS-222 (tricaine methanesulfonate, 0.04% wt/vol). ATP was measured with the ATP bioluminescence kit CLS II (Roche) according to manufacturer's instructions on a Turner Designs luminometer, model TD-20/20. Single retinae were incubated in 50 µL of 1% $HClO_4$ immediately after dissection for precisely 10 minutes at room temperature before the reaction was stopped in 450 µL of boiling Tris buffer (100 mM Tris, 4 mM EDTA, pH 7.75), incubated for 2 minutes at 100ºC, and centrifuged at 1,000 x *g* for 1 minute. The supernant was then transferred to a fresh tube and kept on ice until bioluminescence measurement. In parallel, total protein quantification was assayed on a Qubit 2.0 Fluorometer (Life Technologies) following manufacturer's recommendations. Experimental ATP values were interpolated from a standard curve and normalized to total protein.

Mitochondrial Membrane Potential ($\Delta\Psi_m$) Measurement

Retinal cultures were incubated with 20 nM tetramethylrhodamine, methyl ester (TMRM) at 20ºC for 20 minutes and washed with culture medium before imaging on a Nikon Eclipse TE2000-U (to reduce phototoxicity, lamp fluorescence was limited to 25% and a 0.9 neutral density filter was used). To account for the dependence of F_m on the plasma membrane potential ($\Delta\Psi_p$), $\Delta\Psi_m$ was derived from the ratio of fluorescence intensity between mitochondria (F_m) and mitochondria-poor regions along the axon and in the growth cone (F_c) [259]. Fluorescence measurements were taken by manually tracing mitochondria using Volocity (PerkinElmer); the mitochondria-rich growth cone central domain was analysed as a single unit.

Visualizing Mitochondrial Transport in Cultured Retinal Ganglion Cell Neurons

tpt1-MO- or con-MO-positive retinal explants were incubated with 25 nM MitoTracker Red, a mitochondrion-selective probe, at 20ºC for 20 minutes and, as above, washed with pre-warmed culture medium before imaging on a Nikon Eclipse TE2000-U (to reduce phototoxicity, lamp fluorescence was limited to 25% and a 0.9 neutral density filter was used). Time-lapse imaging was performed immediately after for 5 minutes applying a 5-second interval between each frame. During the analysis process, kymographs were derived for each time-lapse sequence using the KymographTracker module on the freely available Icy image analysis package (created by the Quantitative Image Analysis Unit at the Institute Pasteur). A mobile mitochondrion was only considered as such if its dislocation was ≥ 5 μm over the imaging period [260].

RT-qPCR of Nuclear-encoded Mitochondrial Genes and qPCR Analysis of Mitochondrial DNA Content

All real-time PCR runs were performed using a LightCycler 480 (software release 1.5, Roche). Triplicate 10-μL reaction mixtures were prepared according to manufacturer's instructions (QuantiTect SYBR Green RT-PCR or PCR kits, QIAGEN). RNA purification was performed using RNeasy Mini kit (QIAGEN) and included a DNase-treatment step; QIAamp DNA Micro kit (QIAGEN) was used for DNA purification. Per condition, 7-9 independent samples were collected on different days and each consisted of two retinae dissected from the same embryo (stage 37/38). RNA integrity was assessed on a 2100 Bioanalyzer (Agilent) using a Pico assay. For the quantification of nuclear-encoded mitochondrial genes, reference gene (*ywhaz*, *rps13*, *hprt1* and *tbp1*)[a] normalization was performed using the geNorm module integrated in qbase+ (Biogazelle); the optimal normalization factor was calculated as the geometric mean of reference targets *ywhaz* and *tbp1*; all samples were measured in the same run for a given reference target and statistical analysis was carried out with qbase+. Real-time quantitative PCR mitochondrial DNA content quantification was accomplished with two different primer sets for genomic (glucagon and beta-2-microglobulin) and mitochondrial (mitochondrially encoded tRNA-leucine and ATP synthase 6) loci; efficiency-corrected run analysis was performed within the LightCycler software.

---

a Gene names: *tyrosine 3-monooxygenase/tryptophan 5-monooxygenase activation protein, zeta (ywhaz)*, *ribosomal protein S13* (*rps13*), *hypoxanthine phosphoribosyltransferase 1* (*hprt1*), and *TATA box binding protein* (*tbp1*).

The real-time cycling reaction conditions, as per manufacturer's guidelines, were as follows:

Reverse transcription[a]	30 minutes, 50ºC
PCR Initial Activation Step	15 minutes, 95ºC
Polymerase Chain Reaction (45 cycles)	
Denaturation	15 seconds, 94ºC
Annealing	30 seconds, 57ºC
Extension	30 seconds, 72ºC
Data acquisition	15 seconds, 72ºC
Melting Curve	
1 minutes at 95ºC	
1 minutes at 40ºC	
0.11ºC/second increments from 40ºC to 95ºC and continuous fluorescence readings	

Primary *Rattus norvegicus* Cortex Neuronal Culture and Immunocytochemistry

Foetal neurons derived from cortices of F344 *Rattus norvegicus* E18.5 embryos were obtained commercially from Cyagen Biosciences (dispensed as cryopreserved primary cells), and plated on culture dishes pre-coated with poly-L-lysine (15 μg/mL, Sigma) and laminin (15 μg/mL, Sigma, incubated overnight at 4ºC). Neuronal cultures were grown at 37 ºC in a 5% CO_2 humidified incubator in OriCell Neuron Growth Medium (Cyagen Biosciences) supplemented with L-alanyl-L-glutamine (Life Technologies) and B-27 (Life Technologies) for at least 72 hours before further manipulation. Growth medium was replaced every 36 hours. Immediately before fixation (pre-warmed 4% paraformaldehyde in 1X PBS), cells were washed twice in pre-warmed 1X PBS. After washing the fixative with 1X PBS containing glycine at a 10 mM concentration, cells were permeabilized for 10 minutes with a 0.03% Triton X-100 solution (diluted in PBS). Standard immunocytochemistry protocols were followed henceforth[b]. Alexa

a This step was omitted for qPCR runs.

b Blocking solution: 5% heat-inactivated goat serum in 1X PBS; primary antibodies: anti-Tctp (1:400, Santa Cruz Biotechnology), anti-Mcl1 (1:100, Santa Cruz Biotechnology), and anti-Bcl-X_L (1:100, Santa Cruz Biotechnology), incubated overnight.

Fluor secondary antibodies (Life Technologies) were used at 1:1000. Laser scanning confocal imaging was performed using an Olympus FV1000 microscope.

In situ Proximity Ligation Assay (PLA)

Duolink (Olink Biosciences, distributed by Sigma) *in situ* proximity ligation assays were performed on rat cortex neuronal cultures according to manufacturer's recommendations. Up until the primary antibodies incubation step, all manipulations were performed as detailed above for the immunocytochemistry procedure. The following primary antibody pairs were used: mouse anti-Tctp (1:400, Santa Cruz Biotechnology) and rabbit anti-Mcl1 (1:100, Santa Cruz Biotechnology); mouse anti-Tctp (1:400, Santa Cruz Biotechnology) and rabbit anti-Bcl-X_L (1:100, Santa Cruz Biotechnology). Additionally, a blocking/competition Tctp peptide (Santa Cruz Biotechnology), used at a five-fold excess relative to the anti-Tctp antibody, was included in preliminary experiments to evaluate the specificity of the technique. After overnight primary antibody incubation at 4ºC, all stages of the protocol – except for the washing steps – were performed at 37ºC in a humidity chamber using no more than 100 µL per culture dish. Of note, instead of the supplied probe diluent, mouse and rabbit PLA probes were dispensed in blocking solution. All washes prior to the ligation step utilized PBS; the last wash steps initially included Texas Red-Phalloidin (Life Technologies, incubated for 15 minutes at a 1:40 dilution). Cultures were mounted using a minimal volume of Duolink *In Situ* Mounting medium, which incorporates DAPI in its formulation, and imaged using an UltraView VoX spinning disk confocal imaging system on an Olympus IX81 microscope.

Western Blot

Stage 35/36 eye and/or brain lysates were prepared in ice-cold RIPA buffer (150 mM NaCl, 1% NP-40, 0.5% sodium deoxycholate, 0.1% SDS, 50 mM Tris, pH 8.0) and resolved by SDS-PAGE. Both 'semi-dry' and 'wet' electroblotting methods were applied, depending on the size of the target to be analysed. Nitrocellulose membranes were blotted using the following primary antibodies: rabbit anti-Tctp (1:5000, gift from J. Kubiak); anti-4EBP1 and anti-$p_{T37/46}$4EBP1 (1:2000 and 1:1000, respectively, Cell Signaling); anti-rpS6 (1:500, Abcam) and anti-$p_{S235/236}$S6 (1:4000, Upstate); anti-Akt (1:1000, Cell Signaling); anti-Pgc1α (1:500, Aviva Systems Biology). HRP-conjugated secondary antibodies (Abcam) were used in combination with a chemiluminescence-based detection system (Amersham ECL, GE Healthcare). To evaluate the

efficiency of *tpt1* shRNA knockdown in HCT116 cell lines, a commercial anti-Tctp antibody from Santa Cruz Biotechnology was used (1:500).

Statistical Analysis

Each experiment was repeated at least three times, unless otherwise stated. Details of statistical analysis for each experiment are provided in figure legends. Data were analysed in Prism 5 (GraphPad), except Real-time PCR data. For all experiments, a statistical significance threshold of $\alpha = 0.05$ was used.

Table 1. List of PCR primer sequences

Gene	Primer sequence (5' → 3')	Purpose
tpt1	CCACCATACCATCGGGGTTCATTCTTTC	5' RACE
	CAAACACATCCCATCGGGGGTTTC	'Nested' 5' RACE
	GGGATGTGTTTGGAAGTTGAAGGCAAGG	3' RACE
	ACAGGCTTCACCAAGGACTCTTAC	'Nested' 3' RACE
actb	CCTGTGCAGGAAGATCACAT	RT-PCR (axonal RNA purity assessment)
	TGTTAAAGAGAATGAGCCCC	
hist1h4a	AAAAGGACTGGGGAAAGGAGGCGCCA	RT-PCR (axonal RNA purity assessment)
	CGGTCTTCCTCTTGGCGTGTTCTGTG	
map2	CGATCATCCTTGCCAAGACCTTCCTC	RT-PCR (axonal RNA purity assessment)
	GCGACCTGGAGATTGGGTGATGATTT	
tpt1 5'UTR	TCAGCAGAATTCCCTTTTCTCTCCCCACCCTCCG	Cloning of Kaede constructs
	TCGCGTGGATCCGTTGGCGGCCTAAGTGTTGTAATG	
tpt1 3'UTR	CGCACTGCAGCATTCCGTTTGGTTCTTCCATCTT	
tpt1-S 3'UTR	GGGCCCATATGACAGTGGAGAATCATGGGCTTTAT	
tpt1-L 3'UTR	CGCGGCCATATGTTGTTTAATTCTGTCTTTATTCAGGATC	
T3 promoter + *tpt1* 5'UTR	AATTAACCCTCACTAAAGGCCTTTTCTCTCCCCACCCTCCG	
tpt1 coding sequence	TCCAAAGAGAAGAAGGTGCAA	RT-qPCR analysis of *tpt1* expression
	CTTGGTGAAGCCTGTTTCCT	
tpt1-L unique region	AGAAGCGGACCTTCAGTTTG	RT-qPCR analysis of *tpt1* expression
	CCTTCACGGCCAGAAGTATT	
actb	TACTCTTTTGTTGGCGCTTG	RT-qPCR analysis of *tpt1* expression (Reference gene)
	GGGCAACACTGAGAGGGTAG	
Renilla luciferase	CCAGGATTCTTTTCCAATGC	MS2-BioTRAP RT-qPCR
	TTGAGAACTCGCTCAACGAA	
Firefly luciferase	AACACCCCAACATCTTCGAC	
	TCGCGGTTGTTACTTGACTG	

(continued on next page)

(continued)

cox5a	GCCGTCTGCAGTCTGTCTC TCAGTTCCCAGGCATCAATA	Nuclear-encoded mitochondrial gene RT-qPCR
idh3a	TCTTTGCGCAGGTCTAATTG GAAGAAGAGCAGTGGGGTTG	Nuclear-encoded mitochondrial gene RT-qPCR
rhot1 (*miro1*)	TGTACGACGGAGCTAAACCA TTAACATCAGGACCCCAAGG	Nuclear-encoded mitochondrial gene RT-qPCR
cycs (cytochrome c, somatic)	CCTAAGAAGTACATTCCTGGAACAA ATTAACTGGAGGTTGACTGTTTGAG	Nuclear-encoded mitochondrial gene RT-qPCR
hprt1	CCCTGCATTGTGATTCAAGA ATATCTCGAGCCAGCCTTTC	Nuclear-encoded mitochondrial gene RT-qPCR (Reference Gene)
tbp1	GAAGAAAGCTGGTCAACAGGA GGGACTCCTTACAGTACCCAGA	Nuclear-encoded mitochondrial gene RT-qPCR (Reference Gene)
rps13	CTTCAAACTGGCCAAGAAGG GGCCAGAGCCTTAGACTTGA	Nuclear-encoded mitochondrial gene RT-qPCR (Reference Gene)
gcg (glucagon)	TGATTCAGAACAGCTCAAGGAA AGCCCGTCTGGAGTCTAGGTA	Mitochondrial DNA Content Analysis (Nuclear DNA)
b2m (beta-2-microglobulin)	AATGAGGTGATCTGCTACGTGT TTCCAGTTATGTTGGAATGAGG	Mitochondrial DNA Content Analysis (Nuclear DNA)
ATP synthase F0 subunit 6	CCTGAAGGAACACCAACACC TAGCAGTAAGTCGAACTCCAAGG	Mitochondrial DNA Content Analysis (Mitochondrial DNA)
mtDNA-tRNA-leucine	AATAGGGCATTAGCGACAGC GTGGCATATCATTAAGGGTGGT	Mitochondrial DNA Content Analysis (Mitochondrial DNA)
pgc1a	ATCTGGGTGTTGATCCAAGTGACG CAGTCCCCAGTCACATGACAAAGC	*H. sapiens pgc1a* promoter cloning

3. Results

A – Expression and Regulation of *tpt1*

A.1 *tpt1* is an Abundant Axonal Transcript

I initially sought to validate that *tpt1* transcripts localize to retinal axons and growth cones. *In situ* hybridization of retinal sections showed robust staining in the optic fiber layer (OFL) and in the optic nerve head (ONH), axon-only structures where retinal ganglion cell (RGC) axons collect to exit the eye, indicating that *tpt1* mRNA is expressed in retinal axons *in vivo* **(Figure 3.1A)**. Similarly, in cultured eye explants, I detected *tpt1* mRNA signal in the growth cone of retinal ganglion cell axons **(Figures 3.1D and 3.1E)**. Next, I examined the expression of Tctp protein with a specific antibody against *Xenopus laevis* Tctp [261]; in concordance with *tpt1* mRNA localization, Tctp protein was also detected in the OFL and ONH **(Figure 3.2A)**. Immunostaining on cultured embryonic retinal ganglion cell axons and growth cones confirmed these observations **(Figure 3.2B)**. Ample mRNA and protein signals were also found in the inner and outer plexiform layers (IPL and OPL, respectively), suggestive of localization in the dendrites of retinal ganglion cells and neurites of other retinal neurons **(Figures 3.1A and 3.2A)**. Apart from the retinal neuropil, *tpt1* expression was noticeable in the photoreceptor layer, and in the ciliary marginal zone (CMZ), a well-characterized retinal neurogenic niche **(Figures 3.1A and 3.2A)**. Also of note, *tpt1* mRNA signal was observed in the brain and, particularly, along the optic tract region, where retinal ganglion cell axons navigate en route to the optic tectum, their main synaptic target **(Figure 3.1B)**.

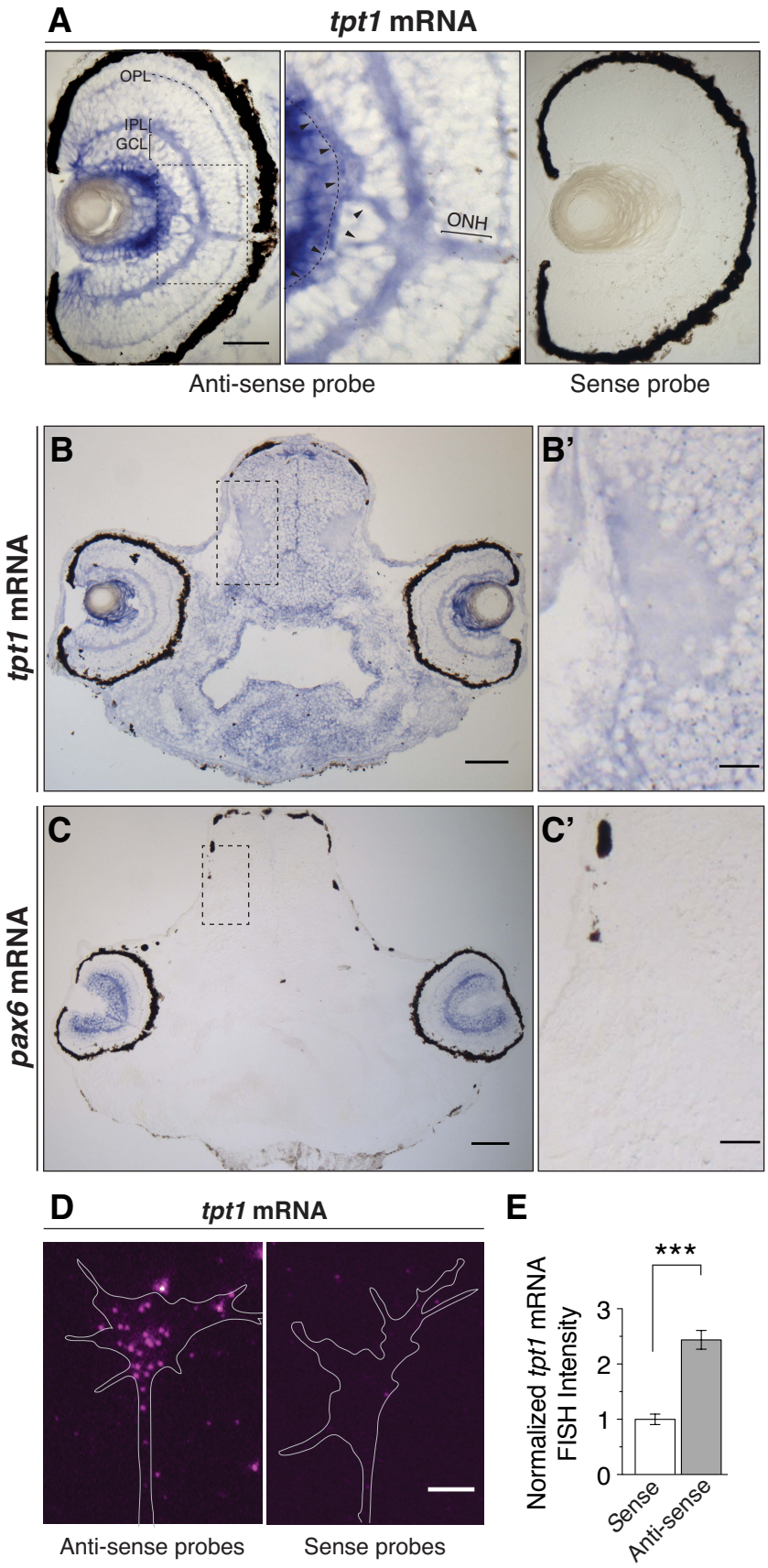

Figure 3.1 – *tpt1* mRNA is expressed in retinal ganglion cell axons and growth cones. (A) *In situ* hybridization (ISH) detection of *tpt1* mRNA on coronal sections of stage 43 retinas (GCL: ganglion cell layer; ONH: optic nerve head; IPL/OPL: inner/outer plexiform layer; arrowheads indicate the optic fiber ▶

layer, OFL). (B and C) ISH detection of *tpt1* and *pax6* mRNAs on coronal sections of stage 43 embryos. The boxed areas, which focus on the lateral surface of the mesencephalon through where retinal axons pass en route to the optic tectum, are shown at a higher amplification in B' and C'. Note the striking contrast between the distribution pattern of *tpt1* and *pax6* mRNAs, the latter encoding for a transcription factor abundantly expressed by retinal ganglion cells [9]. (D and E) ISH detection of *tpt1* mRNA in retinal ganglion cell axons of cultured eye explants (mean ± SEM; *** $P < 0.0001$, one-way ANOVA and Bonferroni). Scale bars: 50 µm in A, 25 µm in B and C, and 5 µm in D.

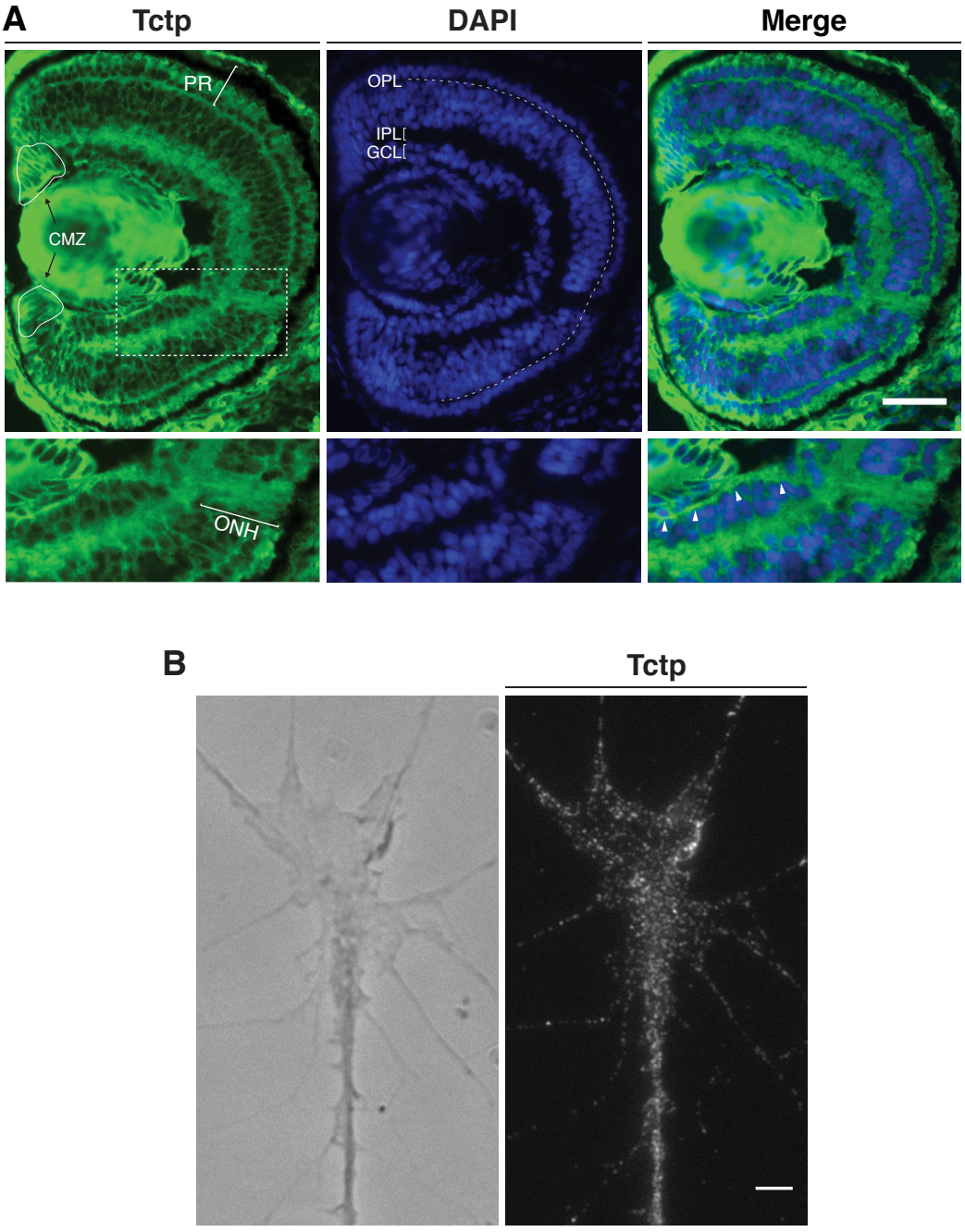

Figure 3.2 – Tctp is expressed in retinal ganglion cell axons and growth cones. (A) Coronal section of stage 43 retina probed for Tctp (CMZ: ciliary marginal zone; PR: photoreceptor layer; arrowheads indicate the OFL). (E) Retinal ganglion cell growth cone stained for Tctp. Scale bars: 50 µm in A, and 5 µm in B.

The human *tpt1* gene is transcribed into two distinct mRNA variants that differ only in the length of their 3' untranslated regions (UTRs) [168]. Since most mRNA regulatory elements, including those that govern subcellular localization and translation, are situated within the untranslated regions [136], I next investigated whether *tpt1* is regulated in an analogous manner in *Xenopus laevis*. Using rapid amplification of 5' and 3' cDNA ends (5' and 3' RACE), two 3'UTR variants of *tpt1* were obtained from eye RNA extracts, comprising a short (*tpt1*-S, 210 bases) isoform and a longer (*tpt1*-L, 607 bases) version, overlapping in its entirety the short form and possessing a unique segment at its 3'-end **(Figure 3.3A)**. Similar to *Homo sapiens*, the exon encoding the 3'UTR in *Xenopus laevis* contains two alternative polyadenylation signals, resulting in transcripts with 3'UTRs of different length but encoding for the same protein **(Figure 3.3B)**. Concomitantly, a single 5'-end was identified, and, as described in *Homo sapiens*, its complete sequencing revealed the existence of a 5'-terminal oligopyrimidine (TOP) motif previously not detected in *Xenopus laevis* **(Figure 3.4)**. In addition, sequence alignment of representative vertebrate species uncovered a highly conserved motif (38 bases) within the 3'UTR of *tpt1*-S, with 79% absolute sequence conservation between *Xenopus laevis* and *Homo sapiens*, and up to 85% between *Homo sapiens* and *Mus musculus* **(Figure 3.5)**. Collectively, these results show that *Xenopus laevis tpt1*, like its human counterpart [168], generates two different mRNA variants, and suggest that *tpt1*, in addition to encoding for a highly conserved protein [16], has remained appreciably unchanged throughout vertebrate evolution.

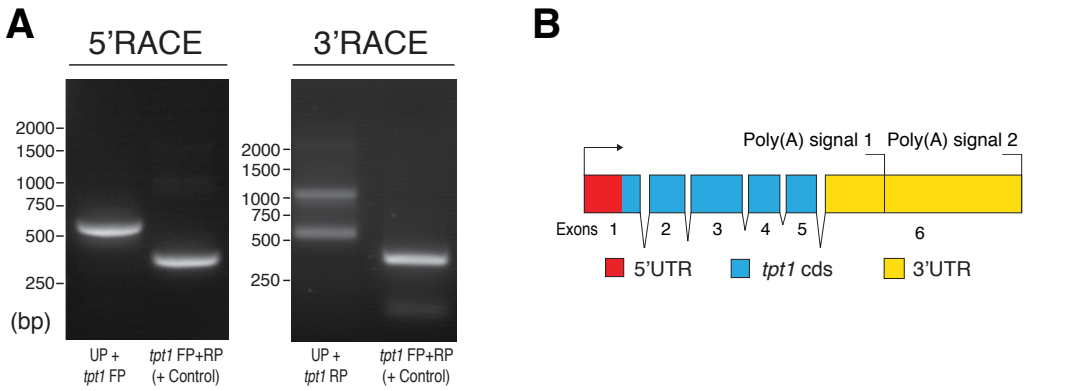

Figure 3.3 – *tpt1* gives rise to two different mRNA isoforms in *Xenopus laevis*. (A) 5' (left) and 3' (right) RACE amplifications of *tpt1* mRNAs using retinal RNA extracts (FP, forward primer: RP; reverse primer; UP, universal primer; NUP, nested universal primer). (B) Organization of the *tpt1* gene in *Xenopus laevis* (cds, coding region; poly(A), polyadenylation).

Figure 3.4 – *tpt1* is a 5'-TOP mRNA. First 25 nucleotides of the *Xenopus laevis tpt1* 5'UTR.

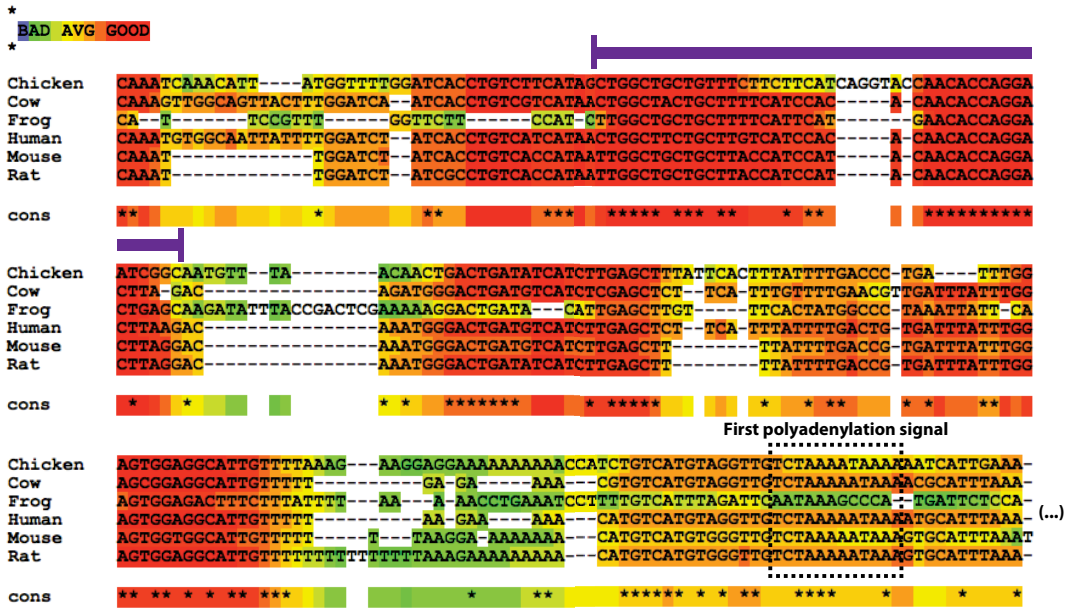

Figure 3.5 – Conserved sequence motif in *tpt1* 3'UTR. (A) *tpt1* 3'UTR multi-species sequence alignment using T-Coffee. Purple line demarks a particularly well-conserved segment within the 3'UTR of the six vertebrate species analysed. The boxed area denotes the location of the first polyadenylation signal (AATAAA).

Differential processing at multiple polyadenylation sites is known to be physiologically regulated in development or by pathological events such as cancer, and can affect the localization and translational properties of the mRNA [262]. For instance, the longer *importinb1* transcript, equally arising from alternative polyadenylation, harbours a signal that enables axonal localization and is specifically required for efficient retrograde signaling in injured axons [153]. I thus explored whether a similar mechanism governed *tpt1* localization in retinal ganglion cell axons. To directly address this, I used laser-capture microdissection (LCM) to harvest axonal extracts [12], a procedure much simplified by retinal ganglion cells being the sole projecting neurons of the eye **(Figure 3.6A)**. To determine whether this approach successfully collected a pure pool of axonal mRNAs, I tested for the presence of mRNAs encoding nuclear proteins, such as histone H4 (*hist1h4a*), and for transcripts described in dendrites but not in axons, such as microtubule-associated protein-2 (*map2*); vitally, no amplification products

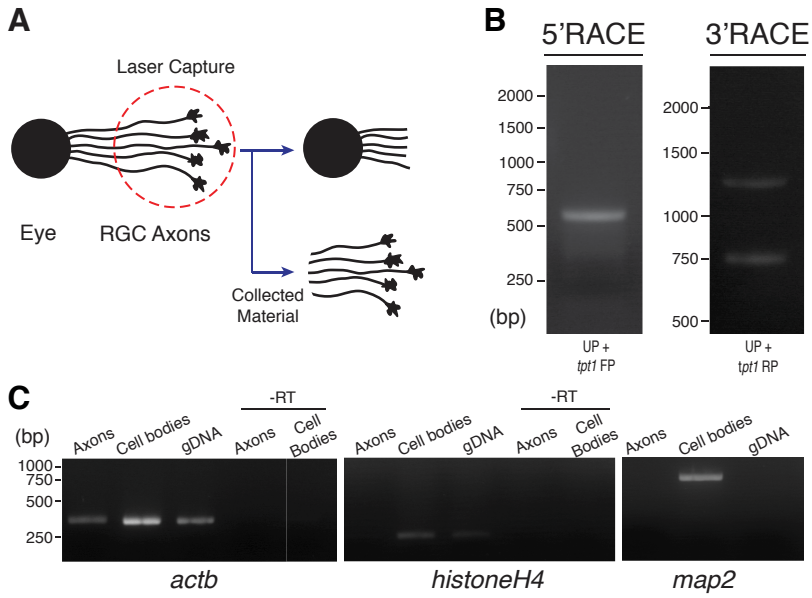

Figure 3.6 – *tpt1*-S and *tpt1*-L localize in retinal ganglion cell axons. (A) Diagram of laser-capture microdissection procedure. (B) 5' (left) 3' (right) RACE amplifications of *tpt1* mRNAs using laser-captured axonal extracts. (C) RT-PCR assessment of laser-captured material. –RT, RNA samples not reverse transcribed; –RGC, retinal ganglion cell.

were detected by RT-PCR (reverse transcription-PCR). By contrast, *actb*, which encodes for β-actin, a transcript previously identified in axons and growth cones [254], was readily amplified, confirming purity **(Figure 3.6C)**. Notably, sequence reads from 5' and 3' RACE reactions using retinal ganglion cell axonal extracts were identical to those obtained from whole eye preparations, implying that both isoforms localize in these axons **(Figure 3.6B)**.

Given the inherent qualitative outcome of RACE PCR, I next employed quantitative RT-PCR (RT-qPCR) to complement my analysis. Specifically, two sets of primers were designed: one directed to a segment of the *tpt1* protein coding region, and a second pair targeting part of the unique region of *tpt1*-L, thus allowing for a direct quantification of this variant **(Figure 3.7A)**. In whole eye extracts, an approximately constant 9:1 *tpt1*-S to *tpt1*-L ratio was obtained in all developmental stages examined. Differently, a striking ~16:1 *tpt1*-S to *tpt1*-L ratio was measured in axonal extracts, indicating that the *tpt1*-S variant is locally enriched in the axonal compartment **(Figure 3.7B)**. Moreover, a near 10-fold ($\Delta Cq_{tpt1:actb}$ = 3.1) enrichment over *actb* mRNA was detected in axons **(Figure 3.7C)**, attesting *tpt1* as a highly abundant transcript in axons. Therefore, unlike other instances where the longer mRNA variants are predominant in neuronal processes [11, 153, 263], these data suggest there is a significant prevalence of the shorter *tpt1* transcript in the axonal compartment.

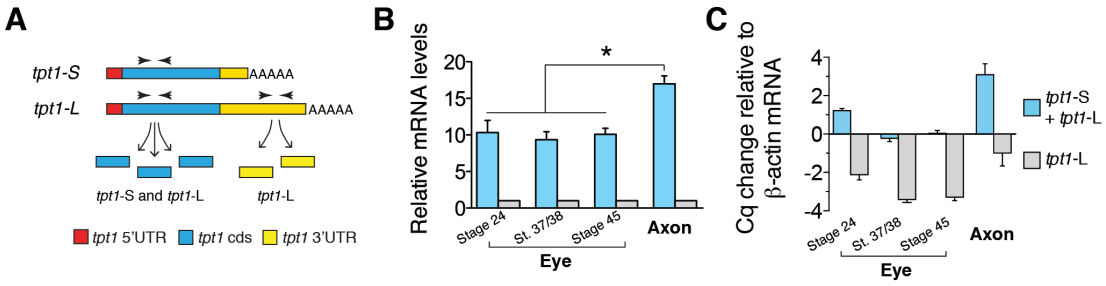

Figure 3.7 – *tpt1*-S is an abundant axonal transcript. (A) RT-qPCR experimental design. (B and C) Axonal and whole-eye content of *tpt1* mRNAs analysed by RT-qPCR and normalized to *actb* expression. In (B), data are plotted as *tpt1*-S + *tpt1*-L and to *tpt1*-L ratios (P = 0.0175, one-way ANOVA), whereas in (C) the quantification cycle (Cq) difference relative to *actb* is shown.

A.2 Netrin-1 Triggers a Translation-dependent Rise in Growth Cone Tctp

The axonal enrichment of *tpt1* transcripts raises the question of whether Tctp protein is synthesized locally in embryonic growth cones. Moreover, previous studies have demonstrated that 5'-TOP-bearing mRNAs are selectively regulated at the translational level by the mTOR complex 1 (mTORC1) in a growth-dependent manner [171], raising the possibility that Tctp growth cone levels can be regulated by guidance cues that activate this signaling pathway. Since Netrin-1 can trigger protein synthesis locally in an mTORC1-dependent manner [144], I reasoned it might specifically regulate *tpt1* mRNA translation in growth cones.

To test this, I initially performed 5-minute Netrin-1 stimulations in cultured eye explants, and used quantitative immunofluorescence (QIF) to examine growth cone Tctp levels. This approach revealed a ~20% increase in the average pixel intensity per unit area in Netrin-1-treated growth cones compared to controls **(Figures 3.8A and 3.8B)**. In parallel, both cycloheximide (CHX), an inhibitor of translation elongation, and rapamycin, an mTORC1 inhibitor, prevented the increase in Tctp signal when applied acutely before the Netrin-1 stimulus **(Figures 3.8A and 3.8B)**. Collectively, these results suggest that Tctp growth cone levels are rapidly regulated by Netrin-1, and that this event is protein synthesis- and mTORC1-dependent[a].

Next, to test directly whether the *tpt1* UTRs drive the synthesis of new protein in response to Netrin-1, I generated Kaede fusion constructs flanked by the 5'UTR and 3'UTRs of *tpt1* (henceforth termed Kaede-S and Kaede-L) **(Figure 3.9A)**. Kaede protein is originally green but can be irreversibly converted to the red form by ultra-violet illumination, thereby allowing for the distinction of new and pre-existing protein [5].

---

[a] Note that the small size of Tctp likely facilitates the swift build-up of its local pool.

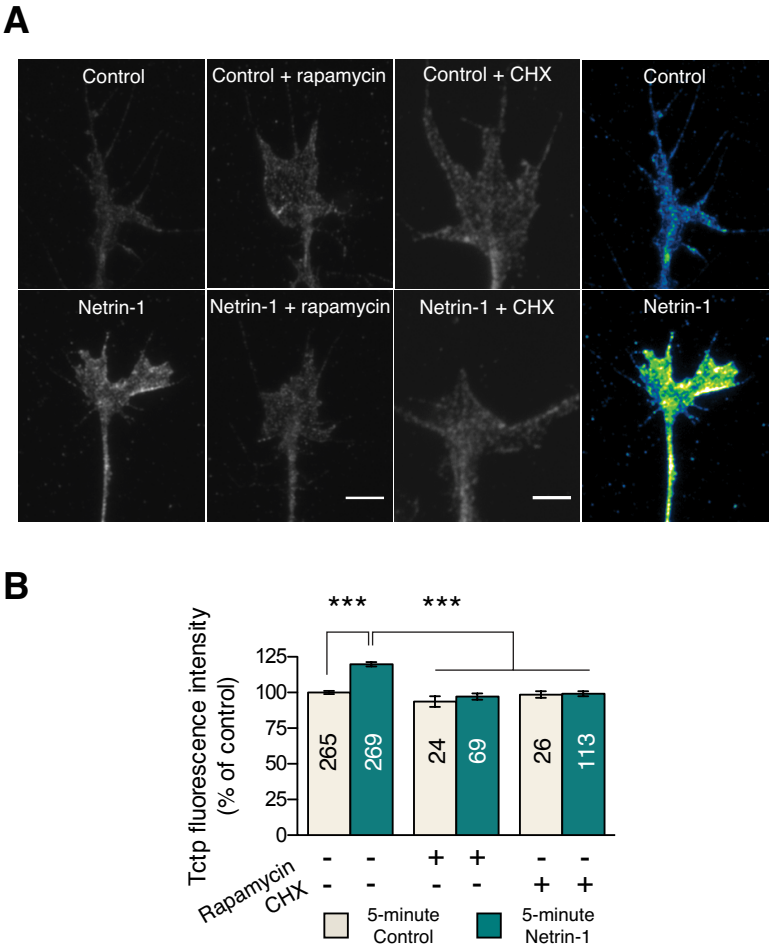

Figure 3.8 – Protein synthesis-dependent rise in Tctp in Netrin-1-treated growth cones. (A and B) Retinal explants were stimulated with Netrin-1 for 5 minutes and stained for Tctp. Netrin-1 induced an increase in growth cone Tctp mean intensity signal relative to control, and this effect was prevented by rapamycin or cycloheximide pre-treatment (mean ± SEM; *n* = no. of growth cones analysed; *** $P <$ 0.0001, Kruskal-Wallis test). Scale bars 5 µm.

Unstimulated, vehicle-treated Kaede-S- or Kaede-L-positive growth cones showed no green fluorescence recovery over the 30-minute course of these experiments **(Figure 3.9B and data not shown)**. However, in Kaede-S-expressing neurons, Netrin-1 significantly increased the reappearance of green signal within 10 minutes of stimulation. Notably, the Netrin-1-induced return of green fluorescence was blocked by cycloheximide added prior to photoconversion, denoting the synthesis of new protein **(Figures 3.9B and 3.9C)**. Furthermore, as this elevation in Kaede-green occurred in axons disconnected from their cell bodies, I excluded soma-derived protein as a possible source of new protein. By contrast, even upon stimulation with Netrin-1, I detected no resurgence of green signal in neurons expressing Kaede-L **(Figures 3.9B and 3.9D)**. Collectively, these data indicate that the 3'UTR of *tpt1*-S can direct the local translation of new pro-

tein in response to Netrin-1. Also, they imply that the *tpt1*-S isoform is the sole origin of the *de novo* synthesized Tctp protein observed upon Netrin-1 stimulation. These findings thus suggest that the longer 3'UTR harbours Netrin-1-insensitive regulatory motifs, while not excluding that different cues or cellular conditions may activate its translation. In fact, *tpt1*-L transcripts are predicted to possess many additional stem-loop structures and miRNA-binding sites within the unique region of its 3'UTR **(Figures 3.10A, 3.10B and 3.11)**, and may therefore associate as part of different ribonucleoprotein particles (mRNPs). Notably, both in *Xenopus laevis* and *Homo sapiens*, the *tpt1* 5'-TOP motif shares complementarity and is predicted to associate with a stretch

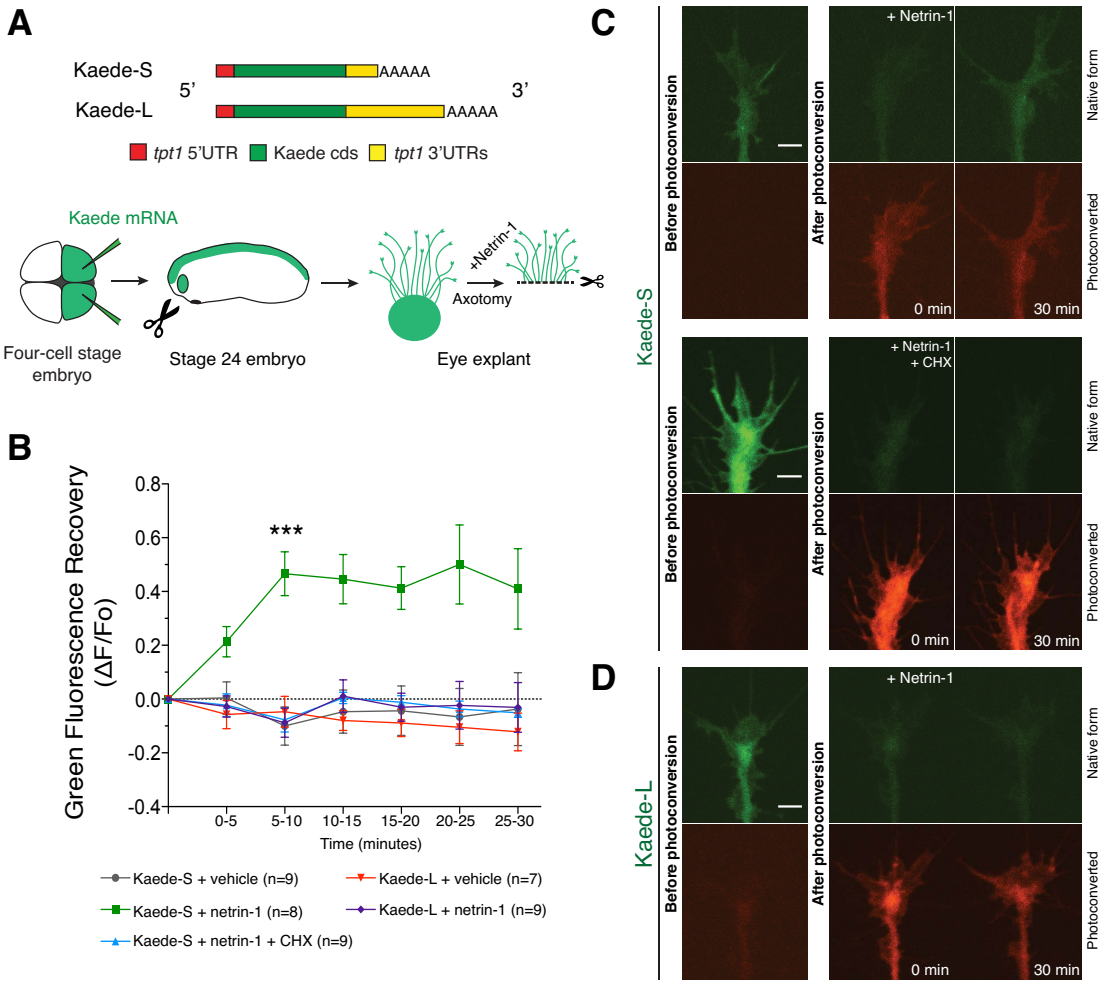

Figure 3.9 – mRNA isoform-specific Tctp upregulation in Netrin-1-treated growth cones. (A) Schematic Kaede constructs and experimental design. (B) Quantification of green fluorescence recovery over multiple time-lapse sequences (*** $P < 0.0001$, two-way ANOVA and Bonferroni). (C and D) Pre- and post-photoconversion images of severed axons expressing Kaede-S or Kaede-L. Fluorescence recovery in response to Netrin-1 was only observed in Kaede-S-expressing neurons, and this effect was prevented by cycloheximide pre-treatment. Scale bars: 5 µm.

of nucleotides located in the unique region of the *tpt1*-L's 3'UTR **(Figure 3.12)**. Thus, it is possible that, in combination with other post-translational regulatory mechanisms, the steric hindrance that such conformation confers to the 5'-TOP motif serves as an additional regulatory layer, rendering this isoform insensitive to mTORC1-activating cues such as Netrin-1. In any case, it is important to stress that these *in silico* data lack any concrete experimental support.

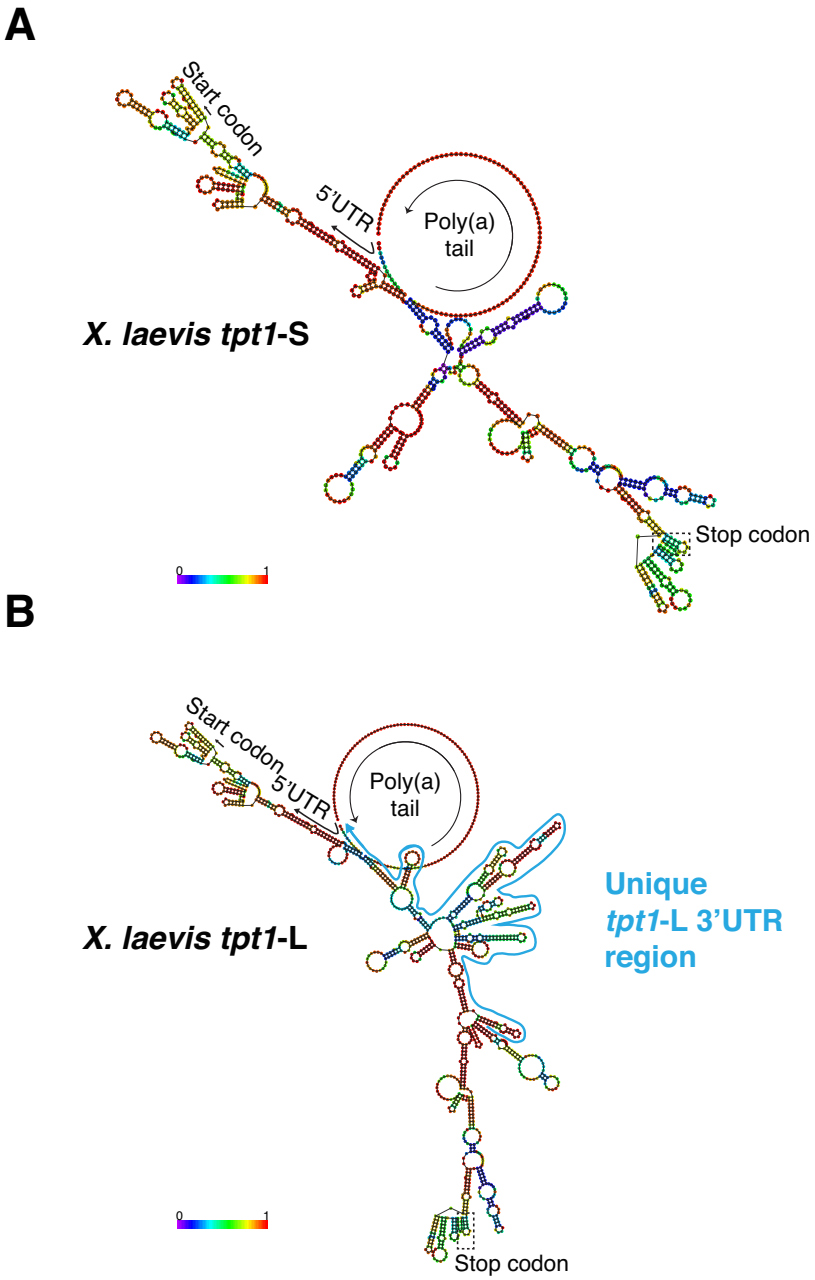

Figure 3.10 – *tpt1* encodes highly structured mRNAs. (A) *Xenopus laevis tpt1*-S and *tpt1*-L secondary structure prediction using the online RNAfold server. The structures are colored by base-pairing probabilities, with pale-colors indicating low base-pairing probabilities. For unpaired regions, the color denotes the probability of being unpaired. The unique segment of the *tpt1*-L 3'UTR is highlighted in light blue. The location of the main RNA landmarks, such as start and stop codons, is also indicated.

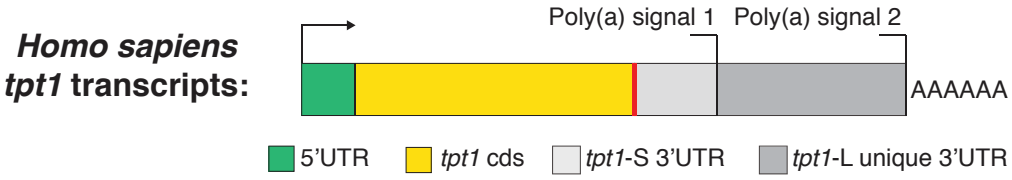

	Selected miRNAs Targeting *H.sapiens tpt1* mRNAs as Predicted by miRNA_targets[a]		Energy[b]	
Common to both *tpt1*-S and *tpt1*-L transcripts	**miR-125a-3p**	miR: 3' ccgaggguUCUUGG-AGUGGACa 5' *tpt1*: 5' auuauuuuGGAUCUAUCACCUGu 3'	-17.96	
	miR-147a	miR: 3' cgucuucguaaAGGUGUGUg 5' *tpt1*: 5' ucugcuugucaUCCACACAa 3'	-13.32	
	miR-489	miR: 3' cgaCGGCAUAUAC--ACUACAGUg 5' *tpt1*: 5' uaaGACAAAUGGGACUGAUGUCAu 3'	-12.24	
	miR-27a/b	miR: 3' cgccuUGAAUCGG--UGACACUu 5' *tpt1*: 5' ucuucAUUUAUUUUGACUGUGAu 3'	-10.56	Validated interaction[c]
	miR-519a-3p	miR: 3' ugugAGAUUU---UCCUACGUGAAa 5' *tpt1*: 5' guugUCUAAAAAUAAAAUGCAUUUa 3'	-11.91	
	miR-519b-3p	miR: 3' uuggAGAUUU---UCCUACGUGAAa 5' *tpt1*: 5' guugUCUAAAAAUAAAAUGCAUUUa 3'	-11.91	
	miR-519c-3p	miR: 3' uaggAGAUUU---UUCUACGUGAAa 5' *tpt1*: 5' guugUCUAAAAAUAAAAUGCAUUUa 3'	-14.27	
tpt1-L transcript specific	**miR-32-3p**	miR: 3' uuUAUAGUGU--GUGUGAUUUAAc 5' *tpt1*: 5' uaAUG-CAUAUUUAAACUAAAUUg 3'	-15.16	
	miR-103a-2-5p	miR: 3' guucCGUCGUGA-CAUUUCUUCGa 5' *tpt1*: 5' uccuGUAGUGUUCCUGGAGAAGCu 3'	-18.21	
	miR-29a-5p	miR: 3' gaCUUGUGGUUUUCUUUAGUca 5' *tpt1*: 5' ugGAAUAUAAAAAAGAAUCAaa 3'	-11.44	
	miR-204-5p	miR: 3' uccguAUCCUAC--UGUUUCCCUu 5' *tpt1*: 5' gauuuUGAGuuGCAAUAAAGGGAa 3'	-13.46	
	miR-96-5p	miR: 3' ucguuuuuacaCGAUCACGGUUu 5' *tpt1*: 5' ccaugcucauaGC-AGUGCCAAc 3'	-13.75	
	miR-181a-2-3p	miR: 3' ccaUGUCAGUUGCCAGUCACCa 5' *tpt1*: 5' aaaAGAGAC-UCAUUCAGUGG- 3'	-11.48	

[a] miRNA_Targets online server uses both miRanda and RNAhybrid for miRNA predictions.

[b] Free energy (kcal/mol) calculated by miRanda algorithm.

[c] Lo, W.Y., Wang, H.J., Chiu, C.W., and Chen, S.F. (2012). miR-27b-regulated TCTP as a novel plasma biomarker for oral cancer: from quantitative proteomics to post-transcriptional study. Journal of proteomics 77, 154-166

Figure 3.11 – miRNAs predicted to bind *tpt1*-S and *tpt1*-L 3'UTRs. Selection of *in silico*-predicted miRNAs targeting *Homo sapiens tpt1* mRNAs. The online 'miRNA_targets' portal (developed by Amit Kumar and Christophe Lefevre, Deakin University, Australia) used in this analysis employs the miRanda and RNAhybrid algorithms in its predictions.

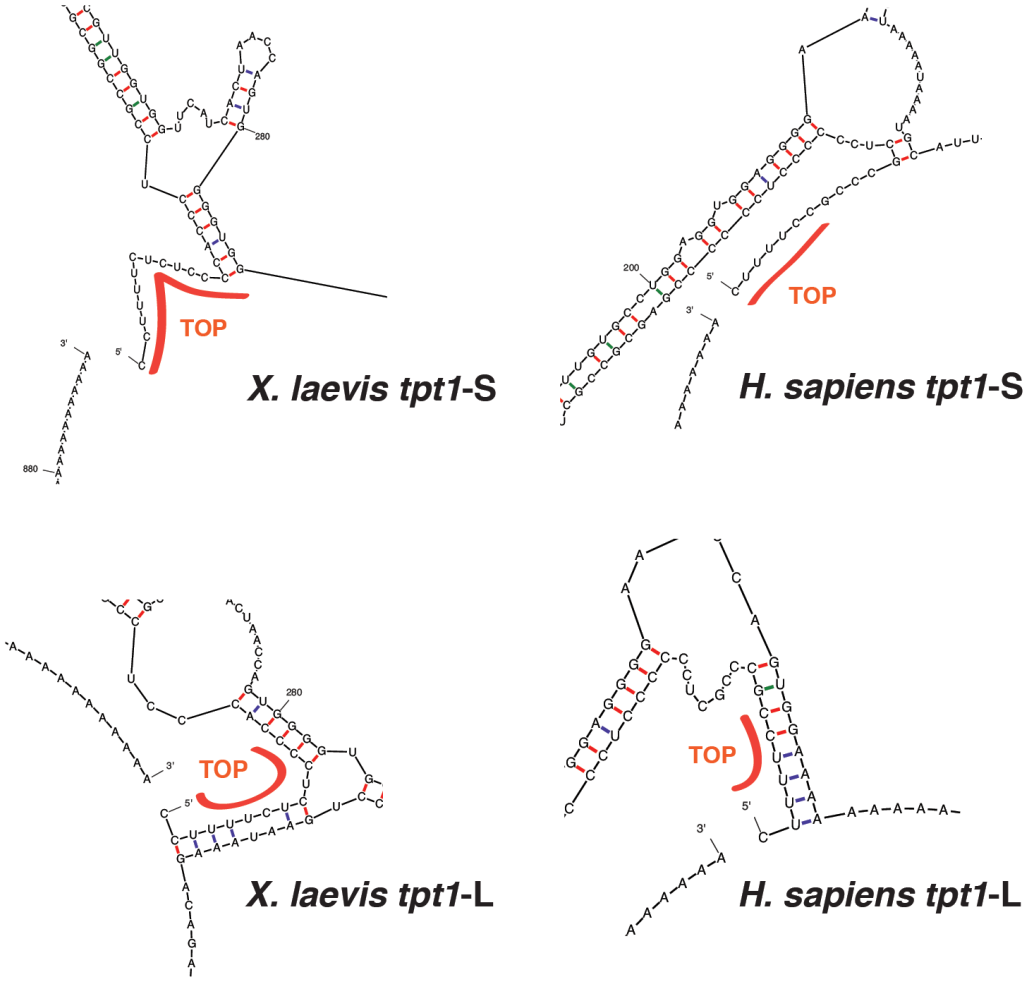

Figure 3.12 – Hypothetical mechanism for the differential regulation of *tpt1* isoforms observed in Netrin-1-treated growth cones. The most stable conformation for *Xenopus laevis* and *Homo sapiens* *tpt1*-L mRNAs is predicted to permit the association between the 5'-TOP motif and a complementary segment exclusive to the *tpt1*-L 3'UTR. Note that the 5'-TOP-complementary segment is not identical in *Xenopus laevis* and *Homo sapiens*; likewise, the 5'-TOP motif in *tpt1* transcripts is not conserved between the two species. This *in silico* structure prediction was generated using the online RNAfold server [264].

A.3 Profiling of *tpt1* mRNA Interacting RNA-binding Proteins

Trans-acting RNA-binding factors, such as RNA-binding proteins and miRNAs, dictate the post-transcriptional fate of mRNAs in terms of their stability, transport, subcellular localization, and translational control [137]. Thus, the profiling and characterization of these factors assumes extraordinary relevance towards an integrated understanding of RNA expression and, in a broader sense, the biology of the cell. If effective prediction criteria used in computational screens for miRNA binding sites have greatly aided the discovery of valid miRNA targets [265], the number of well-defined RNA consensus sequences/motifs for RNA-binding proteins has remained minute. This is, in large part, due to the fact that the secondary structure of the RNA, and not only the linear sequence

of nucleotides, influences its association with protein *trans*-acting factors [266]. On the other hand, the dynamic nature of RNA-protein interactions has proven their comprehensive identification challenging at best. Furthermore, most methodologies employed in the study of RNA-binding proteins use a candidate approach, in that prior knowledge of a particular RNA-binding protein is required for its interactome to be investigated. Such limitations are, however, incompatible with an unbiased analysis of the interactome of a specific mRNA.

Given the inexistence of RNA-binding proteins known to associate with *tpt1* transcripts, I made use of a recently developed RNA-centric approach – MS2 *In Vivo* Biotin Tagged RNA Affinity Purification (MS2-BioTRAP) [256] – in order to elucidate the protein composition of *tpt1* mRNP complexes. In this methodology, a chimeric gene encoding the RNA of interest (or part of it, such as the UTRs) tagged with tandem repeats of stem-loop motifs specifically recognized by the MS2 bacteriophage coat protein is co-expressed '*in-vivo*' with a modified MS2 coat protein [267] [a,b,c]. This allows for the MS2 coat protein, along with the *MS2*-stem-loop tagged RNA that it binds to, as well as any associated RNA-binding protein, to be effectively and rapidly collected by affinity purification. In the last phase of the strategy, the purified RNA-protein complexes are subjected to a SILAC-based quantitative proteomic analysis [268].

I constructed a *tpt1*-derived target for the bacteriophage MS2 coat protein by cloning the *Homo sapiens tpt1*-S 3'UTR (208 base pairs) downstream of the coding sequence of the sea pansy (*Renilla reniformis*) *luc* (luciferase) gene. Four tandem *MS2*-stem-loop repeats were inserted between the luciferase coding sequence and the *tpt1* 3'UTR to tag the *luc-tpt1* chimera for recognition. Of note, the finalized pRL-*Rluc-MS2-tpt1*-3'UTR construct contained an intron (comprised of a 5'-donor splice site, a branch site, and a 3'-acceptor splice site) located downstream of a SV40 enhancer/promoter region, as well as a SV40 polyadenylation signal, guaranteeing that the expressed *Rluc-MS2-tpt1* pre-messenger RNA (pre-mRNA) experiences the major processing events undergone by mature endogenous transcripts. In parallel, a control construct was generated lacking the *tpt1*-S 3'UTR exon (pRL-*Rluc-MS2*-Control), but maintaining all the remaining regulatory landmarks **(Figure 3.13)**.

---

a The engineered MS2 coat protein is tethered to a tag comprising two hexahistidine clusters and a signal sequence for *in vivo* biotinylation (MS2-His-biotin (HB).

b The bacteriophage MS2 coat protein is functional only as a dimer.

c Although HEK (human embryonic kidney)-293 cells were employed in these experiments – namely a stable cell line expressing the modified MS2 coat protein (HEK-293$^{MS2\text{-}HB}$) gifted to me by Dr. Marian Waterman (University of California, Irvine) – the MS2-BioTRAP system can be adapted for use in any other cell line or even in an animal model.

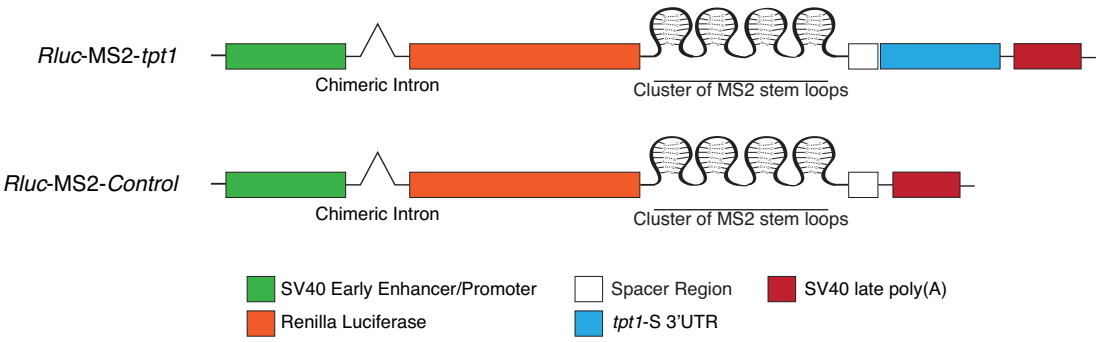

Figure 3.13 – Schematic representation of the *Rluc-MS2-tpt1* and *Rluc-MS2*-Control transgenes.

Critically, both constructs were evaluated for expression in the HEK-293$^{MS2\text{-}HB}$ cell line, as comparable *Rluc-MS2-tpt1* and *Rluc-MS2*-Control mRNA levels were necessary to ensure the final mass spectrometry quantification data held experimental validity. To this end, a RT-qPCR quantification protocol was devised using a co-transfected firefly (*Photinus pyralis*) *luc* reporter for gene expression normalization purposes. Data analysis showed that both mRNAs were expressed at equivalent levels (P = 0.9158, unpaired *t*-test) **(Figure 3.14A)**. Alternatively, the enzymatic activities of the luciferase proteins encoded by the *Rluc-MS2-tpt1* and *Rluc-MS2*-Control constructs were measured, allowing for a quantitative gene expression assessment at the protein level. Relative to the expression of *Rluc-MS2*-Control, I quantified a decrease (circa 20%) in the ratio of *Renilla* to firefly luciferase activity in cells transfected with the *Rluc-MS2-tpt1* construct **(Figure 3.14B)**. Taken together, these results demonstrate that the *Rluc-MS2-tpt1* and *Rluc-MS2*-Control constructs achieve similar levels of mRNA expression, as would be expected of transgenes driven by the same promoter. Moreover, they show that the *tpt1*-S 3'UTR negatively modulates the expression of the *Rluc-MS2-tpt1* mRNA, meaning that this segment confers an extra regulatory layer to the chimeric *Rluc* transcript. Thus, these results suggest that the *tpt1*-S 3'UTR retains functionality when fused to the *Rluc* gene. In any case, it should be stressed that it is the equivalent expression level of the mRNAs, and not that of the proteins, the sole prerequisite of a valid experiment.

After complete SILAC labelling, MS2-HB-associated UV cross-linked mRNP complexes were purified under fully denaturing conditions using streptavidin-coated beads **(Figure 3.15)**. In doing so, only cross-linked RNA-protein associations, and not indirectly interacting factors, were retained, ensuring that a comprehensive, but rigorous, RNA-protein interaction profile for *tpt1* was obtained. In total, three trypsin-treated replicate samples were analysed by mass spectrometry at the Cambridge Centre for

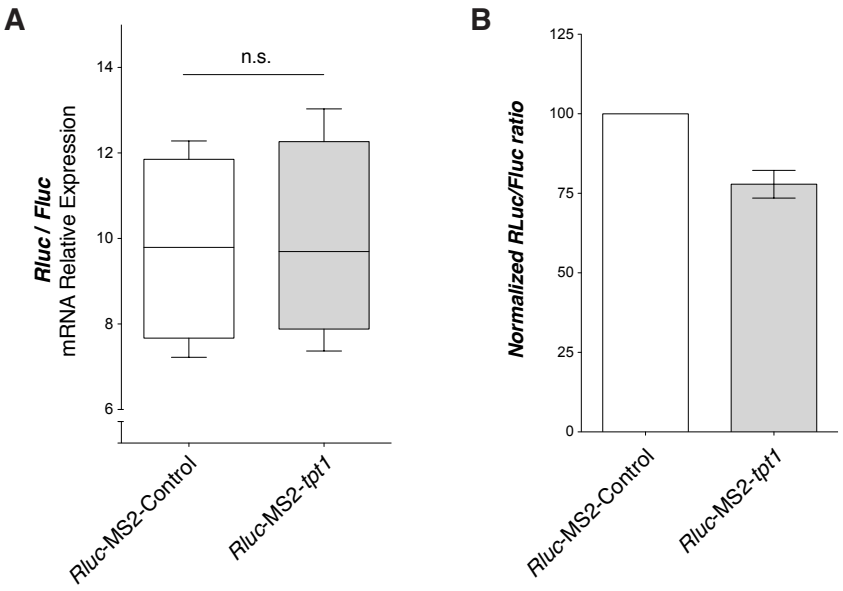

Figure 3.14 – *Rluc*-MS2-*tpt1* and *Rluc*-MS2-Control mRNAs are expressed at equivalent levels in HEK-293MS2-HB cells. (A) RT-qPCR analysis of *Rluc*-MS2-*tpt1* and *Rluc*-MS2-Control mRNA expression. A firefly *luc* reporter (*Fluc*) was included in the transfection protocol to allow for comparisons between conditions (four biological replicates were prepared per condition; $P = 0.9158$, unpaired *t*-test). (B) Analysis of *Rluc*-MS2-*tpt1* and *Rluc*-MS2-Control expression at the protein level using a dual luciferase reporter assay. As in (A), MS2-tagged plasmids were co-transfected with a firefly *luc* reporter for normalization purposes. In (A), boxplot whiskers denote the 5-95 percentile; in (B), error bars specificy the standard error of the mean.

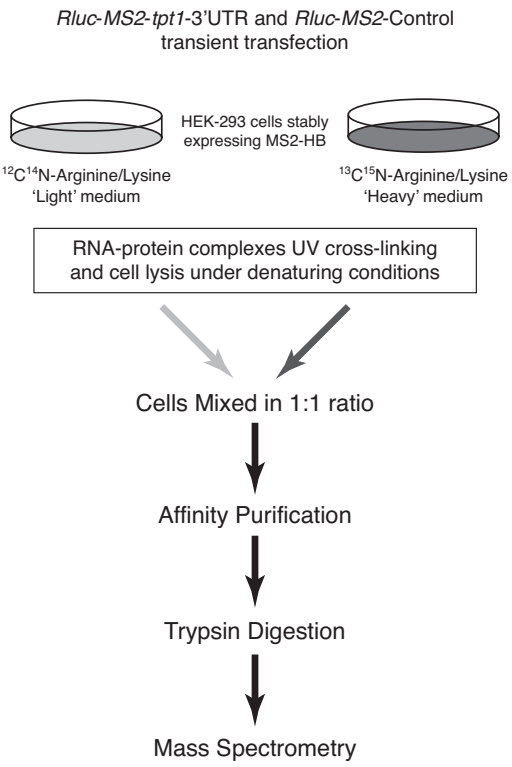

Figure 3.15 – Overview of the MS2 *In Vivo* Biotin Tagged RNA Affinity Purification (MS2-Bio-TRAP) strategy. See text and experimental prodecures for details.

Proteomics. The determination of protein abundance ratios in SILAC-labelled cell populations is possible because peptides with the same amino acid sequence, but different isotopic composition, can be discriminated by mass spectrometry means due to their different masses. If a given RNA-binding protein associates equally with both tagged RNAs, then the 'heavy' to 'light' relative abundance ratio of its digested peptides is, in theory, 1; conversely, a protein that specifically interacts with one of the tagged RNA species will give rise to a relative abundance ratio different from 1. Here, 'heavy' to 'light' relative abundance ratios greater-than 1.5, or less-than 0.66, were judged as specific associations, following published guidelines [268, 269].

Using these analysis parameters, ten known RNA-binding proteins were reproducibly identified as enriched interactors of *MS2*-tagged *tpt1-S* transcripts: RALY heterogeneous nuclear ribonucleoprotein (*raly*), heterogeneous nuclear ribonucleoprotein K (*hnrnpk*), heterogeneous nuclear ribonucleoprotein L (*hnrnpl*), poly(rC) binding protein 1 (*pcbp1*), poly(rC) binding protein 2 (*pcbp2*), polypyrimidine tract binding protein 1 (*ptbp1*), far upstream element-binding protein 2/KH-type splicing regulatory protein (*khsrp*), DEAD (Asp-Glu-Ala-Asp) box helicase 17 (*ddx17*), heterogeneous nuclear ribonucleoprotein H3 (*hnrnph3*), and serine/arginine repetitive matrix 2 (*srrm2*) **(Table 2)**. This dataset was then examined using the STRING (Search Tool for the Retrieval of Interacting Genes/Proteins) database, which catalogues known and predicted protein-protein interactions according to published experimental findings (including high-throughput screens), genomic context, and scientific texts [270, 271]. Notably, STRING analysis revealed the core of *tpt1*-S 3'UTR-enriched factors comprises a highly interactive collection of proteins **(Figure 3.16)**, suggesting that an important portion of the *tpt1*-S mRNP complex may indeed have been captured.

Taken together, and although requiring validation through parallel, protein-centric approaches (e.g. RNA immunoprecipitation), this dataset represents the first snapshot of *tpt1* mRNA *trans*-acting factors, and hence an important novel insight into the regulation of *tpt1* transcripts.

Table 2. RNA-binding protein composition of *tpt1* mRNP complexes

RNA-binding Protein	Biological Overview
hnRNP K	Acts as a docking platform to enable molecular interactions and, simultaneously, as a signal transduction hub. Contains three K homology (KH) domains, which can function in RNA or single-stranded DNA recognition, and shows particular affinity for C-rich motifs. hnRNP K is aberrantly expressed – both in terms of abundance and localization – in many human cancers, suggesting it plays a role in cancer progression [272], and, functionally, has been linked to apoptotic pathways [273]. hnRNP K has been identified in the proteome of growth cones [274]. In addition, it interacts directly or indirectly with *tpt1* mRNA in cultured hippocampal neurons (Graciano Leal and Carlos Duarte, Center for Neuroscience and Cell Biology – University of Coimbra; personal communication).
Pcbp1 and Pcbp2	Together with hnRNP K, poly(C)-binding protein 1 and 2 (Pcbp1 and Pcbp2; also known as hnRNP E1 and hnRNP E2), are the best-characterized elements of a set of evolutionarily related RNA-binding proteins with affinity for C-rich single stranded motifs. Pcbp1 and Pcbp2 share the triple KH domain configuration of hnRNP K, and are involved in mRNA stabilization and translational control processes [275]. Of particular note, Pcbp1 is known to inhibit post-transcriptionally the translation of phosphatase of regenerating liver 3 (PRL-3), a metastasis-associated protein [276]. Likewise, knockdown of Pcbp2 has been shown to inhibit glioma growth by hindering cell cycle progression and promoting Caspase-3-mediated cell death [277]. Pcbp1 is expressed in growth cones [274].
hnRNP L	hnRNP L is involved in many processes of mRNA metabolism, including translational regulation [278], poly(A) site selection [279], and control of mRNA stability [280]. Contains four RNA recognition motif (RRM) domains, and has specificity for CA-rich elements (CAGE). A genome-wide study on hnRNP L binding preferences has revealed that it preferentially associates with intronic and 3' untranslated regions [281]. Significantly, the *Homo sapiens tpt1*-S mRNA contains a highly conserved 16-nt CA-rich region (CATCCACACAACACCA), suggesting that hnRNP L can associate with *tpt1* transcripts via this motif.
Raly	Raly is a member of the heterogeneous nuclear ribonucleoprotein (hnRNP) gene family, and may be involved in pre-mRNA splicing and in embryonic development. Contains a RNA recognition motif (RRM) [282].
Ptbp1	Best known for its involvement in pre-mRNA splicing, Ptbp1 has also been linked to cytoplasmic post-transcriptional processes, including mRNA localization, translational control, and mRNA stability. In mouse, knockout of Ptbp1 results in embryonic lethality, attesting the importance of this RNA-binding protein in development. During early neuronal development, Ptbp1 represses the expression of *postsynaptic density protein 95* (*psd95*), a critical scaffolding protein, by affecting the stability of its mRNA. In cancer biology, Ptbp1 has been shown to regulate apoptosis, cell migration, and growth factor responsiveness. Structurally, Ptbp1 is composed of four RNA recognition motif (RRM) domains [283].
Khsrp	Khsrp is a single-strand nucleic acid binding protein known to promote the decay of mRNAs containing adenylate-uridylate-rich elements (AU-rich elements; AREs) in their 3'UTR [284], such as *tpt1* **(Figure 3.17)**. Khsrp has been shown to destabilize the mRNA encoding for growth-associated protein (Gap)-43 – an axonally synthesized factor [285] – and, by doing so, to constrain axonal outgrowth [286]. Additionally, Khrsp regulates the maturation of a small group of miRNA precursors, and regulates cellular proliferation and differentiation [284]. In terms of structure, Khsrp contains four KH domains [287]. It is also known as Ksrp.
Ddx17	'DEAD box' Ddx17 is a RNA- and ATP-dependent helicase. DEAD box proteins contain a conserved aspartic acid (Asp or D)-glutamic acid (Glu or E)-alanine (Ala or A)-aspartic acid domain (Asp or D), and regulate pre-mRNA splicing and translation initiation processes, among others, by promoting the rearrangement of RNA secondary structures. Its cellular role appears to be context-dependent, as Ddx17 is reported to have both pro- and anti-proliferative functions in cancer cells [288].
hnRNP H3	Like other heterogeneous nuclear ribonucleoproteins, hnRNP H3 regulates the splicing process [289], and plays a role in the early heat shock-induced splicing arrest response [290].
Srrm2	Srrm2 participates in pre-mRNA splicing, although its exact function is yet to be determined. Work in *Saccharomyces cerevisiae* by Grainger et al. indicate that Srrm2 may play a role at the catalytic centre of the spliceosome [291]. Of particular note, Srrm2 dysregulation in terms of the expression of its mRNA isoforms are proposed to serve as a potential blood biomarker in Parkinson's disease [292]. It is also known as SRm300.

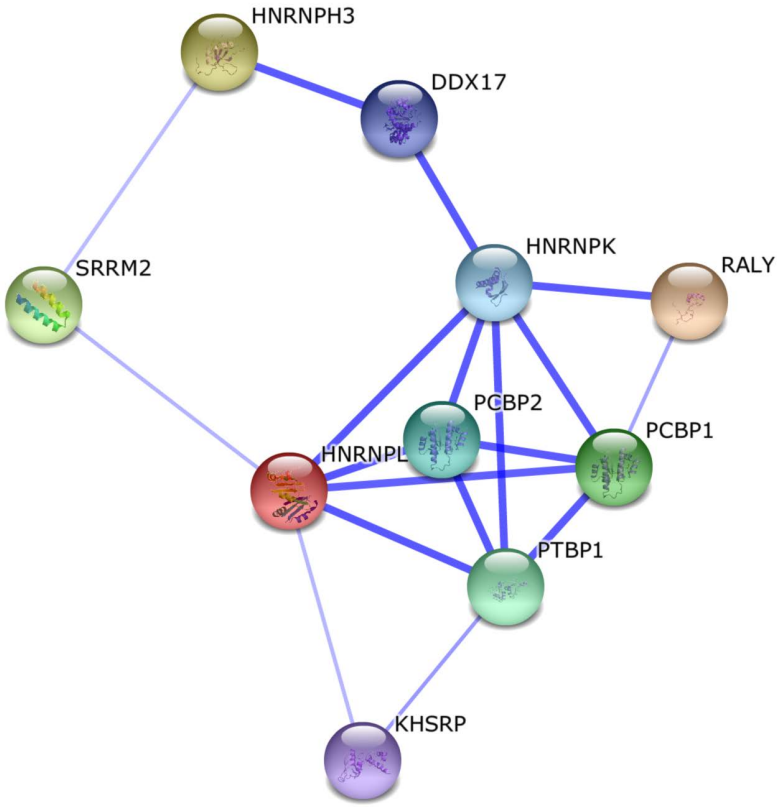

Figure 3.16 – STRING protein network of the ten RNA-binding proteins reproducibly identified as interacting with the *tpt1*-S 3'UTR. Lines between nodes denote the existence of a direct or indirect association. The support for a given association is specified by the thickness of its connecting line.

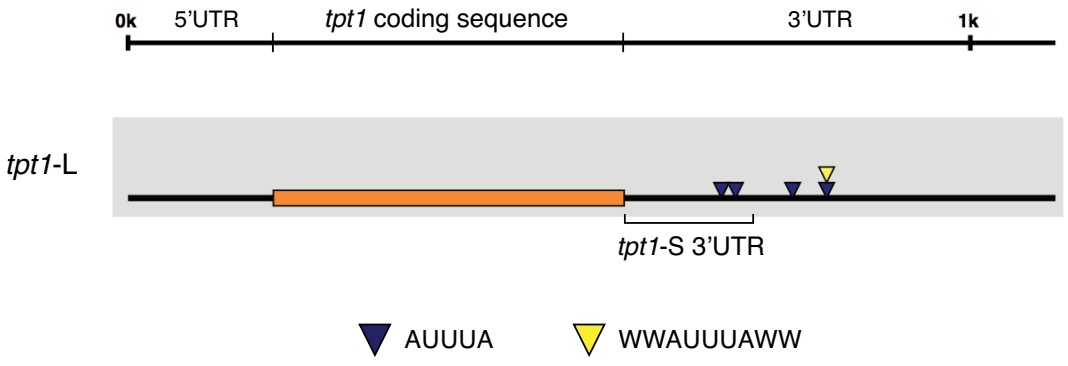

Figure 3.17 – AU-rich elements (ARE) in *tpt1* mRNA. AUUUA site position in *tpt1*-S: 703-707 and 719-723; the two additional AUUUA sites in *tpt1*-L are located at 787-791 and 828-832. WWAUUUAWW site position: 826-834 (sequence: AUAUUUAAA). Analysis performed using the AREsite online resource (University of Vienna). W- A or U residue.

A.4 Growth Cone Tctp Levels Are Downregulated by Ephrin-A1

Growth arrest under a variety of conditions results in the selective repression of 5'-TOP mRNAs, as judged by their shift into the subpolysomal fraction in quiescent cells [172]. A developing axon may be understood to experience an analogous effect upon reaching its synaptic target area, as numerous cues signal for it to halt its extension program and arborize; for example, Eph receptor tyrosine kinases and their ligands, the ephrins, with their graded distribution along the retinal and tectal anterior-posterior and dorso-ventral axes, constitute an effective and well-characterized mode of establishing the correct termination zone coordinates for retinal ganglion cell axons [119]. Of particular note, EphA receptor activation by Ephrin-A has been shown to depress mTORC1 activity and protein synthesis in retinal ganglion cell axons [257]. On the other hand, transcripts encoding for Tctp – as any 5'-TOP-bearing message – are part of a subset of mRNAs specifically regulated by mTORC1 [171], raising the question of whether Ephrin-A1 controls the translation of *tpt1* transcripts in navigating growth cones and, more generally, that of 5'-TOP mRNAs as a whole.

Since EphAs have a high-temporal to low-nasal expression pattern in retinal ganglion cells [120], and hoping to corroborate and simultaneously gain novel insight into the signaling mechanism defined by Nie et al. [257], I initially asked if the aforesaid gradient regulated the inhibitory effects on mTORC1 signaling elicited by Ephrin-A1. To this end, explants from temporal and nasal retinal crescents of stage 32 *Xenopus laevis* embryos were cultured for 24 hours, a duration that approximately equates *in vitro* to the arrival of retinal ganglion cell axons in the Ephrin-A-expressing optic tectum *in vivo* [12, 119]. Notably, following a 10-minute incubation protocol with Ephrin-A1 (5 μg/mL), I observed using quantitative immunofluorescence a significant decrease (approximately 35%; $P < 0.0001$, one-way ANOVA and Tukey's Multiple Comparison Test) in ribosomal protein S6 (rpS6) phosphorylation levels at Ser-235/236, a cardinal marker of mTORC1 activity [293], in retinal ganglion cell growth cones derived from temporal regions of the eye vesicle, but no detectable effects in nasally-originating growth cones **(Figure 3.18)**. Overall, these findings validate and expand on the results of Nie and colleagues [257], as they suggest that the level of expression of EphAs receptors is a fundamental variable in the outcome of Ephrin-A1-induced inhibition of mTORC1.

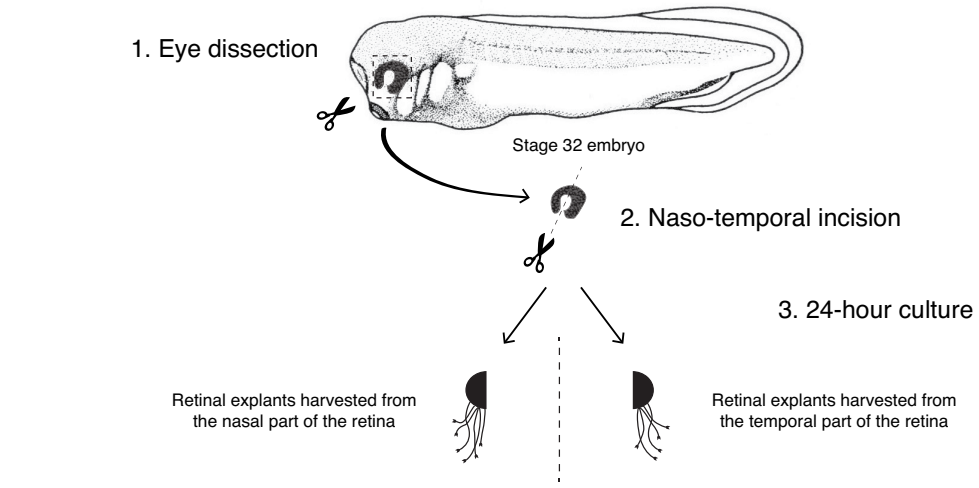

4. Incubation with clustered Ephrin-A1-Fc or clustered Fc for 10 minutes before fixation.

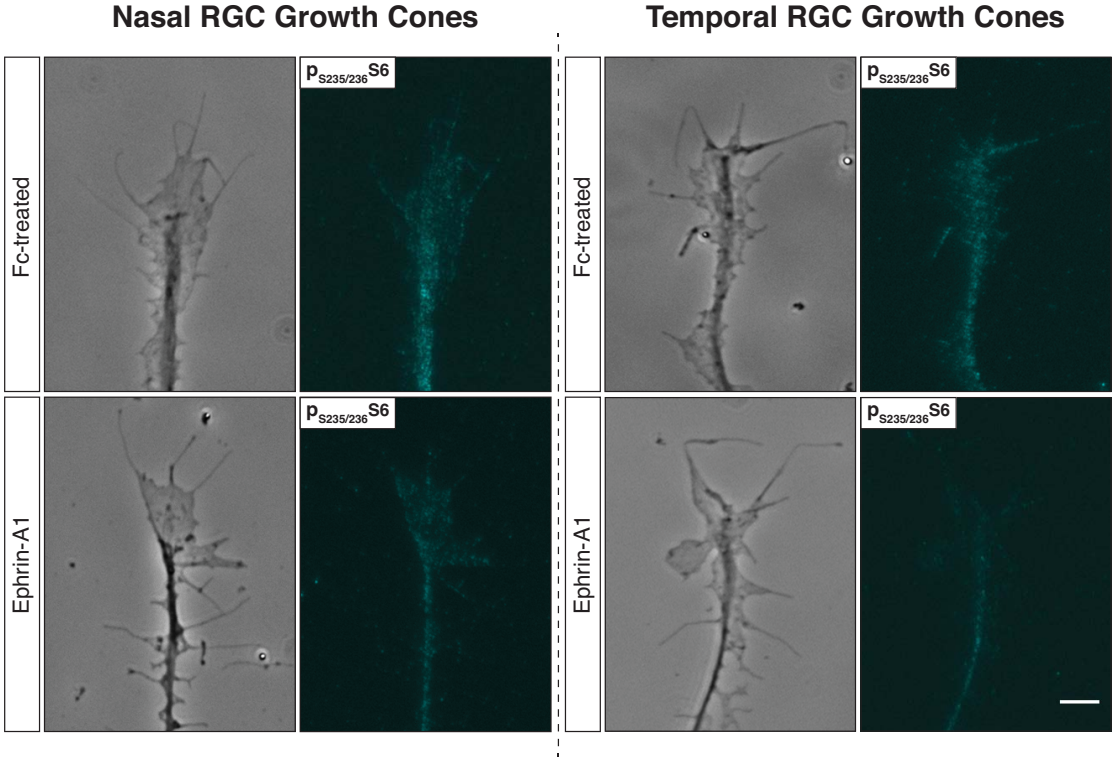

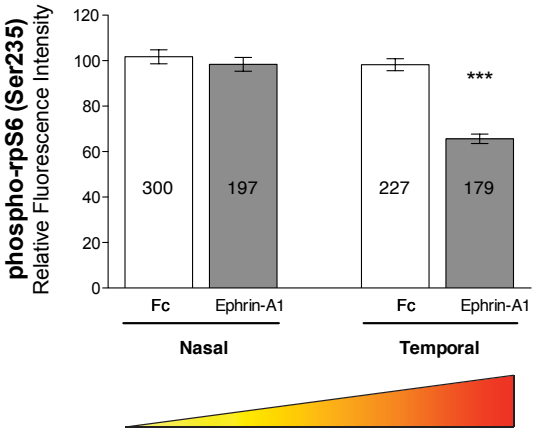

Naso-temporal EphA expression gradient

◀ **Figure 3.18 – Ephrin-A1 differently regulates mTOR activity in nasal and temporal retinal ganglion cell axons.** Nasal and temporal stage 32 retinal explants grown *in vitro* for 24 hours were stimulated with Ephrin-A1-Fc applied at a concentration of 5 μg/mL, and stained with an antibody that specifically recognizes rpS6 when phosphorylated at Ser-235/236. Representative micrographs of control (clustered Fc)- and Ephrin-A1-treated retinal ganglion cell growth cones are shown (mean ± SEM; *n* = no. of growth cones analysed; *** $P < 0.0001$, one-way ANOVA). Scale bar: 5 μm.

Having confirmed that EphrinA1-EphA (forward) signaling modulates the mTOR pathway in *Xenopus laevis* retinal ganglion cells, and employing the same stimulatory protocol as before, I next examined whether EphrinA1-EphA-mediated signaling also regulated the expression of Tctp in the growth cone. Notably, an inverse correlation between EphA activation and Tctp expression was also observed using quantitative immunofluorescence: Tctp protein levels in temporal growth cones showed a reduction of approximately 25% relative to temporal controls ($P < 0.0001$, one-way ANOVA and Tukey's Multiple Comparison Test), accompanied by a smaller but nonetheless significant decline in growth cone Tctp levels in nasal counterparts (circa 10% versus nasal controls; $P < 0.0001$, one-way ANOVA and Tukey's Multiple Comparison Test) **(Figure 3.19)**. Collectively, these results indicate that, at least to some extent, the levels of Tctp reflect the activation of mTORC1 in Ephrin-A1-treated growth cones.

Although my research work eventually took a different direction, I opted for including these preliminary results in my dissertation because they may offer new mechanistic insights into the formation of the retinotectal topographic map. Retinal ganglion cells processes originating from the temporal retina are high-EphA-expressing and project to the anterior-most, low-Ephrin-A1-expressing regions of the optic tectum. Conversely, nasally-derived, low-EphA-expressing retinal ganglion cells extend past the anterior optic tectum towards posterior (and high-Ephrin-A1 expressing) regions of the target field. *Id est*, nasal processes are unresponsive to low-Ephrin-A1-territories that temporal axons find restrictive, and project to the back of the optic tectum, where higher – and increasingly less permissive – Ephrin-A1 concentrations are found. It follows that low-EphA-expressing nasal retinal ganglion cell growth cones must have a higher threshold of response to Ephrin-A1, otherwise they would terminate precociously along the anterior-posterior axis. In other words, the relative progression of the primary axon's growth cone is dependent on the level of EphA receptor expressed on each growth cone's surface, precisely matched to a repellent Ephrin-A1 counter-gradient [119] – it is this molecular duality that defines the anterior-posterior coordinates of each discrete termination zone. At the termination zone, changes in cytoskeleton dynamics leading to actin depolymerization and the collapse of the growth cone cause

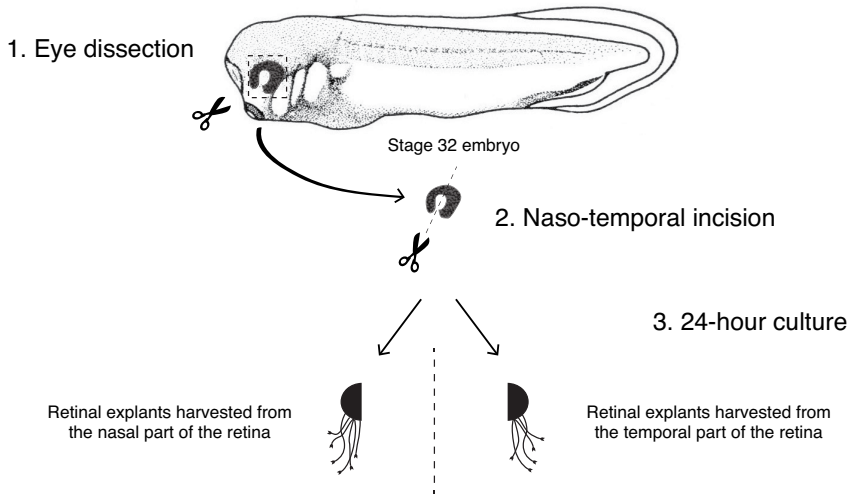

4. Incubation with clustered Ephrin-A1-Fc or clustered Fc for 10 minutes before fixation.

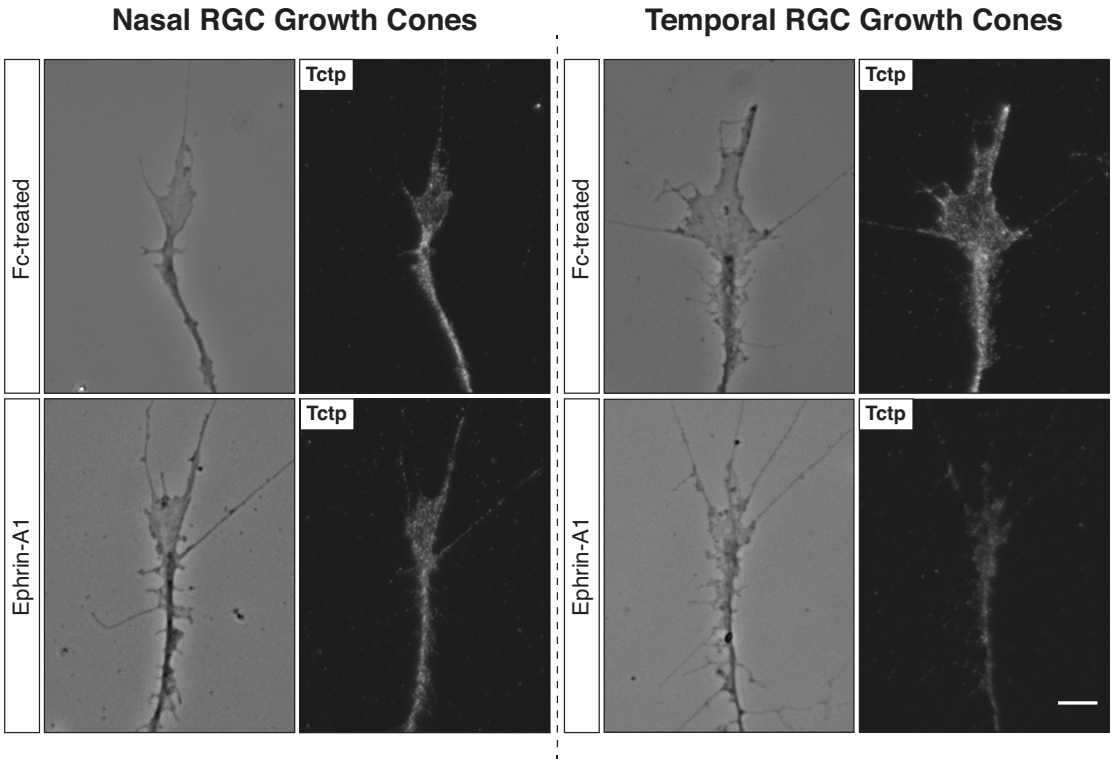

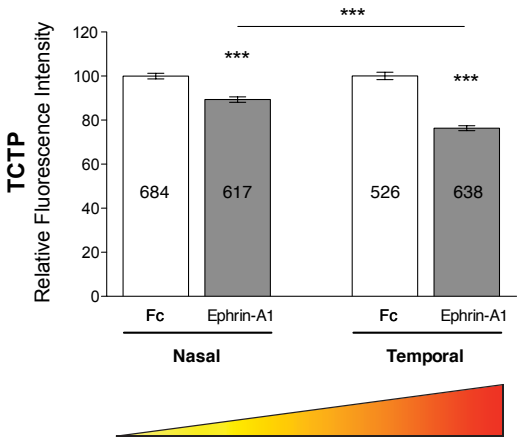

Naso-temporal EphA expression gradient

◀ **Figure 3.19 – Growth cone Tctp expression is correlated with the level of mTOR activation.** Nasal and temporal stage 32 retinal explants grown *in vitro* for 24 hours were stimulated with Ephrin-A1-Fc applied at a concentration of 5 µg/mL, and stained for Tctp. Representative micrographs of control (clustered Fc)- and Ephrin-A1-treated retinal ganglion cell growth cones are shown (mean ± SEM; *n* = no. of growth cones analysed; *** $P < 0.0001$, one-way ANOVA and Tukey's Multiple Comparison Test). Scale bar: 5 µm.

Tukey's Multiple Comparison Test	Mean Diff.[a]	Significant? $P < 0.05$?	Summary	95% CI of diff[b]
Nasal Fc vs Nasal Ephrin-A1	10.65	Yes	***	5.977 to 15.32
Nasal Fc vs Temporal Fc	-0.08356	No	n.s.	-4.964 to 4.797
Nasal Fc vs Temporal Ephrin-A1	23.65	Yes	***	19.02 to 28.28
Nasal Ephrin-A1 vs Temporal Fc	-10.73	Yes	***	-15.73 to -5.739
Nasal Ephrin-A1 vs Temporal Ephrin-A1	13.00	Yes	***	8.252 to 17.75
Temporal Fc vs Temporal Ephrin-A1	23.74	Yes	***	18.78 to 28.69

[a] Difference of the means. [b] Confidence interval on the difference between means.

it to halt its extension and arborize. My findings suggest that the progressive inhibition of mTOR signaling promoted by increasing Ephrin-A1 local concentrations can play a role in the fine modulation of this response, so that it occurs for each given growth cone only when its termination zone is reached and not before **(Figure 3.20)**. Curiously, a set of translationally controlled pro-invasion mRNAs – in their majority (98 out of 144) canonical 5'-TOP-bearing mRNAs, including Tctp – were shown recently to promote prostate cancer invasiveness downstream of aberrant mTOR signaling, a hallmark of advanced human prostate cancers [200]. If a similar rational is applicable to the context of topographic map formation, then the differential attenuation in mTOR signaling elicited by Ephrin-A1 could be understood as a way of reducing the invasive potential of the growth cone only and only when it arrives at its termination zone.

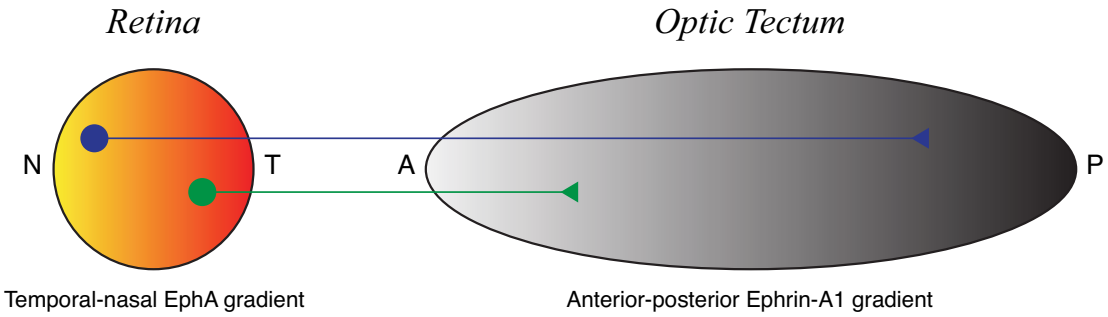

1. Mapping of high-EphA-expressing temporal retinal ganglion cells

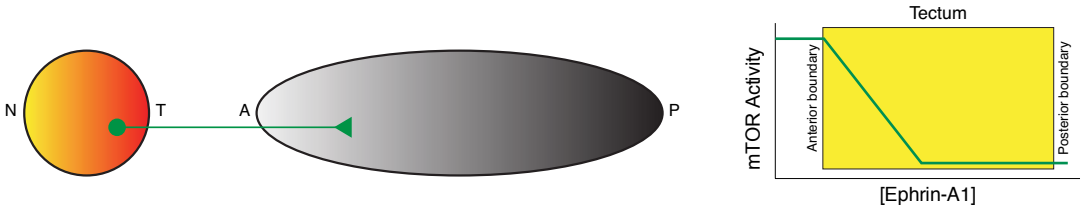

2. Mapping of nasally-derived, low-EphA-expressing retinal ganglion cells

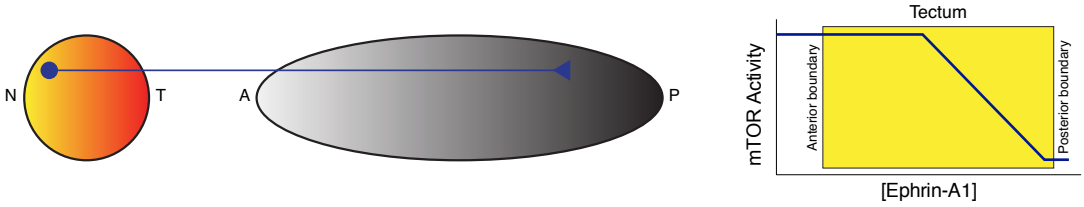

Figure 3.20 – Modulation of mTOR activity by Ephrin-A1-EphA signaling and its hypothetical contribution to retinotectal map formation. TN- temporal-nasal axis; AP- anterior-posterior axis. See text for details.

B – Tctp Regulates Retinal Axon Pathfinding *In Vivo*

B.1 Tctp is Required for Normal Axon Projections

Prompted by the abundant localization of *tpt1* mRNA in the retinal ganglion cell axonal compartment at a time when the retinotectal projection is developing, I next assessed whether Tctp plays a role in retinal axon guidance. To inhibit *tpt1* mRNA translation *in vivo*, I used an antisense morpholino oligonucleotide directed against the start site of *tpt1* mRNA (*tpt1*-MO), which was delivered at the four-cell stage by injection into both dorsal blastomeres **(Figure 3.21A)**. In doing so, I targeted both *tpt1*-S and *tpt1*-L transcripts in the central nervous system, including the neural retina. Western blot analysis validated the efficient knockdown in Tctp levels (ca. 50% in brain and eye lysates; $P = 0.041$, unpaired *t*-test) **(Figure 3.21B)**. In addition, quantitative immunofluorescence analysis of cultured eye explants showed an expression knockdown of approximately 40% in retinal ganglion cell growth cones ($P < 0.0001$, Mann-Whitney test), demonstrating that the axonal pool of Tctp is targeted by this approach **(Figure 3.21C)**. At the morpholino dosage used, Tctp knockdowns appear morphologically normal, with no overt delays in development, albeit showing in most individuals small decreases in eye size (10% on average) **(Figure 3.22A-D)**. Of note, I titrated a morpholino dosage capable of achieving a level of expression knockdown comparable in magnitude to that of *tpt1*$^{+/-}$ mice, which are reported to be viable and fertile, unlike homozygous *tpt1*$^{-/-}$ pups [17, 164].

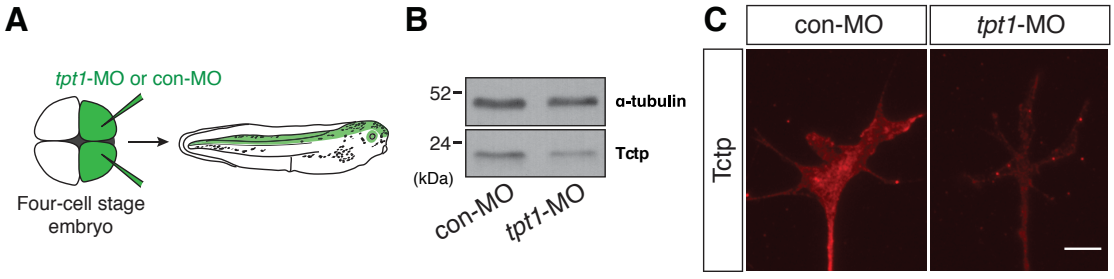

Figure 3.21 – Morpholino-mediated Tctp knockdown in microinjected *Xenopus laevis* embryos. (A) Experimental outline. (B) CNS lysates of control (con)-MO and *tpt1*-MO injected embryos were run on a SDS-PAGE gel and knockdown efficiency verified by western blot. (C) Representative con-MO and *tpt1*-MO-positive growth cones stained for Tctp. Scale bar: 5 µm

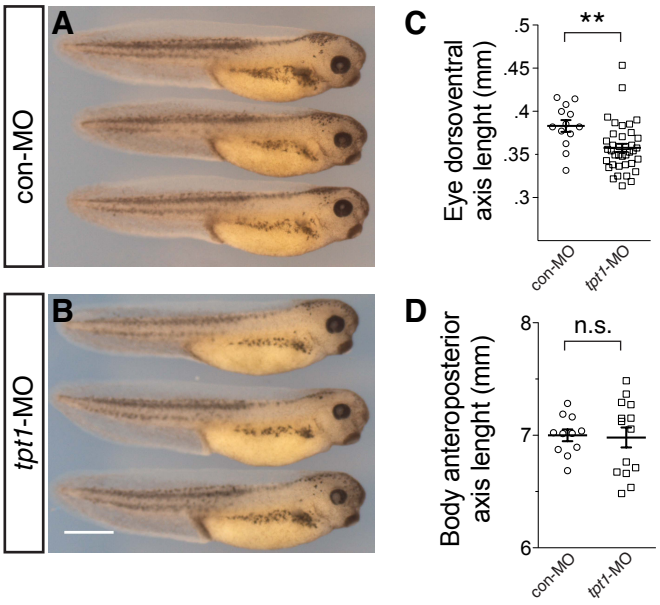

Figure 3.22 – Morphological evaluation of Tctp knockdowns. (A and B) Micrographs of stage 39 con-MO- or *tpt1*-MO-injected embryos. Tctp knockdowns develop at comparable rates relative to control embryos and appear morphologically normal, albeit with smaller eyes. (C) Plot of eye size measurements (mean ± SEM; ** $P < 0.0063$, unpaired *t*-test). (D) Plot of body length (anteroposterior axis) measurements (mean ± SEM; non significant, $P < 0.8614$, unpaired *t*-test). Scale bar: 110 µm.

I first analysed retinal ganglion cell axon trajectories by lipophilic dye (DiI) labelling at stage 40 (~3 day-old embryos), when most axons have completed their stereotyped growth through the optic tract and reached the optic tectum [22]. Whereas control projections consistently coursed a normal trajectory and reached the target region by this stage **(Figure 3.23B)**, most age-matched Tctp knockdowns exhibited significantly shorter projections that failed almost entirely to enter the optic tectum **(Figures 3.23C-E)**. In addition, instead of forming the compact axonal bundle typical of normal projections, retinal ganglion cell axons in Tctp knockdowns grew dispersed and entered inappropriate territories in the diencephalon and telencephalon, which resulted in comparatively wider projections **(Figures 3.23C and 3.23F)**; indeed, the retinal projection in Tctp knockdowns was on average 20-25 µm wider along the mid-optic tract region compared to controls **(Figure 3.23F)**. Remarkably, one day and a half later, at stage 45, when normal axons are undergoing arborization and synaptogenesis in the optic tectum, the retinotectal projection in Tctp knockdowns still contained axons that had not completed their extension through the optic tract **(Figures 3.23)**. Taken together, these data demonstrate that Tctp is necessary for the accurate and timely development of the retinotectal projection.

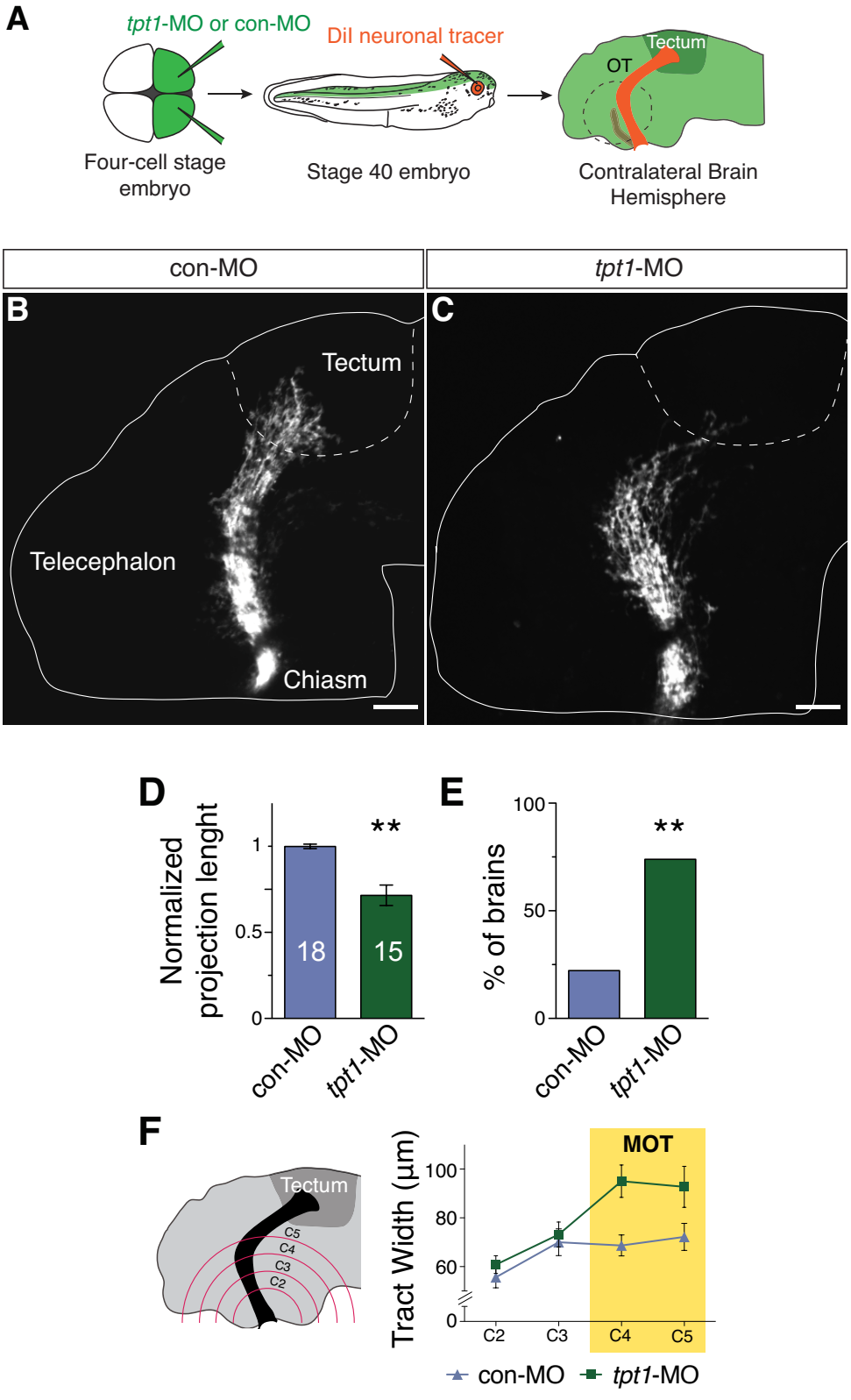

Figure 3.22 – Tctp knockdown perturbs axon development *in vivo*. (A) Schematic representation of the experiment. (B and C) DiI-labeled retinotectal projections in con-MO- or *tpt1*-MO-injected embryos. Dashed lines indicate the tectal boundary. (D) Quantification of retinotectal tract length (mean ± SEM; *n* = no. of brains analysed; ** $P < 0.0014$, Mann-Whitney test). The length of the longest axon was taken for each measurement; since the bulk of the retinotectal projection in Tctp knockdowns is appreciably ▶

◀ shorter, this analysis actually provides a conservative assessment of the phenotype. (E) Percentage of brains displaying axon extension defects (** $P < 0.0016$, Fisher's exact test, performed on number of observations but plotted as percentage). (F) Quantification of mean optic tract width in controls and Tctp knockdowns. C2-5 denote hemi-circumferences centered on the optic chiasm and scaled according to a line connecting the optic chiasm and the posterior pole of the optic tectum. MOT- mid-optic tract.Scale bars: 100 µm.

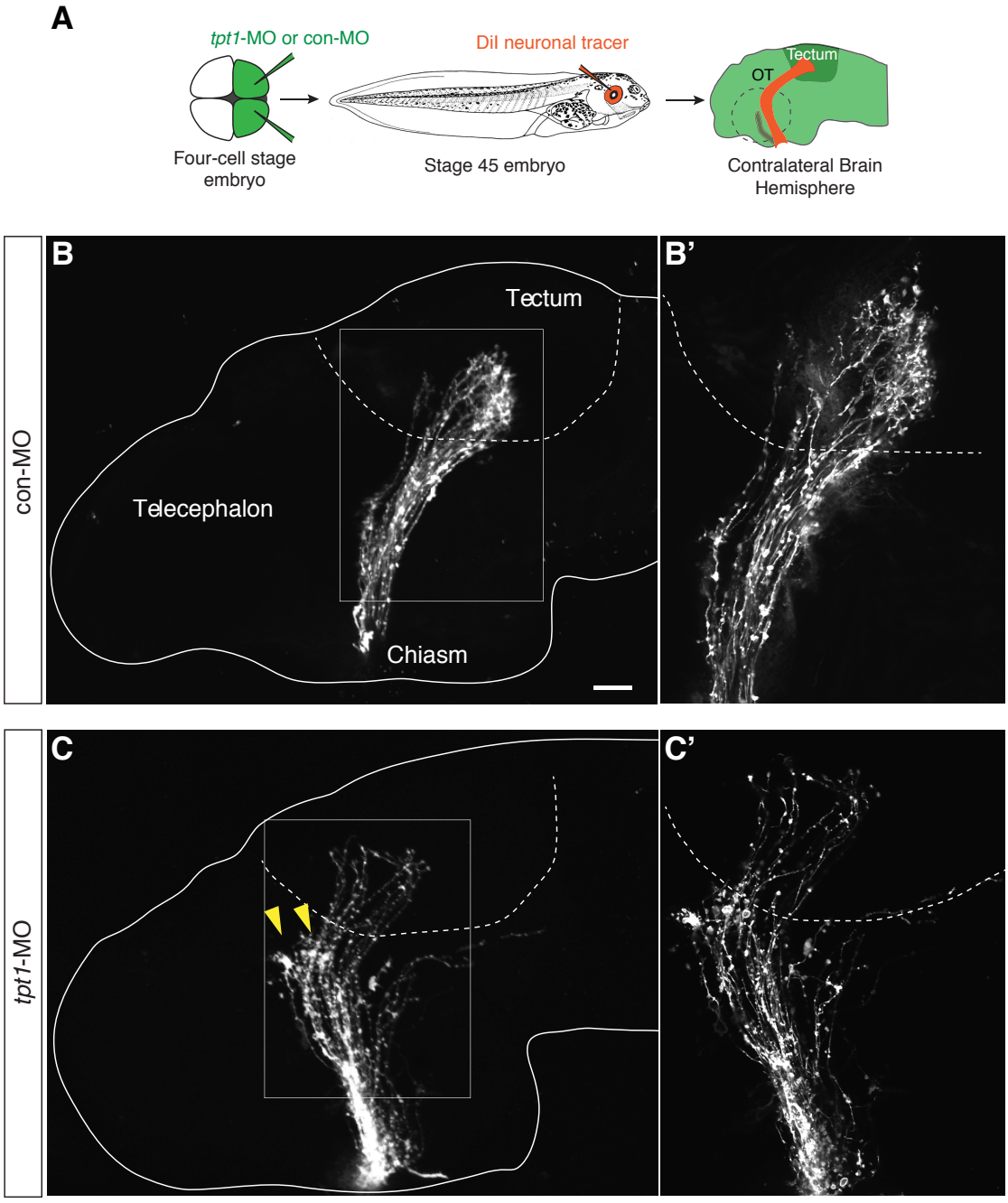

Figure 3.23 – The optic tectum is not fully innervated by stage 45 in Tctp knockdowns. (A) Experimental outline. (B and C) DiI-labeled retinotectal projections in con-MO- or *tpt1*-MO-injected stage 45 embryos. In brains from Tctp morphant embryos, a subset of axons (arrowheads) has not reached the optic tectum by stage 45; seven out of a total of eight embryos analysed were noted to have this phenotype. The boxed areas in (B) and (C) are shown at a higher magnification in panels (B') and (C'). Dashed lines indicate the tectal boundary. (7 out of 8 embryos evinced this phenotype) Scale bar: 100 µm.

Following on these results, and working in collaboration with Hovy Ho-Wai Wong, a fellow doctoral candidate supervised by Christine Holt, we next addressed directly whether Tctp regulates axon elongation *in vivo*. To this end, we made time-lapse movies of control and morphant axons using electroporation to deliver gap-RFP (a membrane-targeted RFP) specifically into the eye **(Figure 3.24A)**. While DiI-fills offered a static glimpse of the axon projection, time-lapse imaging allowed us to directly compare the kinetics of axon growth along the retinotectal pathway. Overall, Tctp-depleted axons advanced through the optic tract at a significantly slower average rate than

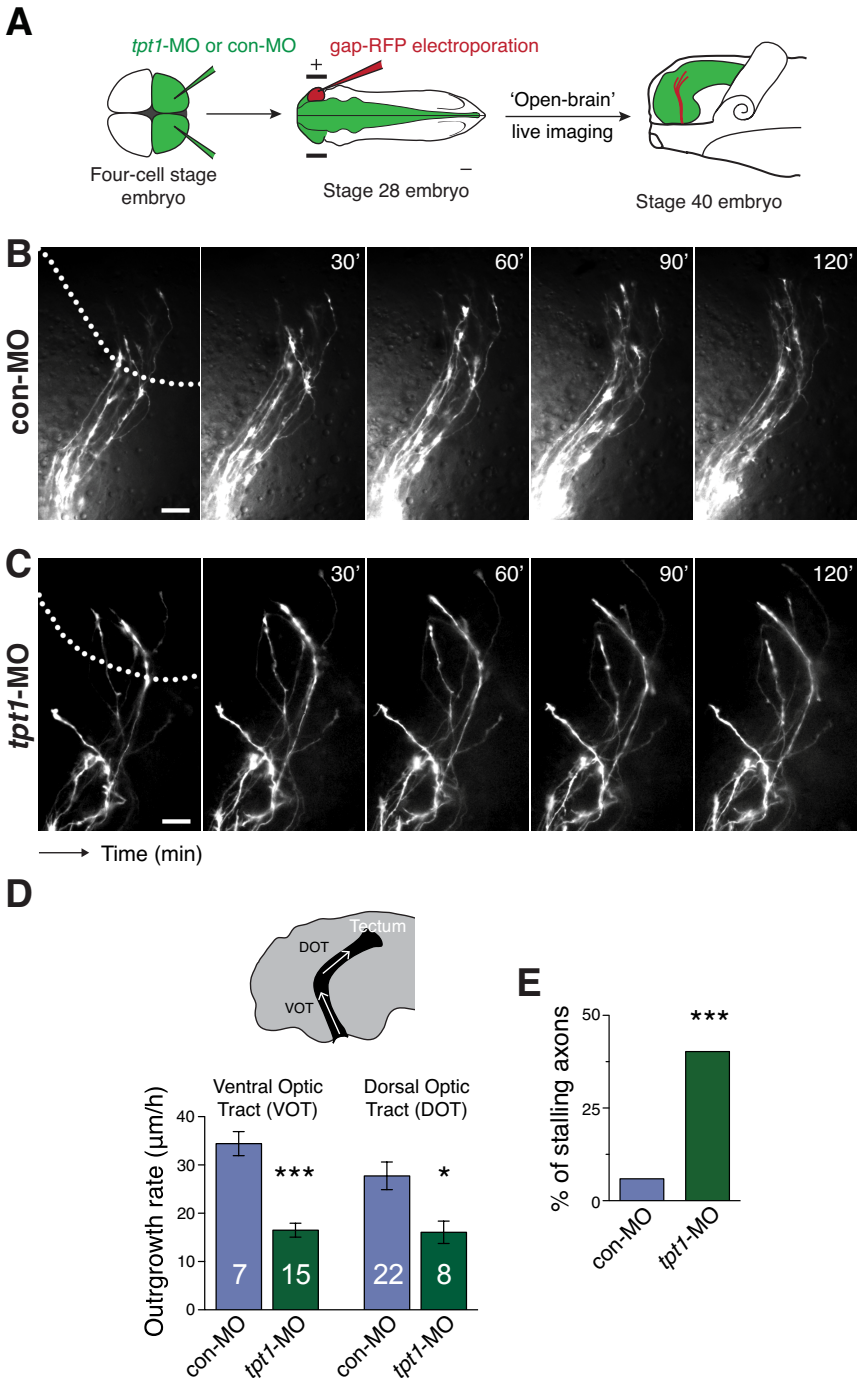

◀ **Figure 3.24 – Tctp knockdown impairs axon extension *in vivo*.** (A) Stage 28 embryos, con-MO- or *tpt1*-MO-injected, were electroporated with gap-RFP to label retinal axons and allowed to develop until stage 40. (B and C) Time-lapse series of gap-RFP-labeled control or Tctp-depleted retinotectal projections coursing through the optic tract. Dashed lines indicate the tectal boundary. (D) Quantification of axon outgrowth rates through the ventral optic tract (VOT) and dorsal optic tract (DOT) in controls and Tctp knockdowns (mean ± SEM; n = no. of axons analysed; VOT: $P < 0.0001$, unpaired t-test; DOT: $P < 0.0273$, unpaired t-test). (E) Percentage of axons with stalling extension. (*** $P < 0.0001$, Fisher's exact test, performed on frequencies but plotted as percentage). Scale bars: 25 μm. *Experiment perfomed in collaboration with Hovy Ho-Wai Wong.*

control axons (ventral optic tract [VOT]: 16.5 μm/h versus 34.4 μm/h; dorsal optic tract [DOT]: 16.1 μm/h versus 27.8 μm/h) **(Figures 3.24B-D)**. In addition, 40% of morphant axons (33 of 82 axons) stalled along the optic tract, a significantly higher proportion than that observed in control samples (5 of 84 axons) **(Figure 3.24E)**. As previously, we observed that the growth of retinal ganglion cell axons in Tctp knockdowns was rather dispersed and erratic, which translated into significantly wider projections relative to controls (mean tract angular spread: 80º versus 30º, $P < 0.0001$, unpaired t-test). Also, degenerating axons, distinguished by their beaded morphology and retraction behaviour, were more frequent along the optic pathway in the *tpt1*-MO:gap-RFP dataset (10 out of 82 axons versus 2 out of 82 axons in controls, $P = 0.0145$, unpaired t-test), suggesting that Tctp could act by promoting axon maintenance and survival. Collectively, these data demonstrate that Tctp is necessary for the accurate development of the retinotectal projection. Moreover, our results show that Tctp knockdown affects the rate of axon elongation, resulting in shorter projections that fail to reach the optic tectum at the precise developmental window.

B.2 Tctp Acts Cell-Autonomously

Tctp displays IgE-dependent histamine-releasing activity and other cytokine-like extracellular functions [162, 175]. It could therefore act non-cell-autonomously in the embryonic environment to promote axon development, as histamine is suggested to have a significant role during neural development [294]. To address this concern, I next investigated whether the axonal phenotype in Tctp-deficient embryos might have a retinal ganglion cell-extrinsic basis.

At the four-cell stage, targeted microinjection into the two dorsal blastomeres delivers the morpholino to the prospective brain as well as the eye, meaning that morphant retinal ganglion cell axons grow into morphant brain tissue. However, as the first cleavage in *Xenopus laevis* eggs separates the future left and right-hand halves of the embryo [295], I was able to generate tadpole chimeras by targeting only one of the

dorsal blastomeres: morpholino-positive in one half of the central nervous system, and wild-type, morpholino-free, in the other **(Figures 3.25A-C)**.

As before, I assessed retinotectal projections at stage 40 using DiI anterograde labelling. Importantly, con-MO-injected embryos consistently developed normal retinotectal projections in both paradigms, verifying the suitability of the strategy **(Figures 3.26B and 3.26D)**. Whereas *tpt1*-MO-positive retinal axons navigating into the contra-

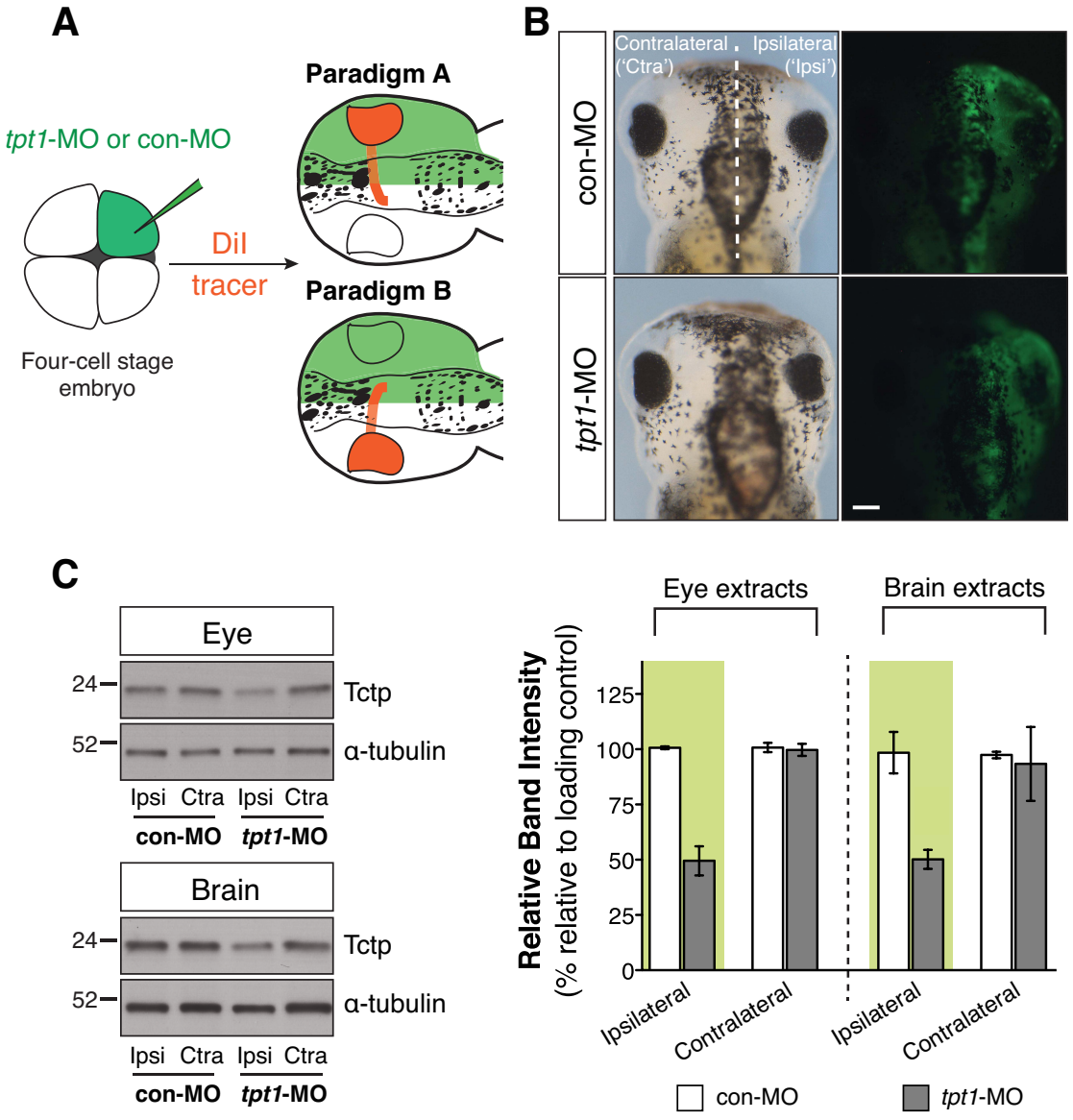

Figure 3.25 – Validation of the experimental strategy devised to investigate cell-autonomy. (A) Experiment outline, depicting unilateral blastomere microinjection of con-MO or *tpt1*-MO, and the two experimental paradigms used to investigate cell-autonomy. (B) Dorsal view of embryos microinjected unilaterally with con-MO or *tpt1*-MO. (C) Western blots of eye or brain lysates probed with Tctp antibody. Ipsilateral ('Ipsi') and contralateral ('Ctra') refer to the side of the embryo injected with morpholino. Eight independent lysates were prepared: con-MO-injected ipsilateral ('Ipsi') and contralateral ('Ctra') eyes or brain hemispheres, plus *tpt1*-MO-injected ipsilateral and contralateral eyes or brain hemispheres (mean ± SEM; no. of independent samples assayed = 2). Scale bars: 100 μm.

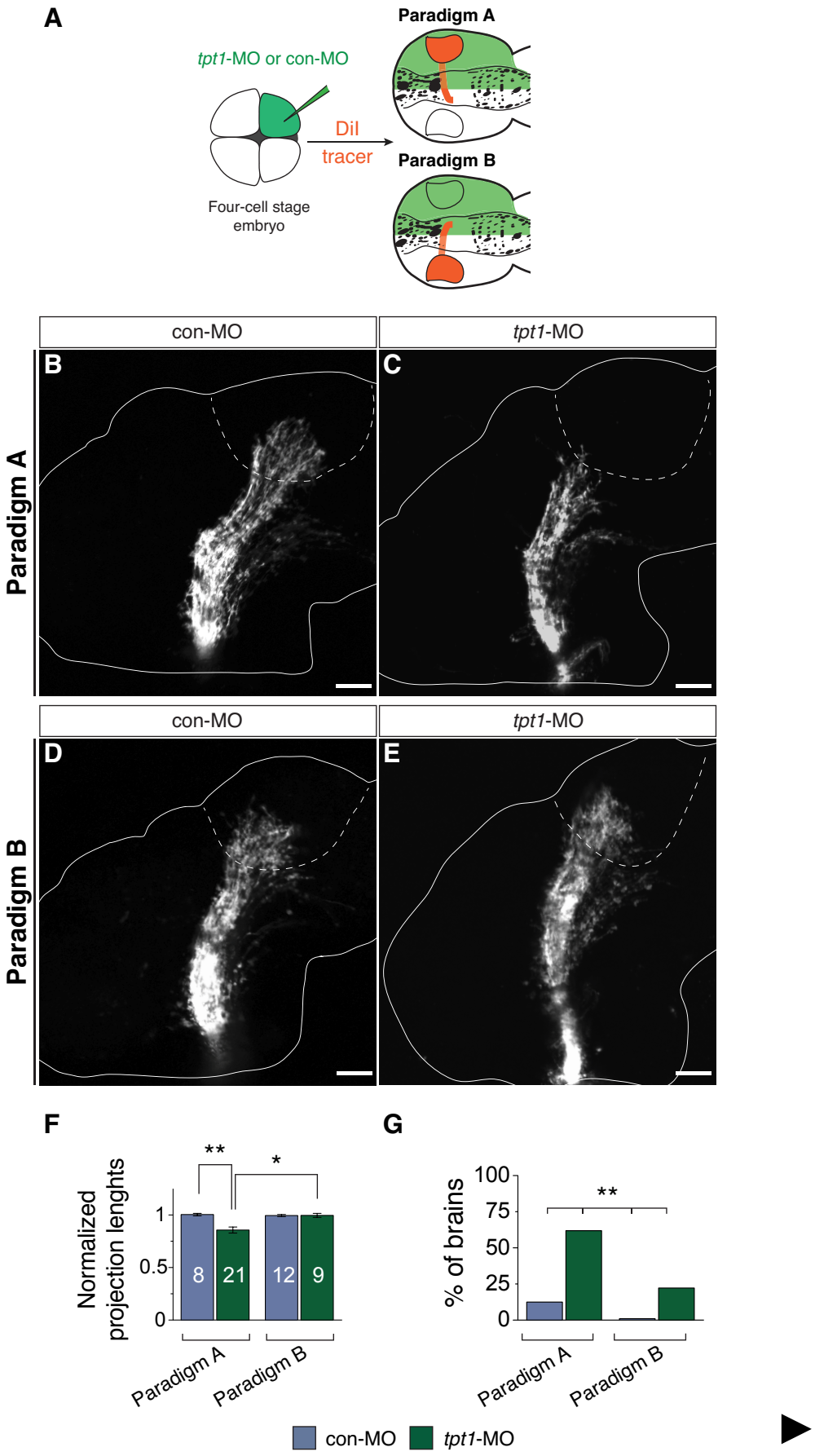
A
tpt1-MO or con-MO
Dil
tracer
Four-cell stage
embryo
Paradigm A
Paradigm B
con-MO
tpt1-MO
B
C
D
E
Paradigm A
Paradigm B
F
Normalized
projection lenghts
**
*
1
0.5
0
8
21
12
9
Paradigm A
Paradigm B
G
% of brains
100
75
50
25
0
**
Paradigm A
Paradigm B
con-MO
tpt1-MO

◀ **Figure 3.26 – Axon extension defect in Tctp morphants is cell-autonomous.** (A) Schematic representation of the experiment, depicting unilateral blastomere microinjection of con-MO or *tpt1*-MO, and the two experimental paradigms used to investigate cell-autonomy. (B-E) DiI-labeled retinotectal projection in unilaterally injected stage 40 embryos. Refer to the diagram in (A) for a graphical outline of each experimental paradigm. Dashed lines indicate the tectal boundary. (F) Quantification of retinotectal tract length (mean ± SEM; *n* = no. of brains analysed; *** *P* = 0.0004, Kruskal-Wallis and Dunn's Multiple Comparison Test). (G) Percentage of brains displaying axon extension phenotypes (** *P* = 0.0011, Chi-square test, performed on frequencies but plotted as percentage). Scale bars: 100 μm.

lateral, *tpt1*-MO-free, hemisphere replicated the same range of phenotypes observed in global Tctp knockdowns **(Figure 3.26C)**, *tpt1*-MO-negative retinal ganglion cell axons projecting into the opposite, *tpt1*-MO-positive, hemisphere showed none of the defects I had previously characterized **(Figure 3.26E)**. Namely, in the former condition, most axons failed to reach the optic tectum, while, in the latter, *tpt1*-MO-negative axons developed unaffected by the morphant brain environment, qualitatively indistinguishable from controls **(Figures 3.26F and 3.26G)**. Taken together, these findings indicate that the axon extension phenotype in Tctp knockdowns is not a consequence of extrinsic perturbations, but a cell-autonomous event.

B.3 Normal Axon Extension When Tctp Translation is Locally Inhibited

Having found that Tctp regulates axon growth, I next investigated the relative contribution of axonally synthesized Tctp to this process. To address this directly, I measured the outgrowth dynamics of transected pathfinding axons in which *tpt1* mRNA translation was subcellularly blocked **(Figure 3.27A)**. In doing so, I specifically targeted the pool of newly synthesized axonal Tctp and, as transected retinal ganglion cell axons can continue to grow and navigate *in vivo* for up to 3 hours [3], simultaneously eliminated the effects of soma-derived protein.

In contrast to microinjected-Tctp knockdowns, the axonal delivery of *tpt1*-MO did not significantly affect the outgrowth dynamics of retinal ganglion cell axons along the optic tract during the 1-hour period of my analysis when compared to controls (ventral optic tract (VOT): 50.5 ± 3.1 μm/h versus 47.8 ± 3.9 μm/h in controls; dorsal optic tract (DOT): 42.7 ± 4.5 μm/h versus 47.9 ± 4.7 μm/h in controls) **(Figures 3.27B-D)**. In addition, a *post hoc* evaluation of axon trajectories did not identify guidance errors arising in either condition, even though a major guidance decision – the caudal turn in the mid-optic tract [22] – was made by many axons in the temporal window of the analysis.

Although these results corroborate previous reports excluding protein synthesis in distal axons as a pre-requisite for axon growth [296], it was impossible to confirm di-

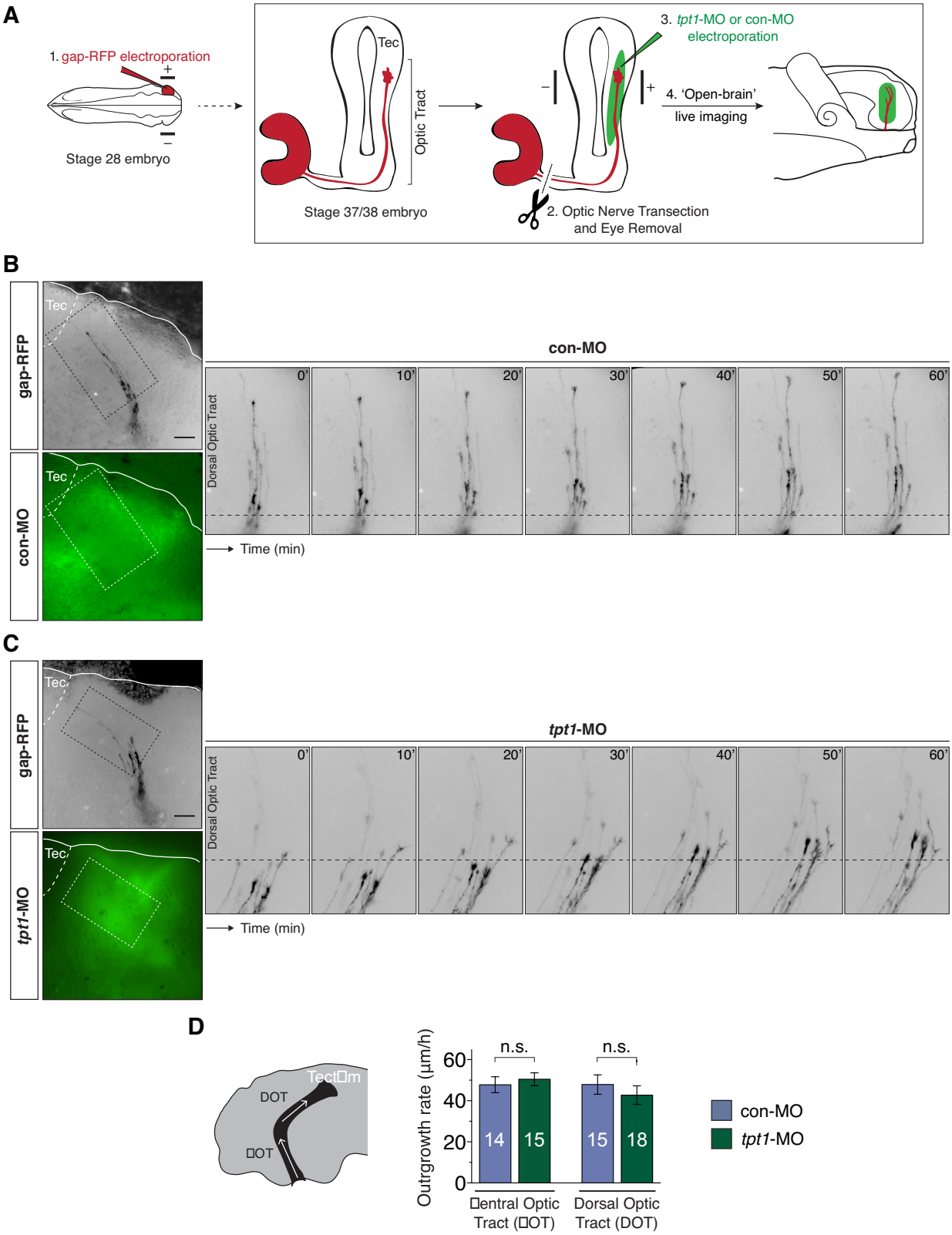

Figure 3.27 – Local synthesis of Tctp is not required for axon extension *in vivo*. (A) Gap-RFP was delivered by eye-targeted electroporation to wild-type stage 28 embryos, when the first retinal ganglion cell axons have just exited the eye, and axon extension kinetics were analysed 21-24 h later (stage 37/38), when most axons are growing up the optic tract towards the optic tectum. Just before imaging, the optic nerve was manually transected, and con-MO or *tpt1*-MO was delivered subcellularly by targeted brain electroporation. Of note, transected retinal ganglion cell axons can continue to grow and navigate accurately *in vivo* for up to 3 hours, well within the 1-hour

◀ period of this experiment. (B and C) Time-lapse series of severed retinal ganglion cell axons coursing through the optic tract in embryos subcellularly electroporated with con- or *tpt1*-MO. (D) Quantification of axon outgrowth rates through the VOT and DOT in embryos subcellularly electroporated with con- or tpt1-MO (mean ± SEM; *n* = no. of axons analszed; VOT: *P* = 0.5956, unpaired t-test; DOT: *P* = 0.4381, unpaired *t*-test; 7-9 replicates were performed per condition; n.s., not significant, unpaired *t*-tests). Scale bars: 50 µm.

rectly whether my experimental approach indeed blocked the axonal synthesis of Tctp. However, recognizing that 5'-TOP-bearing mRNAs such as *tpt1* are specifically regulated by mTORC1 [171], I asked whether the inhibition of this signaling complex could recapitulate the axon phenotype detected in Tctp knockdowns. mTORC1 inhibition, as assessed by the levels of rpS6 phosphorylation at Ser-235/236, is readily achieved in *Xenopus laevis* embryos reared in rapamycin-containing saline [297]. In line with the above results, rapamycin-treated individuals showed normal retinotectal projections in terms of tract length **(Figure 3.28)**, albeit developing seemingly less dense retinotectal projections (not quantified). However, even this approach is not without limitations, as I later came to learn that rapamycin, an allosteric mTOR inhibitor, only blocks p70S6K1/2 activity [200], and *tpt1* is reported to be regulated, at least partly, by the eIF4E-mediated signaling arm of mTOR [199]; therefore, it is possible that the syntehsis of new Tctp protein is not significantly affected in rapamycin-treated embryos [a][143,293].

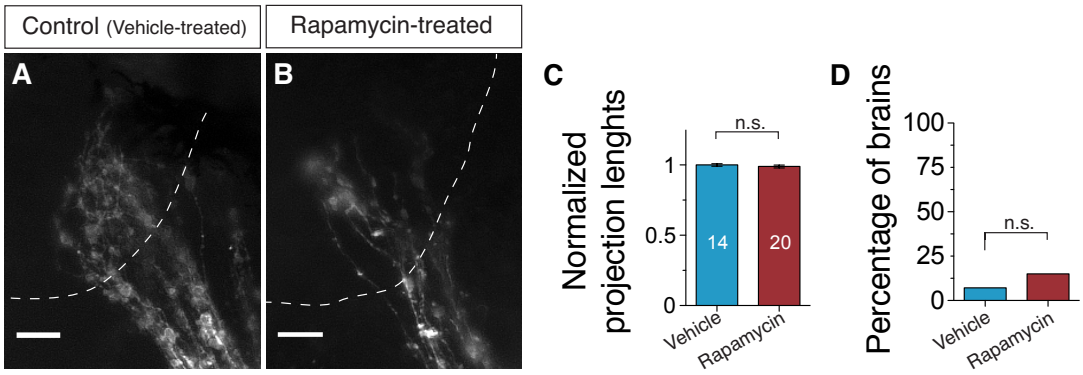

Figure 3.28 – mTOR inhibition does not recapitulate the axon pathfinding defects detected in embryos deficient for Tctp. (A and B) Representative DiI-labeled retinotectal projections from embryos raised in DMSO (vehicle)- or rapamycin-containing saline. The dashed lines represent the anterior boundary of the optic tectum. (C) Quantification of retinotectal tract length (mean ± SEM; *n* = no. of brains analysed; not significant, *P* = 0.5403, Mann-Whitney test). (D) Percentage of brains displaying axon extension phenotypes (not significant, *P* = 1.0000, Fisher's exact test, performed on number of observations but plotted as percentage). Scale bars: 25 µm.

[a] rpS6 is phosphorylated downstream of p70S6K1/2 activation. The p70S6K1/2/rpS6 and the eIF4E-BP/eIF4E pathways are the two main effectors of mTOR signaling.

Collectively, these results suggest that the fine regulation of axonal Tctp expression achieved by local translation mechanisms is not essential in the short-term to support the advance of retinal ganglion cell axons in the optic tract. Thus, as a whole, my results indicate that the axon phenotype detected in Tctp knockdowns arises not as consequence of a regionally delimited dysregulation, but rather from a chronic depletion of Tctp, as would be expected of a protein with constitutive cellular functions. In any case, judging from the enrichment of its mRNA, Tctp is an abundant axonal protein and, owing to its appreciable half-life ($t_{1/2}$ > 6 h) [190], may be able to maintain a sufficient degree of activity when its translation is temporarily inhibited.

B.4 Tctp is Necessary for Photoreceptor Maintenance

I next explored whether the axon phenotype in Tctp knockdowns somehow recapitulated an underlying defect in eye development. Analysis of phalloidin and nuclei-stained retinal sections showed the overall stratification of the retina to be unaffected in morphant embryos, although a relatively disordered neuropil was noted **(Figure 3.29A)**. I substantiated these observations using antibody markers with validated cellular specificity, suggesting that the global cytoarchitecture of the retina is unaffected in *tpt1*-MO-injected embryos **(Figures 3.29B and 3.29C)**.

However, on closer inspection of the outer layer of the neural retina, striking morphological alterations were detected in the cellular domains comprising the inner and outer segments of photoreceptor neurons (PR) in Tctp-deficient individuals **(Figure 3.30A)**. These surprising findings, in addition to the abundant expression of Tctp in the photoreceptor layer of the retina, prompted me to evaluate more closely the effects of Tctp depletion in photoreceptor biology. Briefly, the apical outer segment is a structure densely packed with discs of folded membranes containing the light sensitive photopigments (opsins), whereas the inner segment, which lies between the outer segment and the outer nuclear layer, is dedicated to sustaining the high energy and protein synthesis needs of the photoreceptor [298]. Using opsin markers and a nuclear stain, I first pinpointed the localization of Tctp to the mitochondria-rich inner segments of cone and rod photoreceptors in wild-type specimens **(Figure 3.30A)**. Subsequent quantification of the photoreceptor inner segment (IS) average length in control and Tctp-depleted retinas revealed this structure to be significantly thinner in the latter condition (cone inner segment: 13.7 μm versus 16.1 μm in controls; rod inner segment: 11.8 μm versus 15.8 μm in controls), a defect often accompanied by the complete loss of the outer

segment in a significant proportion of cone and rod photoreceptors **(Figures 3.30B-E)**. Collectively, these data indicate that while Tctp is not essential for the timely development of the retina, it lends an unexpected contribution to photoreceptor maintenance. This is in itself an insightful observation, since previous studies have shown Tctp to be downregulated in conditions associated with mitochondrial defects such as Alzheimer's disease and Down syndrome [128, 207, 336], and photoreceptor degeneration is frequently characterized by bioenergetic decline [298]. Indeed, mitochondrial dysfunction is reported in a number of retinal diseases, including photoreceptor-specific age-related macular degeneration [298], as well as neurodegenerative disorders with prominent axonal phenotypes, such as retinal ganglion cell-specific dominant optic atrophy [130, 131] and Leber's hereditary optic neuropathy [299]. Hence, the phenotypes I have characterized in Tctp-deficient retinal ganglion cell axons and photoreceptors, two cellular domains particularly vulnerable to mitochondrial compromise and where Tctp is abundantly expressed, indicate that Tctp could work by promoting mitochondrial function. I therefore set out to examine the status of mitochondria in Tctp knockdowns

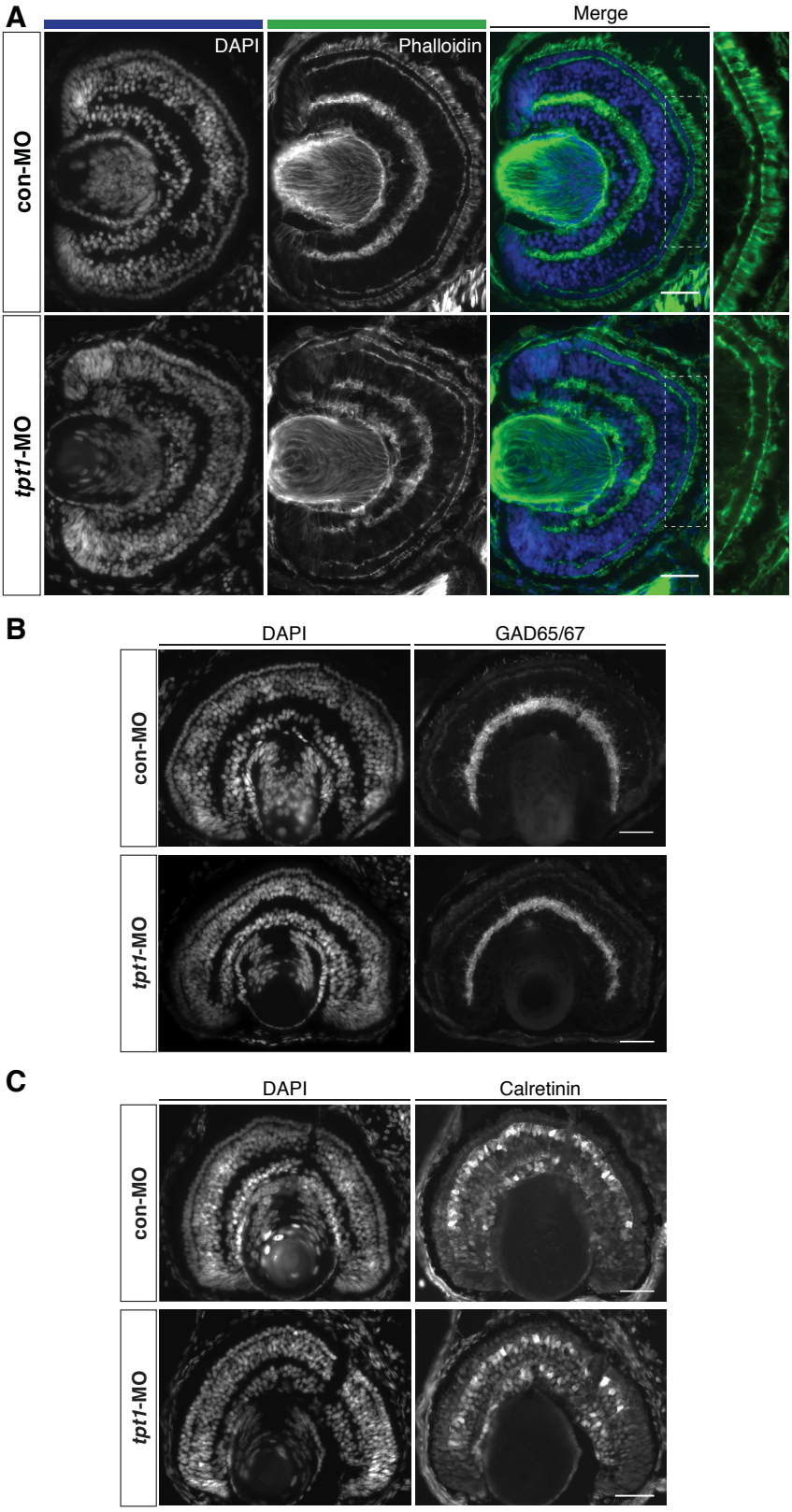

Figure 3.29 – Global retinal architecture is preserved in Tctp morphant embryos. (A) Coronal sections of stage 43 control or Tctp-depleted retinas stained with phalloidin and DAPI. The boxed areas are shown at a higher magnification in the rightmost panels. (B and C) Coronal sections of stage 43 control or Tctp-depleted retinas stained for glutamate decarboxylase (GAD65/67) or calretinin, two cell-type-specific markers (GAD65/67 and Calretinin antisera detect GABAergic amacrine cells, and retinal ganglion cells/bipolar cells, respectively). Scale bars: 50 μm.

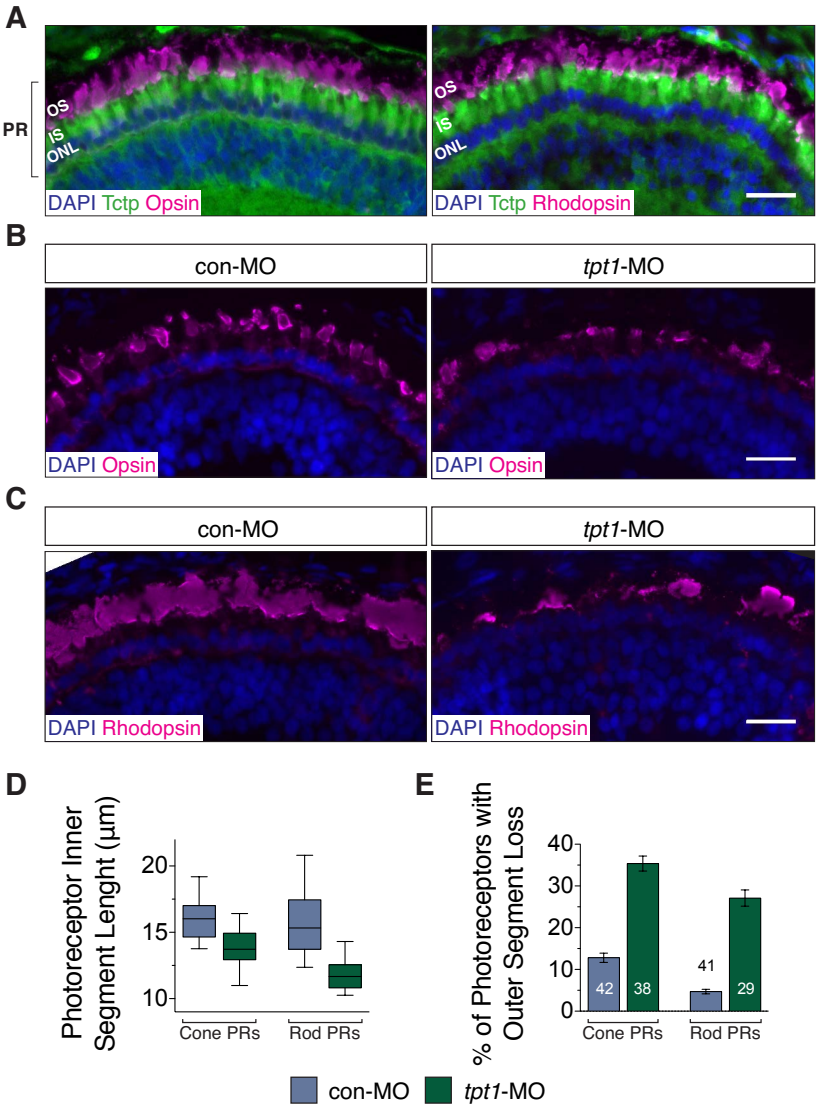

Figure 3.30 – Tctp is necessary for photoreceptor maintenance. (A) Photoreceptor (PR) layer in coronal sections of stage 43 wild-type retinas probed for Tctp and Opsin or Rhodopsin (ONL: outer nuclear layer; IS: PR inner segment; OS: PR inner segment). See also Figure 3.2A. (B and C) Photoreceptor layer in coronal sections of stage 43 control or Tctp-depleted retinas probed for opsin or rhodopsin and counterstained with DAPI. (D) Quantification of the average inner segment length in control and Tctp-depleted embryos (*** $P < 0.0001$, unpaired *t*-tests; boxplot whiskers denote 5-95 percentile). (E) Quantification of the proportion of photoreceptors showing complete outer segment loss in control and Tctp-depleted embryos (n = no. of PR layers analysed; *** $P < 0.0001$, unpaired *t*-test). Scale bars: 25 µm.

C – Mechanistic Insights Into the Role of Tctp in Neural Development

C.1 Tctp Knockdown Leads to Mitochondrial Compromise

I initially gained direct insight of the metabolic status of Tctp-depleted embryos by using a bioluminescence assay to determine total ATP concentration [258]. The energy content in Tctp-depleted retinas was found to be on average 30% lower relative to controls (Figure 3.31), suggesting that the function of mitochondria, the cell's powerhouses and key organelles behind axon survival [126], is affected in Tctp knockdowns. Following on this result, I sought to measure the mitochondrial membrane potential ($\Delta\Psi_m$) in retinal explant cultures, a parameter related to a cell's capacity to generate ATP by oxidative phosphorylation and, for this reason, a cardinal indicator of mitochondrial function [300]. Notably, in Tctp knockdowns, I found a significantly lower accumulation of the cationic fluorescent probe tetramethylrhodamine methyl ester (TMRM) in the mitochondria-rich growth cone central domain (~20% in respect to control), denoting $\Delta\Psi_m$ depolarization **(Figures 3.32A and 3.32B)**. A significant decrease in the number of axonal mitochondria was also noted in these experiments, which I confirmed *in vitro* with a mitochondrial stain (approximately 30% fewer mitochondria), and *in vivo*, working in collaboration with Hovy Ho-Wai Wong, by co-labelling retinal ganglion cell axons with mitochondrion-targeted GFP (mt-GFP) and gap-RFP (approximately 23% fewer mitochondria) **(Figures 3.33A-C and 3.34)**. Consequently, these findings raised concerns about my assessment of mitochondrial depolarization in Tctp-depleted growth cones, as a decrease in axonal mitochondrial density would be expected to affect to some extent the accumulation of mitochondria at the growth cone central domain; however, analysis of individual mitochondria distributed throughout the axonal compartment showed a comparable $\Delta\Psi_m$ reduction in Tctp knockdowns **(Figure 3.32C)**, supporting my initial conclusions regarding mitochondrial function in these embryos. In spite of these results, mitochondrial morphology in Tctp-depleted axons, as assessed by measuring the

length of axonal mitochondria, was not overtly different from controls **(Figure 3.33D)**. Taken together, these results show a significant reduction, both *in vitro* and *in vivo*, in axonal mitochondrial density in Tctp-depleted axons, as well as a decrease in axonal mitochondrial function and global energy levels, thus establishing a framework for understanding the axon outgrowth defects we have characterized in Tctp knockdowns.

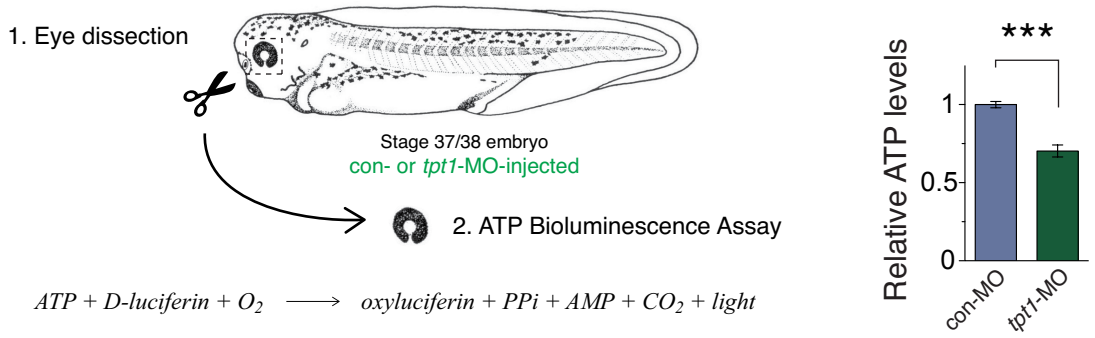

Figure 3.31 – Decreased energy levels in Tctp knockdowns. (A) Relative ATP levels per retina normalized to total protein (mean ± SEM; $n = 17$ per condition, *** $P < 0.0001$, unpaired t-test).

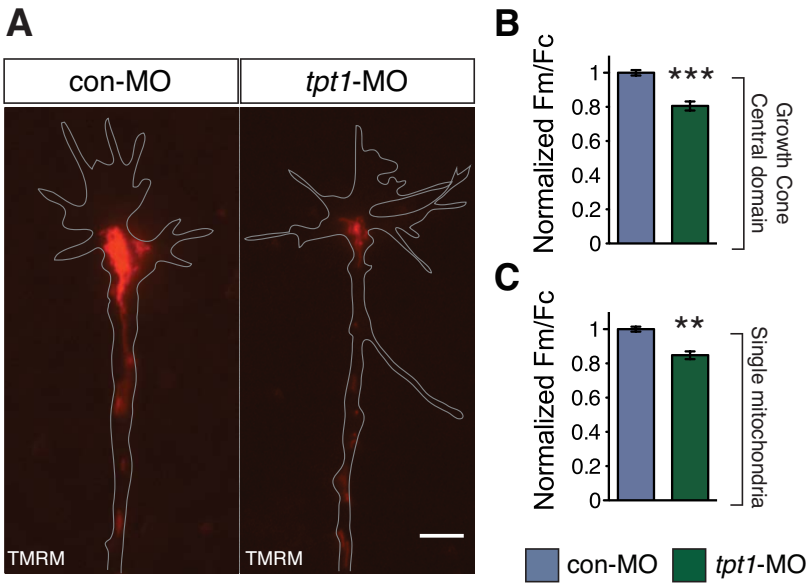

Figure 3.32 – Mitochondrial dysfunction in Tctp-depleted axons. (A) Representative con-MO and *tpt1*-MO-positive retinal ganglion cell growth cones loaded with TMRM. (B) Quantification of TMRM fluorescence intensity in the mitochondria-rich growth cone central domain (mean ± SEM; *** $P = 0.0002$, Mann-Whitney test). (C) Quantification of TMRM fluorescence intensity in individual mitochondria along the axonal compartment (mean ± SEM; ** $P < 0.0012$, Mann-Whitney test). A ΔΨp-controlled assessment of ΔΨm was derived from the ratio of fluorescence intensity between mitochondria (Fm) and mitochondria-poor regions (Fc) [259, 300]. Up to 10 replicate experiments were performed per condition, totaling 427 growth cones and 4918 individual mitochondria analysed. Scale bar: 5 µm.

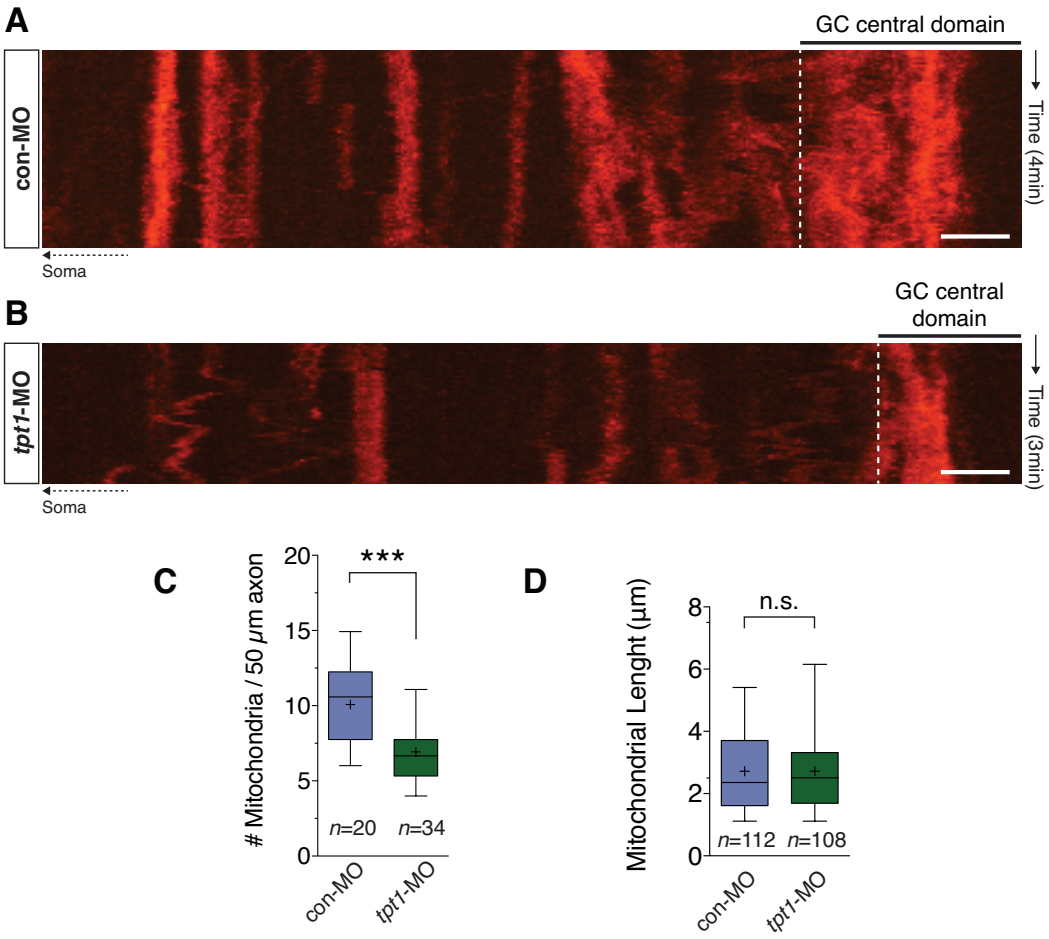

Figure 3.33 – Decreased mitochondrial density in Tctp-depleted axons – *in vitro* analysis. (A-C) Kymographs of MitoTracker-labeled mitochondria in con-MO- or *tpt1*-MO-positive retinal ganglion cell axons and quantification of axonal mitochondrial density (mean ± SEM; *n* = no. of axons analysed; *** $P < 0.0001$, Mann-Whitney test). Note also the weaker mitochondrial loading in Tctp-depleted axons (like TMRM, MitoTracker dyes are lipophilic cationic compounds; thus, their accumulation inside mitochondria is dependent on $\Delta\Psi_m$). (D) Quantification of mitochondrial length in cultured retinal ganglion cell axons. Scale bars: 5 µm. *This in vitro dataset complements the embryo data presented in Figure 3.34.*

C.2 Normal Mitochondrial Biogenesis and Mass in Tctp Morphants

The generation of new mitochondria in neurons is thought to occur mainly in the neuronal soma, being distributed from there to the cell periphery [260]. Thus, I next addressed whether the decrease in mitochondrial density detected in Tctp-depleted retinal ganglion cell axons stemmed from a global impairment of mitochondrial biogenesis. First, I documented normal mitochondria DNA copy numbers (*id est*, the ratio of mitochondrial to nuclear DNA), as evaluated by quantitative PCR (qPCR), in Tctp-depleted retinas **(Figure 3.35A)**. Western blot analysis of Tctp-depleted tissues showed, in addition, unaltered levels of

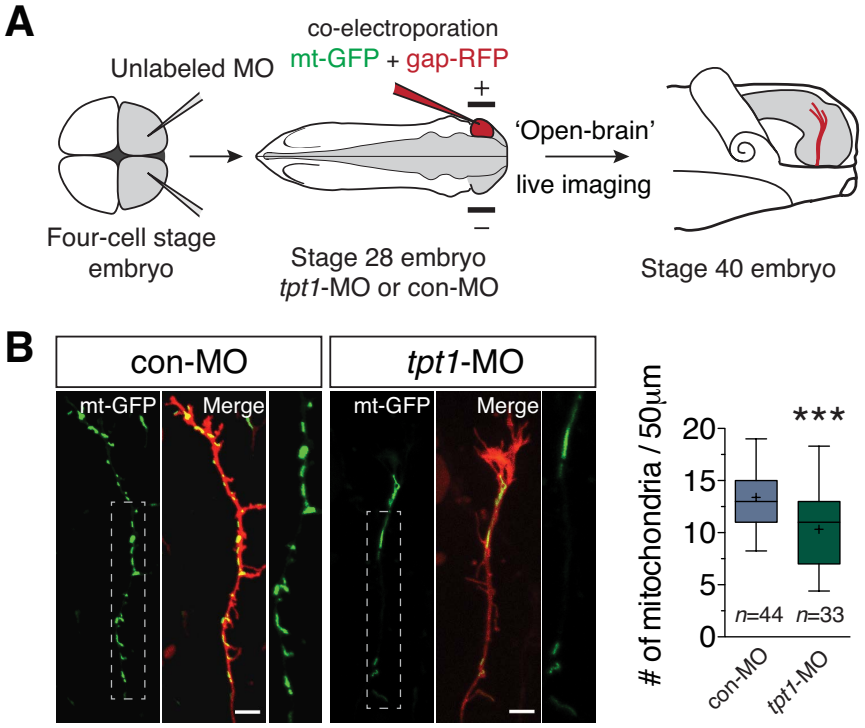

Figure 3.34 – Decreased mitochondrial density in Tctp-depleted axons – *in vivo* analysis. (A) Schematic representation of the experiment. (B) Micrographs of retinal ganglion cell axons co-labelled with mt-GFP and gap-RFP, plus quantification of axonal mitochondrial density (*n* = no. of axons analyzed; *** *P* = 0.0002, unpaired *t*-test; boxplot: whiskers cover 5-95 percentile, '+' denotes the mean value). Note that the boxed areas in the control and morphant backgrounds are shown at a higher magnification in the rightmost panels. *Experiment perfomed in collaboration with Hovy Ho-Wai Wong.*

Pgc1α (peroxisome proliferator-activated receptor gamma, coactivator 1 alpha), a master inducer of mitochondrial biogenesis and regulator of mitochondrial density in neurons [301] **(Figures 3.35B)**. I obtained a similar result with a luciferase reporter assay where the promoter region of human *pgc1a* was cloned upstream of the luciferase gene cassette and transfected into *tpt1* or control shRNA-infected HCT116 cells; here, measurements of reporter activity were not different between the two conditions, even though the decrease in Tctp expression was as high as 85% in these cells **(Figures 3.36A-C)**. Further corroborating these findings, the mRNA expression levels of the nuclear-encoded mitochondrial genes examined (*idh3a*, isocitrate dehydrogenase 3 (NAD^+) alpha; *cox5a*, cytochrome c oxidase subunit Va; *cysc*, cytochrome c, somatic), were unchanged relative to control retinas **(Figure 3.37A)**. Cytochrome c protein levels were also examined by western blot, confirming its normal expression in Tctp knockdowns **(Figure 3.37B)**. Collectively, these data strongly indicate that mitochondrial biogenesis and mass are unaffected in Tctp knockdowns, and consequently imply that the decrease in mitochondrial density detected in Tctp-depleted axons results from a secondary perturbation.

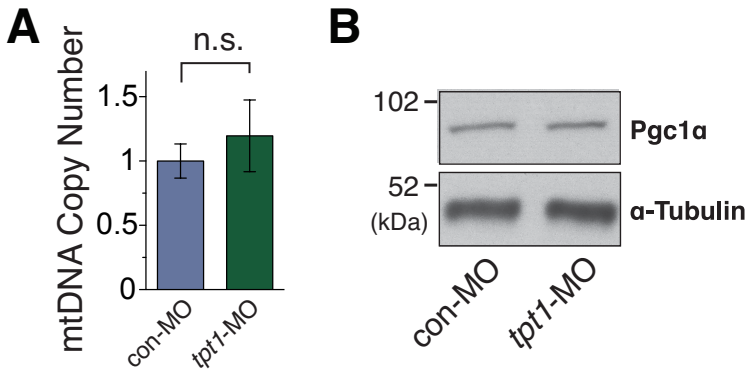

Figure 3.35 – Normal mitochondrial biogenesis in Tctp knockdowns. (A) The ratio of mitochondrial to nuclear DNA was determined by qPCR in control and Tctp-depleted retinas (mean ± 95% confidence interval; n = 7 paired retinas per condition; n.s., P = 0.23, Mann-Whitney test). (B) Protein samples prepared from con-MO- or *tpt1*-MO-injected embryos were run on a SDS-PAGE gel and Pgc1α was subjected to immunoblot analysis (n =3 independent samples; n.s., P = 0.8048, unpaired t-test).

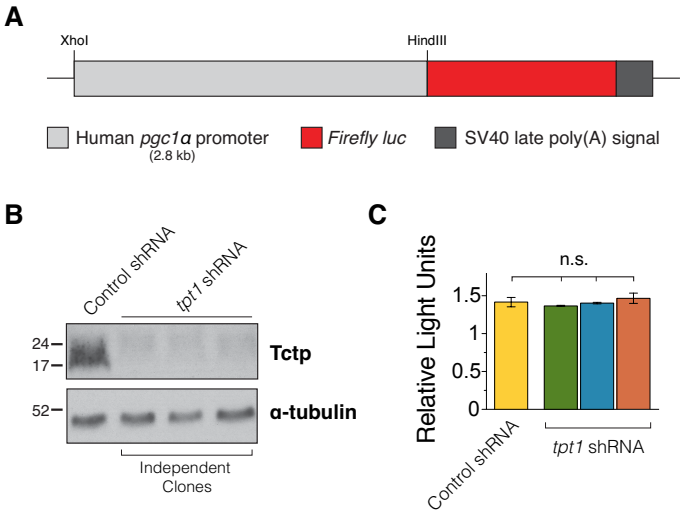

Figure 3.36 – Normal *pgc1a* expression in HCT116 cells deficient for Tctp. The rational for applying this seemingly indirect approach is not immediate. I knew *a priori* that basal P53 levels were elevated in *tpt1*$^{+/-}$ mice [24]. In turn, I later learned that the expression of *pgc1a* was repressed by the activation of P53 in the context of telomere dysfunction [340]. Since the mitochondrial traits I had identified in Tctp morphants were highly reminiscent of dysfunctional Pgc1α activity [301], I hypothesised that the activation of P53 in Tctp-deficient backgrounds could result in mitochondrial dysfunction due to its repression of *pgc1a* expression. Hence the strategy used here, for it allowed me to evaluate the expression of *pgc1a* at the transcriptional level. (A-C) The promoter region of human *pgc1a* (2.8 kb) was cloned upstream of the luciferase gene cassette and stably transfected into *tpt1* or control shRNA-infected HCT116 cells. Subsequently, lysates of *tpt1* or control shRNA-infected HCT116 cells were run on a SDS-PAGE gel and Tctp protein expression verified by western blot. Tctp expression knockdown was as high as 85% in these cells. Also shown is a plot of the average relative light units (RLU) measured in cells co-transfected with *pgc1a-luc* and a control plasmid (mean ± SEM; six biological replicates of *tpt1*-shRNA-infected cells were measured in triplicate in the two independent rounds of experiments conducted; *** P = 0.5544, one-way ANOVA).

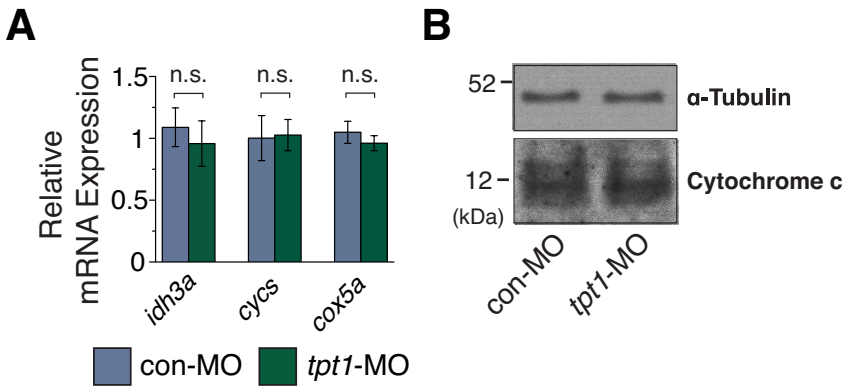

Figure 3.37 – Normal mitochondrial mass in Tctp knockdowns. (A) RT-qPCR analysis of nuclear-encoded metabolic genes in control and Tctp-depleted retinas (mean ± 95% confidence interval; $n = 9$ retinas per condition, Mann-Whitney test). (B) Protein samples prepared from con-MO- or *tpt1*-MO-injected embryos were run on a SDS-PAGE gel and Cytochrome c was subjected to immunoblot analysis ($n = 3$ independent samples; n.s., $P = 0.5989$, unpaired *t*-test)..

C.3 Tctp Knockdown Affects Mitochondrial Transport Dynamics in Axons

Having excluded impaired mitochondrial biogenesis, and because mitochondrial distribution and transport are inherently interdependent, I next investigated whether Tctp deficiency affects mitochondrial dynamics in axons. I was particularly intrigued by reports linking mitochondrial dysfunction in axons – which is present in Tctp knockdowns – to the transport of these organelles back to the cell body for recycling [302], a mechanism with a potential negative impact on axonal mitochondrial density. Analysis of time-lapse movies of labelled mitochondria showed a nonsignificant decrease in the number of motile mitochondria in Tctp-depleted axons (30.4% versus 37.2% in controls, $P = 0.3193$), accompanied by a higher proportion of mitochondria moving in the retrograde direction (8.7% versus 1.9% in controls, $P = 0.0358$) and fewer mitochondria moving anterogradely (21.7% versus 35.2% in controls, $P = 0.0353$) **(Figures 3.38A and 3.38B)**. This translated into a mean net movement in the anterograde direction of +4.4 µm versus +8.9 µm in controls – *id est*, considering the analysed population of mitochondria as a whole, including stationary and retrogradely trafficked organelles, the overall displacement of mitochondria in Tctp-depleted axons was smaller than in control axons, albeit still in the anterograde direction **(Figures 3.38A-D)**. Whereas a global characterization of mitochondrial transport dynamics had initially been sought, I next centred my analysis on the subset of axonal mitochondria undergoing fast transport,

A

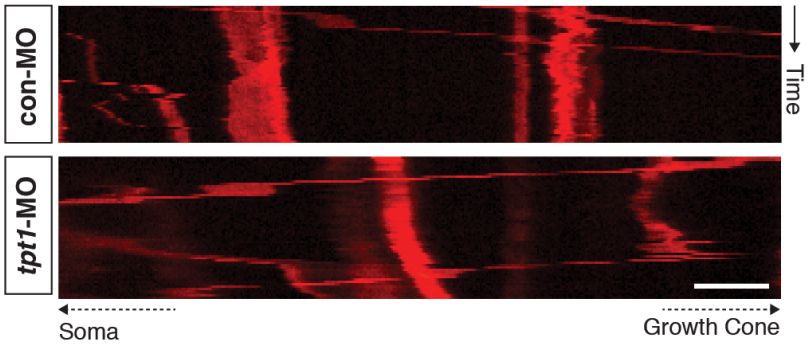

B

	con-MO[a]	*tpt1*-MO[b]	*P*-value
Anterogradely Transported Mitochondria	37/105 (35.24%)	25/115 (21.74%)	0.0353
Retrogadely Transported Mitochondria	2/105 (1.91%)	10/115 (8.70%)	0.0358
Stationary Mitochondria (Displacement ≤ 5 µm)	66/105 (62.86%)	80/115 (69.57%)	0.3193

[a] *n* = 14 axons [b] *n* = 16 axons

C

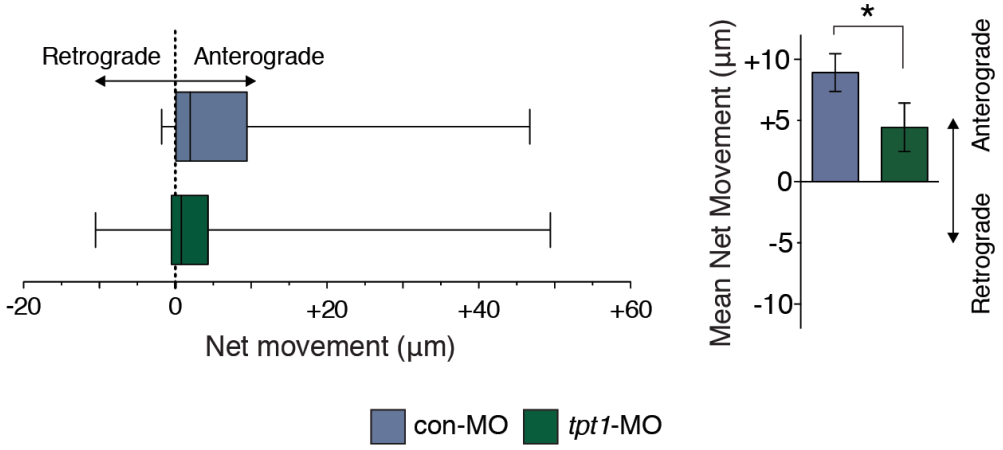

D

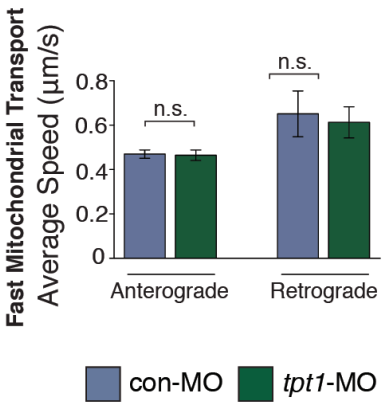

E

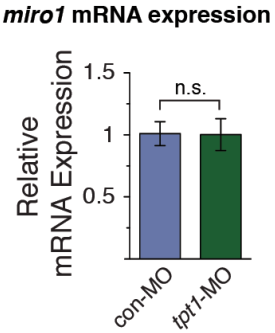

◀ **Figure 3.38 – Tctp knockdown affects mitochondrial transport dynamics in retinal ganglion cell axons.** (A) Kymographs showing the motility of MitoTracker-labeled retinal ganglion cell axonal mitochondria. (B) Summary of changes in axonal mitochondrial dynamics (Fisher's exact test). (C) Quantification of the relative mitochondrial motility and mean net movement in retinal ganglion cell axons (boxplot whiskers denote 5-95 percentile; right panel: mean ± SEM; * $P < 0.0117$, Mann-Whitney test). (D) Quantitative analysis of fast mitochondrial transport (mean ± SEM; $P = 0.9468$ (anterograde direction), $P = 0.7308$ (retrograde direction), Mann-Whitney tests). (E) RT-qPCR analysis of nuclear-encoded *miro1* in control and Tctp-depleted retinas (mean ± 95% confidence interval; $n = 9$ retinas per condition, $P = 1.00$ Mann-Whitney test). Scale bar: 5 µm.

which was *a priori* defined as encompassing those moving at average velocities of ≥ 0.3 µm/s. Notably, in this dataset, the velocity of transport in the anterograde and retrograde directions were not significantly different between both groups **(Figure 3.38D)**. Plus, using RT-qPCR, I found that the mRNA expression level of *miro1* (mitochondrial Rho GTPase 1, also known as *rhot1*), a key regulator of mitochondrial transport, was unchanged in Tctp knockdowns **(Figure 3.38E)**. Taken together, these findings show that mitochondrial dynamics are appreciably altered in Tctp-depleted retinal ganglion cell axons, with more mitochondria being trafficked retrogradely and fewer anterogradely. Additionally, they suggest that the mitochondrial transport machinery itself is not compromised upon Tctp knockdown. In any case, it must be stressed that this analysis was based on 5-minute long time-lapse movies; hence, what at first could be understood as a relatively small perturbation on mitochondrial trafficking dynamics, has in effect the potential to orchestrate a prominent decrease in axonal mitochondrial density over the course of axon development.

C.4 Axonal Tctp Interacts with Pro-survival Mcl1 and Bcl-X_L

How does mitochondrial dysfunction occur in Tctp-depleted axons? An attractive possibility stems from findings implicating Tctp as a positive modulator of mTOR signaling [19], a master kinase that controls cell growth and mitochondrial function [303, 304]. However, like reported by others [164, 305], I have not detected alterations in global mTORC1 activation in Tctp knockdown embryos, nor did treatment with bisperoxovanadium (bpV), a PI3K-Akt-mTOR signaling-promoting drug [297], ameliorate mitochondrial function in Tctp-depleted axons **(Figures 3.39A-D)**. Furthermore, as was documented in a previous section, rapamycin-treated embryos do not recapitulate the axon phenotype detected in Tctp knockdowns **(Figures 3.28A-D)**. Taken together, these findings strongly suggest that mTORC deregulation is unlikely to be at the core of the observed mitochondrial defects in Tctp knockdowns.

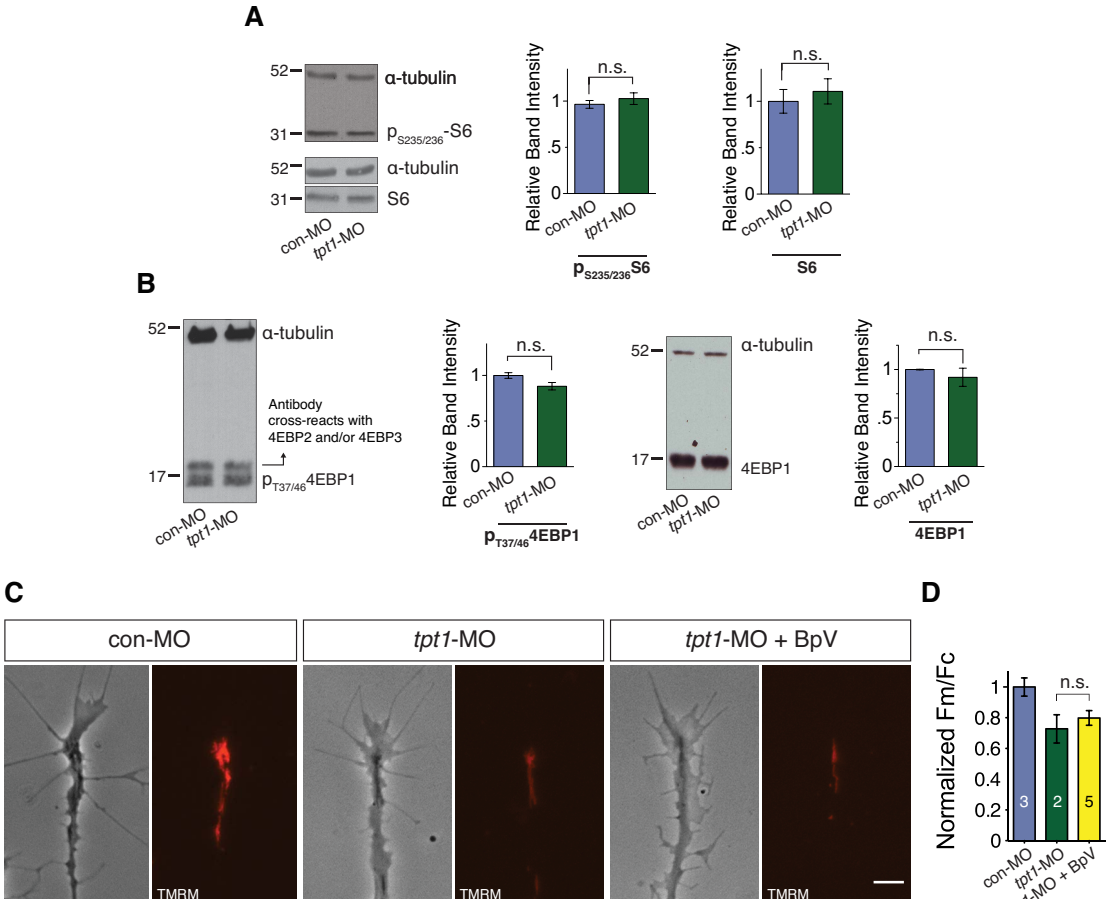

Figure 3.39 – Unaffected mTORC1 signaling in Tctp knockdown embryos. (A and B) CNS lysates of con-MO and *tpt1*-MO injected embryos were run on a SDS-PAGE gel and mTOR activation verified by western blot using antibodies that specifically recognize the mTORC1-mediated phosphorylation of rpS6 and 4EBP1. (mean ± SEM; n.s., not significant, unpaired *t*-tests; *n* =3). (C) Representative retinal ganglion cell growth cones loaded with TMRM. Of particular note, Tctp knockdowns raised in bisperoxovanadium (BpV), a PI3K/Akt/mTOR signaling-promoting drug, show no recovery in terms of ΔΨm. (D) Quantification of TMRM fluorescence intensity in the mitochondria-rich growth cone central domain (mean ± SEM; *n* = no. of independent experiments; '*tpt1*-MO' versus '*tpt1*-MO + BpV': n.s. *P* = 0.4809, unpaired *t*-test). A ΔΨp-controlled assessment of ΔΨm was derived from the ratio of fluorescence intensity between mitochondria (Fm) and mitochondria-poor regions (Fc) [259, 300]. Each replicate included four retinal explants; a total of 72 control, 47 Tctp-depleted, and 119 Tctp-depleted and BpV-treated axons were analysed in the course of this experiment. Scale bar: 5 μm.

An alternative hypothesis builds on reports documenting the interplay between Tctp and the B cell lymphoma-2 (Bcl-2) family of proteins, which comprises key cellular mediators of mitochondrial integrity [306]. Indeed, although it lacks the characteristic Bcl-2 homology domains shared by the members of this family, Tctp has been shown to interact with the anti-apoptotic oncoproteins myeloid cell leukaemia 1 (Mcl1) and Bcl-2-like protein 1 (Bcl-X_L) [189-191], and to interfere with Bcl-2 associated X protein (Bax) homodimerization in the mitochondrial outer membrane [17]. In addition, despite

Tctp being a cytosolic protein and lacking a membrane-binding region, its expression is documented as part of the mitochondrial proteome [307, 308], and Tctp has in fact been shown to anchor in the mitochondrial membrane [17], where much of the interplay between the Bcl-2 family members takes places [127]. Curiously, embryonic sensory neurons depleted of Bcl-2, the prototypic member of this family, have reduced axon growth rates [309], and the Bcl-2 family is associated in many instances with photoreceptor disease [310-312]. Hence, the phenotypes I have characterized in Tctp-deficient axons and photoreceptors, together with its close links to the Bcl-2 family, prompted me to explore Tctp's potential interactions in neuronal cells.

First, I investigated if Mcl1 is expressed *in vivo* by retinal ganglion cells using an antibody raised against the *Xenopus laevis* protein [313]. Similarly to Tctp, Mcl1 was expressed throughout the neural retina and particularly in the inner plexiform layer (IPL), the outer plexiform layer (OPL) and the inner segment of photoreceptors **(Figures 3.40A and 3.40D)**. Mcl1 was also detected in the ganglion cell layer (GCL), the optic fiber layer (OFL) and the optic nerve head (ONH), indicating that Mcl1 localizes to retinal ganglion cell axons *in vivo* **(Figure 3.40B)**. Supporting these results, immunofluorescence studies on cultured eye explants confirmed Mcl1 expression in retinal ganglion cell axons and growth cones **(Figure 3.40C)**. Regrettably, the lack of a specific antibody against Bcl-X_L precluded the analysis of its expression in the embryonic *Xenopus laevis* retina, but in rat this protein is reported to specifically localize to the

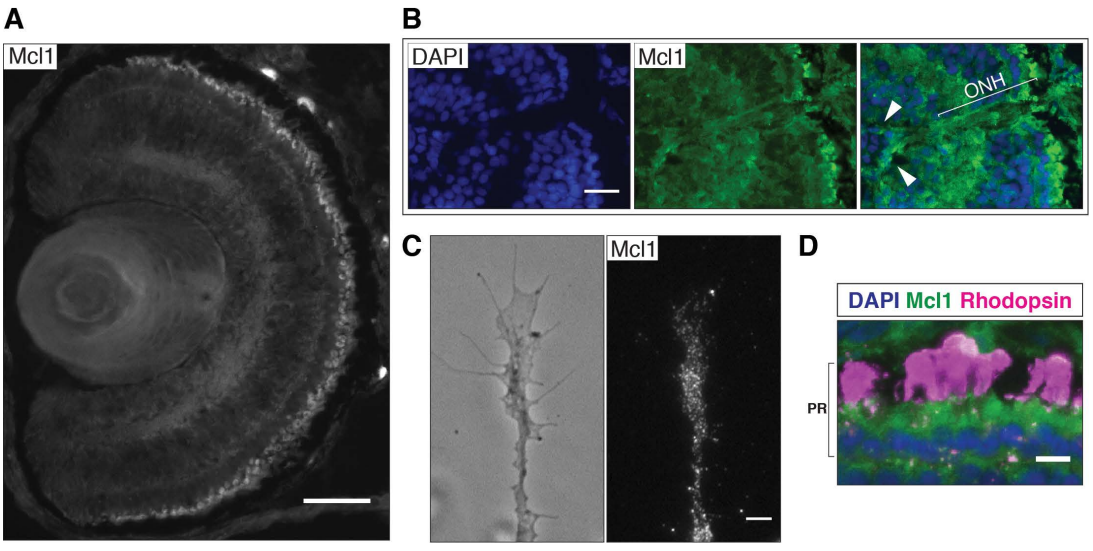

Figure 3.40 – Mcl1 is expressed in retinal ganglion cell axons and growth cones. (A and B) Coronal section of stage 43 wild-type retina probed for Mcl1. In (B), Mcl1 can be seen localizing in the optic fiber layer and optic nerve head (ONH). Arrowheads indicate the optic fiber layer. (C) Growth cone stained for Mcl1. (D) Photoreceptor (PR) layer of a stage 43 wild-type retina probed for Mcl1 and Rhodopsin. Scale bars: 50 μm in (A), 25 μm in (B), 5 μm in (C), and 10 μm in (D).

ganglion cell layer, the inner plexiform layer, the outer plexiform layer, and the inner segment of photoreceptors [314]. In line with these data, both Mcl1 and Bcl-X_L were detected in axons and dendrites of cultured *Rattus norvegicus* cortical neurons, confirming that, like Tctp, these proteins are present in neurites **(Figures 3.41A-C)**.

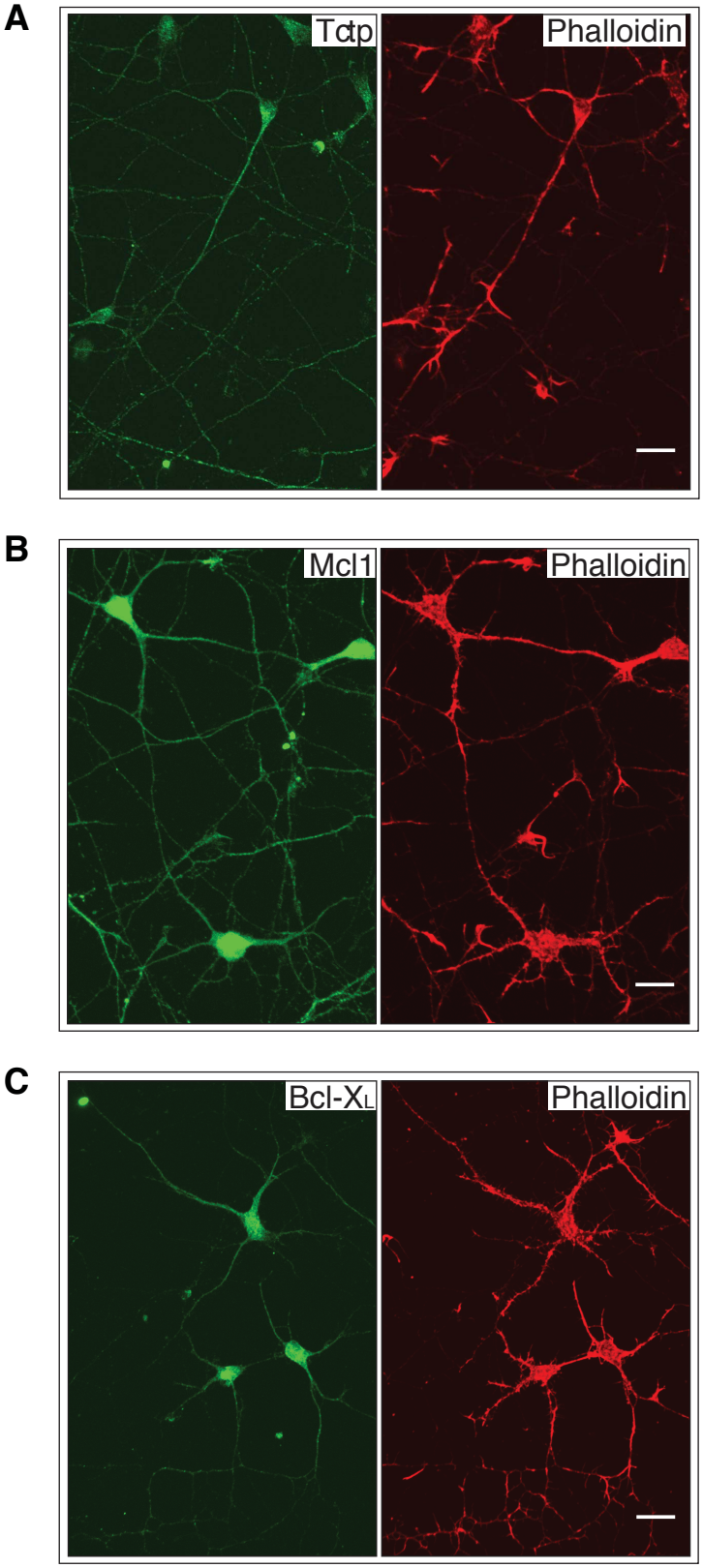

Figure 3.41 – Mcl1 and Bcl-X_L are expressed in the neurites of *Rattus norvegicus* cortical neurons. (A-C) Cultured rat cortical neurons (E18.5 + 3DIV) stained for Tctp, Mcl1 or Bcl-XL, and counterstained with Phalloidin. Scale bars: 25 µm.

I then tested whether Tctp physically interacts in axons with Mcl1 and Bcl-X_L using a proximity ligation assay (PLA)[a] [315]. I resorted to rat cortical neurons in these studies due to my inability to locate matching sets of *Xenopus laevis*-specific primary antibodies raised in different hosts, a central requirement of this methodology. Tctp-Mcl1 PLA dots, *id est*, pairs of Tctp and Mcl1 epitopes, were abundantly detected in the cell body, but also along the axon, dendrites and growth cone central domain of rat cortical neurons (E18.5 + 3 DIV) **(Figure 3.42A)**. I obtained an even more profuse signal in cultures aged *in vitro* for 14 days, suggesting these interactions are not transient phenomena **(Figure 3.42B)**. Similarly, pairs of Tctp and Bcl-X_L epitopes were also detected in these cells, mimicking the distribution of Tctp-Mcl1 interaction events, but occurring much less extensively at E18.5 + 3 DIV and to a comparable degree at E18.5 + 14 DIV **(Figure 3.44)**.

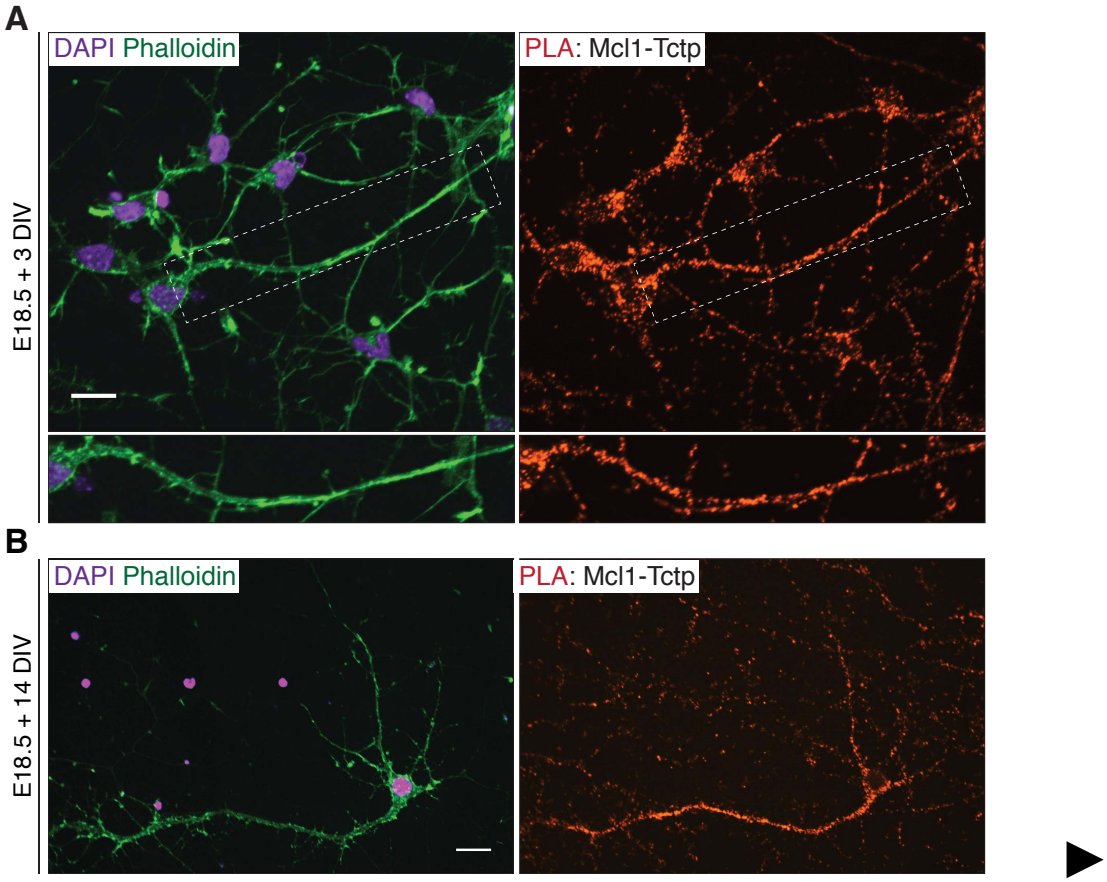

[a] A PLA reaction generates a positive signal only when the two target epitopes are in close vicinity, the theoretical maximum working distance between two proteins of interest being 30-40 nm. Thus, this method allows protein-protein interactions to be analysed *in situ*.

Figure 3.42 – Axonal Tctp interacts with pro-survival Mcl1. (A) PLA signal for Tctp and Mcl1 in cultured rat cortical neurons (E18.5 + 3 DIV) counterstained with DAPI and Phalloidin. Note that the boxed area is shown at a higher magnification in the bottom panels. (B) PLA signal for Tctp and Mcl1 in cultured rat cortical neurons (E18.5 + 14 DIV) counterstained with DAPI and Phalloidin. Scale bars: 10 µm.

```
Human Mcl1    249 VMIHVFSDGVTNWGRIVTLISFGAFVAKHLKTINQE 284
Rat Mcl1      251 VMVHVFSDGVTNWGRIVTLISFGAFVAKHLKSINQE 286
Mouse Mcl1    251 VMVHVFSDGVTNWGRIVTLISFGAFVAKHLKSINQE 286
Rabbit Mcl1   230 VMVHVFKDGVTNWGRIVTLISFGAFVAKHLKSVNQE 265
Chick Mcl1    230 VAAHVFNDGVTNWGRVVTLISFGAFVAKHLKSINQE 265
X. laevis Mcl1 174 VPALVFNDGVTNWGRIVTVISFGAFVAKHLKSLNLE 209
                   *  **  *********.***.**************..*  *
```

Figure 3.43 – The critical lysine residue for Mcl1 to interact with Tctp is conserved from *Homo sapiens* to *Xenopus laevis*. (A) Amino acid sequence alignment of vertebrate Mcl-1. The key lysine residue for Tctp:Mcl-1 interaction, as defined by Liu et al. [190], is shown in green. The Bcl-2 homology (BH)-1 domain is indicated in yellow. Asterisks indicate fully conserved residues; colons and periods denote residues with strongly similar and weakly similar properties, respectively.

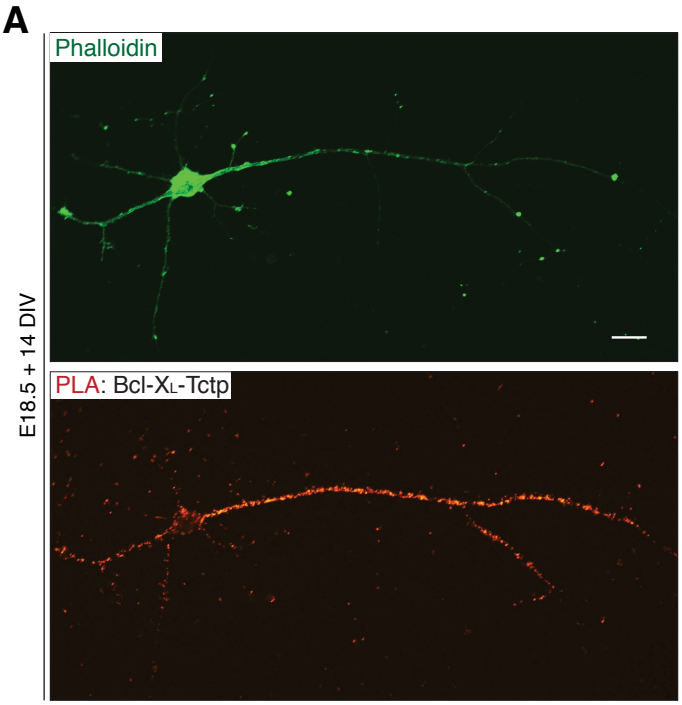

Figure 3.44 – Axonal Tctp interacts with pro-survival Bcl-X_L. (A) PLA signal derived for Tctp and Bcl-X_L interactions in cultured rat cortical neurons (E18.5 + 14 DIV) counterstained with Phalloidin. Scale bar: 10 µm.

Mechanistically, the pro-survival members of the Bcl-2 family (e.g. Mcl1 and Bcl-X_L) operate by sequestering initiator and executioner pro-apoptotic proteins (e.g. Bax), thus preventing the release of Cytochrome c from the mitochondrial intermembrane space and subsequent activation of caspases; as such, the interactions between the members of this family are dictated by local equilibria that are dependent on their relative protein concentrations and binding affinities [126, 127]. Of particular note, Tctp stabilizes and enhances Mcl1 biological activity [190], and promotes P53 degradation [24, 316], which itself neutralizes the pro-survival actions of Bcl-X_L and Bcl-2 at the mitochondria [317]. Therefore, I reasoned that Tctp-depleted axons might develop a detrimental balance between the pro- and anti-apoptotic arms of the Bcl-2 family. While *Xenopus laevis* retinal ganglion cell axons and growth cones depleted of Tctp did not manifest altered levels of Mcl1 **(data not shown)**, I found using quantitative immunofluorescence that P53 expression levels were significantly upregulated in this subcellular domain **(Figure 3.45)**, corroborating the findings by Telerman and colleagues in various organs of *tpt1*$^{+/-}$ mice [24]. In line with this evidence, I measured a 50% increase in active Caspase-3 mean signal relative to controls **(FIgure 3.46)**. Collectively, these data validate previous biochemical reports and add a hitherto unexplored subcellular dimension to them, revealing that Tctp-Mcl1 and Tctp-Bcl-X_L interactions occur in the cell body and processes of neuronal cells. In addition, while caspases mediate normal physiologic processes in neurons [193], including growth cone chemotropic responses [318], the levels of P53 and cleaved Caspase-3 indicate that mitochondrial dysfunction in Tctp-depleted axons can arise as a result of unbalanced, and therefore detrimental, pro-apoptotic signaling.

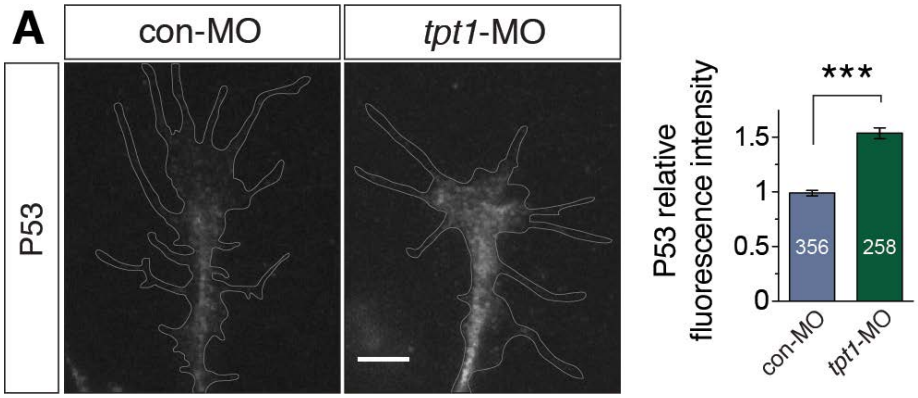

Figure 3.45 – Expression of P53 in growth cones is upregulated in Tctp morphants. (A) Representative con-MO and *tpt1*-MO-positive retinal ganglion cell growth cones stained for P53, and respective quantification (mean ± SEM; *n* = no. of growth cones analysed; *** *P* = 0.0002, unpaired *t*-test). Scale bar: 5 µm.

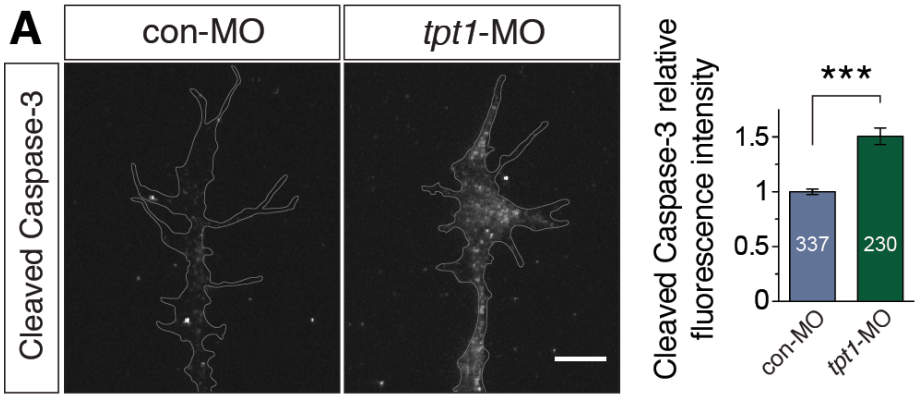

Figure 3.46 – Increased Caspase-3 activation in the growth cones of Tctp-depleted embryos. (A) Representative con-MO and *tpt1*-MO-positive retinal ganglion cell growth cones probed with an antibody that specifically recognizes the cleaved form of Caspase-3, and respective quantification (mean ± SEM; *n* = no. of growth cones analysed; *** *P* = 0.0002, unpaired *t*-test). Scale bar: 5 μm.

4. Discussion

Neurons are highly compartmentalized cells with great energy demands. Given their elongated morphology and unique metabolic requirements, mitochondrial operation needs to be appropriately regulated in these cells to sustain neuronal processes. This assumes particular relevance at distal axon terminals, which require the localized presence of mitochondria to support axon growth, maintenance, and synaptic transmission [260]. Significantly, the results herein identify axonally enriched Tctp as a cell-autonomous checkpoint for the normal development of the retinotectal projection by promoting axon survival. In particular, my findings show that Tctp-deficient retinal ganglion cell neurons have impaired axon outgrowth rates *in vivo*, and that mitochondrial homeostasis is compromised in this subcellular domain.

4.1 Tctp and Cellular Homeostasis

Tctp expression has been linked to cell growth in multiple contexts, including during bone development and in cancer [19, 25, 174, 180, 181, 194]. Still, perhaps the strongest molecular clue corroborating its involvement in growth programs comes from the identification of a 5'-terminal oligopyrimidine (TOP) motif in vertebrate *tpt1* transcripts [319, and my own observations], a hallmark of a subset of mRNAs specifically regulated by mTORC1 that shift to the translationally active polysome fraction when resting cells are induced to grow or proliferate [171, 320]. Although archetypal examples of TOP mRNAs include those encoding ribosomal proteins and elongation factors – effectively the build-up of the translational apparatus is needed to accommodate the increased demand for protein synthesis during growth programs [172] – the findings

herein presented suggest that Tctp may function in axons as an indirect growth 'enabler' rather than a de facto growth 'promoter', by participating in the maintenance of a permissive cellular environment for axonal growth. Indeed, following on previous biochemical reports [189-191], I show that Tctp interacts in axons with key pro-survival members of the Bcl-2 family, and that P53, which itself neutralizes the actions of Bcl-2 and Bcl-X_L [317], is upregulated in Tctp-deficient axons. Moreover, Tctp is reported to protect cells from oxidative stress [167], a detrimental by-product of growth programs when not adequately counteracted. Consistent with these considerations, one day after reaching the optic tectum, when most retinal ganglion cells have effectively stopped extending their axons and synaptogenesis is under way, *tpt1* mRNA and its encoded protein are still present in the axonal compartment. Furthermore, *tpt1* is expressed throughout the adult central nervous system [168] and, in particular, still ranks among the most enriched transcripts in adult sensory axons [13], indicating that Tctp remains important after the development of the nervous system, as indeed would be expected of a protein that contributes to cellular homeostasis.

4.2 On the Axonal Expression and Regulation of *tpt1*

In concordance with genome-wide transcriptomic evidence by several independent research groups [11-14], my data show that *tpt1* is expressed abundantly in the axonal compartment of retinal ganglion cells. Indeed, my results indicate that *tpt1* transcripts are nearly 10-times more prevalent in axons than *actb*, widely regarded as the standard axon-enriched message [4, 5, 254]. Moreover, differently from other known axon-targeted mRNAs, *tpt1* transcripts containing the shorter 3'UTR variant (*tpt1*-S) were here documented to be the predominant form expressed in retinal ganglion cell axons. This is a surprising finding in the field of neuronal mRNA localization, considering that longer 3'UTRs have been known to harbour unique *cis*-regulatory elements that allow for the distal trafficking of transcripts [136, 262]. Prominent examples of this paradigm include *importinb1* and *impa1* in axons [11, 153], in addition to *bdnf* and *camk2a* in dendrites [262, 263][a]. At first glance, the most parsimonious explanation for this result is that the longer *tpt1* mRNA variant (*tpt1*-L) contains a soma-restricting element of some sort. However, careful examination of the data presented in Figure 3.7C of the Results Section argues against this possibility, since the expression level of *tpt1*-L transcripts in

a Gene names: *karyopherin (importin) beta 1* (*importinb1*), *inositol(myo)-1(or 4)-monophosphatase 1* (*impa1*), *brain-derived neurotrophic factor* (*bdnf*), and *calcium/calmodulin-dependent protein kinase (CaM kinase) II alpha* (*camk2a*).

the axonal compartment appears to be almost on a par with that of *actb* ($\Delta Cq_{tpt1\text{-}L:actb} \approx -1$, meaning that, for every *tpt1*-L message populating the axon, there are two encoding for β-actin). That is, on these terms, *tpt1*-L cannot be ruled as a weakly expressed isoform in axons; instead, this result suggests that the *tpt1*-L mRNA variant is actively trafficked into axons. In any case, it is noteworthy that shorter 3'UTRs are associated with more efficient translation kinetics [337], a feature that can partly justify why an 'uncomplicated' transcript encoding for a protein with constitutive axonal functions such as Tctp might actually be favoured in a 'housekeeping' context. Still, the clearest hint to the overall cellular significance of *tpt1*-S is perhaps found in the genomes of *Mus musculus* and *Rattus norvegicus*: to the best of my knowledge, these species, unlike *Xenopus laevis*, *Oryctolagus cuniculus* (rabbit) [168], and *Homo sapiens* [168], do not express *tpt1* mRNA variants bearing longer 3'UTRs. This enigmatic evolutionary history inherently implies that the core of Tctp 'signature' functions is regulated solely through *tpt1*-S. Conversely, the reappearance of longer *tpt1* mRNA variants in *Oryctolagus cuniculus* and *Homo sapeins* with relatively little homology to *Xenopus laevis tpt1*-L suggests that newer biological functions may have been acquired by Tctp later in vertebrate evolution **(Figure 4.1)**.

4.3 Axonal Tctp and Local Translation

Several lines of study have established that Tctp cellular levels are regulated in response to extra- and intracellular signals, including growth signals and certain cytokines [159, 163, 196, 197], though the biological significance of this modulation remains unknown. Comparably, I observed protein synthesis-dependent increases in growth cone Tctp expression levels after acute treatment with Netrin-1, an mTORC1-inducing chemotropic guidance cue encountered by navigating and target-arrived retinal ganglion cell axons [144, 321], suggesting that the local translation of Tctp is subcellularly regulated during development.

It is well documented that caspases can be physiologically activated during multiple aspects of normal neuronal development and operation without signaling for the destruction of the entire cell [193]. Indeed, the localized activation of caspases, as seen in long-term depression (LTD) [322] or downstream of Slit1a-Robo2 signaling to control axonal arborization [323], might be understood as a form of subcellular apoptosis, with cellular and functional alterations that are limited in time and space [193]. Notably, the activation of Caspase-3 in retinal ganglion cell growth cones is also required for the chemotropic guidance responses induced by Netrin-1 [318]. Upstream of caspases,


A
X. laevis – H. sapiens 3'UTR Sequence Homology
tpt1-S
73%
tpt1-L
45%
tpt1-S + tpt1-L
56%
BAD AVG GOOD
Frog : 56
Human : 56
cons : 56
First polyadenylation signal
B
O. cuniculus – H. sapiens 3'UTR Sequence Homology
tpt1-S
97%
tpt1-L
94%
tpt1-S + tpt1-L
95%
BAD AVG GOOD
Human : 95
Rabbit : 95
cons : 95
First polyadenylation signal

◀ **Figure 4.1 – Poor sequence conservation between *Xenopus laevis* and *Homo sapiens tpt1*-L.** The *tpt1* 3'UTR in *Xenopus laevis* and *Homo sapiens* (A), or in *Oryctolagus cuniculus* (rabbit) and *Homo sapiens* (B), were aligned using the T-Coffee web resource. Note that upstream of the first polyadenylation signal (*id est*, the segment encompassing *tpt1*-S) both *Xenopus laevis* and *Oryctolagus cuniculus* show appreciable sequence homology relative to *Homo sapiens*, suggesting that *tpt1*-S is under the same regulatory constrains in these species. By contrast, the level of sequence conservation relative to *Homo sapiens* drops significantly in *Xenopus laevis* downstream of this motif (that is, in the unique region of the *tpt1*-L 3'UTR), but remains nearly unchanged between *Oryctolagus cuniculus* and *Homo sapiens*. Hence, this *in silico* dataset indicates that *tpt1*-L and the pool of Tctp protein in encodes for may have acquired over the course of vertebrate evolution additional regulatory domains and new biological functions, respectively. The boxed areas denote the location of the first polyadenylation signal (AATAAA).

pro-apoptotic Bcl-2-associated agonist of cell death (Bad) and Bcl-2 antagonist/killer (Bak) are also necessary for LTD induction, implicating the Bcl-2 family in this neurophysiologic paradigm [324]. Hence, it follows as necessary that local mechanisms be in place to control the physiologic activation of apoptotic cascades and neutralize these destructive programs [193].

Critically, Bax is reported to act upstream of the caspase pathway in the context of trophic deprivation-induced axonal degeneration [341], while both Mcl1 and Bcl-X_L, pro-survival Tctp interactors, have been shown to block Bax- and Bak-mediated apoptotic programs [193]. Thus, due to its association with members of the apoptotic machinery, Tctp is potentially apt to influence the regulation of axonal caspase cascades. Indeed, the spatiotemporal precision conferred to newly synthesized Tctp molecules may influence, through the stabilization and enhancement of Mcl1 biological activity [190], or the inhibition of Bax dimerization on a local scale [17], the confined modulatory response required to limit the effects of the regional activation of caspases. In line with these considerations, ribosome immunopurification data recently obtained in the Holt laboratory indicate that pro-apoptotic Bax is locally translated in target-arrived retinal ganglion cell axons *in vivo* (Hosung Jung, Toshiaki Shigeoka, and Christine Holt, unpublished observations). Furthermore, it is noteworthy that neurotrophin stimulation of nerve terminals promotes *de novo* synthesis of another pro-survival factor, Bcl-2-like protein 2 (Bcl-w), which was shown to prevent axonal degeneration by counteracting caspase activation subcellularly [133]. Like Tctp [a][17], Bcl-w is known to associate with Bax and inhibit Bax-induced mitochondrial outer membrane permeabilization [325]. Whether Tctp, Bcl-w and Bax are locally and synchronously regulated during axon development is, therefore, an enticing direction of investigation.

---

a As mentioned in the Introduction Section, Susini et al. reported that Tctp *indirectly* inhibits Bax dimerization and consequent Bax-induced mitochondrial outer membrane permeabilization. The authors suggest that it may do so by recruiting Mcl1 and Bcl-X_L to the mitochondrial membrane [17].

4.4 Mitochondrial Density in Tctp-deficient Axons

The axonal transport of cargos, be it organelles, synaptic vesicles or RNA granules, requires a constant provision of ATP to power the activity of dynein and kinesin motors [135]. However, unlike vesicular fast axonal transport, which is reliant on the glycolytic pathway for its energetic needs [338], the trafficking of mitochondria is dependent on the ATP produced by oxidative phosphorylation [338, 339]. Thus, considering the disruption of mitochondrial membrane potential observed in Tctp-depleted axons, a parameter correlated with the capacity of mitochondria to generate ATP by oxidative phosphorylation, and that embryos depleted of Tctp actually have a lower ATP content than age-matched controls[a], the defective accumulation of mitochondria at the neuronal periphery was perhaps, in hindsight, a predictable outcome of my analysis. In turn, it has been reported that dysfunctional mitochondria in neurons are transported back to the cell body for repair and/or degradation [260, 302][b], and, more recently, that mitophagy of damaged mitochondria can take place locally in axons [327]. Thus, the mechanisms identified by these studies have the potential to exacerbate any mitochondrial distribution defect already existing in Tctp-depleted neurons. While the subcellular component of mitophagy was not addressed herein, the increased numbers of retrogradely transported mitochondria in Tctp-depleted axons suggests that the mechanism elucidated by Miller and Sheetz contributes towards the overall mitochondrial phenotype in Tctp-deficient axons [302]. Indeed, the subcellular insult to mitochondria in these axons – whether exclusively a consequence of the imbalance in pro- and anti-apoptotic signaling, or arising in concert with an complementarily acting pathway – may in effect potentiate a secondary perturbation on mitochondrial dynamics, with more organelles being shuttled back to the cell body for repair. These ideas are thoroughly supported by my findings on normal mitochondrial biogenesis and mass in Tctp knockdowns, as they imply that the reduced mitochondrial density detected in Tctp-depleted axons does not stem from an inability of the neuron to generate mitochondria. Furthermore, given that

---

a Note that the data collected on the total ATP content of Tctp knockdowns does not discriminate between a decline in glycolysis or oxidative phosphorylation. Still, given that postmitotic retinal cells in *Xenopus laevis* are known to be more dependent on oxidative phosphorylation than on glycolysis for its energetic needs [258], and considering the overwhelmingly superior output in terms of energy production of the former process, it stands to reason that the decline in total ATP levels results, at least to some extent, from an impairment in mitochondrial ATP production.

b Miller and Sheetz demonstrated that the direction of transport of individual mitochondrion in axons is correlated with the mitochondrial membrane potential ($\Delta\Psi_m$). In particular, approximately 9 out of 10 mitochondria with a high $\Delta\Psi_m$ were observed to progress in the anterograde direction (that is, towards the growth cone), whereas circa 8 out of 10 mitochondria with low $\Delta\Psi_m$ moved retrogradely towards the neuronal cell body [302].

fast mitochondrial transport is unaltered in Tctp-deficient axons, it is equally unlikely that defects at the level of the transport machinery account *per se* for the decreased mitochondrial density observed. Likewise, the comparable proportion of stationary mitochondria in control and morphant axons indicates that adequate mitochondrial docking mechanisms are still in operation, whereas the normal length of these organelles in Tctp-deficient axons rejects deregulated mitochondrial fusion and/or fission as the basis for the decrease in axonal mitochondrial numbers. Hence, this body of work collectively points to the conclusion that the axonal mitochondrial loss seen in Tctp-deficient retinal ganglion cell axons arises from an impairment in mitochondrial function.

4.5 Tctp and Mitochondrial Function

How does axonal Tctp promote mitochondrial function? Although Tctp is a multifunctional protein, which potentially could have limited the interpretation of any finding, the range of phenotypes detected in Tctp knockdowns – compromised axon outgrowth rates arising in a cell-autonomous fashion, photoreceptor degeneration, and mitochondrial dysfunction – ultimately permitted to narrow down the list of possible candidates. Pro-survival members of the Bcl-2 protein family, such as Mcl1 and Bcl-X_L, work primarily by sequestering and neutralizing Bcl-2-related pro-apoptotic factors (e.g. Bax), which, if left uncontrolled, negatively impact on the integrity of mitochondria [127]. A fitting analogy would be a molecular tug of war contest, with pro- and anti-apoptotic Bcl-2-related factors on opposite sides of a rope, playing for mitochondrial homeostasis. According to the model put forward by Susini et al. [17], Tctp's pro-survival activity results from it blocking Bax dimerization, a key mitochondrial outer membrane permeabilization (MOMP)-inducing event, by binding and reconfiguring Mcl1 and Bcl-X_L in such a way that their inhibitory actions on Bax are effectively promoted. In this regard, Tctp is proposed to act as a cell survival *enhancer*. It is thus reasonable to assume that in axons chronically depleted of Tctp, part of the insult to mitochondria likely occurs due to a shift in the equilibrium between the pro- and anti-apoptotic arms of the Bcl-2 family. Indeed, the increased levels of cleaved Caspase-3 detected in Tctp-depleted axons serve as a key insight into the local over-activation of pro-apoptotic signaling. Crucially, though, considering that apoptosis is, in essence, a 'yes' or 'no' process [328], my observations also indicate that a full-scale cell death program does not occur in Tctp-deficient retinal ganglion cells – at least during the developmental stages analysed. Instead, the cellular insult produced in these neurons seems to impair mitochondrial integrity to a degree that repair responses are still deemed appropriate

by the cell.

Tctp may also promote mitochondrial integrity and axon survival indirectly through the negative regulation it exerts on P53 expression [24, 316, and corroborated by my own observations in Tctp-depleted axons]. In fact, P53 activation may influence axon development programs in a number of ways, since it can act both as a nuclear transcription factor and as a modulator of apoptosis in the cytoplasm [329, 330]. Of particular note, cytoplasmic P53 is known to translocate to the mitochondria under a range of cellular stresses [329], where it associates with and offsets Bcl-2 and Bcl-X_L pro-survival actions [317]. Similarly, cytoplasmic P53 has also been shown to interact with pro-apoptotic Bcl-2 homologous antagonist/killer (Bak) at the mitochondrial membrane[a], liberating it from the inhibitory effects constitutively exerted by Mcl1 [331]. Thus, as a whole, mitochondrially-translocated P53 can potentially exacerbate any pre-existing unbalance between pro- and anti-apoptotic signalling in Tctp-depleted neurons ensuing from Tctp's direct involvement in this pathway.

Based on the evidence discussed above, I propose that in Tctp-deficient axons a detrimental shift in the balance between the pro- and anti-apoptotic arms of the Bcl-2 family is produced and mitochondrial integrity is consequently compromised. Ultimately, this translates into mitochondrial dysfunction and an energy state that is insufficient to sustain the continuous expansion and rearrangement of a growing axon **(Figure 4.2)**. In other words, Tctp impacts on axon development by having an effect on the homeostatic mechanisms of the neuron.

4.6 The Tumour Suppressor P53 in Neurite Outgrowth

Above, for the sake of a coherent argument, I presented a rather one-sided view on how the activation of P53 can affect axon development. In fact, P53 biological activities are much more diversified, and the cellular significance of its upregulation in Tctp-depleted axons difficult to interpret. Two related reasons justify this initial oversimplification on my part: P53 mode of action is context-specific and is impacted by various post-translational modifications. Broadly speaking, P53 can be understood as having transcriptional and non-transcriptional functions [329]. Working as a transcription factor, P53 promotes the expression of an extensive list of genes involved in apoptosis (including *bax*,

a Like Bax, Bak can induce the permeabilization of the mitochondrial outer membrane.

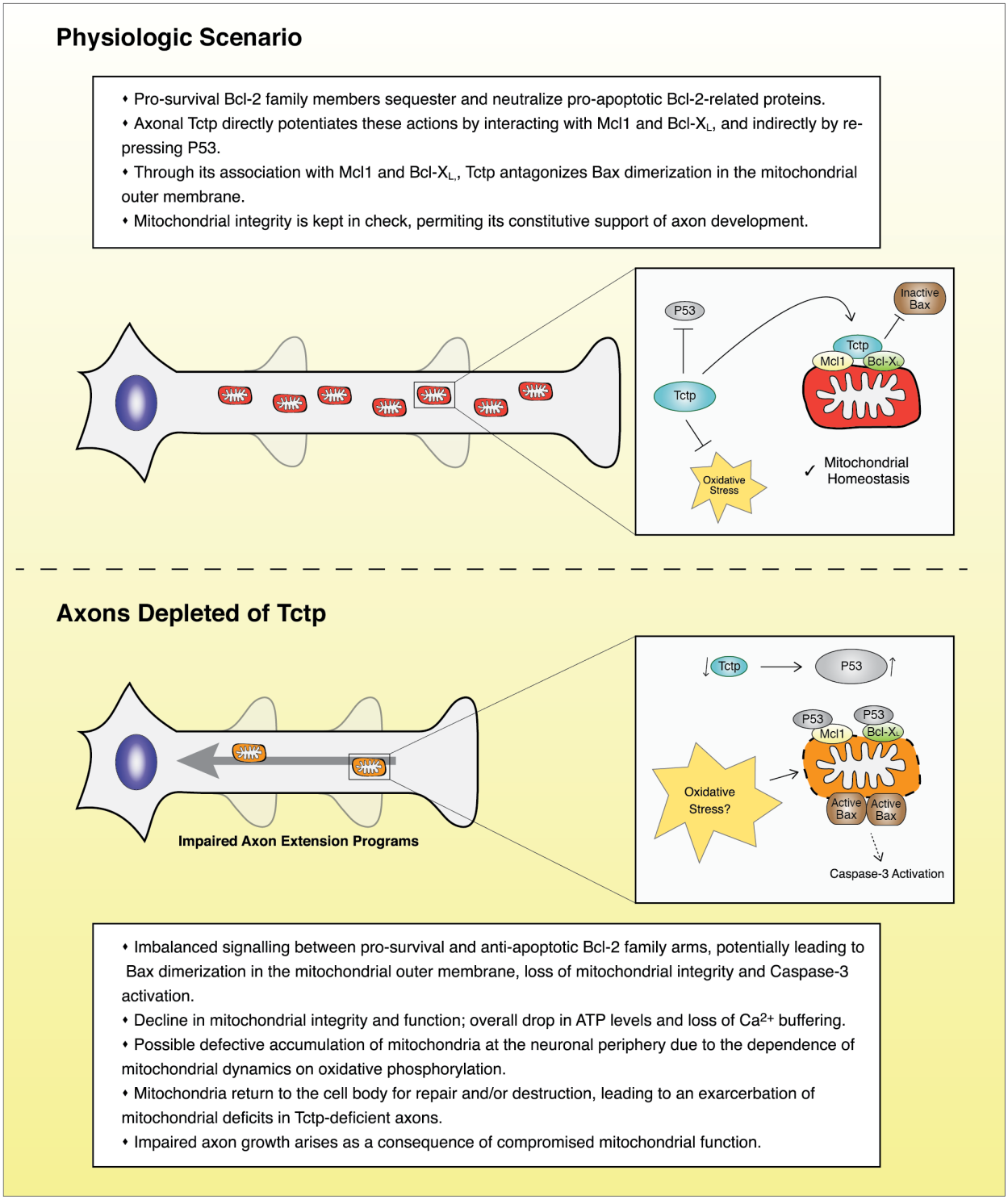

Figure 4.2 – A role for Tctp in neural circuitry formation - graphical overview.

as well as *puma* and *pmaip1*/*noxa*, which encode for BH3-only Bcl-2 proteins[a]), cell senescence, cell cycle progression, and metabolism, among others [329]. Furthermore, it is now well established that P53 specifically modulates the cytoskeletal response associated with neurite outgrowth elicited by neurotrophin- and cue-mediated signaling [342]. It does so by integrating these signals at the nuclear level, where it binds to the promoter region and activates the expression of a number of cytoskeleton-related genes, including *coronin1b* (which encodes for an actin-binding protein), *gap43* and *prkg1* [342][b]. Also of note, emerging evidence suggests that various classical axon guidance genes are similarly under the control of P53 in the context of tumorigenesis [343]. Cytoplasmic P53, on the other hand, in addition to associating with the mitochondrial outer membrane under a number of apoptosis-inducing conditions, where it counteracts the actions of Bcl-2 family pro-survival proteins [317], is also reported to inhibit autophagy and mitophagy [329, 344, 345], which, in the context of Tctp depletion, could accentuate the decline in mitochondrial integrity over the course of development. Moreover, although less well characterized, a direct, transcription-independent role for P53 in the regulation of the growth cone cytoskeleton has been recently defined [342]. Of particular importance, P53 antagonizes growth cone Rho-associated protein kinase (Rock) activity [346], and participates in Semaphorin 3A-induced growth cone collapse responses [347].

Given P53 often opposing roles, how can its many and spatially heterogeneous cellular effects be brought about? In general terms, the transcriptional versus non-transcriptional functions of P53 are determined, as already alluded to, by a plethora of post-translational modifications at several domains (e.g. ubiquitination, neddylation, sumoylation phosphorylation, and acetylation) that shape the balance of its nuclear and cytoplasmic pools, and its association with other proteins [329]. For example, unlike the mitochondrial translocation of P53, which is initially regulated by monoubiquitination[c] and carboxy-terminal phosphorylation events, P53 neurite outgrowth-promoting

---

a Gene names: *p53 upregulated modulator of apoptosis* (*puma*), also known as *bcl-2-binding component 3* (*bbc3*), and *phorbol-12-myristate-13-acetate-induced protein 1* (*pmaip1*), which encodes for a protein commonly known as Noxa.

b Gene name: *protein kinase, cGMP-dependent, type 1* (*pkrg1*).

c Note that P53 is apoptotically active in its non-ubiquitinated form – once at the mitochondria it gets deubiquitinated by herpesvirus-associated ubiquitin-specific protease (Hausp).

transcriptional activity appears to be mainly modulated by acetylation [329, 342]. Differently, P53-mediated inhibition of Rock at the growth cone is controlled by the phosphorylation of a serine residue in its N-terminus [346]. That is, as would be expected of a protein whose effects influence cells at so many different levels, P53 *modus operandi* is governed by an intricate network of regulatory signals, and, therefore, the outcome of its upregulation cannot be subjected to a one-dimensional evaluation. For this reason, it seems fruitless to elaborate much further on the possible transcription-dependent effects evoked by P53, as I have only characterized its expression in the growth cone of retinal ganglion cells. If anything, considering its negative impact on *pgc1a* transcription in the context of telomere dysfunction [340], and the apparently unaffected *pgc1a* expression levels in Tctp knockdown embryos and cells, one can perhaps infer that P53 activation in Tctp-depleted backgrounds might have a predominantly cytoplasmic component. Still, providing that is indeed the case, establishing the actual consequences of its upregulation in the axonal compartment of Tctp-deficient neurons will require additional experimental work to distinguish between its cytoskeletal and mitochondrial effects.

5. Future Perspectives

Whereas during my studies I have focused exclusively on examining the role of Tctp in the context of axon pathfinding, future work should aim at elucidating its implications in the adult nervous system. Indeed, the finding that *tpt1* is still one the most abundant transcripts in adult sensory axons [13], together with reports of deregulated Tctp protein expression in Down syndrome and Alzheimer's disease [128, 207, 336], two conditions associated with mitochondrial dysfunction, prompt speculation on whether Tctp may hold an important lifelong axonal function. However, given that Tctp contributes to the formation of neural circuits, temporal control over its knockdown will be a key aspect of any successful approach aimed at elucidating this question. New tools to meet such requisites *in vivo* are at tantalizing distance, since two different *Mus musculus* lines containing *floxed tpt1* alleles have already been established [17, 164]; *id est*, Tctp inactivation in a precisely limited temporal window could be achieved by crossing these animals with an inducible Cre recombinase strain. Considering that proper mitochondrial operation is an imperative of synaptic homeostasis [260], such strategy would, for example, allow one to study Tctp in the context of synaptic plasticity independently of underlying defects in neural circuitry formation.

It would also be important to investigate Tctp's axon and cell body roles separately. Indeed, judging from the immunofluorescence studies I conducted, Tctp is abundantly expressed not only throughout neuronal processes, but also in the soma of these cells, suggesting that its contribution to neuronal homeostasis may have a compartment-specific component. These considerations assume particular relevance given

the many functions that have been ascribed to Tctp over the past 20 years of scrutiny. This is, I believe, an important limitation of my doctoral work, as I have not been able to directly differentiate between global and axon-specific effects in the context of Tctp knockdown. Cumbersome genetics in *Xenopus laevis* – this frog species has an allotetraploid genome [91] – justifies this obstacle in large part, as effective genome-editing tools did not exist until very recently[a][332, 333]. By contrast, well-established gene knockdown methods like morpholinos target the different cellular pools of a given mRNA indiscriminately, precluding this type of analysis *in vivo*. A potential future strategy around these drawbacks could, for example, exploit the control exerted by the untranslated regions – and, in particular, that of the 3'UTR [136] – on the subcellular distribution of a transcript. To limit the axonal accumulation of *tpt1* transcripts, a *Xenopus laevis* or *Mus musculus* line could be engineered to have the *tpt1* 3'UTR substituted for that of a soma-restricted transcript, such as *tubb* (β-tubulin) [263, 334], or *actg1* (γ-actin) [254] – *id est*, *tpt1-tubb* or *tpt1-actg1* chimeras in place of the endogenous *tpt1* gene. Alternatively, the exon encoding for the 3'UTRs could be removed altogether from the *tpt1* gene. Still, supposing the proposed strains are viable, this approach would only partly succeed in reducing the expression of *tpt1* in axons, as *de novo* synthesis of Tctp protein would cease to occur locally, but axonal transport of cell body-derived protein – if it happens – would remain uncompromised. In any case, given the local enrichement of this mRNA species, it stands to reason to expect this type of approach to yield a better *in vivo* understanding of the axon-specific functions of Tctp (or, indeed, any other protein encoded by a subcellularly-targeted transcript).

At a molecular level, further research is also needed to characterize the regulatory duality of *tpt1* mRNA isoforms observed in growth cones exposed to Netrin-1[b]. This was, in fact, what led me to pursue the profiling of *tpt1* mRNPs in the first place. Had it not been for time constraints, the MS2-BioTRAP strategy applied simultaneously to the analysis of *tpt1*-S and *tpt1*-L mRNPs would likely have permitted the identification of some of the *trans*-acting factors behind the differential regulation exhibited by the two *tpt1* variants. In parallel, additional experiments using the *tpt1*-Kaede translation reporters in different stimulatory contexts (e.g. Semaphorin 3A or Slit 2, which, like Netrin-1, signal through the mTOR pathway, but induce repulsive turning responses in growth cones [115, 144]; as another option, a protocol with axon survival-promoting

a This paradigm has changed with the recent advent of CRISPR-Cas and TALEN technology.

b Although much less abundant in axons than *tpt1*-S, the expression of *tpt1*-L in retinal ganglion cell axons is almost on a par with that of *actb* mRNA, suggesting it plays an important subcellular function.

neurotrophins could be tried [133]), may achieve additional understanding regarding the modes of regulation behind *tpt1* expression. Overall, the questions posed by the differential regulation of *tpt1* isoforms echo on the necessity to globally elucidate the mechanisms regulating mRNA-specific translation programs in axonal processes populated by thousands of transcripts.

Concluding Remarks

Many mitochondrial dysfunctions lead to neurodegenerative conditions with prominent axonal phenotypes [129-131], suggesting that axons may be particularly vulnerable to mitochondrial compromise. A developing axon is all the more dependent on adequate mitochondrial operation, as it requires a continuous provision of energy and Ca^{2+} buffering for its expansion in the embryonic brain. The corollary to these ideas is that neurons must operate, as well as preserve, a tightly regulated mitochondrial network to sustain an axon's growth potential.

Many parallels can be drawn between the normal processes of migratory growth cones during axon development and the disease mechanisms of cancer cell invasion. Here, motivated by the abundance of its mRNA in diverse axonal populations, I pioneered the study of tumorigenic Tctp in the context of neural connectivity. Given the importance of maintaining an operational mitochondrial network to axon development and overall neuronal function, it is perhaps not surprising that all axonal populations analysed to date at the transcriptome level contain a large proportion of nuclear-encoded mitochondria-related mRNAs [2]. In fact, it has been estimated that up to 25% of all locally synthesized proteins are transported to the mitochondria [335]. Hence, my efforts to characterize Tctp in the context of axon development typify the significant biological investment put into supporting these organelles subcellularly.

In summary, the data collected over the course of my doctoral work indicate that Tctp regulates axon development by impacting on the homeostatic mechanisms of the neuron. My findings thus suggest a novel and fundamental role for Tctp in vertebrate neural circuitry formation.

References

1. Azevedo, F.A., et al., *Equal numbers of neuronal and nonneuronal cells make the human brain an isometrically scaled-up primate brain.* J Comp Neurol, 2009. **513**(5): p. 532-41.
2. Jung, H., B.C. Yoon, and C.E. Holt, *Axonal mRNA localization and local protein synthesis in nervous system assembly, maintenance and repair.* Nat Rev Neurosci, 2012. **13**(5): p. 308-24.
3. Harris, W.A., C.E. Holt, and F. Bonhoeffer, *Retinal axons with and without their somata, growing to and arborizing in the tectum of Xenopus embryos: a time-lapse video study of single fibres in vivo.* Development, 1987. **101**(1): p. 123-33.
4. Yao, J., et al., *An essential role for beta-actin mRNA localization and translation in Ca2+-dependent growth cone guidance.* Nat Neurosci, 2006. **9**(10): p. 1265-73.
5. Leung, K.M., et al., *Asymmetrical beta-actin mRNA translation in growth cones mediates attractive turning to netrin-1.* Nat Neurosci, 2006. **9**(10): p. 1247-56.
6. Wu, K.Y., et al., *Local translation of RhoA regulates growth cone collapse.* Nature, 2005. **436**(7053): p. 1020-4.
7. Brittis, P.A., Q. Lu, and J.G. Flanagan, *Axonal protein synthesis provides a mechanism for localized regulation at an intermediate target.* Cell, 2002. **110**(2): p. 223-35.
8. Natera-Naranjo, O., et al., *Local translation of ATP synthase subunit 9 mRNA alters ATP levels and the production of ROS in the axon.* Mol Cell Neurosci, 2012. **49**(3): p. 263-70.
9. Yoon, B.C., et al., *Local translation of extranuclear lamin B promotes axon maintenance.* Cell, 2012. **148**(4): p. 752-64.
10. Aschrafi, A., et al., *MicroRNA-338 regulates local cytochrome c oxidase IV mRNA levels and oxidative phosphorylation in the axons of sympathetic neurons.* J Neurosci, 2008. **28**(47): p. 12581-90.
11. Andreassi, C., et al., *An NGF-responsive element targets myo-inositol monophosphatase-1 mRNA to sympathetic neuron axons.* Nat Neurosci, 2010. **13**(3): p. 291-301.
12. Zivraj, K.H., et al., *Subcellular profiling reveals distinct and developmentally regulated repertoire of growth cone mRNAs.* J Neurosci, 2010. **30**(46): p. 15464-78.
13. Gumy, L.F., et al., *Transcriptome analysis of embryonic and adult sensory axons reveals changes in mRNA repertoire localization.* RNA, 2011. **17**(1): p. 85-98.
14. Taylor, A.M., et al., *Axonal mRNA in uninjured and regenerating cortical mammalian axons.* J Neurosci, 2009. **29**(15): p. 4697-707.
15. Minis, A., et al., *Subcellular transcriptomics-dissection of the mRNA composition in the axonal compartment of sensory neurons.* Dev Neurobiol, 2014. **74**(3): p. 365-81.
16. Thaw, P., et al., *Structure of TCTP reveals unexpected relationship with guanine nucleotide-free chaperones.* Nat Struct Biol, 2001. **8**(8): p. 701-4.
17. Susini, L., et al., *TCTP protects from apoptotic cell death by antagonizing bax function.* Cell Death Differ, 2008. **15**(8): p. 1211-20.
18. Kamath, R.S., et al., *Systematic functional analysis of the Caenorhabditis elegans genome using RNAi.* Nature, 2003. **421**(6920): p. 231-7.
19. Hsu, Y.C., et al., *Drosophila TCTP is essential for growth and proliferation through regulation of dRheb GTPase.* Nature, 2007. **445**(7129): p. 785-8.

20. Acunzo, J., et al., *TCTP as therapeutic target in cancers.* Cancer Treat Rev, 2014. **40**(6): p. 760-9.
21. Ramón y Cajal, S., *A quelle époque apparaissent les expansions des cellules nerveuses de la moelle épinière du poulet?* Anatomischer Anzeiger, 1890. **5**: p. 609-613.
22. Leung, L.C., et al., *Coupling of NF-protocadherin signaling to axon guidance by cue-induced translation.* Nat Neurosci, 2013. **16**(2): p. 166-73.
23. Tuynder, M., et al., *Biological models and genes of tumor reversion: cellular reprogramming through tpt1/TCTP and SIAH-1.* Proc Natl Acad Sci U S A, 2002. **99**(23): p. 14976-81.
24. Amson, R., et al., *Reciprocal repression between P53 and TCTP.* Nat Med, 2012. **18**(1): p. 91-9.
25. Kaarbo, M., et al., *TCTP is an androgen-regulated gene implicated in prostate cancer.* PLoS One, 2013. **8**(7): p. e69398.
26. Xenbase. *Gene Nomenclature Guidelines*. [cited 2015 January 2015]; Available from: http://www.xenbase.org/gene/static/geneNomenclature.jsp.
27. Lodish, H.F., in *Molecular Cell Biology*. 2008, W.H. Freeman: New York. p. 1028.
28. Sanes, J.R. and S.L. Zipursky, *Design principles of insect and vertebrate visual systems.* Neuron, 2010. **66**(1): p. 15-36.
29. Weiss, P., *Selectivity controlling the central-peripheral relations in the nervous system.* Biological Reviews of the Cambridge Philosophical Society, 1936. **11**(4): p. 494-531.
30. Meyer, R.L., *Roger Sperry and his chemoaffinity hypothesis.* Neuropsychologia, 1998. **36**(10): p. 957-80.
31. Langley, J.N., *Note on Regeneration of Prae-Ganglionic Fibres of the Sympathetic.* J Physiol, 1895. **18**(3): p. 280-4.
32. Sperry, R.W., *Visuomotor coordination in the newt (Triturus viridescens) after regeneration of the optic nerve.* Journal of Comparative Neurology, 1943. **79**(1): p. 33-55.
33. Sperry, R.W., *Optic nerve regeneration with return of vision in anurans.* Journal of Neurophysiology, 1944. **7**(1): p. 57-69.
34. Sperry, R.W., *Chemoaffinity in the Orderly Growth of Nerve Fiber Patterns and Connections.* Proc Natl Acad Sci U S A, 1963. **50**: p. 703-10.
35. Zipursky, S.L. and J.R. Sanes, *Chemoaffinity revisited: dscams, protocadherins, and neural circuit assembly.* Cell, 2010. **143**(3): p. 343-53.
36. Crossland, W.J., et al., *The specification of the retino-tectal projection in the chick.* J Comp Neurol, 1974. **155**(2): p. 127-64.
37. Lance-Jones, C. and L. Landmesser, *Pathway selection by chick lumbosacral motoneurons during normal development.* Proc R Soc Lond B Biol Sci, 1981. **214**(1194): p. 1-18.
38. Holt, C.E. and W.A. Harris, *Order in the initial retinotectal map in Xenopus: a new technique for labelling growing nerve fibres.* Nature, 1983. **301**(5896): p. 150-2.
39. Raper, J.A., M. Bastiani, and C.S. Goodman, *Pathfinding by neuronal growth cones in grasshopper embryos. I. Divergent choices made by the growth cones of sibling neurons.* J Neurosci, 1983. **3**(1): p. 20-30.
40. Dickson, B.J. and G.F. Gilestro, *Regulation of commissural axon pathfinding by slit and its Robo receptors.* Annu Rev Cell Dev Biol, 2006. **22**: p. 651-75.
41. Klambt, C., J.R. Jacobs, and C.S. Goodman, *The midline of the Drosophila central nervous system: a model for the genetic analysis of cell fate, cell migration, and growth cone guidance.* Cell, 1991. **64**(4): p. 801-15.
42. Hibbard, E., *Orientation and directed growth of Mauthners cell axons form duplicated vestibular nerve roots.* Exp Neurol, 1965. **13**(3): p. 289-301.
43. Tessier-Lavigne, M. and C.S. Goodman, *The molecular biology of axon guidance.* Science, 1996. **274**(5290): p. 1123-33.
44. O'Donnell, M., R.K. Chance, and G.J. Bashaw, *Axon growth and guidance: receptor regula-*

tion and signal transduction. Annu Rev Neurosci, 2009. **32**: p. 383-412.

45. Charron, F., et al., *The morphogen sonic hedgehog is an axonal chemoattractant that collaborates with netrin-1 in midline axon guidance.* Cell, 2003. **113**(1): p. 11-23.
46. Ruiz de Almodovar, C., et al., *VEGF mediates commissural axon chemoattraction through its receptor Flk1.* Neuron, 2011. **70**(5): p. 966-78.
47. Augsburger, A., et al., *BMPs as mediators of roof plate repulsion of commissural neurons.* Neuron, 1999. **24**(1): p. 127-41.
48. Mehlen, P., C. Delloye-Bourgeois, and A. Chedotal, *Novel roles for Slits and netrins: axon guidance cues as anticancer targets?* Nat Rev Cancer, 2011. **11**(3): p. 188-97.
49. Squire, L.R., in *Fundamental Neuroscience*. 2012, Academic Press. p. 368-372.
50. Pasterkamp, R.J., *Getting neural circuits into shape with semaphorins.* Nat Rev Neurosci, 2012. **13**(9): p. 605-18.
51. Pasquale, E.B., *Eph receptors and ephrins in cancer: bidirectional signalling and beyond.* Nat Rev Cancer, 2010. **10**(3): p. 165-80.
52. Lyuksyutova, A.I., et al., *Anterior-posterior guidance of commissural axons by Wnt-frizzled signaling.* Science, 2003. **302**(5652): p. 1984-8.
53. Liu, Y., et al., *Ryk-mediated Wnt repulsion regulates posterior-directed growth of corticospinal tract.* Nat Neurosci, 2005. **8**(9): p. 1151-9.
54. Kidd, T., K.S. Bland, and C.S. Goodman, *Slit is the midline repellent for the robo receptor in Drosophila.* Cell, 1999. **96**(6): p. 785-94.
55. Zou, Y., et al., *Squeezing axons out of the gray matter: a role for slit and semaphorin proteins from midline and ventral spinal cord.* Cell, 2000. **102**(3): p. 363-75.
56. Chen, Z., et al., *Alternative splicing of the Robo3 axon guidance receptor governs the midline switch from attraction to repulsion.* Neuron, 2008. **58**(3): p. 325-32.
57. Stein, E. and M. Tessier-Lavigne, *Hierarchical organization of guidance receptors: silencing of netrin attraction by slit through a Robo/DCC receptor complex.* Science, 2001. **291**(5510): p. 1928-38.
58. Lowery, L.A. and D. Van Vactor, *The trip of the tip: understanding the growth cone machinery.* Nat Rev Mol Cell Biol, 2009. **10**(5): p. 332-43.
59. Vitriol, E.A. and J.Q. Zheng, *Growth cone travel in space and time: the cellular ensemble of cytoskeleton, adhesion, and membrane.* Neuron, 2012. **73**(6): p. 1068-81.
60. Lin, D.M., et al., *Genetic analysis of Fasciclin II in Drosophila: defasciculation, refasciculation, and altered fasciculation.* Neuron, 1994. **13**(5): p. 1055-69.
61. Caudy, M. and D. Bentley, *Pioneer growth cone steering along a series of neuronal and non-neuronal cues of different affinities.* J Neurosci, 1986. **6**(6): p. 1781-95.
62. Goodman, C.S., et al., *Cell recognition during neuronal development.* Science, 1984. **225**(4668): p. 1271-9.
63. Raper, J.A., M.J. Bastiani, and C.S. Goodman, *Pathfinding by neuronal growth cones in grasshopper embryos. IV. The effects of ablating the A and P axons upon the behavior of the G growth cone.* J Neurosci, 1984. **4**(9): p. 2329-45.
64. Bastiani, M.J., J.A. Raper, and C.S. Goodman, *Pathfinding by neuronal growth cones in grasshopper embryos. III. Selective affinity of the G growth cone for the P cells within the A/P fascicle.* J Neurosci, 1984. **4**(9): p. 2311-28.
65. Kamiguchi, H., *The role of cell adhesion molecules in axon growth and guidance.* Adv Exp Med Biol, 2007. **621**: p. 95-103.
66. Lodish, H.F., in *Molecular Cell Biology*. 2008, W.H. Freeman: New York. p. 801-811.
67. Burnette, D.T., et al., *Myosin II activity facilitates microtubule bundling in the neuronal growth cone neck.* Dev Cell, 2008. **15**(1): p. 163-9.
68. Medeiros, N.A., D.T. Burnette, and P. Forscher, *Myosin II functions in actin-bundle turnover*

in neuronal growth cones. Nat Cell Biol, 2006. **8**(3): p. 215-26.

69. Mitchison, T. and M. Kirschner, *Cytoskeletal dynamics and nerve growth.* Neuron, 1988. **1**(9): p. 761-72.
70. Gordon-Weeks, P.R., *Microtubules and growth cone function.* J Neurobiol, 2004. **58**(1): p. 70-83.
71. Lee, A.C. and D.M. Suter, *Quantitative analysis of microtubule dynamics during adhesion-mediated growth cone guidance.* Dev Neurobiol, 2008. **68**(12): p. 1363-77.
72. Suter, D.M., A.W. Schaefer, and P. Forscher, *Microtubule dynamics are necessary for SRC family kinase-dependent growth cone steering.* Curr Biol, 2004. **14**(13): p. 1194-9.
73. Schaefer, A.W., N. Kabir, and P. Forscher, *Filopodia and actin arcs guide the assembly and transport of two populations of microtubules with unique dynamic parameters in neuronal growth cones.* J Cell Biol, 2002. **158**(1): p. 139-52.
74. Parsons, J.T., A.R. Horwitz, and M.A. Schwartz, *Cell adhesion: integrating cytoskeletal dynamics and cellular tension.* Nat Rev Mol Cell Biol, 2010. **11**(9): p. 633-43.
75. Govek, E.E., S.E. Newey, and L. Van Aelst, *The role of the Rho GTPases in neuronal development.* Genes Dev, 2005. **19**(1): p. 1-49.
76. Koh, C.G., *Rho GTPases and their regulators in neuronal functions and development.* Neurosignals, 2006. **15**(5): p. 228-37.
77. Lee, H., et al., *The microtubule plus end tracking protein Orbit/MAST/CLASP acts downstream of the tyrosine kinase Abl in mediating axon guidance.* Neuron, 2004. **42**(6): p. 913-26.
78. Zhou, F.Q., et al., *NGF-induced axon growth is mediated by localized inactivation of GSK-3beta and functions of the microtubule plus end binding protein APC.* Neuron, 2004. **42**(6): p. 897-912.
79. Bunge, M.B., *Fine structure of nerve fibers and growth cones of isolated sympathetic neurons in culture.* J Cell Biol, 1973. **56**(3): p. 713-35.
80. Bunge, M.B., *Initial endocytosis of perioxidase or ferritin by growth cones of cultured nerve cells.* J Neurocytol, 1977. **6**(4): p. 407-39.
81. Tojima, T., et al., *Attractive axon guidance involves asymmetric membrane transport and exocytosis in the growth cone.* Nat Neurosci, 2007. **10**(1): p. 58-66.
82. Tojima, T., R. Itofusa, and H. Kamiguchi, *Asymmetric clathrin-mediated endocytosis drives repulsive growth cone guidance.* Neuron, 2010. **66**(3): p. 370-7.
83. Hines, J.H., M. Abu-Rub, and J.R. Henley, *Asymmetric endocytosis and remodeling of beta1-integrin adhesions during growth cone chemorepulsion by MAG.* Nat Neurosci, 2010. **13**(7): p. 829-37.
84. Kolpak, A.L., et al., *Negative guidance factor-induced macropinocytosis in the growth cone plays a critical role in repulsive axon turning.* J Neurosci, 2009. **29**(34): p. 10488-98.
85. Tojima, T., et al., *Second messengers and membrane trafficking direct and organize growth cone steering.* Nat Rev Neurosci, 2011. **12**(4): p. 191-203.
86. Bloom, O.E. and J.R. Morgan, *Membrane trafficking events underlying axon repair, growth, and regeneration.* Mol Cell Neurosci, 2011. **48**(4): p. 339-48.
87. Piper, M., et al., *Endocytosis-dependent desensitization and protein synthesis-dependent resensitization in retinal growth cone adaptation.* Nat Neurosci, 2005. **8**(2): p. 179-86.
88. Harris, W.A., et al., *Growth cones of developing retinal cells in vivo, on culture surfaces, and in collagen matrices.* J Neurosci Res, 1985. **13**(1-2): p. 101-22.
89. Leung, K.M. and C.E. Holt, *Live visualization of protein synthesis in axonal growth cones by microinjection of photoconvertible Kaede into Xenopus embryos.* Nat Protoc, 2008. **3**(8): p. 1318-27.
90. Falk, J., et al., *Electroporation of cDNA/Morpholinos to targeted areas of embryonic CNS in*

Xenopus. BMC Dev Biol, 2007. **7**: p. 107.

91. Xenbase. *Introduction to Xenopus, the frog model*. [cited 2014 August 17]; Available from: http://www.xenbase.org/anatomy/intro.do.
92. Holt, C.E., *A single-cell analysis of early retinal ganglion cell differentiation in Xenopus: from soma to axon tip.* J Neurosci, 1989. **9**(9): p. 3123-45.
93. Randlett, O., et al., *The oriented emergence of axons from retinal ganglion cells is directed by laminin contact in vivo.* Neuron, 2011. **70**(2): p. 266-80.
94. Ohta, K., et al., *Embryonic lens repels retinal ganglion cell axons.* Dev Biol, 1999. **211**(1): p. 124-32.
95. Erskine, L. and E. Herrera, *The retinal ganglion cell axon's journey: insights into molecular mechanisms of axon guidance.* Dev Biol, 2007. **308**(1): p. 1-14.
96. Bao, Z.Z., *Intraretinal projection of retinal ganglion cell axons as a model system for studying axon navigation.* Brain Res, 2008. **1192**: p. 165-77.
97. Kolpak, A., J. Zhang, and Z.Z. Bao, *Sonic hedgehog has a dual effect on the growth of retinal ganglion axons depending on its concentration.* J Neurosci, 2005. **25**(13): p. 3432-41.
98. Brittis, P.A. and J. Silver, *Multiple factors govern intraretinal axon guidance: a time-lapse study.* Mol Cell Neurosci, 1995. **6**(5): p. 413-32.
99. Thompson, H., et al., *Slit proteins regulate distinct aspects of retinal ganglion cell axon guidance within dorsal and ventral retina.* J Neurosci, 2006. **26**(31): p. 8082-91.
100. Deiner, M.S., et al., *Netrin-1 and DCC mediate axon guidance locally at the optic disc: loss of function leads to optic nerve hypoplasia.* Neuron, 1997. **19**(3): p. 575-89.
101. Serafini, T., et al., *Netrin-1 is required for commissural axon guidance in the developing vertebrate nervous system.* Cell, 1996. **87**(6): p. 1001-14.
102. Nakagawa, S., et al., *Ephrin-B regulates the Ipsilateral routing of retinal axons at the optic chiasm.* Neuron, 2000. **25**(3): p. 599-610.
103. Manns, R.P., et al., *Differing semaphorin 3A concentrations trigger distinct signaling mechanisms in growth cone collapse.* J Neurosci, 2012. **32**(25): p. 8554-9.
104. Nedelec, S., et al., *Concentration-dependent requirement for local protein synthesis in motor neuron subtype-specific response to axon guidance cues.* J Neurosci, 2012. **32**(4): p. 1496-506.
105. Williams, S.E., et al., *Ephrin-B2 and EphB1 mediate retinal axon divergence at the optic chiasm.* Neuron, 2003. **39**(6): p. 919-35.
106. Kruger, K., et al., *Retinal ganglion cell axon progression from the optic chiasm to initiate optic tract development requires cell autonomous function of GAP-43.* J Neurosci, 1998. **18**(15): p. 5692-705.
107. Zhang, F., et al., *GAP-43 mediates retinal axon interaction with lateral diencephalon cells during optic tract formation.* Development, 2000. **127**(5): p. 969-80.
108. Ringstedt, T., et al., *Slit inhibition of retinal axon growth and its role in retinal axon pathfinding and innervation patterns in the diencephalon.* J Neurosci, 2000. **20**(13): p. 4983-91.
109. Fricke, C., et al., *astray, a zebrafish roundabout homolog required for retinal axon guidance.* Science, 2001. **292**(5516): p. 507-10.
110. Thompson, H., et al., *Slits contribute to the guidance of retinal ganglion cell axons in the mammalian optic tract.* Dev Biol, 2006. **296**(2): p. 476-84.
111. Ichijo, H. and I. Kawabata, *Roles of the telencephalic cells and their chondroitin sulfate proteoglycans in delimiting an anterior border of the retinal pathway.* J Neurosci, 2001. **21**(23): p. 9304-14.
112. Walz, A., et al., *Chondroitin sulfate disrupts axon pathfinding in the optic tract and alters growth cone dynamics.* J Neurobiol, 2002. **53**(3): p. 330-42.

113. Stone, K.E. and D.S. Sakaguchi, *Perturbation of the developing Xenopus retinotectal projection following injections of antibodies against beta1 integrin receptors and N-cadherin.* Dev Biol, 1996. **180**(1): p. 297-310.
114. Rhee, J., et al., *Activation of the repulsive receptor Roundabout inhibits N-cadherin-mediated cell adhesion.* Nat Cell Biol, 2002. **4**(10): p. 798-805.
115. Piper, M., et al., *Signaling mechanisms underlying Slit2-induced collapse of Xenopus retinal growth cones.* Neuron, 2006. **49**(2): p. 215-28.
116. Campbell, D.S., et al., *Semaphorin 3A elicits stage-dependent collapse, turning, and branching in Xenopus retinal growth cones.* J Neurosci, 2001. **21**(21): p. 8538-47.
117. McFarlane, S., L. McNeill, and C.E. Holt, *FGF signaling and target recognition in the developing Xenopus visual system.* Neuron, 1995. **15**(5): p. 1017-28.
118. Holt, C.E. and W.A. Harris, *Target selection: invasion, mapping and cell choice.* Curr Opin Neurobiol, 1998. **8**(1): p. 98-105.
119. McLaughlin, T. and D.D. O'Leary, *Molecular gradients and development of retinotopic maps.* Annu Rev Neurosci, 2005. **28**: p. 327-55.
120. Cang, J. and D.A. Feldheim, *Developmental mechanisms of topographic map formation and alignment.* Annu Rev Neurosci, 2013. **36**: p. 51-77.
121. Simon, D.K. and D.D. O'Leary, *Relationship of retinotopic ordering of axons in the optic pathway to the formation of visual maps in central targets.* J Comp Neurol, 1991. **307**(3): p. 393-404.
122. Plas, D.T., J.E. Lopez, and M.C. Crair, *Pretarget sorting of retinocollicular axons in the mouse.* J Comp Neurol, 2005. **491**(4): p. 305-19.
123. Mann, F., et al., *Topographic mapping in dorsoventral axis of the Xenopus retinotectal system depends on signaling through ephrin-B ligands.* Neuron, 2002. **35**(3): p. 461-73.
124. Hindges, R., et al., *EphB forward signaling controls directional branch extension and arborization required for dorsal-ventral retinotopic mapping.* Neuron, 2002. **35**(3): p. 475-87.
125. Dekkers, M.P., V. Nikoletopoulou, and Y.A. Barde, *Cell biology in neuroscience: Death of developing neurons: new insights and implications for connectivity.* J Cell Biol, 2013. **203**(3): p. 385-93.
126. Pease, S.E. and R.A. Segal, *Preserve and protect: maintaining axons within functional circuits.* Trends Neurosci, 2014. **37**(10): p. 572-582.
127. Shamas-Din, A., et al., *Mechanisms of action of Bcl-2 family proteins.* Cold Spring Harb Perspect Biol, 2013. **5**(4): p. a008714.
128. Friedman, J.R. and J. Nunnari, *Mitochondrial form and function.* Nature, 2014. **505**(7483): p. 335-43.
129. Nunnari, J. and A. Suomalainen, *Mitochondria: in sickness and in health.* Cell, 2012. **148**(6): p. 1145-59.
130. Alexander, C., et al., *OPA1, encoding a dynamin-related GTPase, is mutated in autosomal dominant optic atrophy linked to chromosome 3q28.* Nat Genet, 2000. **26**(2): p. 211-5.
131. Delettre, C., et al., *Nuclear gene OPA1, encoding a mitochondrial dynamin-related protein, is mutated in dominant optic atrophy.* Nat Genet, 2000. **26**(2): p. 207-10.
132. Davies, A.M., *The neurotrophic hypothesis: where does it stand?* Philos Trans R Soc Lond B Biol Sci, 1996. **351**(1338): p. 389-94.
133. Cosker, K.E., et al., *Target-derived neurotrophins coordinate transcription and transport of bclw to prevent axonal degeneration.* J Neurosci, 2013. **33**(12): p. 5195-207.
134. Barnes, A.P. and F. Polleux, *Establishment of axon-dendrite polarity in developing neurons.* Annu Rev Neurosci, 2009. **32**: p. 347-81.
135. Hirokawa, N. and R. Takemura, *Molecular motors and mechanisms of directional transport in neurons.* Nat Rev Neurosci, 2005. **6**(3): p. 201-14.

136. Andreassi, C. and A. Riccio, *To localize or not to localize: mRNA fate is in 3'UTR ends.* Trends Cell Biol, 2009. **19**(9): p. 465-74.
137. Gebauer, F., T. Preiss, and M.W. Hentze, *From cis-regulatory elements to complex RNPs and back.* Cold Spring Harb Perspect Biol, 2012. **4**(7): p. a012245.
138. Jung, H., et al., *Remote control of gene function by local translation.* Cell, 2014. **157**(1): p. 26-40.
139. Kelleher, R.J., 3rd and M.F. Bear, *The autistic neuron: troubled translation?* Cell, 2008. **135**(3): p. 401-6.
140. Liu-Yesucevitz, L., et al., *Local RNA translation at the synapse and in disease.* J Neurosci, 2011. **31**(45): p. 16086-93.
141. Ramaswami, M., J.P. Taylor, and R. Parker, *Altered ribostasis: RNA-protein granules in degenerative disorders.* Cell, 2013. **154**(4): p. 727-36.
142. Wang, W., et al., *RNA transport and localized protein synthesis in neurological disorders and neural repair.* Dev Neurobiol, 2007. **67**(9): p. 1166-82.
143. Zoncu, R., A. Efeyan, and D.M. Sabatini, *mTOR: from growth signal integration to cancer, diabetes and ageing.* Nat Rev Mol Cell Biol, 2011. **12**(1): p. 21-35.
144. Campbell, D.S. and C.E. Holt, *Chemotropic responses of retinal growth cones mediated by rapid local protein synthesis and degradation.* Neuron, 2001. **32**(6): p. 1013-26.
145. Hamilton, A.M. and K. Zito, *Breaking it down: the ubiquitin proteasome system in neuronal morphogenesis.* Neural Plast, 2013. **2013**: p. 196848.
146. Huttelmaier, S., et al., *Spatial regulation of beta-actin translation by Src-dependent phosphorylation of ZBP1.* Nature, 2005. **438**(7067): p. 512-5.
147. Sasaki, Y., et al., *Phosphorylation of zipcode binding protein 1 is required for brain-derived neurotrophic factor signaling of local beta-actin synthesis and growth cone turning.* J Neurosci, 2010. **30**(28): p. 9349-58.
148. Jung, H., C.M. O'Hare, and C.E. Holt, *Translational regulation in growth cones.* Curr Opin Genet Dev, 2011. **21**(4): p. 458-64.
149. Lasek, R.J., C. Dabrowski, and R. Nordlander, *Analysis of axoplasmic RNA from invertebrate giant axons.* Nat New Biol, 1973. **244**(136): p. 162-5.
150. Hengst, U., et al., *Axonal elongation triggered by stimulus-induced local translation of a polarity complex protein.* Nat Cell Biol, 2009. **11**(8): p. 1024-30.
151. van Kesteren, R.E., et al., *Local synthesis of actin-binding protein beta-thymosin regulates neurite outgrowth.* J Neurosci, 2006. **26**(1): p. 152-7.
152. Cox, L.J., et al., *Intra-axonal translation and retrograde trafficking of CREB promotes neuronal survival.* Nat Cell Biol, 2008. **10**(2): p. 149-59.
153. Perry, R.B., et al., *Subcellular knockout of importin beta1 perturbs axonal retrograde signaling.* Neuron, 2012. **75**(2): p. 294-305.
154. Verma, P., et al., *Axonal protein synthesis and degradation are necessary for efficient growth cone regeneration.* J Neurosci, 2005. **25**(2): p. 331-42.
155. Ben-Yaakov, K., et al., *Axonal transcription factors signal retrogradely in lesioned peripheral nerve.* EMBO J, 2012. **31**(6): p. 1350-63.
156. Michaelevski, I., et al., *Signaling to transcription networks in the neuronal retrograde injury response.* Sci Signal, 2010. **3**(130): p. ra53.
157. Miao, X., et al., *TCTP overexpression is associated with the development and progression of glioma.* Tumour Biol, 2013. **34**(6): p. 3357-61.
158. Yenofsky, R., I. Bergmann, and G. Brawerman, *Messenger RNA species partially in a repressed state in mouse sarcoma ascites cells.* Proc Natl Acad Sci U S A, 1982. **79**(19): p. 5876-80.

159. Bohm, H., et al., *The growth-related protein P23 of the Ehrlich ascites tumor: translational control, cloning and primary structure.* Biochem Int, 1989. **19**(2): p. 277-86.
160. Benndorf, R., P. Nurnberg, and H. Bielka, *Growth phase-dependent proteins of the Ehrlich ascites tumor analyzed by one- and two-dimensional electrophoresis.* Exp Cell Res, 1988. **174**(1): p. 130-8.
161. Bommer, U.A. and B.J. Thiele, *The translationally controlled tumour protein (TCTP).* Int J Biochem Cell Biol, 2004. **36**(3): p. 379-85.
162. MacDonald, S.M., et al., *Molecular identification of an IgE-dependent histamine-releasing factor.* Science, 1995. **269**(5224): p. 688-90.
163. Zhang, J., et al., *Role of the translationally controlled tumor protein in DNA damage sensing and repair.* Proc Natl Acad Sci U S A, 2012. **109**(16): p. E926-33.
164. Chen, S.H., et al., *A knockout mouse approach reveals that TCTP functions as an essential factor for cell proliferation and survival in a tissue- or cell type-specific manner.* Mol Biol Cell, 2007. **18**(7): p. 2525-32.
165. Xenbase. [cited 2014 September 17]; Available from: http://gbrowse.xenbase.org/fgb2/gbrowse/xl7_1/?name=Scaffold14978:6124999-6130443&.
166. Andree, H., et al., *Expression of the human TPT1 gene coding for translationally controlled tumor protein (TCTP) is regulated by CREB transcription factors.* Gene, 2006. **380**(2): p. 95-103.
167. Chen, W., et al., *Tumor protein translationally controlled 1 is a p53 target gene that promotes cell survival.* Cell Cycle, 2013. **12**(14): p. 2321-8.
168. Thiele, H., et al., *Expression of the gene and processed pseudogenes encoding the human and rabbit translationally controlled tumour protein (TCTP).* Eur J Biochem, 2000. **267**(17): p. 5473-81.
169. Tay, Y., J. Rinn, and P.P. Pandolfi, *The multilayered complexity of ceRNA crosstalk and competition.* Nature, 2014. **505**(7483): p. 344-52.
170. Chitpatima, S.T., et al., *Nucleotide sequence of a major messenger RNA for a 21 kilodalton polypeptide that is under translational control in mouse tumor cells.* Nucleic Acids Res, 1988. **16**(5): p. 2350.
171. Thoreen, C.C., et al., *A unifying model for mTORC1-mediated regulation of mRNA translation.* Nature, 2012. **485**(7396): p. 109-13.
172. Meyuhas, O., *Synthesis of the translational apparatus is regulated at the translational level.* Eur J Biochem, 2000. **267**(21): p. 6321-30.
173. Bommer, U.A., et al., *The mRNA of the translationally controlled tumor protein P23/TCTP is a highly structured RNA, which activates the dsRNA-dependent protein kinase PKR.* RNA, 2002. **8**(4): p. 478-96.
174. Brioudes, F., et al., *Translationally controlled tumor protein is a conserved mitotic growth integrator in animals and plants.* Proc Natl Acad Sci U S A, 2010. **107**(37): p. 16384-9.
175. Kim, M., J. Maeng, and K. Lee, *Dimerization of TCTP and its clinical implications for allergy.* Biochimie, 2013. **95**(4): p. 659-66.
176. Nuoffer, C., et al., *Mss4 does not function as an exchange factor for Rab in endoplasmic reticulum to Golgi transport.* Mol Biol Cell, 1997. **8**(7): p. 1305-16.
177. Wixler, V., et al., *Identification and characterisation of novel Mss4-binding Rab GTPases.* Biol Chem, 2011. **392**(3): p. 239-48.
178. Lowther, W.T., et al., *The mirrored methionine sulfoxide reductases of Neisseria gonorrhoeae pilB.* Nat Struct Biol, 2002. **9**(5): p. 348-52.
179. Drazic, A. and J. Winter, *The physiological role of reversible methionine oxidation.* Biochim Biophys Acta, 2014. **1844**(8): p. 1367-82.
180. Kang, H.S., et al., *Molecular identification of IgE-dependent histamine-releasing factor as a B cell growth factor.* J Immunol, 2001. **166**(11): p. 6545-54.

181. Zhang, M., et al., *Microarray analysis of perichondral and reserve growth plate zones identifies differential gene expressions and signal pathways.* Bone, 2008. **43**(3): p. 511-20.
182. Cans, C., et al., *Translationally controlled tumor protein acts as a guanine nucleotide dissociation inhibitor on the translation elongation factor eEF1A.* Proc Natl Acad Sci U S A, 2003. **100**(24): p. 13892-7.
183. Gachet, Y., et al., *The growth-related, translationally controlled protein P23 has properties of a tubulin binding protein and associates transiently with microtubules during the cell cycle.* J Cell Sci, 1999. **112 (Pt 8)**: p. 1257-71.
184. Miyara, F., et al., *Non-equivalence of embryonic and somatic cell nuclei affecting spindle composition in clones.* Dev Biol, 2006. **289**(1): p. 206-17.
185. Yarm, F.R., *Plk phosphorylation regulates the microtubule-stabilizing protein TCTP.* Mol Cell Biol, 2002. **22**(17): p. 6209-21.
186. Koziol, M.J., N. Garrett, and J.B. Gurdon, *Tpt1 activates transcription of oct4 and nanog in transplanted somatic nuclei.* Curr Biol, 2007. **17**(9): p. 801-7.
187. Li, F., D. Zhang, and K. Fujise, *Characterization of fortilin, a novel antiapoptotic protein.* J Biol Chem, 2001. **276**(50): p. 47542-9.
188. Graidist, P., A. Phongdara, and K. Fujise, *Antiapoptotic protein partners fortilin and MCL1 independently protect cells from 5-fluorouracil-induced cytotoxicity.* J Biol Chem, 2004. **279**(39): p. 40868-75.
189. Yang, Y., et al., *An N-terminal region of translationally controlled tumor protein is required for its antiapoptotic activity.* Oncogene, 2005. **24**(30): p. 4778-88.
190. Liu, H., et al., *Stabilization and enhancement of the antiapoptotic activity of mcl-1 by TCTP.* Mol Cell Biol, 2005. **25**(8): p. 3117-26.
191. Zhang, D., et al., *Physical and functional interaction between myeloid cell leukemia 1 protein (MCL1) and Fortilin. The potential role of MCL1 as a fortilin chaperone.* J Biol Chem, 2002. **277**(40): p. 37430-8.
192. Jung, J., et al., *Interaction of translationally controlled tumor protein with Apaf-1 is involved in the development of chemoresistance in HeLa cells.* BMC Cancer, 2014. **14**: p. 165.
193. Hyman, B.T. and J. Yuan, *Apoptotic and non-apoptotic roles of caspases in neuronal physiology and pathophysiology.* Nat Rev Neurosci, 2012. **13**(6): p. 395-406.
194. Hong, S.T. and K.W. Choi, *TCTP directly regulates ATM activity to control genome stability and organ development in Drosophila melanogaster.* Nat Commun, 2013. **4**: p. 2986.
195. Kim, M., et al., *Dimerization of translationally controlled tumor protein is essential for its cytokine-like activity.* PLoS One, 2009. **4**(7): p. e6464.
196. Nielsen, H.V., et al., *Identification of a basophil leukocyte interleukin-3-regulated protein that is identical to IgE-dependent histamine-releasing factor.* Allergy, 1998. **53**(7): p. 642-52.
197. Teshima, S., et al., *Macrophage colony-stimulating factor stimulates synthesis and secretion of a mouse homolog of a human IgE-dependent histamine-releasing factor by macrophages in vitro and in vivo.* J Immunol, 1998. **161**(11): p. 6356-66.
198. Gross, B., et al., *cDNA sequence coding for a translationally controlled human tumor protein.* Nucleic Acids Res, 1989. **17**(20): p. 8367.
199. Bommer, U.A., et al., *Translational regulation of the mammalian growth-related protein P23: involvement of eIF-4E.* Cell Mol Biol Res, 1994. **40**(7-8): p. 633-41.
200. Hsieh, A.C., et al., *The translational landscape of mTOR signalling steers cancer initiation and metastasis.* Nature, 2012. **485**(7396): p. 55-61.
201. Sage-Ono, K., et al., *Dark-induced accumulation of mRNA for a homolog of translationally controlled tumor protein (TCTP) in Pharbitis.* Plant Cell Physiol, 1998. **39**(3): p. 357-60.

202. Sturzenbaum, S.R., P. Kille, and A.J. Morgan, *Identification of heavy metal induced changes in the expression patterns of the translationally controlled tumour protein (TCTP) in the earthworm Lumbricus rubellus1.* Biochim Biophys Acta, 1998. **1398**(3): p. 294-304.
203. Baudet, C., et al., *Differentially expressed genes in C6.9 glioma cells during vitamin D-induced cell death program.* Cell Death Differ, 1998. **5**(1): p. 116-25.
204. Walsh, B.J., et al., *Identification of macrophage activation associated proteins by two-dimensional gel electrophoresis and microsequencing.* J Leukoc Biol, 1995. **57**(3): p. 507-12.
205. Bonnet, C., et al., *Identification and transcription control of fission yeast genes repressed by an ammonium starvation growth arrest.* Yeast, 2000. **16**(1): p. 23-33.
206. Xu, A., A.R. Bellamy, and J.A. Taylor, *Expression of translationally controlled tumour protein is regulated by calcium at both the transcriptional and post-transcriptional level.* Biochem J, 1999. **342 Pt 3**: p. 683-9.
207. Kim, S.H., et al., *Decreased brain histamine-releasing factor protein in patients with Down syndrome and Alzheimer's disease.* Neurosci Lett, 2001. **300**(1): p. 41-4.
208. Thomas, G., G. Thomas, and H. Luther, *Transcriptional and translational control of cytoplasmic proteins after serum stimulation of quiescent Swiss 3T3 cells.* Proc Natl Acad Sci U S A, 1981. **78**(9): p. 5712-6.
209. Sinha, P., et al., *Identification of novel proteins associated with the development of chemoresistance in malignant melanoma using two-dimensional electrophoresis.* Electrophoresis, 2000. **21**(14): p. 3048-57.
210. Chung, S., et al., *Expression of translationally controlled tumor protein mRNA in human colon cancer.* Cancer Lett, 2000. **156**(2): p. 185-90.
211. Telerman, A. and R. Amson, *The molecular programme of tumour reversion: the steps beyond malignant transformation.* Nat Rev Cancer, 2009. **9**(3): p. 206-16.
212. Tamagnone, L., *Emerging role of semaphorins as major regulatory signals and potential therapeutic targets in cancer.* Cancer Cell, 2012. **22**(2): p. 145-52.
213. Biankin, A.V., et al., *Pancreatic cancer genomes reveal aberrations in axon guidance pathway genes.* Nature, 2012. **491**(7424): p. 399-405.
214. Bonnet, D. and J.E. Dick, *Human acute myeloid leukemia is organized as a hierarchy that originates from a primitive hematopoietic cell.* Nat Med, 1997. **3**(7): p. 730-7.
215. Chaffer, C.L. and R.A. Weinberg, *A perspective on cancer cell metastasis.* Science, 2011. **331**(6024): p. 1559-64.
216. Valastyan, S. and R.A. Weinberg, *Tumor metastasis: molecular insights and evolving paradigms.* Cell, 2011. **147**(2): p. 275-92.
217. Nieto, M.A., *Epithelial plasticity: a common theme in embryonic and cancer cells.* Science, 2013. **342**(6159): p. 1234850.
218. Bissell, M.J. and W.C. Hines, *Why don't we get more cancer? A proposed role of the microenvironment in restraining cancer progression.* Nat Med, 2011. **17**(3): p. 320-9.
219. Wolfe, J.N., *Risk for breast cancer development determined by mammographic parenchymal pattern.* Cancer, 1976. **37**(5): p. 2486-92.
220. Boyd, N.F., et al., *Mammographic density and the risk and detection of breast cancer.* N Engl J Med, 2007. **356**(3): p. 227-36.
221. Joyce, J.A. and J.W. Pollard, *Microenvironmental regulation of metastasis.* Nat Rev Cancer, 2009. **9**(4): p. 239-52.
222. Itoh, Y., et al., *Scratch regulates neuronal migration onset via an epithelial-mesenchymal transition-like mechanism.* Nat Neurosci, 2013. **16**(4): p. 416-25.
223. Hirabayashi, Y. and Y. Gotoh, *Epigenetic control of neural precursor cell fate during development.* Nat Rev Neurosci, 2010. **11**(6): p. 377-88.
224. Yi, J.J., et al., *TGF-beta signaling specifies axons during brain development.* Cell, 2010. **142**(1): p. 144-57.

225. Polleux, F. and W. Snider, *Initiating and growing an axon.* Cold Spring Harb Perspect Biol, 2010. **2**(4): p. a001925.
226. Mehlen, P., et al., *The DCC gene product induces apoptosis by a mechanism requiring receptor proteolysis.* Nature, 1998. **395**(6704): p. 801-4.
227. Fearon, E.R., et al., *Identification of a chromosome 18q gene that is altered in colorectal cancers.* Science, 1990. **247**(4938): p. 49-56.
228. Fitamant, J., et al., *Netrin-1 expression confers a selective advantage for tumor cell survival in metastatic breast cancer.* Proc Natl Acad Sci U S A, 2008. **105**(12): p. 4850-5.
229. Raval, A., et al., *Downregulation of death-associated protein kinase 1 (DAPK1) in chronic lymphocytic leukemia.* Cell, 2007. **129**(5): p. 879-90.
230. Furne, C., et al., *Netrin-1 is a survival factor during commissural neuron navigation.* Proc Natl Acad Sci U S A, 2008. **105**(38): p. 14465-70.
231. Nishida, N., et al., *Angiogenesis in cancer.* Vasc Health Risk Manag, 2006. **2**(3): p. 213-9.
232. Chauvet, S., et al., *Gating of Sema3E/PlexinD1 signaling by neuropilin-1 switches axonal repulsion to attraction during brain development.* Neuron, 2007. **56**(5): p. 807-22.
233. Bellon, A., et al., *VEGFR2 (KDR/Flk1) signaling mediates axon growth in response to semaphorin 3E in the developing brain.* Neuron, 2010. **66**(2): p. 205-19.
234. Pasquale, E.B., *Eph receptor signalling casts a wide net on cell behaviour.* Nat Rev Mol Cell Biol, 2005. **6**(6): p. 462-75.
235. Ong, C.K., et al., *Exome sequencing of liver fluke-associated cholangiocarcinoma.* Nat Genet, 2012. **44**(6): p. 690-3.
236. Ballard, M.S. and L. Hinck, *A roundabout way to cancer.* Adv Cancer Res, 2012. **114**: p. 187-235.
237. Werbowetski-Ogilvie, T.E., et al., *Inhibition of medulloblastoma cell invasion by Slit.* Oncogene, 2006. **25**(37): p. 5103-12.
238. Yiin, J.J., et al., *Slit2 inhibits glioma cell invasion in the brain by suppression of Cdc42 activity.* Neuro Oncol, 2009. **11**(6): p. 779-89.
239. Heuberger, J. and W. Birchmeier, *Interplay of cadherin-mediated cell adhesion and canonical Wnt signaling.* Cold Spring Harb Perspect Biol, 2010. **2**(2): p. a002915.
240. Tseng, R.C., et al., *SLIT2 attenuation during lung cancer progression deregulates beta-catenin and E-cadherin and associates with poor prognosis.* Cancer Res, 2010. **70**(2): p. 543-51.
241. Macias, H., et al., *SLIT/ROBO1 signaling suppresses mammary branching morphogenesis by limiting basal cell number.* Dev Cell, 2011. **20**(6): p. 827-40.
242. Paget, S., *The Distribution of Secondary Growths in Cancer of the Breast.* The Lancet, 1889. **133**(3421): p. 571-573.
243. Fidler, I.J., *The pathogenesis of cancer metastasis: the 'seed and soil' hypothesis revisited.* Nat Rev Cancer, 2003. **3**(6): p. 453-8.
244. Vaccinex-Inc. *Evaluation of Safety, Tolerability, PK & PD of Intravenous VX15/2503 in Patients With Advanced Solid Tumors*. In: Clinicaltrials.gov [Internet] [cited 2014 September 15]; Available from: http://clinicaltrials.gov/ct2/show/NCT01313065?term=semaphorin&rank=3.
245. Genentech. *A Study of MNRP1685A in Patients With Locally Advanced or Metastatic Solid Tumors*. In: Clinicaltrials.gov [Internet] [cited 2014 September 15]; Available from: http://clinicaltrials.gov/ct2/show/NCT00747734?term=neuropilin&rank=1.
246. M.D.AndersonCancerCenter. *EphA2 Gene Targeting Using Neutral Liposomal Small Interfering RNA Delivery*. In: Clinicaltrials.gov [Internet] [cited 2014 September 15]; Available from: http://clinicaltrials.gov/ct2/show/NCT01591356?term=epha2&rank=1.

247. California, U.o.S. *Recombinant Albumin Fusion Protein sEphB4-HSA in Treating Patients With Metastatic or Recurrent Solid Tumors*. In: Clinicaltrials.gov [Internet] [cited 2014 September 15]; Available from: http://clinicaltrials.gov/ct2/show/NCT01642342?term=ephb4&rank=3.
248. KadmonCorporationLLC. *Study of XL647 Administered Orally Daily to Patients With Solid Tumors*. In: Clinicaltrials.gov [Internet] [cited 2014 September 15]; Available from: http://clinicaltrials.gov/ct2/show/NCT00336765?term=ephb4&rank=1.
249. KadmonCorporationLLC. *Study of XL647 in Subjects With Non-Small-Cell Lung Cancer*. In: Clinicaltrials.gov [Internet] [cited 2014 September 15]; Available from: http://clinicaltrials.gov/ct2/show/NCT00364780?term=ephb4&rank=2.
250. Nieuwkoop, P.D. and J. Faber, *Normal table of Xenopus laevis (Daudin) : a systematical and chronological survey of the development from the fertilized egg till the end of metamorphosis*. 1994, New York: Garland Pub. 252 p., 10 leaves of plates.
251. Xue, X.Y. and W.A. Harris, *Using myc genes to search for stem cells in the ciliary margin of the Xenopus retina.* Dev Neurobiol, 2012. **72**(4): p. 475-90.
252. Shimamura, K., et al., *Wnt-1-dependent regulation of local E-cadherin and alpha N-catenin expression in the embryonic mouse brain.* Development, 1994. **120**(8): p. 2225-34.
253. Broadbent, J. and E.M. Read, *Wholemount in situ hybridization of Xenopus and zebrafish embryos.* Methods Mol Biol, 1999. **127**: p. 57-67.
254. Bassell, G.J., et al., *Sorting of beta-actin mRNA and protein to neurites and growth cones in culture.* J Neurosci, 1998. **18**(1): p. 251-65.
255. Pfaffl, M.W., *A new mathematical model for relative quantification in real-time RT-PCR.* Nucleic Acids Res, 2001. **29**(9): p. e45.
256. Tsai, B.P., et al., *Quantitative profiling of in vivo-assembled RNA-protein complexes using a novel integrated proteomic approach.* Mol Cell Proteomics, 2011. **10**(4): p. M110 007385.
257. Nie, D., et al., *Tsc2-Rheb signaling regulates EphA-mediated axon guidance.* Nat Neurosci, 2010. **13**(2): p. 163-72.
258. Agathocleous, M., et al., *Metabolic differentiation in the embryonic retina.* Nat Cell Biol, 2012. **14**(8): p. 859-64.
259. Marks, J.D., C. Boriboun, and J. Wang, *Mitochondrial nitric oxide mediates decreased vulnerability of hippocampal neurons from immature animals to NMDA.* J Neurosci, 2005. **25**(28): p. 6561-75.
260. Sheng, Z.H. and Q. Cai, *Mitochondrial transport in neurons: impact on synaptic homeostasis and neurodegeneration.* Nat Rev Neurosci, 2012. **13**(2): p. 77-93.
261. Bazile, F., et al., *Complex relationship between TCTP, microtubules and actin microfilaments regulates cell shape in normal and cancer cells.* Carcinogenesis, 2009. **30**(4): p. 555-65.
262. Di Giammartino, D.C., K. Nishida, and J.L. Manley, *Mechanisms and consequences of alternative polyadenylation.* Mol Cell, 2011. **43**(6): p. 853-66.
263. An, J.J., et al., *Distinct role of long 3' UTR BDNF mRNA in spine morphology and synaptic plasticity in hippocampal neurons.* Cell, 2008. **134**(1): p. 175-87.
264. ViennaRNA. *RNAfold WebServer*. 2014 [cited 2013 January 15]; Available from: http://rna.tbi.univie.ac.at/cgi-bin/RNAfold.cgi.
265. Dweep, H., C. Sticht, and N. Gretz, *In-Silico Algorithms for the Screening of Possible microRNA Binding Sites and Their Interactions.* Curr Genomics, 2013. **14**(2): p. 127-36.
266. Wan, Y., et al., *Understanding the transcriptome through RNA structure.* Nat Rev Genet, 2011. **12**(9): p. 641-55.
267. Keryer-Bibens, C., C. Barreau, and H.B. Osborne, *Tethering of proteins to RNAs by bacteriophage proteins.* Biol Cell, 2008. **100**(2): p. 125-38.
268. Ong, S.E., et al., *Stable isotope labeling by amino acids in cell culture, SILAC, as a simple and accurate approach to expression proteomics.* Mol Cell Proteomics, 2002. **1**(5): p. 376-86.

269. Guerrero, C., et al., *An integrated mass spectrometry-based proteomic approach: quantitative analysis of tandem affinity-purified in vivo cross-linked protein complexes (QTAX) to decipher the 26 S proteasome-interacting network.* Mol Cell Proteomics, 2006. **5**(2): p. 366-78.
270. *Search Tool for the Retrieval of Interacting Genes/Proteins*. [cited 2013 July]; Available from: http://string-db.org.
271. Franceschini, A., et al., *STRING v9.1: protein-protein interaction networks, with increased coverage and integration.* Nucleic Acids Res, 2013. **41**(Database issue): p. D808-15.
272. Barboro, P., N. Ferrari, and C. Balbi, *Emerging roles of heterogeneous nuclear ribonucleoprotein K (hnRNP K) in cancer progression.* Cancer Lett, 2014. **352**(2): p. 152-9.
273. Charroux, B., et al., *The levels of the bancal product, a Drosophila homologue of vertebrate hnRNP K protein, affect cell proliferation and apoptosis in imaginal disc cells.* Mol Cell Biol, 1999. **19**(11): p. 7846-56.
274. Hornberg, H. and C. Holt, *RNA-binding proteins and translational regulation in axons and growth cones.* Front Neurosci, 2013. **7**: p. 81.
275. Choi, H.S., et al., *Poly(C)-binding proteins as transcriptional regulators of gene expression.* Biochem Biophys Res Commun, 2009. **380**(3): p. 431-6.
276. Wang, H., et al., *PCBP1 suppresses the translation of metastasis-associated PRL-3 phosphatase.* Cancer Cell, 2010. **18**(1): p. 52-62.
277. Han, W., et al., *RNA-binding protein PCBP2 modulates glioma growth by regulating FHL3.* J Clin Invest, 2013. **123**(5): p. 2103-18.
278. Majumder, M., et al., *The hnRNA-binding proteins hnRNP L and PTB are required for efficient translation of the Cat-1 arginine/lysine transporter mRNA during amino acid starvation.* Mol Cell Biol, 2009. **29**(10): p. 2899-912.
279. Hung, L.H., et al., *Diverse roles of hnRNP L in mammalian mRNA processing: a combined microarray and RNAi analysis.* RNA, 2008. **14**(2): p. 284-96.
280. Shih, S.C. and K.P. Claffey, *Regulation of human vascular endothelial growth factor mRNA stability in hypoxia by heterogeneous nuclear ribonucleoprotein L.* J Biol Chem, 1999. **274**(3): p. 1359-65.
281. Rossbach, O., et al., *Crosslinking-immunoprecipitation (iCLIP) analysis reveals global regulatory roles of hnRNP L.* RNA Biol, 2014. **11**(2): p. 146-55.
282. UniProt. *RNA-binding protein Raly*. January 2015; Available from: http://www.uniprot.org/uniprot/Q9UKM9.
283. Keppetipola, N., et al., *Neuronal regulation of pre-mRNA splicing by polypyrimidine tract binding proteins, PTBP1 and PTBP2.* Crit Rev Biochem Mol Biol, 2012. **47**(4): p. 360-78.
284. Briata, P., et al., *Functional and molecular insights into KSRP function in mRNA decay.* Biochim Biophys Acta, 2013. **1829**(6-7): p. 689-94.
285. Donnelly, C.J., et al., *Axonally synthesized beta-actin and GAP-43 proteins support distinct modes of axonal growth.* J Neurosci, 2013. **33**(8): p. 3311-22.
286. Bird, C.W., et al., *KSRP modulation of GAP-43 mRNA stability restricts axonal outgrowth in embryonic hippocampal neurons.* PLoS One, 2013. **8**(11): p. e79255.
287. UniProt. *Far upstream element-binding protein 2/KH-type splicing regulatory protein*. Available from: http://www.uniprot.org/uniprot/Q92945.
288. Fuller-Pace, F.V. and H.C. Moore, *RNA helicases p68 and p72: multifunctional proteins with important implications for cancer development.* Future Oncol, 2011. **7**(2): p. 239-51.
289. Honore, B., *The hnRNP 2H9 gene, which is involved in the splicing reaction, is a multiply spliced gene.* Biochim Biophys Acta, 2000. **1492**(1): p. 108-19.
290. Mahe, D., et al., *Cloning of human 2H9 heterogeneous nuclear ribonucleoproteins. Relation with splicing and early heat shock-induced splicing arrest.* J Biol Chem, 1997. **272**(3): p. 1827-36.

291. Grainger, R.J., et al., *Physical and genetic interactions of yeast Cwc21p, an ortholog of human SRm300/SRRM2, suggest a role at the catalytic center of the spliceosome.* RNA, 2009. **15**(12): p. 2161-73.
292. Shehadeh, L.A., et al., *SRRM2, a potential blood biomarker revealing high alternative splicing in Parkinson's disease.* PLoS One, 2010. **5**(2): p. e9104.
293. Ma, X.M. and J. Blenis, *Molecular mechanisms of mTOR-mediated translational control.* Nat Rev Mol Cell Biol, 2009. **10**(5): p. 307-18.
294. Molina-Hernandez, A., N.F. Diaz, and J.A. Arias-Montano, *Histamine in brain development.* J Neurochem, 2012. **122**(5): p. 872-82.
295. Jones, C.M. and J.C. Smith, *An overview of Xenopus development.* Methods Mol Biol, 1999. **97**: p. 331-40.
296. Blackmore, M. and P.C. Letourneau, *Protein synthesis in distal axons is not required for axon growth in the embryonic spinal cord.* Dev Neurobiol, 2007. **67**(7): p. 976-86.
297. Love, N.K., et al., *A nutrient-sensitive restriction point is active during retinal progenitor cell differentiation.* Development, 2014. **141**(3): p. 697-706.
298. Wright, A.F., et al., *Photoreceptor degeneration: genetic and mechanistic dissection of a complex trait.* Nat Rev Genet, 2010. **11**(4): p. 273-84.
299. Wallace, D.C., et al., *Mitochondrial DNA mutation associated with Leber's hereditary optic neuropathy.* Science, 1988. **242**(4884): p. 1427-30.
300. Perry, S.W., et al., *Mitochondrial membrane potential probes and the proton gradient: a practical usage guide.* Biotechniques, 2011. **50**(2): p. 98-115.
301. Wareski, P., et al., *PGC-1{alpha} and PGC-1{beta} regulate mitochondrial density in neurons.* J Biol Chem, 2009. **284**(32): p. 21379-85.
302. Miller, K.E. and M.P. Sheetz, *Axonal mitochondrial transport and potential are correlated.* J Cell Sci, 2004. **117**(Pt 13): p. 2791-804.
303. Ramanathan, A. and S.L. Schreiber, *Direct control of mitochondrial function by mTOR.* Proc Natl Acad Sci U S A, 2009. **106**(52): p. 22229-32.
304. Cunningham, J.T., et al., *mTOR controls mitochondrial oxidative function through a YY1-PGC-1alpha transcriptional complex.* Nature, 2007. **450**(7170): p. 736-40.
305. Rehmann, H., et al., *Biochemical characterisation of TCTP questions its function as a guanine nucleotide exchange factor for Rheb.* FEBS Lett, 2008. **582**(20): p. 3005-10.
306. Czabotar, P.E., et al., *Control of apoptosis by the BCL-2 protein family: implications for physiology and therapy.* Nat Rev Mol Cell Biol, 2014. **15**(1): p. 49-63.
307. Rezaul, K., et al., *A systematic characterization of mitochondrial proteome from human T leukemia cells.* Mol Cell Proteomics, 2005. **4**(2): p. 169-81.
308. Fountoulakis, M., et al., *The rat liver mitochondrial proteins.* Electrophoresis, 2002. **23**(2): p. 311-28.
309. Hilton, M., G. Middleton, and A.M. Davies, *Bcl-2 influences axonal growth rate in embryonic sensory neurons.* Curr Biol, 1997. **7**(10): p. 798-800.
310. Yang, L., et al., *Preventing retinal detachment-associated photoreceptor cell loss in Bax-deficient mice.* Invest Ophthalmol Vis Sci, 2004. **45**(2): p. 648-54.
311. Nir, I., et al., *Expression of Bcl-2 protects against photoreceptor degeneration in retinal degeneration slow (rds) mice.* J Neurosci, 2000. **20**(6): p. 2150-4.
312. Chen, J., et al., *bcl-2 overexpression reduces apoptotic photoreceptor cell death in three different retinal degenerations.* Proc Natl Acad Sci U S A, 1996. **93**(14): p. 7042-7.
313. Tsuchiya, Y. and S. Yamashita, *Anti-apoptotic activity and proteasome-mediated degradation of Xenopus Mcl-1 protein in egg extracts.* J Biol Chem, 2011. **286**(18): p. 15806-14.
314. Levin, L.A., et al., *Identification of the bcl-2 family of genes in the rat retina.* Invest Ophthalmol Vis Sci, 1997. **38**(12): p. 2545-53.

315. Soderberg, O., et al., *Direct observation of individual endogenous protein complexes in situ by proximity ligation.* Nat Methods, 2006. **3**(12): p. 995-1000.
316. Rho, S.B., et al., *Anti-apoptotic protein TCTP controls the stability of the tumor suppressor p53.* FEBS Lett, 2011. **585**(1): p. 29-35.
317. Vaseva, A.V. and U.M. Moll, *The mitochondrial p53 pathway.* Biochim Biophys Acta, 2009. **1787**(5): p. 414-20.
318. Campbell, D.S. and C.E. Holt, *Apoptotic pathway and MAPKs differentially regulate chemotropic responses of retinal growth cones.* Neuron, 2003. **37**(6): p. 939-52.
319. Thiele, H., et al., *Structure of the promoter and complete sequence of the gene coding for the rabbit translationally controlled tumor protein (TCTP) P23.* Eur J Biochem, 1998. **257**(1): p. 62-8.
320. Stolovich, M., et al., *Transduction of growth or mitogenic signals into translational activation of TOP mRNAs is fully reliant on the phosphatidylinositol 3-kinase-mediated pathway but requires neither S6K1 nor rpS6 phosphorylation.* Mol Cell Biol, 2002. **22**(23): p. 8101-13.
321. Shewan, D., et al., *Age-related changes underlie switch in netrin-1 responsiveness as growth cones advance along visual pathway.* Nat Neurosci, 2002. **5**(10): p. 955-62.
322. Li, Z., et al., *Caspase-3 activation via mitochondria is required for long-term depression and AMPA receptor internalization.* Cell, 2010. **141**(5): p. 859-71.
323. Campbell, D.S. and H. Okamoto, *Local caspase activation interacts with Slit-Robo signaling to restrict axonal arborization.* J Cell Biol, 2013. **203**(4): p. 657-72.
324. Jiao, S. and Z. Li, *Nonapoptotic function of BAD and BAX in long-term depression of synaptic transmission.* Neuron, 2011. **70**(4): p. 758-72.
325. Kim, E.M., et al., *Bcl-w promotes cell invasion by blocking the invasion-suppressing action of Bax.* Cell Signal, 2012. **24**(6): p. 1163-72.
326. Koziol, M.J. and J.B. Gurdon, *TCTP in development and cancer.* Biochem Res Int, 2012. **2012**: p. 105203.
327. Ashrafi, G., et al., *Mitophagy of damaged mitochondria occurs locally in distal neuronal axons and requires PINK1 and Parkin.* J Cell Biol, 2014. **206**(5): p. 655-70.
328. Chipuk, J.E., L. Bouchier-Hayes, and D.R. Green, *Mitochondrial outer membrane permeabilization during apoptosis: the innocent bystander scenario.* Cell Death Differ, 2006. **13**(8): p. 1396-402.
329. Green, D.R. and G. Kroemer, *Cytoplasmic functions of the tumour suppressor p53.* Nature, 2009. **458**(7242): p. 1127-30.
330. Muller, P.A., K.H. Vousden, and J.C. Norman, *p53 and its mutants in tumor cell migration and invasion.* J Cell Biol, 2011. **192**(2): p. 209-18.
331. Leu, J.I., et al., *Mitochondrial p53 activates Bak and causes disruption of a Bak-Mcl1 complex.* Nat Cell Biol, 2004. **6**(5): p. 443-50.
332. Sander, J.D. and J.K. Joung, *CRISPR-Cas systems for editing, regulating and targeting genomes.* Nat Biotechnol, 2014. **32**(4): p. 347-55.
333. Joung, J.K. and J.D. Sander, *TALENs: a widely applicable technology for targeted genome editing.* Nat Rev Mol Cell Biol, 2013. **14**(1): p. 49-55.
334. Paradies, M.A. and O. Steward, *Multiple subcellular mRNA distribution patterns in neurons: a nonisotopic in situ hybridization analysis.* J Neurobiol, 1997. **33**(4): p. 473-93.
335. Gioio, A.E., et al., *Nerve terminals of squid photoreceptor neurons contain a heterogeneous population of mRNAs and translate a transfected reporter mRNA.* Eur J Neurosci, 2004. **20**(4): p. 865-72.
336. Pagano, G., and Castello, G. (2012). *Oxidative stress and mitochondrial dysfunction in Down syndrome.* Advances in experimental medicine and biology **724**, 291-299.

337. Sandberg, R., et al., (2008). *Proliferating cells express mRNAs with shortened 3' untranslated regions and fewer microRNA target sites.* Science **320**, 1643-1647.
338. Zala, D., et al., *Vesicular glycolysis provides on-board energy for fast axonal transport.* Cell, 2013. **152**(3): p. 479-91.
339. Rintoul, G.L., et al., *Glutamate decreases mitochondrial size and movement in primary forebrain neurons.* J Neurosci, 2003. **23**(21): p. 7881-8.
340. Sahin, E., et al., *Telomere dysfunction induces metabolic and mitochondrial compromise.* Nature, 2011. **470**(7334): p. 359-65.
341. Schoenmann, Z., et al., *Axonal degeneration is regulated by the apoptotic machinery or a NAD+-sensitive pathway in insects and mammals.* J Neurosci, 2010. **30**(18): p. 6375-86.
342. Di Giovanni, S. and K. Rathore, *p53-Dependent pathways in neurite outgrowth and axonal regeneration.* Cell Tissue Res, 2012. **349**(1): p. 87-95.
343. Arakawa, H., *p53, apoptosis and axon-guidance molecules.* Cell Death Differ, 2005. **12**(8): p. 1057-65.
344. Hoshino, A., et al., *Inhibition of p53 preserves Parkin-mediated mitophagy and pancreatic beta-cell function in diabetes.* Proc Natl Acad Sci U S A, 2014. **111**(8): p. 3116-21.
345. Hoshino, A., et al., *Cytosolic p53 inhibits Parkin-mediated mitophagy and promotes mitochondrial dysfunction in the mouse heart.* Nat Commun, 2013. **4**: p. 2308.
346. Qin, Q., et al., *A novel function for p53: regulation of growth cone motility through interaction with Rho kinase.* J Neurosci, 2009. **29**(16): p. 5183-92.
347. Qin, Q., et al., *Role of calpain-mediated p53 truncation in semaphorin 3A-induced axonal growth regulation.* Proc Natl Acad Sci U S A, 2010. **107**(31): p. 13883-7.

IMAGES SOURCED FROM ACADEMIC BOOKS:

348. Squire, Larry R. *Fundamental Neuroscience.* Amsterdam: Elsevier / Academic Press, 2008.
349. Sanes, Dan Harvey, Thomas A Reh, and William A Harris. *Development Of The Nervous System.* Amsterdam: Elsevier, 2012.

List of Abbreviations

5’-TOP	5’-terminal oligopyrimidine motif
$\Delta\Psi_m$	mitochondrial membrane potential
$\Delta\Psi_p$	plasma membrane potential
A	adenine
Å	angstrom
Alpha (α)	level of significance
ANOVA	analysis of variance
Apaf1	apoptotic peptidase-activating factor 1 [a]
ARNm	ácido ribonucleico mensageiro
Bax	Bcl-associated X protein
Bcl-2	B-cell lymphoma 2
Bcl-X_L	Bcl-2-like protein 1
Bdnf	brain-derived neurotrophic factor
Bmp	bone morphogenic protein
C	cytosine
cAMP	cyclic adenosine monophosphate
Cdc42	cell division control protein 42
ceRNA	competing endogenous RNA
CHX	cycloheximide
CMZ	ciliary marginal zone
CNS	central nervous system
CNV	copy number variation
Cq	(in qPCR) quantification cycle
$\Delta Cq_{X:actb}$	quantification cycle difference of X relative to *actb*
CRE	cAMP response element
Cspg	chondroitin sulfate proteoglycan
CST	cancer stem cell
DAPI	4’,6-diamidino-2-phenylindole
Dcc	deleted in colorectal carcinoma
DIG	digoxigenin
DiI	1,1’-dioctadecyl-3,3,3’,3’-tetramethylindocarbocyanine perchlorate
DMSO	dimethyl sulfoxide
DNA	deoxyribonucleic acid
DOT	dorsal optic tract
dsRNA	double-stranded RNA-dependent
ECM	extracellular matrix
e.g.	exempli gratia
F-actin	filamentous-actin
Fc	fragment crystallizable
Fgf	fibroblast growth factor
FISH	fluorescence in situ hybridization
G	guanine

[a] Note that, although gene/protein names and symbols in *Xenopus* are based on the nomenclature of their human counterparts, protein symbols are first letter capital only.

Gap-43	growth associated protein-43
GC	growth cone
GDI	guanine nucleotide dissociation inhibitor
GDP	guanosine diphosphate
GFP	green fluorescent protein
GPI	glycosylphosphatidylinositol
GTP	guanosine triphosphate
Gsk3β	glycogen synthase kinase 3β
h	hour
HEK 293	human embryonic kidney two hundred and ninety-three cells
$HEK^{MS2\text{-}HB}$	HEK 293 cells expressing a modified MS2 coat protein tethered to a His-biotin (HB) tag
IgE	immunoglobulin E
IgG	immunoglobulin G
ISH	*in situ* hybridization
IPL	inner plexiform layer
kDa	kilodalton
LCM	laser-capture microdissection
LGN	lateral geniculate nucleus
LTD	long-term depression
M-phase	mitotic phase
Mag	myelin-associated glycoprotein
MBS	Modified Barth's Saline
Mcl1	myeloid cell leukemia 1
Mdm2	MDM2 proto-oncogene, E3 ubiquitin protein ligase
min	minute
miRNA	microRNA
MO	morpholino antisense oligomer
MOM	mitochondrial outer membrane
MOMP	mitochondrial outer membrane permeabilization
mRNA	messenger ribonucleic acid
mRNP	messenger ribonucleoprotein
MS-222	Tricaine methanesulfonate
MS2-BioTRAP	MS2 *in vivo* biotin tagged RNA affinity purification
MsrB	methionine sulfoxide reductase gene B
Mss4	mammalian suppressor of yeast
mtDNA	mitochondrial DNA
mTOR	mechanistic/mammalian target of rapamycin
mTORC1	mammalian TOR complex 1
MOT	mid-optic tract
Ngf	nerve growth factor
no.	number
NP-40	nonyl phenoxypolyethoxylethanol
Nt	neurotrophin
OFL	optic fiber layer
ONH	optic nerve head
OPL	outer plexiform layer

PBS	phosphate buffer saline
PCR	polymerase chain reaction
Pkr	protein kinase R
PLA	*in situ* proximity ligation assay
Poly(A)	polyadenylation
PR	photoreceptor
QIF	quantitative immunofluorescence
qPCR	quantitative real-time polymerase chain reaction
RACE	rapid amplification of cDNA ends
RBP	RNA-binding protein
RGC	retinal ganglion cell
Rheb	Ras homolog enriched in brain
RhoA	Ras homolog gene family, member A
RIPA buffer	radioimmunoprecipitation assay buffer
RFP	red fluorescent protein
RNA	ribonucleic acid
RT-PCR	reverse transcriptase-polymerase chain reaction
s	second
SAGE	sequential analysis of gene expression
SDS	sodium dodecyl sulfate
SDS-PAGE	sodium dodecyl sulfate-polyacrylamide gel electrophoresis
SEM	standard error of the mean
Shh	sonic hedgehog
shRNA	small hairpin RNA
SILAC	stable isotope labeling by amino acids in cell culture
srGAP	Slit-Robo-specific GTPase-activating protein
STRING	Search Tool for the Retrieval of Interacting Genes/Proteins
T	thymine
TAF	*trans*-acting factor
Tctp	translationally controlled tumor protein (protein)
TMRM	tetramethylrhodamine methyl ester
tpt1	*tumor protein, translationally-controlled 1* (gene)
tpt1-L	long 3'UTR variant of the *tpt1* mRNA
tpt1-S	short 3'UTR version of the *tpt1* mRNA
U	uracil
UPS	ubiquitin proteasome system
UTR	untranslated region
V	volt
Vamp2	vesicle-associated membrane protein 2
Vegf	vascular endothelial growth factor
VOT	ventral optic tract
Zbp1	zipcode-binding protein 1

Figure and Table Index

1. INTRODUCTION

2. EXPERIMENTAL PROCEDURES

3. RESULTS

A – Expression and Regulation of *tpt1*

B – Tctp Regulates Retinal Axon Pathfinding In Vivo

C – Mechanistic Insights Into the Role of Tctp in Neural Development

4. DISCUSSION